UNIVERSITE DE BORDEAUX 1

ÉCOLE DOCTORALE DES SCIENCES & ENVIRONNEMENTS (ED 304)

THESE

POUR OBTENIR LE GRADE DE DOCTEUR
SPÉCIALITÉ : Géoressources, patrimoines et environnements
Présentée par

Yohana Vanesa STUPAR

Trends and rates of mercury and arsenic in sediments accumulated in the last ~80 years in the climatic-sensitive Mar Chiquita system, Central Argentina

Doctorat en co-direction avec la Universidad National de Córdoba, Argentina

Directeur de thèse: M. Philippe LE COUSTUMER
Co-directrice de thèse: Mme. María Gabriela GARCÍA

Soutenue le 06 décembre 2013
devant la commission d'examen

M. David AMOUROUX	Directeur de recherches, LCABIE-IPREM, UMR 5254 CNRS, Université de Pau et des Pays de l'Adour (UPPA)	Rapporteur
M. Mikael MOTELICA-HEINO	Professeur, ISTO, UMR7327 CNRS, Université d'Orléans	Rapporteur
M. Jörg SCHÄFER	Professeur, UMR 5805 EPOC - Université de Bordeaux 1	Président
Mme. María Gabriela GARCÍA	Professeur, Universidad Nacional de Córdoba, Argentina	Examinatrice
M. Frédéric HUNEAU	Professeur, Université de Corse Pascal Paoli, Corte	Examinateur
M. Philippe LE COUSTUMER	Maître de Conférences, HDR	Examinateur

UNIVERSITÉ DE BORDEAUX

EA 4592 G&E Géoressources & Environnement

I2M BORDEAUX

Acknowledgement

Wow!! Three years ago this moment seemed to be so far away, but thanks God it has arrived! However, it could have not been possible without many people that were next to me in one way or another all along this journey.

First and above all, I want to thank God. His Word, the Bible says in the book of Isaiah 41:10:

So do not fear, for I am with you;
Do not be dismayed, for I am your God.
I will strengthen you and help you;
I will uphold you with my righteous right hand.

During this adventure, there were ups and downs and sometimes more downs than ups but God was next to me all the time. The faith on Him strengthened me every day and I could not be more grateful! Thank you Lord!

Thanks to David Amoroux and Mikael Motelica-Heino and all the members of the jury for accepting to examine this thesis.

Thank Philippe Le Coustumer and Frédéric Huneau for helping me with all the administrative procedures (not few in France!) to start my thesis. Thank you Philippe likewise, for making this work end in good conditions.

An enormous thank to María Gabriela García and Jörg Schäfer! Thank you both for being my mentors, for your explanations, your patience, for putting your smocks on and coming to the lab when the things weren't working out and for all the time that you have dedicated to this thesis. Your experience and contributions helped me to make this work what it is. It was such a pleasure to work with you! Thank you Gabriela for being so close to this work even counting the 11000 km that separate Bordeaux from Córdoba.

Thanks to Eduardo Piovano and Sabine Schmidt for your valuable contributions along this thesis and for answering every single and numerous mails!!

Thanks to the "house" that saw me grow up as professional: the Universidad Nacional de Córdoba and all the member of CIGeS laboratory: Gabriela, Eduardo, Diego, Karina, Andrea, Stella, Myriam, Pedro, Jorge and the PhD students Verena, Lucía, Stefanía and Lucio. To my geology friends, especially those who started in 2003 and share many adventures with me!

Many thanks to those that came with me to the field trips to collect the samples that were traduced in the results of the thesis: Gabriela, Eduardo, Verena, Marina, Guillermo and my dad.

Thanks to my second "house", the EGID now ENSEGID. It is hard to start to write and to put into words what I have lived here because countless thoughts come to my mind! To this big family that welcomed me in a way that I couldn't have imagined. I feel so grateful to have spent 3 years in this great place with such an amazing group of people!! Where to start from? Well, probably by the direction and his director. Thank you very much Alain for allowing me to take one "hydro" places even if I'm not fully hydrogeologist. I wish you all the best for this new period for you and for the institution! To the ancient director, Jean-Marie, your daily "l'equipe" made more than one person make a comment about sport during lunch... and yes, I am still a Boxers fan! To those who I had the privilege to share the daily lunch with: Alicia and the equal Argentinean taste, Christine, Maïlys trying to give the original recipe for couscous to Francis but he didn't care much as long as he had one dessert nearby. Thanks Morgan, Alex P. and Vincent for introducing us to the bio culture and to Michel, Amélie and Jimmy for let us know which is the best shop to get the better deals in the "Capucins Marché". Thanks also to Francois, Sandrine, Sophie, Marian, Rapaël, Olivier A., Corine, Florence, Frédéric... without you lunch in the "cafet" wouldn't have been the same.

Serge and Léa, thank you very much for dedicating time to my samples and the numerous DRX analyses.

To those who are also part of the institution: Adrian, Philippe R., Myriam, Laurent, Olivier L.R., Nesrine, Samia, Line...

Thanks Christine for the help that you provided me especially at the end of this thesis. Thanks Florence for all your work in the library and for name me "reader of the month in July"! I hope mushrooms stop growing!!

Thanks to Franck and Sébastian for making ~~internet~~ the informatic system work every day. Although I think I will always have problems with the printers until I leave....

To the INNOVASOL group with Marian and Sarah... and the goats... and the sheeps... surely the ENSEGID is the pearl of the IPB!!

Thanks to Sambala and Chantal, it feels great to have a clean office and talk (talk talk talk talk talk talk) every morning!

I will also would like to say thanks to those who after 3 years usually leave the ENSGID (I say usually because after spending tine here, it is hard to leave...): Amélie, Johan, Estefanía, Fanny, Alex B., Nazeer, Morgan, Aurelié, Florie, Greg, Benoit B., Hugo, Yohann, Wei,

Elicia... Thank for sharing the quotidian, laughters, and from time to time barbequeues and a glass of wine, or two..... Sooner or later the end arrives... Greg you have won the “pages battle”! Congrats on your PhD and new postdoc position. I’m glad that we could share the last months of writing especially in summer! And thanks to Michel that encourage us with the “bibis”!

Benoit H. and Benoit B., thank you very much for your help with the analysis of the satellite images and remote sensing. It was great to learn with you! Benoit H., your desserts are dearly missed...!

But how to name the PhD student without mentioning those who share with me most of my days at the office? Two are gone but other two are still going through this “thesis adventure”. Olivier, thank you for being there for me from the first moment of my arrival. Everything started printing an article, sharing many cups of coffee, laughters, then it continued going to the hockey matches, movies, restaurants... Thank you for your loving regards, your attentions, your caring, your love, your daily help, for readying the entire thesis and doing great remarks... well, thank you for everything that you do for me! I thank God for your life and for becoming the man that walks besides me. Jessy, I still don’t understand why you said that you could do another doctorate but I do agree with you that at the end, it is a great experience. Thank you for being an ear when things weren’t that easy and thanks for sharing your laughter, kindness and your disponibility when I needed help. I hope that Corse treats you, Béné and Louise better than ever! Nazeer, your arrival made me think mine: not being able to communicate in French wasn’t easy! Thank you, Rim and Iamen for treating me like a little sister! I really appreciated it. Morgan... well... what to say...? I’m joking! I must to say that I didn’t know what to expect of you being in the same office than us but after you say that you liked mate, everything changed. Thank you for sharing litres and litres of mate in the rainy days (that were many)! This year I stopped the count in 22 consecutive days but I’m sure they were lot more! Or for sharing the tererés when the thermometer raised up to 39 °C in the office. Jessy was right when he said that I will continue to improve my French with you but I warn you that the phrases “les fenêtres sont crades” or “j'ai mal aux pattes” will still continue to be among my favourite ones!! Haha!

To those that I had the pleasure to cross by at the ENSEGID even if not for so long, Cyril and Jehane, thank you very much for introducing me to the French culture after some days of my arrival and Christophe thanks for your funny character that could make explode in laughter!

To the ex-GHYMAC lab and the (ex)PhD students that I had the pleasure of meeting: Saber, Rasool, Yuliya, Thibault, Jessica. Nicole, thanks so much for your help especially in the last part of the analysis of my samples!

I will like to thank as well, the GBU (Groupe Biblique Universitaire) and in special the groups in Talence and Centre Ville. It was great to share with you so many activities, weekends, Bible studies, everything to learn more about He that gave his life for us: Jesus Christ. Thanks for living and sharing your unconditional love with me! Thanks God you are many, so I prefer not to name you in the case I might forget one of you. Thanks to the Razzano family and the church in Cauderan for your prayers, friendship and fraternal love. Thanks to the church that saw me grow up in Córdoba since I was a 3 years old little girl. Your constant prayers and your love to me through messages, e-mails, calls made shorten distances between these two continents.

Thanks to my flat mates: Vere, Nam, Mariam and Philippe…. And the students that thanks ERASMUS I got to meet.

Thanks to my closer family: grandmother, uncles, aunts, cousins and closer friends those from Argentina, South Africa and spread all around the globe for being there all the time, for asking how I was. I surely miss you deeply!

And finally to my family: My dad Daniel, my mom Norma, my sisters Cintia and Pamela and my brother Jonatán. You have no idea how much I have missed you during these years!!! Our hugs, long talking sessions, movies, praying together or a simple mate to share what the day had brought. I pray every day for you and I can't wait the end of December to end up these two long years apart. Thank you for your example, your words given at the right time, your encouragement, your prayers. Mom, dad, thank you for everything that you have taught me in these 30 years. You are an example of love, caring, trust in the Lord… I know that saying thanks is never going to be enough, but this thesis is for you. I would like to return a bit of everything that you have given me. I LOVE you all deeply!!

I hope that I did not forget any of those who helped me all the way, but if I did, it wasn't my intention!

Thanks to all of you for walking with me and arriving to the end of this journey…

Yohana

Résumé

En Amérique du Sud et notamment en Argentine, le comportement du mercure (Hg) et de l'arsenic (As) principalement dans les sédiments est encore peu compris. Le système de Mar Chiquita et plus particulièrement le lac Laguna del Plata, recevant les eaux de la rivière Suquía, sert ici de cadre à l'étude de la dynamique de ces deux éléments trace. Leurs distributions dans l'espace et le temps sont analysées en lien avec l'influence anthropique et les conditions hydrologiques qui ont changé de manière importante au cours du dernier siècle.

L'approche retenue a consisté tout d'abord à examiner la distribution spatiale du mercure et de l'arsenic à travers l'analyse des eaux et sédiments pris le long de la rivière Suquía et dans Laguna del Plata. Dans un second temps, l'étude fine d'une carotte de sédiment prélevée dans Laguna del Plata a permis d'analyser les variations temporelles de Hg et As.

De plus, la réalisation d'extractions sélectives a conduit à l'identification des phases porteuses de Hg et As. L'interprétation globale des résultats et l'appui des images satellites ont révélé le rôle majeur joué par les changements climatiques et les variations hydrologiques dans le contrôle du comportement du mercure et de l'arsenic au sein du système de Mar Chiquita.

Au final, l'association des différentes approches a démontré les comportements différents du mercure et de l'arsenic. Les concentrations de mercure sont faibles quand les conditions climatiques sont plus arides et le niveau du lac bas. Elles sont principalement associées aux sulfures transportés par les sédiments de la rivière Suquía. La hausse des précipitations régionales aboutit à un ruissellement plus important et une montée du niveau du lac conduisant à l'augmentation d'accumulation de mercure. Durant cette période, Hg est principalement associé à la matière organique. L'arsenic, quant à lui, est apporté en solution par les eaux jusqu'au lac et, durant les périodes plus sèches, un apport supplémentaire s'effectue par les vents balayant la plaine loessique de Chaco Pampean. Dans la carotte de sédiment, l'arsenic est associé aux oxyhydroxydes réactifs de fer et de manganèse. Ses fortes concentrations dans la partie basse de la carotte sont également liées aux sulfures mais sont aussi associées, dans les parties moyenne et haute, aux carbonates.

Mots-clés: Mercure - arsenic – variations hydrologiques – Laguna del Plata – changement climatique

Abstract

In South America and especially in Argentina, the behaviour of mercury (Hg) and arsenic (As) mainly in sediments remains poorly understood. The Mar Chiquita system and more particularly the Laguna del Plata with its associated Suquía River basin is used here as a case study to identify the dynamic of these two trace elements. Their distribution in space and time are studied in relation with the anthropic presence and the hydrological conditions that importantly changed in the last century.

The methodology consisted first to study the spatial distribution of mercury and arsenic thanks to the analysis of water and sediments taken all along the Suquía River and Laguna del Plata. Secondly, the sampling and study of a sediment core taken in Laguna del Plata allowed to evaluate variations of Hg and As with time.

The implementation of selective extractions allowed to better identify Hg and As bearing phases. The global interpretation of the results and the support of satellites images revealed the important role played by climate changes and hydrological variations in the control of mercury and arsenic behaviour within the Mar Chiquita system.

The combination of these different approaches revealed that the dynamic of mercury and arsenic shows contrast behaviour. Hg concentrations are low when the climate conditions are dry and lake-level is low. They are mainly associated to sulphurs carried by the Suquía River. The augmentation in regional precipitations produced higher runoff, rise in the lake-level and an increment in Hg accumulations. In this period Hg is mainly associated to the organic matter. As instead is contributed to the lake in solution and by the influence of winds from the loessic Chaco Pampean Plain in drier periods. As is associated to reactive Fe and Mn oxyhydroxides throughout the core. High concentrations in the bottom of the core are also associated to sulphides while in the middle and upper part As concentrations are as well associated with carbonates.

Keywords: Mercury - arsenic – hydrological variations – Laguna del Plata – climate change

Résumé étendu

Au centre de l'Argentine, la plaine Chaco-pampéenne forme une vaste plaine loessique qui s'étend depuis la Cordillère des Andes à l'Ouest jusqu'à l'Océan atlantique à l'Est. Elle couvre une surface d'environ $1x10^6$ km^2 représentant ~36 % du territoire argentin. Sur la bordure est de la plaine (30°S to 37°S), une série de lac est disposée le long d'un axe nord-sud. L'analyse des sédiments accumulés dans ces lacs indique qu'ils présentent une forte sensibilité aux changements climatiques qui se produisent depuis le Petit Age Glaciaire (PAG). Cette sensibilité s'illustre remarquablement dans le système de Mar Chiquita qui se compose de Laguna Mar Chiquita, de Laguna del Plata et des zones humides du Río Dulce. En période de hautes eaux, Laguna Mar Chiquita devient le lac salé le plus grand d'Amérique du Sud mais aussi un des plus grands du monde. En outre, la taille du lac a varié de ~6000 km^2 dans les périodes plus humides à ~2000 km^2 de nos jours mais a par le passé été encore plus petit en atteignant ~1000 km^2 (Piovano *et al.,* 2009) quand un climat sec a prévalu. Dans le sud-ouest du système, la Laguna del Plata est un petit lac formant une baie avec Laguna Mar Chiquita durant les hautes eaux (Oroná *et al.,* 2010) alors qu'il n'est connecté que par un petit canal en basses eaux. Laguna del Plata reçoit les eaux de la rivière Suquía qui prend sa source dans la chaine des Sierras Pampeanas, à l'Ouest. En amont, la plupart de ses affluents sont retenus par le barrage de San Roque (31°22'13.43"S; 64°27'41.40"W, 643 m.a.s.l.). Plus en aval, la rivière traverse la ville de Córdoba et la plaine lœssique chaco-pampéenne après avoir parcouru près de 200 km puis se jette dans Laguna del Plata. Cette région est soumise à un développement urbain et industriel important depuis le milieu du $20^{ème}$ siècle ayant probablement impacté la chimie de la rivière. Plusieurs auteurs (i.e., Pesce and Wunderlin, 2000; Wunderlin *et al.,* 2001; Monferrán *et al.,* 2011; Pasquini *et al.,* 2011) ont observé une diminution de la qualité de l'eau depuis les territoires vierges, en amont du bassin versant, vers le lac. Gaiero *et al.* (1997) ont remarqué une augmentation des concentrations des métaux en trace dans les sédiments de la rivière d'amont en aval, l'attribuant à l'influence urbaine. A l'heure actuelle, aucune donnée ne permet de comprendre sur le long terme les variations des taux de métaux dans les sédiments de la rivière Suquía.

L'évolution environnementale d'une région peut-être enregistrée correctement dans un environnement sédimentaire relativement stable (Oldfield and Appleby, 1984). Par conséquent, l'étude des sediments accumulés dans un lac revêt une grande importance pour

l'analyse des processus environnementaux, sur la base d'une chronologie précise et fine au ^{210}Pb (Sanchez-Cabeza *et al.*, 2000).

Dans la présente étude, les évolutions historiques des concentrations de deux contaminants ont été analysés dans les sédiments accumulés durant les 80 dernières années environ dans Laguna del Plata, avec l'objectif d'identifier leurs variations en lien avec celles des conditions climatiques et hydrologiques qui ont régné sur le nord de la région chaco-pampéenne. D'un côté, un élément d'origine atmosphérique, le mercure (Hg), a été retenu pour cette étude du fait de sa sensibilité aux changements globaux. De l'autre côté, l'arsenic (As), un contaminant géogénique, dont la présence a été largement rapportée dans la région Chaco-pampéenne, est analysé en se focalisant sur son comportement géochimique vis-à-vis de l'alternance des conditions eau salée et eau douce.

Les objectifs spécifiques de cette étude sont:

- Contribuer à une meilleure connaissance de la distribution spatiale du mercure et de l'arsenic au sein du système Mar Chiquita,
- Analyser la variabilité de leurs concentrations dans les sédiments accumulés au cours des 80 dernières années,
- Identifier leurs sources et leur dynamique au cours des processus de transport et d'accumulation,
- Évaluer leur comportement vis-à-vis des fluctuations hydrologiques du système.

Dans ce but, différentes méthodologies ont été appliquées.

Tout d'abord, une synthèse bibliographique est proposée afin de comprendre les spécificités géologiques, hydrologiques et climatiques de la région et leurs impacts géo-physicochimiques sur le système Mar Chiquita. Les dynamiques de Hg et As sont également étudiées et leur présence dans le monde et plus spécifiquement en Argentine sont abordés.

Dans un second temps, plusieurs campagnes de terrain ont été menées dans le but de collecter des échantillons de sédiments et d'eau. Les différentes stations d'échantillonnage sont situées en amont de la rivière Suquía, dans la chaine des Sierras Pampeanas, puis le long de la rivière jusqu'à Laguna del Plata et Laguna Mar Chiquita. Différents paramètres ont été mesurés *in situ* dans les rivières tels que le total de solides dissous (TDS), la conductivité, le pH ou encore l'oxygène dissous. En laboratoire, les échantillons d'eau ont été filtrés et analysés pour

déterminer leurs concentrations en ions majeurs et mineurs par chromatographie et spectrométrie de masse à plasma à couplage inductif (ICP-MS). La composition des sédiments a été déterminée par diffraction de rayon X (DRX). Enfin, la teneur en mercure a été mesurée par la spectrométrie d'absorption atomique à vapeur froide (CV-AAS).

En complément, à l'embouchure de la rivière Suquía avec Laguna del Plata, une carotte de sédiment a été prélevée. Sa chimie a été analysée par fluorescence de rayons X (XRF). Ensuite, elle a été échantillonnée toutes les 0,5 cm et différents paramètres ont été mesurés tels que le pH, la porosité, le carbone organique et inorganique, la granulométrie et enfin une datation a été effectuée. Sur les échantillons, le processus d'extractions sélectives a été réalisé à l'aide d'une solution d'ascorbate (enlève des éléments traces associés à des oxydes de Mn et de la fraction la plus réactive de l'oxyde de Fe), d'une solution de H_2O_2 (attaque la matière organique mais les sulfures sont également partiellement oxydés au cours de cette étape), d'une solution de HCl (comprend les métaux associés aux oxydes amorphes et cristallines de Mn et de Fe, les carbonates, les silicates hydratés de Al et les sulfures volatils en acides - AVS) et d'une solution de HF pour l'attaque totale de sédiment. Les sédiments restants et les surnageants ont été analysés pour déterminer les concentrations de Hg, As, Fe et Mn.

L'ensemble des résultats a permis de réviser le modèle hydro-géochimique proposé par Piovano *et al.* (2002) en affinant davantage le fonctionnement de Laguna del Plata et en incluant les phases porteuses principales de Hg et As identifiées dans la région.

Dans la figure, les précipitations (P) et l'évaporation (E) sont représentées par des flèches dont la longueur est proportionnelle au volume. Le ruissellement de la rivière, qui s'est intensifié à partir des années 1970, est indiqué par une flèche pleine. En revanche, la flèche apparait en pointillés lorsque les débits de la rivière deviennent faibles, conditions hydrologiques qui prédominent durant la période sèche. L'épaisseur des flèches, associées à différentes phases du Hg et As étudiées dans la région, est proportionnelle à l'importance de leurs flux respectifs. Avant les annés 1970, la période sèche domine et s´accompagne de niveaux des lacs bas. Les entrées de Hg dans le lac provenaient alors principalement de sources naturelles comme le mercure associé aux particules (notamment aux sulfures) qui ont été transportées vers le lac depuis la partie supérieure du bassin de la rivière Suquía ou encore le Hg atmosphérique (dépôt sec). Dans des conditions de hautes eaux (après 1970), ces deux sources ont augmenté leurs contributions en raison d'une augmentation des précipitations (dépôt

humide) et de l'érosion des sols dans la partie supérieure du bassin versant mais aussi de l'augmentation globale du flux de Hg dans l'atmosphère. Les conditions plus humides entraînent une augmentation de la production primaire du lac et donc une plus grande affinité du Hg pour la matière organique particulaire qui se trouve dans les sédiments accumulés au cours de cette période.

En revanche, l'arsenic est principalement associé aux (hydr)oxydes de Mn et Fe dans la phase aqueuse, ceci étant favorisé par les conditions de pH élevé du lac en basses et hautes eaux. En outre, dans des conditions plus sèches, l'entrée de l'As dans le lac a été renforcée par les vents dominants qui ont porté les particules de lœss riches en cet élément. Dans des conditions plus humides, l'entrée d'As depuis l'atmosphère devient moins important et il est surtout présent dans le lac associé aux particules provenant de la rivière. En plus d'être associé aux (hydr)oxydes de Mn et Fe, l'As est associé à la pyrite dans la partie inférieure de la carotte sédimentaire et à la calcite dans les parties médiane et supérieure. Par ailleurs, l'arsenic résiduel qui ne peut pas être expliqué par les extractions sélectives peut être fixé sur la pyrite non réactive.

Les sources de Hg et d'As dans les sédiments de Laguna del Plata sont le plus souvent attribuées à des sources naturelles. Dans le cas du Hg, une contribution des flux mondiaux devrait être considérée ainsi que de certaines autres sources anthropiques locales. Ces dernières sont devenues de plus en plus importantes à partir des années 1970 suite au développement industriel de la région. L'activité volcanique qui a eu lieu au début des années 1990 aurait pu également augmenter le signal du Hg. En ce qui concerne l'As, l'entrée principale est clairement associée à la contribution croissante des particules lœssiques pendant la période sèche qui a régné dans la région avant les années 1970.

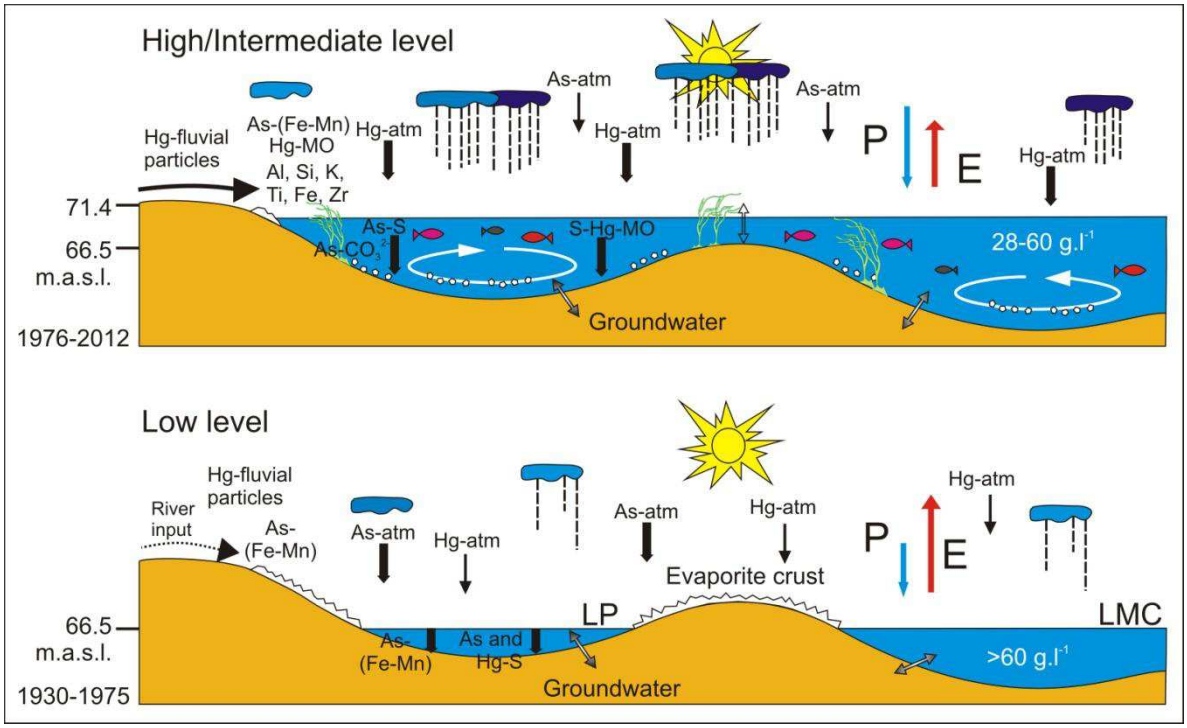

Principales entrées de Hg et As en lien avec les variations des conditions hydrologiques de Laguna del Plata (modifié de Piovano *et al.*, 2002).

Table of content

List of figures

List of tables

Introduction

In the central Argentina, the Chaco Pampean Plain is a vast loessic plain that extends from the Andean Cordillera in the west to the Atlantic Ocean in the east. It covers an area of around $1x10^6$ km^2 that represents ~36 % of the Argentinean territory. A series of lakes is found along a N-S bar located in the eastern border of the plain (30°S to 37°S). The analyses of the sediments accumulated in these lakes have shown high sensitivity to the climatic changes that have occurred since the last Little Ice Age (LIA). The most conspicuous example is the Mar Chiquita system is composed of the Laguna Mar Chiquita, Laguna del Plata and the Río Dulce wetlands. During highstands, Laguna Mar Chiquita becomes not only the largest saline lake in South America but also one of the largest in the world. Furthermore, the lake has varied its size from ~6000 km^2 in the wettest periods to the ~2000 km^2 that shows nowadays but it was even smaller with ~1000 km^2 in the past (Piovano *et al.,* 2009) when a dry climate prevailed. In the southernmost margin of the Laguna Mar Chiquita, the Laguna del Plata is a small lake that forms a bay with it during highstands (Oroná *et al.,* 2010) and stays connected through a small channel during lowstands. Laguna del Plata receives the runoff waters of the Suquía River whose headwaters are located in the Sierras Pampeanas Range, in the west. Most of these tributaries in the upper catchments are stored in the San Roque Dam (31°22'13.43"S; 64°27'41.40"W, 643 m.a.s.l.). Downflow, the river crosses the city of Córdoba and the loessic plain of the Chaco Pampean Plain, after travelling around 200 km. Finally, the Suquía River discharges into the Laguna del Plata. This system is subject to a growing urban and industrial development since the mid 20^{th} Century that had probably impacted in the chemistry of the river. Some authors (i.e., Pesce and Wunderlin, 2000; Wunderlin *et al.,* 2001; Monferrán *et al.,* 2011; Pasquini *et al.,* 2011) observed a decrease in the water quality from pristine regions in the upper fluvial catchments to the proximity of the lake. Gaiero *et al.* (1997) noticed increasing trace metal concentrations in riverbed sediments downflow, which was attributed to the urban impact. At present there is no comprehensive data on the long-term change in metal contents of the Suquía river sediment load.

The environmental evolution of a region can be well-recorded in the relatively stable sedimentary environment (Oldfield and Appleby, 1984). Therefore, the study of the sediments

accumulated in lakes has a great importance for the analysis of the environmental processes, based on a detailed and accurate ^{210}Pb chronology (Sanchez-Cabeza *et al.*, 2000).

In the present study, the historical records of two contaminants were analyzed in the sediments accumulated in the last ~80 years in the Laguna del Plata, with the aim of identifying their variability with the hydrological and climatic conditions predominant in the last 80 years in the northern Chaco Pampean region. On one hand, a typical atmospheric-borne element such as Hg was selected due to its already documented sensibility to global changes. On the other hand, a geogenic contaminant such as arsenic, whose presence has been largely reported in the Chaco Pampean region is analyzed focusing on its geochemical behaviour under alternating saline and freshwater conditions.

The **hypothesys** of the present work are:

- The climate variations in the Mar Chiquita system have influence on its chemical composition, and particularly on the dynamics of the studied trace elements
- Hg sources are likely associated with the global flow of this element,
- The record of As in the lake sediments likely responds to the variable contributions from the loessic sediments that cover the Chaco Pampean Plain
- The volcanic eruptions in the Andes Cordillera are a potential source of trace elements (such as Hg) that accumulate in the sedimentary record of the Mar Chiquita system.

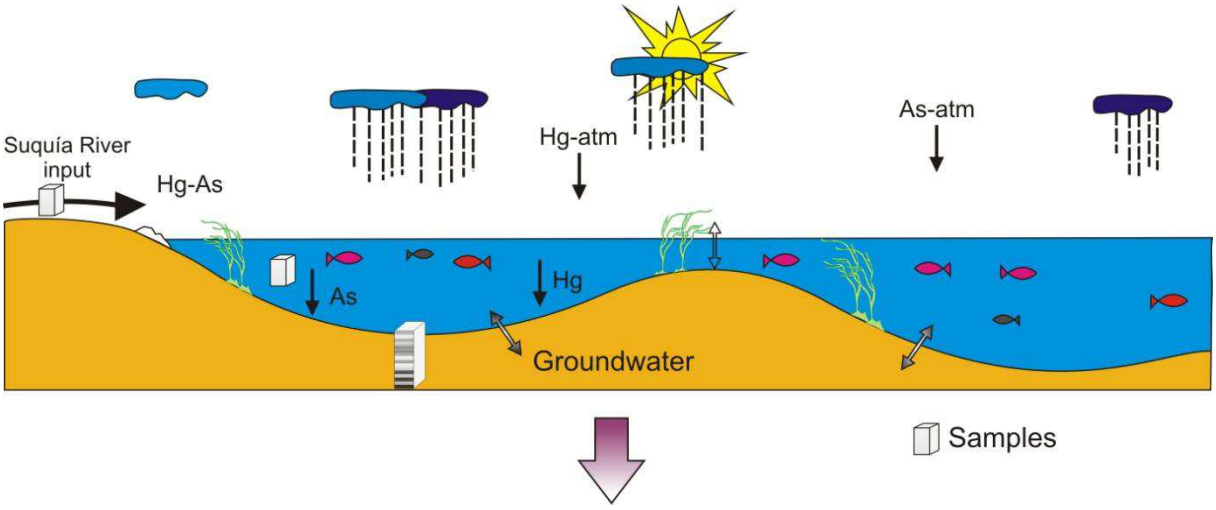

Following these hypothesis, the **specific objectives** of this study were defined as:

- To evaluate the response of Hg and As concentrations measured in the sedimentary record of laguna del Plata to the hydrological fluctuations in the basin.

- To contribute to a better knowledge of the spatial distributions of mercury and arsenic in the basin,
- To analyze the variability of their concentrations in the sediments accumulated in the past 80 years,
- To identify their sources and dynamics during transport and accumulation,

To achieve these objectives, a large set of geochemical, isotopic, hydrological and limnogeologial tools were used.

The approach to achieve these objectives is outlined in the six parts of this thesis.

First chapter:

It provides the information to place the study area into its geographical context. It allows as well to understand the climatic features that triggered the climate changes and the geo-physicochemical consequences over the Mar Chiquita system.

Second chapter

This chapter contains general information about the occurrence of Hg and As in the environment. Primary sources, dynamics, chemical associations and previous works in the world and Argentina are discussed.

Third chapter

In this chapter, all methodological aspects are described. Details of the sampling methodology, analytical methods for water and sediment analysis, selective extractions, determination of sediment´s mineralogy, core dating and satellite image interpretation are included.

Fourth chapter

It presents all the results obtained. For a better understanding the results show firstly the information obtained in the Suquía River basin and its spatial distribution. Secondly, the results corresponding to the sedimentary core that give the temporal distribution are presented.

Fifth chapter

The results presented in the previous chapter are interpreted and discussed.

Sixth chapter

Finally, a hydro-geochemical model for the Mar Chiquita system including Hg and As bearing phases is described as well as the perspectives of this work.

1. Regional context of Laguna Mar Chiquita and Laguna del Plata

1.1 Location

Laguna Mar Chiquita system (Laguna Mar Chiquita, Laguna del Plata and the Dulce River wetlands) is located in the provinces of Córdoba and Santiago del Estero occupying a vast area that goes between 26° to 31° S and 62° to 63°' W in the geological province of the Chaco Pampean Plain. The system plays an important biological role due to its rich and abundant biodiversity as well as anthropological interest to the point that was declared a Ramsar site by the United Nations (http://ramsar.wetlands.org).

The Laguna Mar Chiquita system catchment covers an area of around 127,000 km^2 (Fig. 1-1). At the present time, there are three rivers that flow into the lake: The Suquía, Xanaes and Dulce Rivers.

- The Suquía River (200 km) headwaters are located in the Sierras Pampeanas de Córdoba (between 29°00' - 33°30'S and 64°00' - 65°30'W) where different mining activities (mainly rock quarries) and land-use have been developed. The San Roque reservoir (643 m.a.s.l. - 31°22′41″S, 64°28′10″W) located upstream from Córdoba city, collects the waters from the catchment's tributaries and is used for flood control and drinking water reservoir. Downflow, the river crosses from west to east of the city of Córdoba which is the second biggest of Argentina (1.3 million inhabitants) after Buenos Aires. Automobile industry, machinery manufacturing, food and paint production are the main economical activities in the city. In its lower stretch, the Suquía River crosses the loessic depression of the Chaco Pampean Plain (Zárate, 2003) which is one of the most important agricultural areas of the country. Finally the river discharges into the Laguna del Plata situated in the South West margin of the Laguna Mar Chiquita and connects to it during high lake-level periods.

- The Xanaes River (300 km) has its headwaters also in the Sierras Pampeanas Range and originates in the confluence of the Anizacate and Los Molinos rivers. In the Chaco Pampean plain, it runs with a W-E direction (Vázquez *et al.*, 1979) parallel to the Suquía River until reaching Laguna Mar Chiquita.

- The Dulce River (812 km) is the most important of the three rivers owed to its volume. Its headwaters are located in the limit between the provinces of Salta and Tucumán (NW region of Argentina). After 100 kilometres the river discharges into the Río Hondo Dam (27°31'34.76"S; 64°58'37.65"W with an extension of 330 km^2 at ~350 m.a.s.l.) and a few

kilometres downflow the output it divides into two branches. One of them (Saladillo River) crosses the Ambargasta salt pan raising the salinity of its waters and binds anew to the Dulce River. Finally, the highly saline river flows into the Laguna Mar Chiquita (Vázquez *et al.*, 1979) from its northern coast.

The combined average annual discharge of both Suquía and Xanaes Rivers is 725 hm^3 while the discharge of Dulce River ascends to 2996 hm^3 (Reati *et al.*, 1997).

Several authors (e.g., Kröhling and Iriondo, 1999; Piovano *et al.*, 2002; Bucher *et al.*, 2006; Leroy *et al.*, 2010) have mentioned the dramatic lake levels fluctuations that Mar Chiquita has suffered all along its history. These hydrological fluctuations are evident not only through the sedimentary record, but also through the continuous variations of lake area registered in the last 30 years by satellites images (Fig. 1-2). Laguna Mar Chiquita is the largest saline lake in South America and one of the biggest in the world (Piovano *et al.*, 2002, 2004a,b). It reached its maximum level (71.4 m.a.s.l.) in 2003 with an extension of ~6500 km^2. At the moment of this work, Laguna Mar Chiquita shows a reduction in its area of ~50 % reaching an extension of ~2220 km^2 and a lake-level of 68.1 m.a.s.l. Bucher *et al.* (2006) divided this area in two sub-regions: the Dulce River wetlands which include a series of small lakes located in the NE part of the Laguna Mar Chiquita and the present channel of the Dulce River. The landscape is characterised by a plain covered with scrub vegetation that is intentionally burnt twice a year to improve the palatability for the cattle. The other region is the one occupied by the actual Laguna Mar Chiquita.

On the east side, the lake is limited by the San Guillermo high lifted up by the Tostado-Selva fault (Mon and Gutierrez, 2009). The southern margin is a potentially flooded depression cut by some remaining sandy elevations formed during the past driest periods. Farming and cattle are the main economic activities in this area. The eastern flanks of the Sierras Pampeanas foothills reach the western margin of the Mar Chiquita Lake, where agricultural expansion produced an elevated deforestation. Finally, the North shore is characterised by the presence of muddy and salty playas derived from the intense hydrological fluctuations that affect the region.

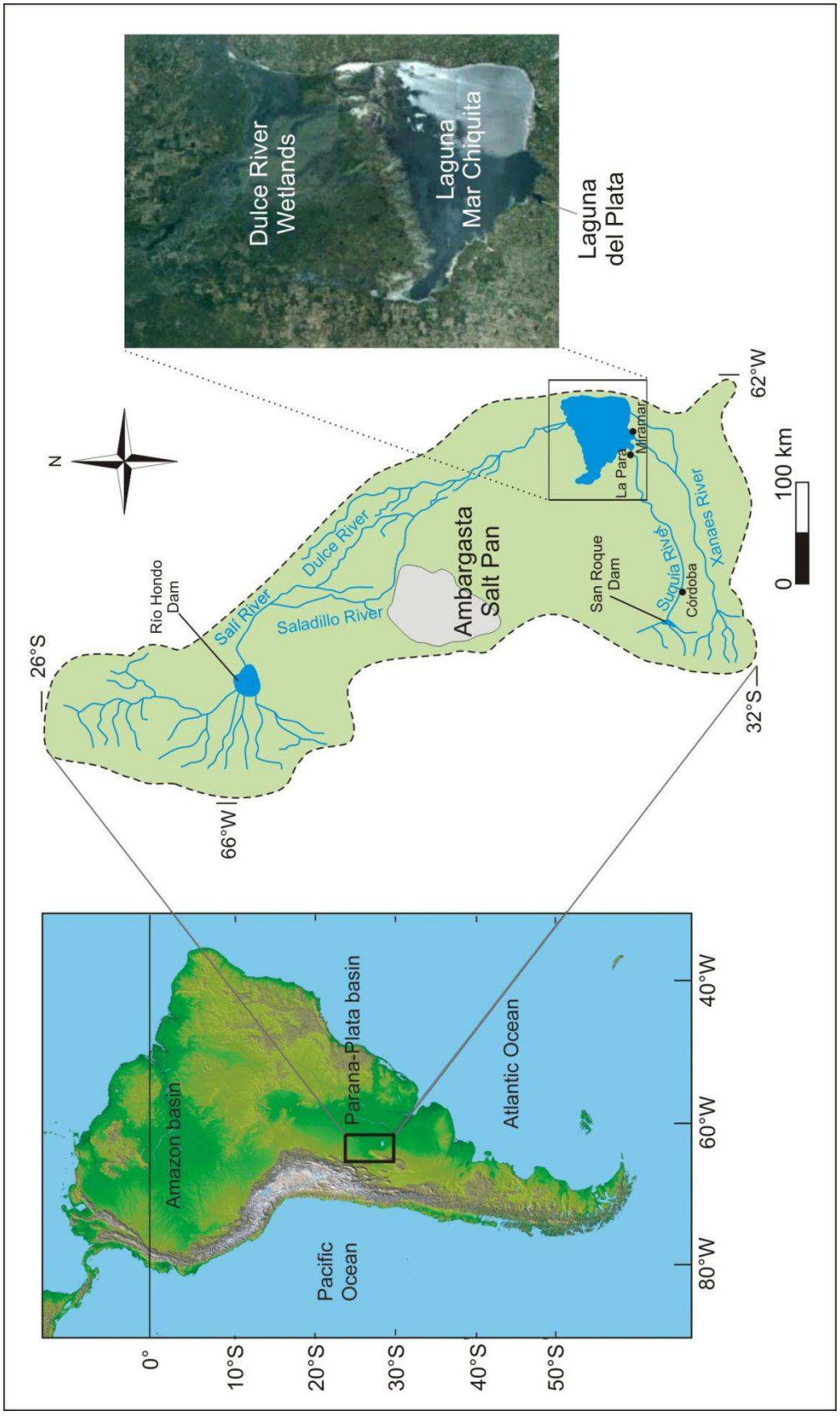

Fig. 1-1 : Study area location. (Modified from Piovano *et al.*, 2006 and Troin *et al.*, 2010)

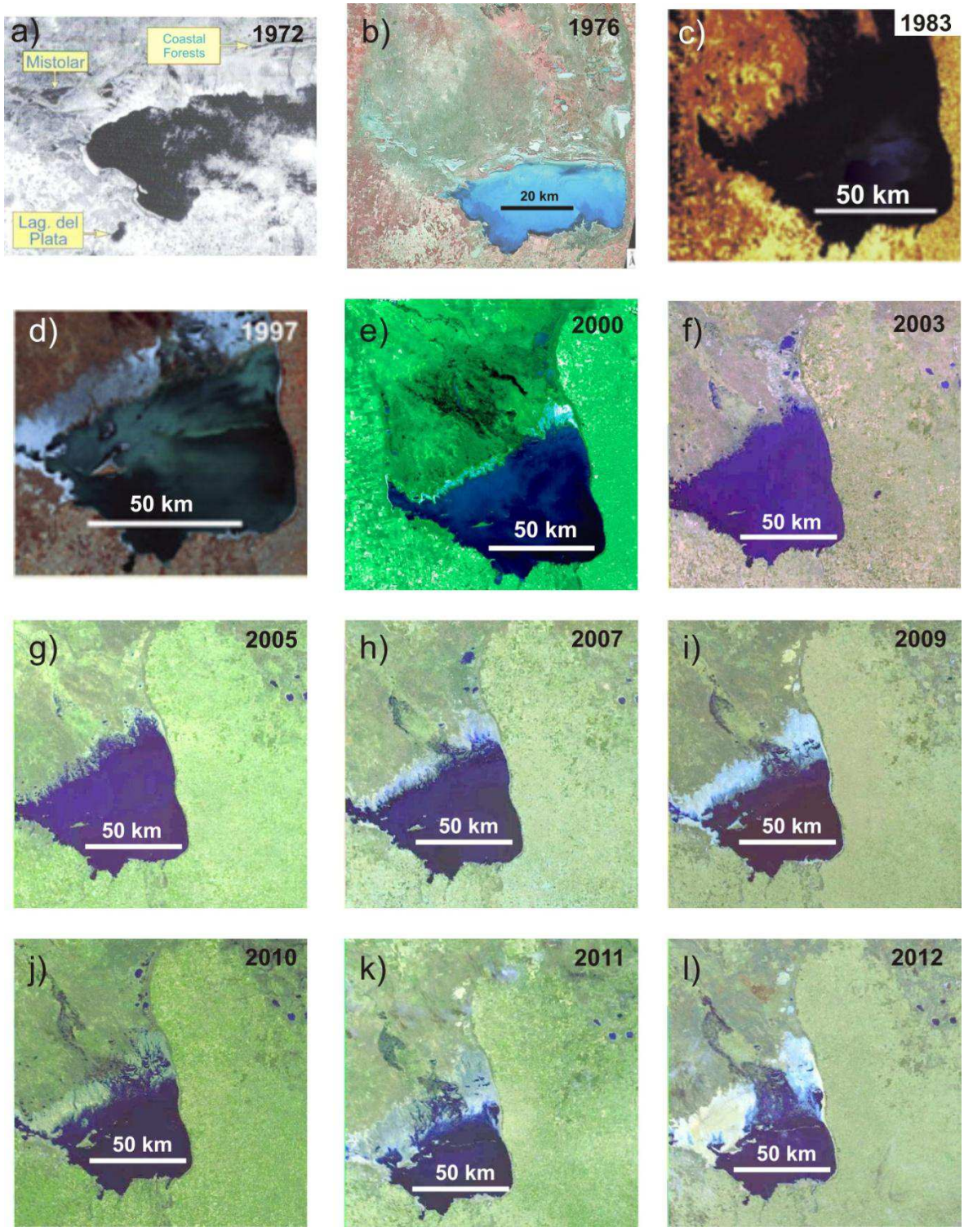

Fig. 1-2 : Laguna Mar Chiquita size variations in 40 years through aerial pictures and satellite images; a) Bucher *et al.*, 2006, b) INPE Brazil, c) and d) Troin *et al.*, 2010, e) to l) CONAE, http://catalogos.conae.gov.ar

1.2 Regional Climate

1.2.1 Modern Climate

South American climate is complex and exhibits tropical, subtropical and extratropical climatic features that extent from 10°N to 53°S (Garreaud *et al.*, 2009). These authors have well summarized the present-day South American climate where significant differences are given at both sides of the Andes Cordillera that acts as a meridional topographic barrier controlling the diversity of precipitation, temperature and wind patterns (Garreaud, 2009).

A major characteristic of the seasonal climate variability in South America is the occurrence of a monsoon-like system (Vera *et al.*, 2006) that extends southward from the tropical continental region during the austral summer. It connects the Atlantic Inter Tropical Convergence Zone (ITCZ) with the South Atlantic Convergence Zone (SACZ) by means of a large-scale atmospheric circulation containing a low-level jet (Fig. 1-3). The South American Low-Level Jet (SALLJ) starts in the northern part of South America at the foot of the Andes and, driven by the Chaco Low, provides moisture to South Eastern South America (SESA) (Nogués-Paegle and Mo 1997; Labraga *et al.* 2000) and basically determines the hydrological balance of the region (Berbery and Collini 2000; Saulo *et al.* 2000; Berbery and Barros 2002). Summer precipitation maxima and dry winters (in the Southern Hemisphere) characterize a large area east of the Andes, between 22º S and 40º S, where the only external sources of water vapour are the tropical latitudes and the south Atlantic Ocean (Doyle and Barros, 2002). During austral summer, light easterly flow extends down to 21º S and the subtropical westerly jet weakens and reaches its southernmost position. In contrast, during austral winter the easterly winds are restricted to the north of 10º S and the subtropical westerly jet becomes stronger with its core at 30º S (Garreaud, 2009). The westerlies act as a largely symmetric belt south of 35°S due to the absence of significant land masses at these latitudes (Garreaud *et al.* 2009). Other important climatic features are the sporadic incursions of polar air outbreaks (Antarctic Oscillation – AAO) east of the Andes (Marengo and Rogers 2001; Garreaud *et al.* 2009), the Pacific Decadal Oscillation (PDO) and ENSO (El Niño-Southern Oscillation) teleconnections controlling precipitation and, hence, the hydrology of major riverine systems (Aceituno 1988; Depetris *et al.* 1996; Silvestri 2004; Boulanger *et al.* 2005; Pasquini *et al.*,

2006). These last two features have similar anomalies but differ in their amplitudes (PDO is half of ENSO) (Garreaud 2009).

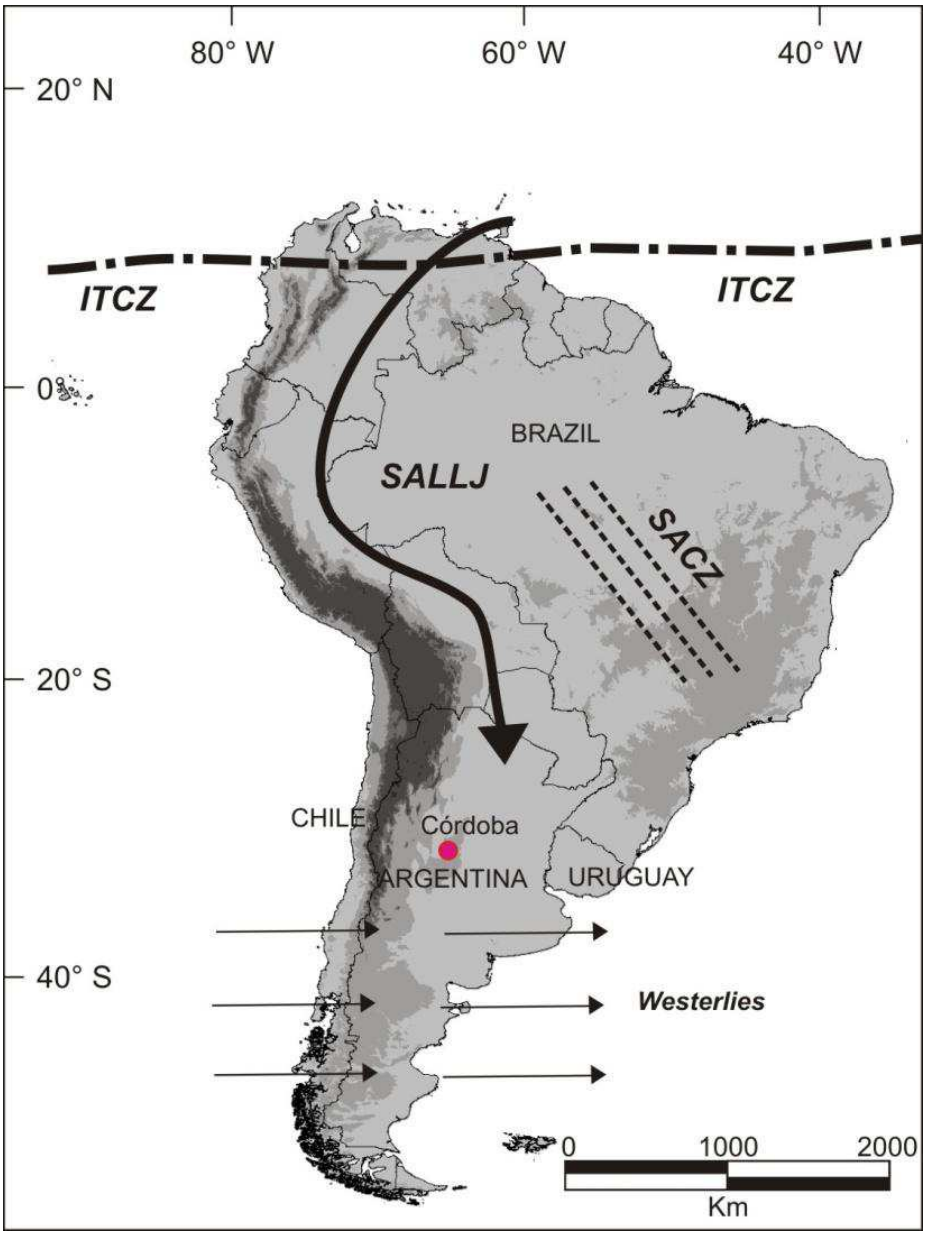

Fig. 1-3: Main climatic features that operate in Southern America. ITCZ: Inter Tropical Convergence Zone, SALLJ: South American Low-Level Jet, SACZ: South Atlantic Convergence Zone and westerly belt south of 35°S. (Adapted from Garreaud, 2009 and Zular *et al.*, 2013)

1.2.2 Paleoclimate

Paleoenvironmental evolution of the Late Pleistocene and Holocene (last 13.0 ka) for Southern South America and east of the Andes was reconstructed by Piovano *et al.* (2009). Concerning Laguna Mar Chiquita system, several authors (Piovano *et al.*, 2004a,b, 2009) consider it as a "sensitive hydroclimatic indicator" in South America mid-latitudes due to its sharp lake-level fluctuations. The paleoclimate reconstruction was performed taking into account limnogeological features observed in sedimentary cores retrieved from Laguna Mar Chiquita, interpretation of satellite images, meteorological records, historical sources and fieldwork. According to Piovano *et al.* (2009), the hydroclimatic record indicates positive hydrological balance and therefore highstand onset at ca. (*circa*) 13.0 cal ka BP (calibrated thousand years Before Present). This period was followed by extremely dry conditions that triggered the precipitation of evaporates and more positive isotope composition of carbonates and organic matter. After 6.8 cal ka BP there was an increase in the temperature gradient as a result of an enhanced influence of the Southeast Pacific anticyclone, larger Antarctic sea-ice extend (Gilli *et al.*, 2005) and the effect of changes in insolation (Markgraf, 1998) that derived on the strengthening of the Southern Westerlies. The most intense magnitude was dated around 4.7 cal ka BP, this cold and dry phase of the Middle Holocene is consistent with a reduced latitudinal convey of moisture from the tropics to the subtropics as a consequence of a weakened Monsoonal circulation. These conditions extended until the middle of the first millennia when less extreme lowstands can be inferred by 1.5 cal ka BP. The timing of the droughts for the first and second millennia is poorly resolved due to the occurrence of several sedimentary hiatuses indicated by gypsum-halite layers. Several climatic indicators suggest that warm and humid conditions prevailed from 1400-800 y BP in the Central Region of Argentina known as "Medieval Warm Period (MWP)" (Kröhling and Iriondo, 1999), that allowed soil development and expansion of fluvial and lacustrine systems. This heating (Fig. 1-4) is explained as an enhancement of the South Atlantic Anticyclone (Cioccale, 1999). The "Little Ice Age (LIA)" characterized by cold conditions started around 1300 (Cardich, 1980). The LIA was not a homogeneous event; it was formed by two cold pulses separated by an intermediate period of more benign conditions. The first cold pulse extended from the first decades of the 15th Century until the end of the 16th Century. The intermediate period began at

the end of the 16th Century and was prolonged until the beginning of the 18th Century (Cioccale, 1999). From ~1770 sedimentation is more constant and was dated by ^{210}Pb (Piovano *et al.*, 2002) indicating less extreme conditions with the occurrence of short-lived humid pulses during the second half of the 19th Century (1850-1870) (Piovano *et al.*, 2009). Finally, the second cold pulse spanned from the beginning of the 18th Century until the beginning of the 19th Century being the coldest part of the LIA and where the southern Andes glaciers reached their maximum extension (Cioccale, 1999).

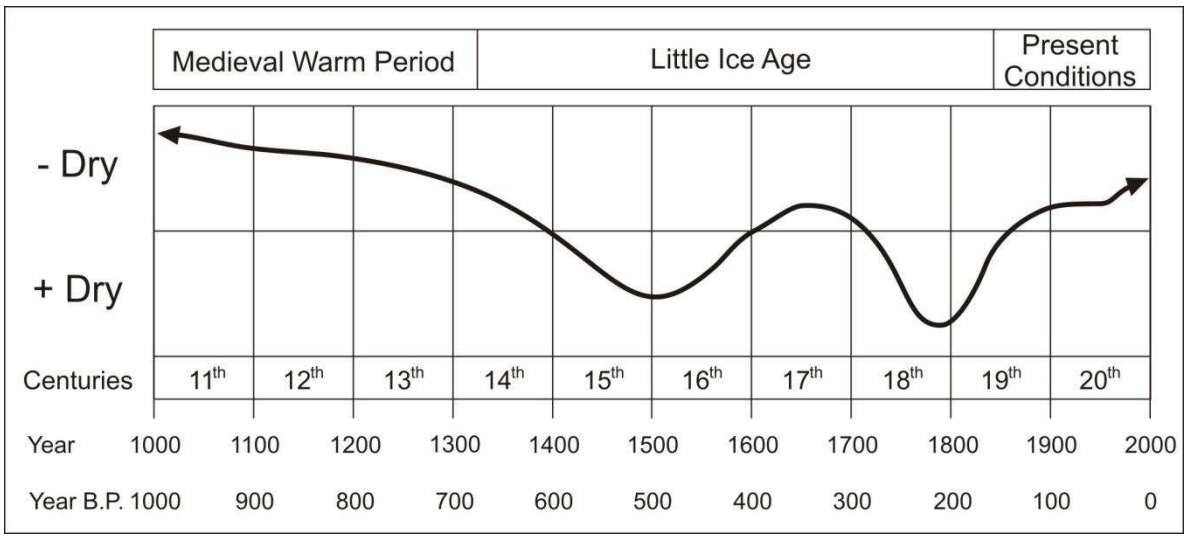

Fig. 1-4: Climatic fluctuations in the Central Region of Argentina during the last 1000 years (Cioccale, 1999).

1.3 Vegetation

The diversity and spatial distribution of vegetation in the study area are determined by the interaction between the landscape and the hydrology. The size of vegetation decreases with increasing water table influence and soil salinity. The correspondence between vegetation and the hydro-topographic gradient varies as follow: chaco forest (characterized by *Aspidosperma quebracho-blanco, Ziziphus mistol* and *Prosopis spp.)* ➡ transition shrubland ➡ halophytic scrub ➡flooded savanna (pajonal ➡ reed bed ➡ totoral➡ prairie). This spatial variation is manifested along the Dulce River (Fig. 1-5) (Menghi *et al.*, 2006).

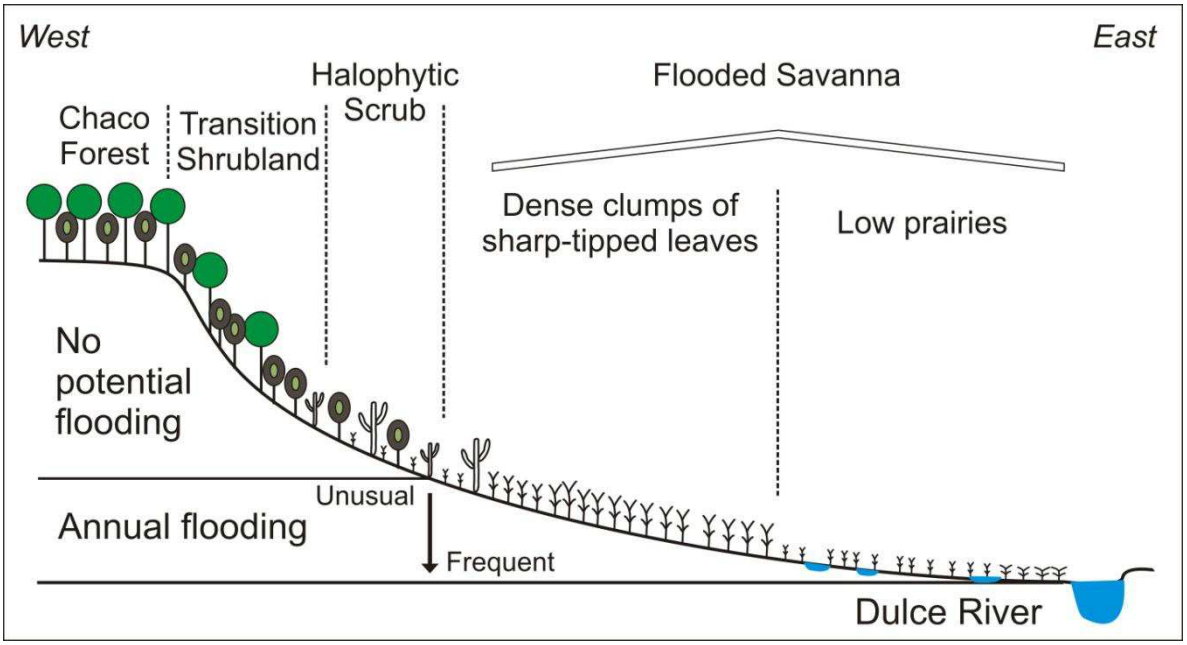

Fig. 1-5: Scheme profile of the typical landscape and vegetation variation from the borders of Mar Chiquita depression to Dulce River channel, close to its mouth in the lake. (From Menghi, 2006).

Menghi (2006) recognized three major physiognomic groups: a) Xerophyllous forests on the dry elevated margins; b) woody vegetation of low to medium size, characterized by xero-hallophyllous plant species, in elevated areas inside the depression and under water table effects, and c) herbaceous vegetation, with higro-hallophyllous plant species, dominant on lowlands under fluvial and water table influences.

Flooding and biomass fires are also system modellers. Periodic Dulce River flooding events are vital to maintain soil fertility, habitats biodiversity, vegetation quality and productivity (both livestock and floristic diversity purposes) and animal wildlife associated as well as sediments deposition and removal, salt wash from the soils and nutrient inputs (Menghi *et al.*, 2001; Bucher and Bucher, 2006b). The second one (biomass fires) is frequent in flooded savannas around the world (Whelan, 1995). The wet period that follows the floods favours the production of grassland biomass and a grand majority dries at the end of the dry season becoming highly flammable fuel. Under these conditions and even without human influence, the grassland can easily burn due to solar rays (Bucher and Bucher, 2006b). The effect of the biomass burning will depend on its intensity but there are some common patterns in the fire-vegetation interaction. Fire does not allow woody vegetation expansion, favours grass development and harms shrubberies and trees grow (Bucher and Bucher, 2006a). Biomass burning liberates components by volatilization predominating greenhouse gasses and other chemically active components such as carbon monoxide, nitric acid and sulphur oxides. At the same time, fire mineralizes soil organic matter ions and as a consequence there is a rise in pH, conductivity, calcium, magnesium, potassium, phosphorous, and ammonium values that could last even one year after the burning (Schmalzer and Hinkle, 1992). In the burnt areas there is a nude soil and an ash layer remaining that is easily removed by the water and wind and could accumulate in Mar Chiquita (Bucher and Bucher, 2006b). Furthermore biomass burning is increased by human activity even up to twice a year to control the growth of woody species and promote the development of softer grasses that improve the palatability of the cattle (Menghi *et al.*, 2001; Bucher and Bucher, 2006b).

1.4 Geology and geomorphology

The study area is located in two large geomorphological regions: the Sierras Pampeanas Range and the Pampean Plain (Fig. 1-6).

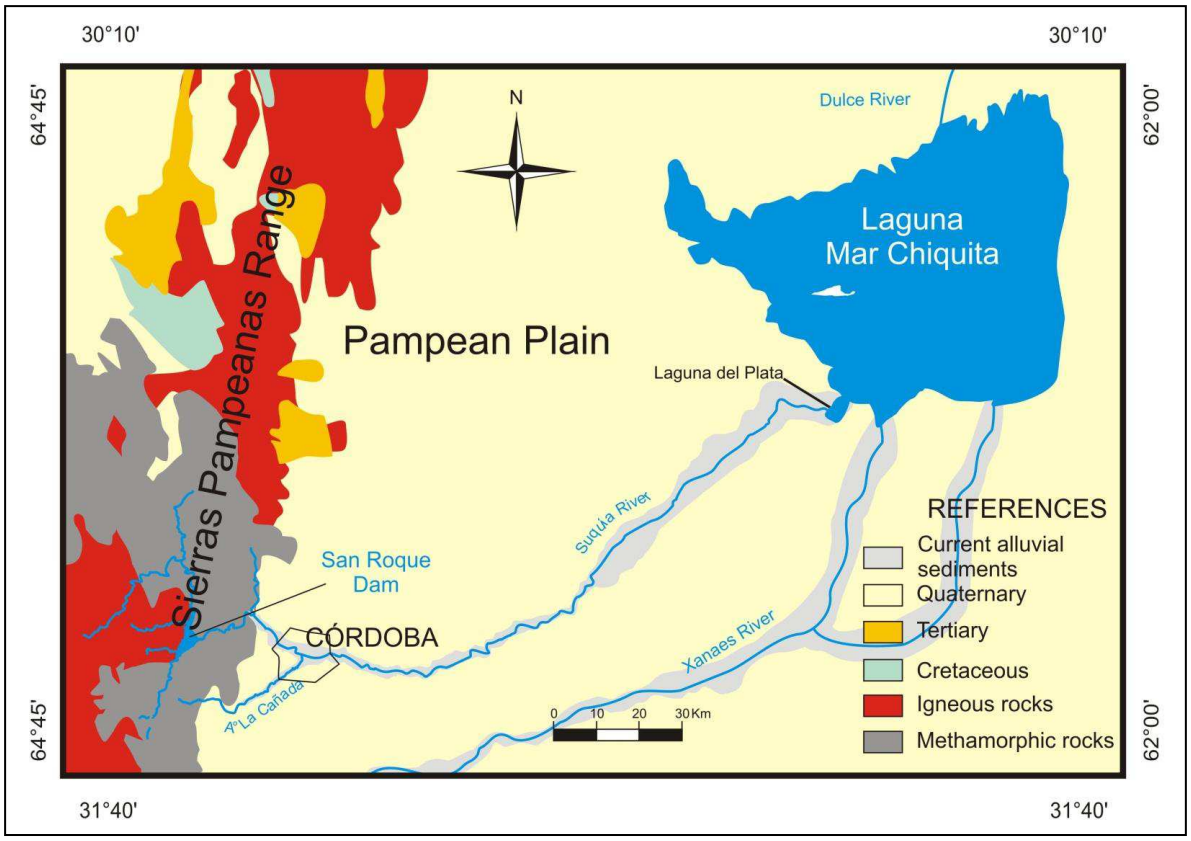

Fig. 1-6: Simplified main geological outcrops of the region. Based on geological maps from Argentina (Cruz del Eje – 3166 II, Jesús María - 3163 I, Villa Dolores - 3166 IV and Córdoba - 3163 III. Scale 1:250000. SEGEMAR).

The Sierras Pampeanas Range, located to the West, is an old crystalline massif that corresponds to the Orogenic Pampean Cycle (600-520 Ma) (Aceñolaza and Toselli, 1976; Ramos, 1988 a,b; Kraemer *et al.*, 1995). It has suffered successive erosive events, forming a landscape characterized by relicts of erosional surfaces, fractured and tilted during the Andean movements that started ~50-40 Ma ago (Carignano, 1997; Linares *et al.*, 2002). This group of mountains present a western abrupt flank that corresponds to large fault scarps, and an

oriental extended slope where the old erosion surfaces are preserved, sometimes covered by Tertiary and Quaternary sediments (Cioccale, 1999) deposited by a serie of coalescent alluvial fans. These fluvial sediments become finer towards the East where they gradually mix with the Aeolian sediments of the loessic Pampean Plain (Carignano, 1997). The Aeolian sediments are classified as typical loess with grain size dominated by coarse silt. They are composed of metamorphic and igneous rocks and volcaniclastic material belonging to the Andes Cordillera, Sierras Pampeanas Range, Paraná basin and Uruguayan shield (Zárate, 2003) and transferred by southern winds that formed the Pampean Aeolian System (Brunetto and Iriondo, 2007).

The Chaco Pampean Plain was traditionally considered as a stable area but recent studies showed that in fact it was affected by neotectonic activity and that Andean deformations reached regions located more than 700 km from the Andean chain (Fig. 1-7) (Mon and Gutierrez, 2009). During the Lower Pleistocene, an uplift occurred in the northern end of the Sierras Pampeanas Ranges leading to a deviation of the Dulce River from its original course and the formation of the Salado River. The uplift of the San Guillermo high due to the activation of the Tostado-Selva fault in the Middle Pleistocene (Iriondo, 1989, 1997), and the accumulation of the fans of Suquía and Xanaes Rivers against it, closed the Dulce River thus generating the Mar Chiquita impounding (Costa, 1999; Mon and Gutierrez 2009). The elevation of this high generated an important reorganization of the drainage design (Castellanos, 1959) as well as a considerable influence of the environmental and geomorphological evolution of the region.

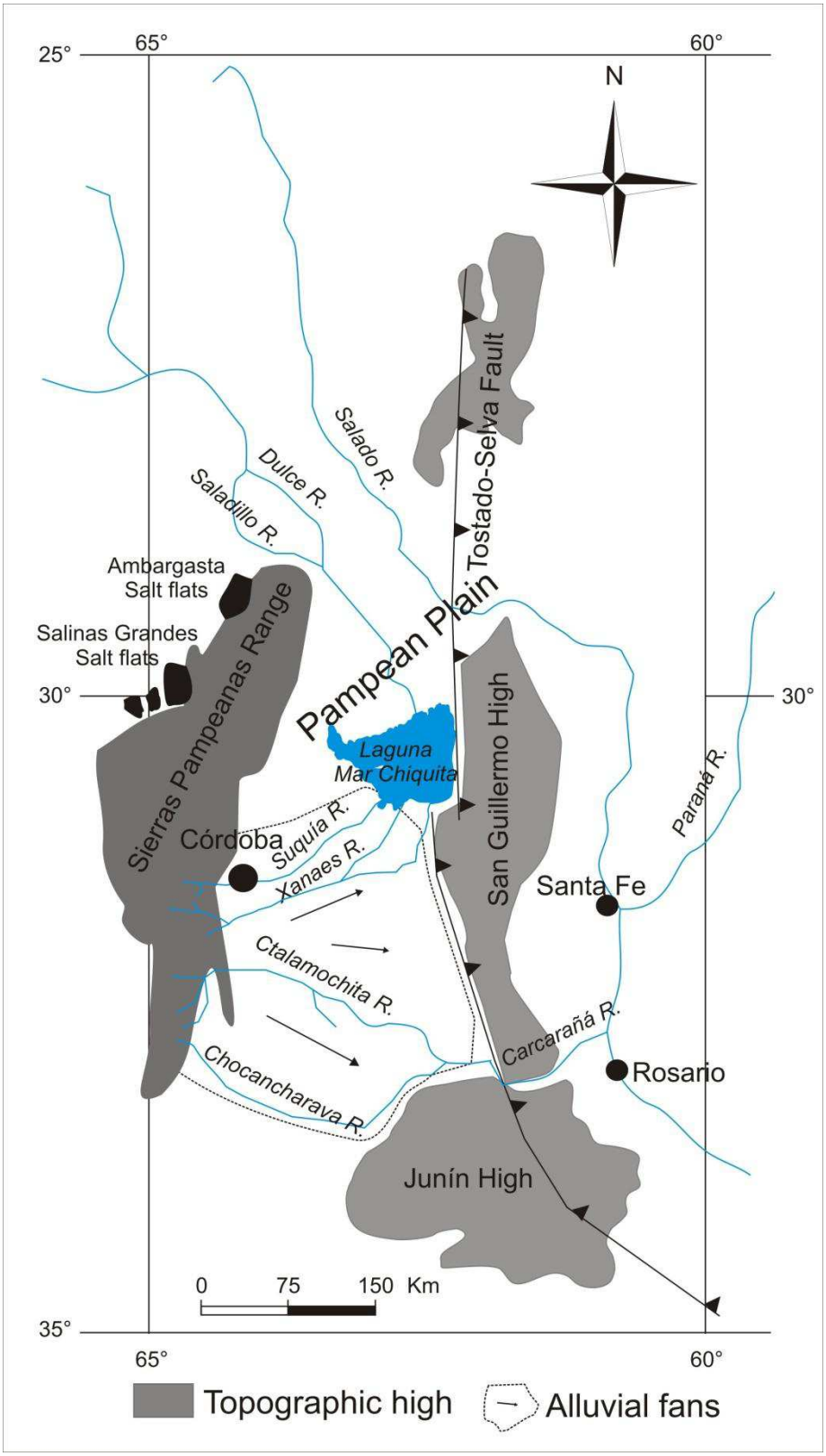

Fig. 1-7: Main geomorphological and tectonic features that characterize the region (Modified from Mon and Gutierrez, 2009 and Kröhling and Iriondo, 1999).

1.5 Sources of modern sediments

Based on geochemical and sedimentological interpretation of the Mar Chiquita bottom sediments, Martínez *et al.* (1994) and Kröhling and Iriondo (1999) recognized six different domains (Fig. 1-8):

- Central and northern part of the lake, where silty sand and alluvial sediments transported from the Dulce River accumulate.
- The main depocenter that corresponds to an evaporitic area characterized by abundant gypsum precipitates.
- A secondary depocenter represented by a mud rich in gypsum.
- Campo Maare Unit that extends along the western flank and remains permanently flooded, composed of aeolian sands.
- Lagunilla del Plata Formation, that consists of alluvial sediments deposited by the Xanaes River that were recently flooded (post Little Ice Age).
- Transitional area, corresponding to marginal or mixed environments.

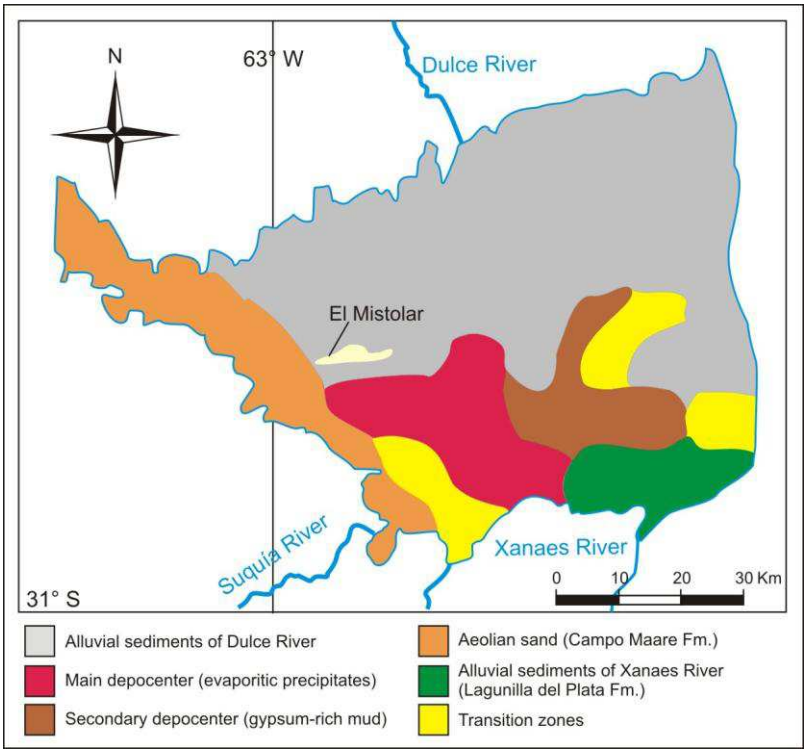

Fig. 1-8: Depositional regions in the bottom of Laguna Mar Chiquita (modified from Martinez *et al.*, 1994 and Kröhling and Iriondo 1999).

1.6 Water Mass Circulation and Hydrological modelling

Water mass circulation

The water mass movement in lakes is the result of the interaction of several factors such as wind, solar radiation, gravity and Earth rotation (Coriolis force) and the currents generated by the entrance of the tributary rivers (Tilzer and Serruya 1990). Wind is the main factor in the majority of the cases, like Mar Chiquita that furthermore is shallow, with a flat and soft bottom, situated in a non mountainous area with regular shores and soft slope, therefore, lot of wind (Pozzi *et al.*, 2006). Here, the prevailing winds are from the N (16.4 %) and SE (16 %) with observed intensities up to 70 km/h (Corral *et al.*, 2006).

Main water movements in a lake are:

- Waves: produced by the wind friction over the water surface. The wave length is related to the water depth; therefore they are bigger in the centre of the lake.
- Currents: generated mainly by the wind but they are as well influenced by atmospheric pressure change and by the entrance of tributary rivers. The contact of waters with different density and velocity generates vortexes (Imbodem, 1990). When they rotate in vertical sense, they are called "Langmuir Cells" producing parallel foam lines in the wind direction. They are important because facilitate the mixture of water, heat, dissolved gases, phyto and zooplankton (Rich, 2002).
- Rotation: includes the rotary movement of the whole lake due to the Coriolis force that should have an anti-clockwise whirl, when no other forces act.
- Meteorological tide: is the inclination of the lake surface produced by the wind (wind setup). The wind "carries" the water to one of the sides of the lake accumulating the coast where the wind blows to producing a descent on the opposite side leaving the shore exposed. When the wind stops, there is an oscillating movement until the surface returns to the initial situation.
- Astronomical tides: produced by the Moon and Sun gravitational forces twice a day but they are not significant in lakes.

In Mar Chiquita, fine sediments from its tributaries remain in suspension for a long period of time due to the higher density of the salt water, becoming a "natural marker" to determine currents in the lake. The main contrasting input comes from the Dulce River in the North and in lesser extent from the Suquía and Xanaes Rivers from the South. This is owed to their volume and the soils these rivers cross (Gorgas and Tassile, 2003; Pozzi *et al.*, 2006). Winds tend to homogenise differences in the water bodies and sediment removal and relocation.

Hydrological Modeling

Numerical Hydrological models have been applied to Laguna Mar Chiquita and Laguna del Plata to evaluate different climatic scenarios and management alternatives. Bathymetry was used as base for the modelling which was updated with satellite images. Laguna Mar Chiquita major depths are located in the centre-South region (Fig. 1-9). To the North and Northeast a big plain with low steep extends covering 50 % of the area occupied by the lake in 2005 (Corral *et al.*, 2006).

Rodriguez *et al.*, 2005 used the Lambda 2 Model (2004 version) that is based on a "box balance" (Fig. 1-10) taking into account the water that enters and leaves ("transfers") the system for time unit developed from the available climatic and hydrological data.

The equations calculate the balance between the system "deposits" or "banks" (in this case the accumulated water in the lake) and the transfers within the system. The inputs are given by the tributary rivers (Suquía, Xanaes and Dulce Rivers) and precipitations on the lake, wetlands and the middle catchment of the Dulce River. The outputs are given by the evapotranspiration and evaporation. For the period that goes between 1967 and 1997, the annual average of Dulce River input was 1092 $m^3 s^{-1}$ while for both Suquía and Xanaes Rivers it was 262 $m^3 s^{-1}$. Lambda 2 helped to deduce the volume and levels in which the lake could vary when reaching conditions of meso, hyper and mega salinities (below 50 g L^{-1}, between 50 and 100 g L^{-1} and above 100 g L^{-1}, respectively) as well as the volume required to ensure the survival of pejerrey fish (*Odontesthes bonariensis*) at salinities between 50 g l^{-1} (limit to complete its reproduction cycle) and 60 g l^{-1} (Tsuzuki *et al.*, 2000). The Dulce River is the major influencing input in the system therefore it will determine the necessary volume to keep certain lake levels in equilibrium. In Table 1-1, Laguna Mar Chiquita levels are shown

together with the necessary Dulce River discharge to keep that level stable. If Laguna Mar Chiquita receives an inferior discharge from Dulce River for a period of three continuous months, the lake level drops. Instead, if the lake receives a major volume, the level tends to rise.

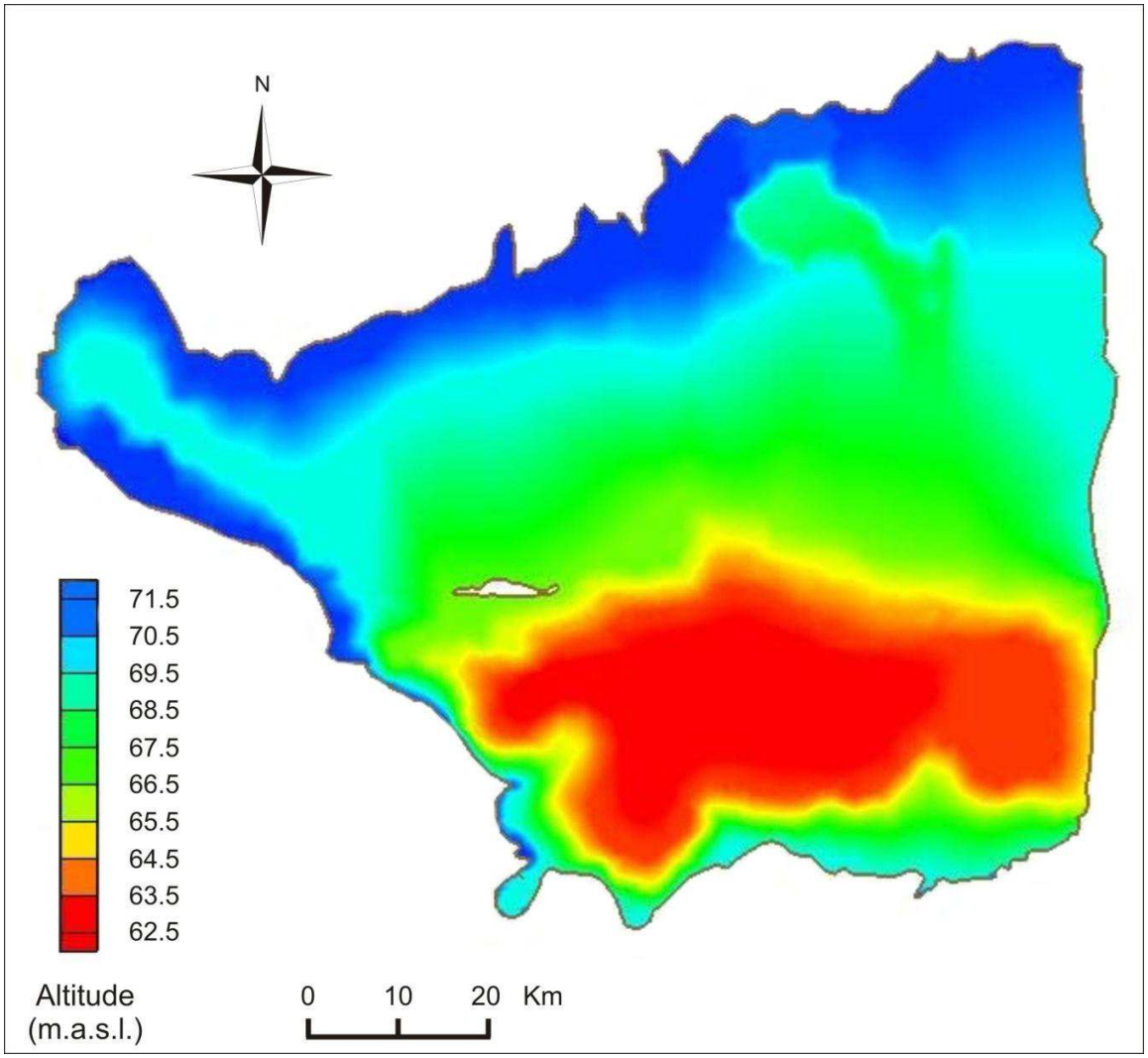

Fig. 1-9: Laguna Mar Chiquita bathymetry between levels 61 and 72 m.a.s.l (Pozzi *et al.*, 2005). Red colours corresponds to the deepest area and blue ones to the shallowest.

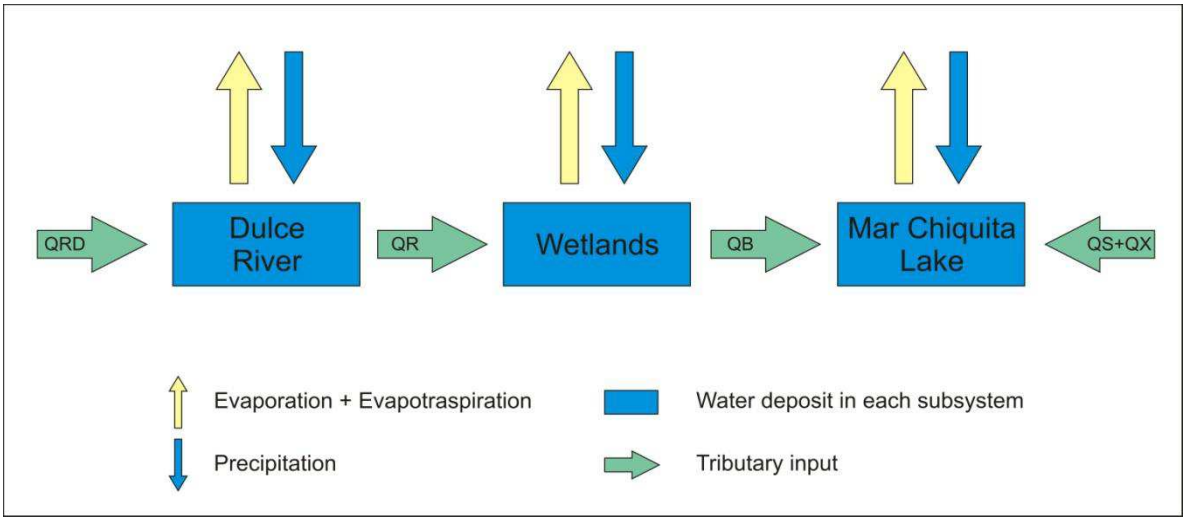

Fig. 1-10: Schematic diagram of the main components treated in the Lambda 2 model. QRD: Dulce River input; QR: Dulce River input at the wetlands entry; QB: Wetlands input to the lake; QS+QX: Suquía and Xanaes Rivers input (Modified from Rodriguez *et al.*, 2005).

Lake level (m.a.s.l.)	Discharge ($m^3 s^{-1}$)	Salinity ($g L^{-1}$)
71.5	142.2	25
71.0	105.7	30
70.5	89.0	34
70.0	80.3	40
69.5	74.1	45
69.0	67.8	52
68.5	58.3	60
68.0	47.7	69
67.5	40.3	79
67.0	30.7	91
66.5	21.9	104
66.0	14.6	120
65.5	8.9	137
65.0	4.6	156
64.5	0.1	181

Table 1-1: Necessary Dulce River discharge to keep the different Laguna Mar Chiquita levels and the estimated salinity in each case (Rodriguez *et al.*, 2005).

Another model carried out by Troin *et al.*, 2010 pretended to estimate the link between climate and lake level variations. They applied a lake water balance model measuring the dynamic of the lake by the lake water balance equation expressed as:

$$\frac{\Delta V}{\Delta t} = A(V)(P - E) + Q_{in} - G_{out} \quad \text{(Eq. 1)}$$

Where ΔV is the lake volume variation (m^3) for the monthly time step Δt;

A is the lake area (m^2), as a function of lake volume V;

P is the on-lake precipitation estimated from the six rainfall stations (m);

E is the evaporation from the lake's surface (m);

Q_{in} is the water inflow from the catchment (m^3);

G_{out} is the groundwater outflow (m^3).

This model predicted a significant water loss with the available data from 1926 to 2006. As a consequence, a chloride balance was applied in order to measure groundwater outflow (G_{out}). The results showed that G_{out} represented at most 3 % of the water loss, suggesting that groundwater seepage from the lake was negligible and that the water loss is mainly due to evaporation and evapotranspiration. Based on the variations in precipitation and river discharge, two contrasted climatic situations were extracted and defined: Dry (1967-1972 average) and wet (1976-1985 average). The model showed that the evaporation component is the most sensitive parameter of all. If a 10 % evaporation increase is maintained during a dry scenario, the simulated lake level equilibrium was 62.7 m.a.s.l close to the total lake drying. In the other hand, if a 10 % evaporation reduction is modelled, during the wet climate scenario, it induced a lake level increase of 0.75 m.

This model estimated as well that 92 % of the lake level variations are attributed to a runoff increase in the upper Dulce River catchment and it is possible to attend a lake drying when river discharge decreases only a 5 % during a dry scenario.

Corral *et al.* (2005) modelled two situations for the Laguna del Plata (Fig. 1-11): the first case studied was the dilution that the Suquía River may cause when entering into Laguna del Plata and the second one the action of the wind that determines the water input from Mar Chiquita to the small lake. In this instance the numerical three-dimensional model COHERENS (Luyten *et al.*, 1999) was used. In the first case the model showed a marked difference of salinity between the Suquía River and Laguna del Plata. The values range between 0.70 and 0.72 g L^{-1} for the river and between 27.29 and 35.52 g L^{-1} for the lake taking into account bottom and surface water mass measurements which are similar to those measured in Mar Chiquita. The model was calculated with the estimated Suquía River flooding of 100 m^3 s^{-1} and the water surface rose up to a maximum of 0.08 m and the radial influence was less than 1 km, thus concluding that Suquía River discharge does not present major influences in the system hydrodynamic. The salinity gradient is abrupt in a radial extension less than 1.5 km and it is present in all vertical layers acting as an uniform vertical front that moves forward until total dilution is reached.

For the second case, constant NE winds produce surface water circulations. It was possible to determine 3 layers with water circulation in different directions. In the first layer almost parallel vectors are produced with a SW direction. Wind speeds are higher on the shores (0.30 m.s^{-1}) and lower in the central region of the lake (0.10 m s^{-1}). Right in the connexion between both lakes the flux enters to Laguna del Plata with speeds about 0.35 m s^{-1}. The middle water layer presents three flow directions: two located on the shores with a Southwest direction and the other one in the central area towards to the Northeast with a speed of 0.15 m s^{-1}. In the bottom layer, although speed is almost not existent, there is one flow direction in the central area towards the Northeast. In conclusion, this shows that due to the strong winds that occur in the region, the water column from Laguna del Plata is well mixed as the one from Laguna Mar Chiquita is.

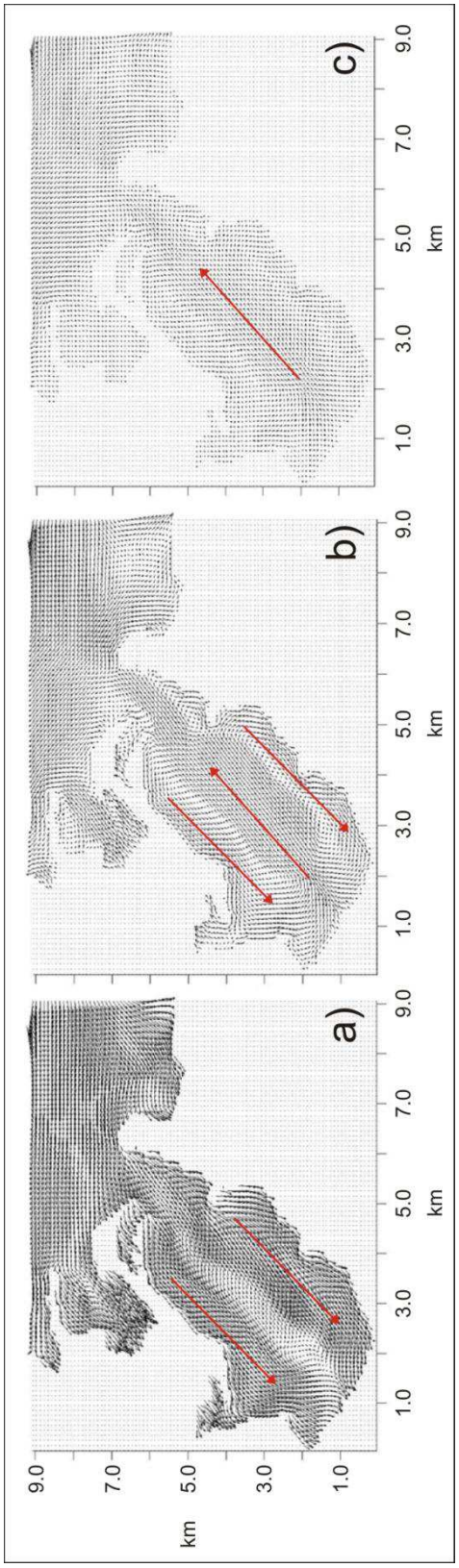

Fig. 1-11: Water flow directions in Laguna del Plata from COHERENS Model in the a) superficial, b) middle and c) bottom layers (Modified from Corral *et al.*, 2005).

1.7 Paleolimnology

Recent studies allowed to reconstruct the environmental fluctuations from the late Pleistocene (last 14000 year) using the sedimentological record of different short cores taken at Laguna Mar Chiquita and Laguna del Plata (Piovano *et al.*, 2006). As it was mentioned before, Mar Chiquita has suffered changes in its size due to the variable water inputs from its main tributaries which respond to increasing and decreasing average regional precipitation. High or low lake levels were defined whether they are over or below the altitude of 66.5 m.a.s.l. (Piovano *et al.*, 2002). High salinity values were measured during the low level periods that occurred in the 20th Century: 360 g L^{-1} in 1911 (Frank, 1915), 251 g L^{-1} in 1951 (Bertoldi de Pomar, 1953) and 270 g L^{-1} in 1970 (Martinez, 1991). This intense deficit in the water budget is attributed to the strongly negative hydrological balance that affected central Argentina during the first 70 years of the 20th Century (Piovano *et al.*, 2009; Troin *et al.*, 2010). An onset of higher regional precipitations started early in the 1970s and the Laguna Mar Chiquita lake level started to rise generating the connection of this lake with Laguna del Plata that persist nowadays (Piovano *et al.*, 2002; 2004a,b). In 1986 Martinez (1991) measured salinities of 29 g L^{-1} and three years later this value rose to 35 g L^{-1} in coincidence with a 1.3 m water depth decrease. He also compared the compositional relationships founding that they reminded the same for the major ions (Na, Cl and SO_4^{-2}). Mar Chiquita waters are classified as of the Na-Cl- SO_4^{-2} type.

Using ^{210}Pb dating, Piovano *et al.* (2002, 2006) determined sediment ages in two cores taken from Laguna Mar Chiquita (TMC-5 and TMC-14; Fig. 1-12).The determination of sediment ages along with the description of the sedimentological characteristics and the analysis of meteorological data, allowed a reconstruction of the hydrological history of the lake. Sediments accumulated during the 20th Century correspond to the first 50 cm of the core. High lake levels were recognized from 1977 to present, while a period of low lake levels extended from 1968 to 1972. During the high level phase, the sedimentation rate in Laguna Mar Chiquita varied between 0.77 and 1.12 cm y^{-1}, while during low lake-levels values were between 0.25 to 0.34 cm y^{-1}. The average sedimentation rate (ASR) was calculated through a linear regression along the treated section (54 cm) resulting in 0.41 and 0.49 cm y^{-1}. Older ages below 54 cm were obtained using the mean ASR value and assuming constant rates.

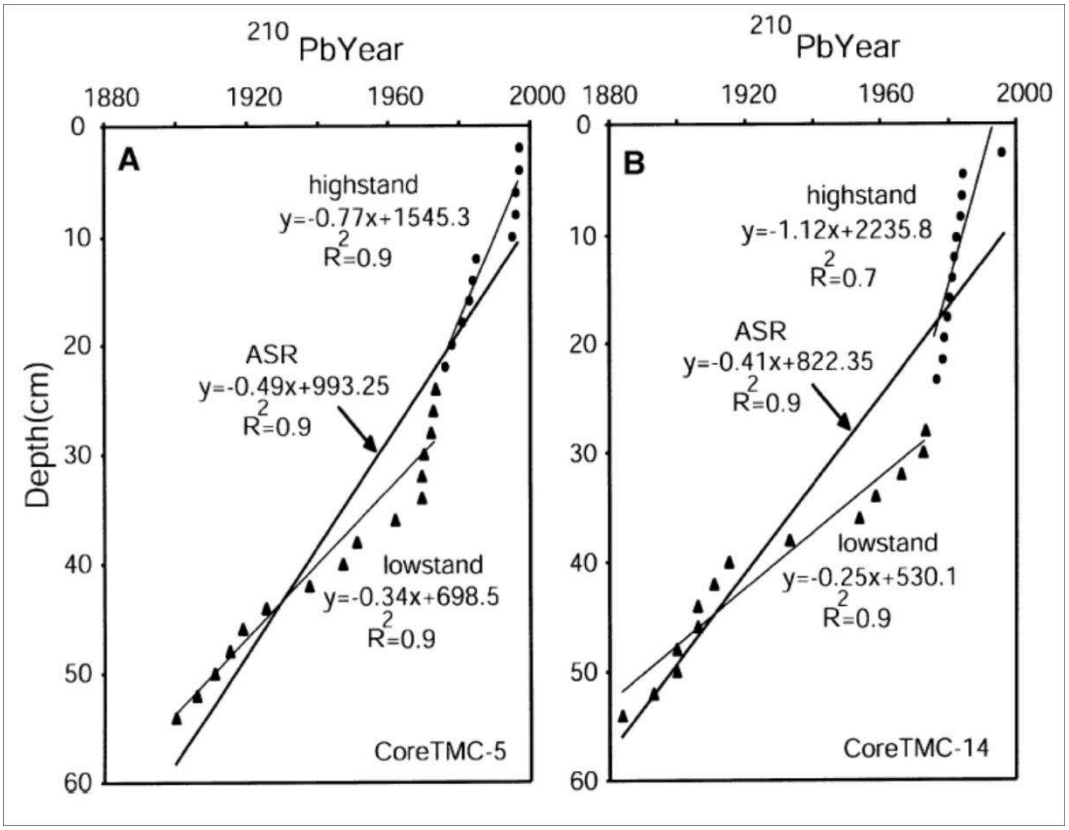

Fig. 1-12: Age ^{210}Pb profile and sedimentation rates for high and low stands, obtained from the slope of the best-fit linear equation. ASR, average sedimentation rate for the entire dated interval (Piovano *et al.*, 2002).

Cores from Laguna Mar Chiquita present a laminated sequence of sedimentation. They cannot be described as typical varves because they do not originate as a consequence of seasonal variations but due to cyclic wet and dry climatic periods.

Piovano *et al.* (2002, 2004a,b and 2006) proposed to divide the sequences in 4 facies:

- Facies A - High Level sedimentation: composed of laminated to banded muds with dark colours and with a high organic matter content. There is a development of very thin lamination (<2 mm) and banded intervals (<10 mm). Gypsum crystals are found in the mud. The content of Total Organic Carbon (TOC) correspond to the highest values registered (1.8-3.2 %) and the carbonates present the lowest values (0.4-6.6 %).

- Facies B - Low Level sedimentation: it is characterized by salt rich muds formed by Calcite-Gypsum-Halite, which could reach 2 cm thick. These units represent periods

of very low lake levels and high salinities. They contain high carbonate concentrations (25 %) and low TOC (0.5-1.6 %).

- Facies C – Intermediate Level sedimentation: it presents intermediate characteristics compared to the previous two facies of high and low levels. They are laminated to banded muds with intermediate contents of TOC and carbonates. It is possible to find these units between the very salt rich levels and the organic matter rich ones. TOC ranges between 1.3 and 2.4 % and carbonates between 5.6 and 13.3 %.
- Facies D – Short Pulses of Intermediate Level sedimentation: they are organic matter rich muds with very thin calcite laminas. They present up to 2.1 % of TOC, gypsum crystals. They were sedimented when the lake level was intermediate and last for a short period.

Energy, nutrients and evaporitic mineral precipitation fluxes are controlled by the variation in salinity associated to the lake level changes (Martínez 1991; Reati *et al.*, 1997) resulting in organic matter rich facies in high levels and evaporitic rich facies during low levels. The abundant clastic fraction present in the sediments shows that during the positive water balances, the fluvial input is significant (Piovano *et al.*, 2006).

Some studies concerning the isotopic record in Mar Chiquita were done by Dapeña *et al.* (1997), Dapeña and Panarello (2001) and Piovano *et al.* (2004a, 2006). The shallowness of Mar Chiquita and the well mixed state of its waters allows to perform an isotopic balance (Reati *et al.*, 1997; Dapeña and Panarello 2001). Piovano *et al.* (2004b, 2006), carried out some analysis concerning carbon, carbonate and oxygen isotope analysis. Analyses of $\delta^{18}O_{carb}$ and $\delta^{13}C_{carb}$ showed that facies A contains the most negative values (-3.1 ‰ and between -5.3 and -2.1 ‰ respectively). In the other hand, facies B and D show the less negative values ($\delta^{18}O_{carb}$ = 0.8 ‰; $\delta^{13}C_{carb}$ = -1.3 ‰ and $\delta^{18}O_{carb}$ = 1.7 ‰; $\delta^{13}C_{carb}$ = -0.5‰ respectively) while facies C presents intermediate isotopes values ($\delta^{18}O_{carb}$ = -1.0 ‰ and $\delta^{13}C_{carb}$ = -2.5 ‰).

Therefore, a model representing the lake level fluctuations and the associated sedimentary record was performed. Sediments reflect their precipitation from waters with different isotopic compositions which is the consequence of varying P-E (Precipitation – Evaporation) ratios (Fig. 1-13, Piovano *et al.*, 2002, 2004a,b, 2006):

- Facies like A were characterised by periods where P>E with lower salinities (28-60 g L^{-1}) and high organic matter level due to a high biological activity are registered for example between 1997-2005.
- Facies C and D are represented by P=E with intermediate salinities (80 g L^{-1}) indicating an evolution in the system, progressing water dilution as consequence of fresh water input, increasing levels of organic matter accumulation and a diminution on the carbonates precipitation, the period between 1972 and 1977 is an example of this situation.
- Facies like B are given when P<E, characterized by a negative water balance with high salinities (360 g L^{-1}), low water levels, high carbonates accumulation rate, development of evaporitic levels (Piovano *et al.*, 2006) and diminution of the biological activity with a decrease in the organic matter accumulation (Reati *et al.*, 1997). Periods like this were registered in 1911 (Frank, 1915). The isotopic study helped to confirm that the water losses are only due to evaporation discarding the groundwater leaking (Dapeña and Panarello, 2001).

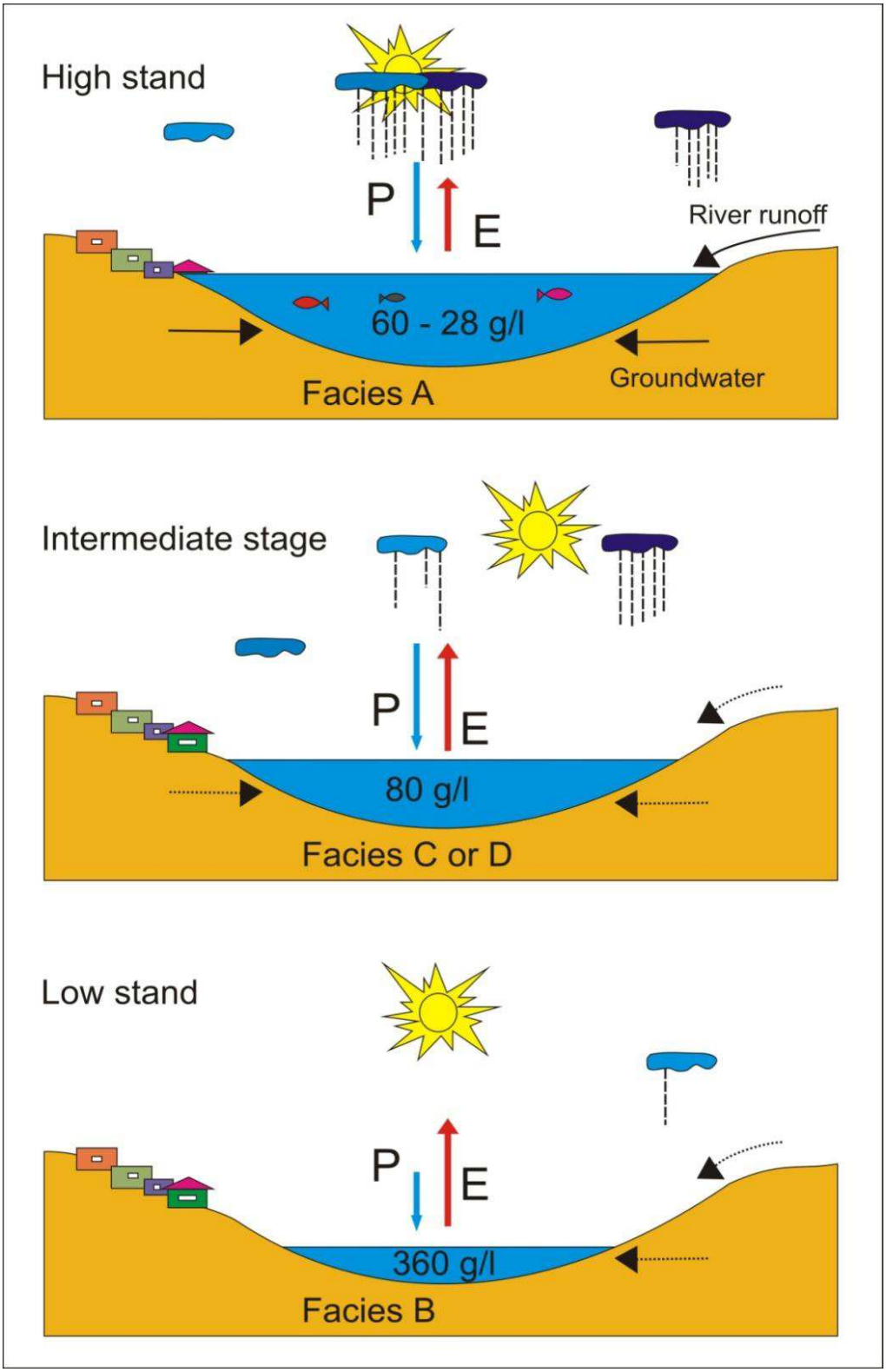

Fig. 1-13: Model that represents lake level variations and the associated sedimentary record. Arrows indicate Precipitation (P) and Evaporation (E) balance; their relative lengths indicate the predominance of P or E. Higher river runoff and groundwater inputs are indicated in solid arrows and lower inputs are indicated in dotted arrows (from Piovano *et al.*, 2002).

2. Hazardous elements in the environment: Mercury and Arsenic

Elements that occur in the Earth's crust in amounts less than 0.1 % (1000 mg kg^{-1}) are known as "trace metals". Many elements are present as trace amounts in living matter. Some of these elements are essential for the growth, development and health of organisms, but the quantitative difference between essential amounts and biological excess (therefore hazardous) is very small (Kabata-Pendias, 2010). In this study the distribution and geochemistry of mercury (Hg) and arsenic (As) is presented for the Suquía River basin and the saline lake of Laguna del Plata. Hg has been widely studied as a global flux indicator especially in the Northern Hemisphere (e.g., Fitzgerald and Mason, 1997; Fitzgerald et al., 1998; Fitzgerald and Lamborg, 2003) but in the Southern Hemisphere and notably Argentina studies are scarce. In this context, the study of Hg accumulation in the sedimentary record in Laguna del Plata is a contribution to understand the fluxes of global Hg in a climatic-sensitive region of southern South America (e.g. Piovano *et al.*, 2004a,b). On the other hand, As has been widely studied in the Chaco Pampean Region due to the high concentration of this element in groundwater (that in most of the cases exceeds the recommended guideline value for drinking water) and its strong association to the loess present in the region (e.g. Smedley and Kinniburgh, 2002). But studies concerning fresh water and the relationship to saline systems are rare.

2.1 Mercury

2.1.1 Mercury in the environment

Mercury is a chemical element with the particularity to be the only common metal liquid at ordinary temperatures, rarely occurs free in nature. The main ore is *cinnabar* (HgS – Fig. 2-1), when it is heated in a current air and by condensing the vapour it is possible to obtain the metal. Mercury is widely used in laboratory work for making thermometers, barometers, diffusion pumps, and many other instruments, as well as in making pesticides, mercury cells for caustic soda and chlorine production, dental preparations, antifouling paint, batteries, and catalysts (Hammond, 2005).

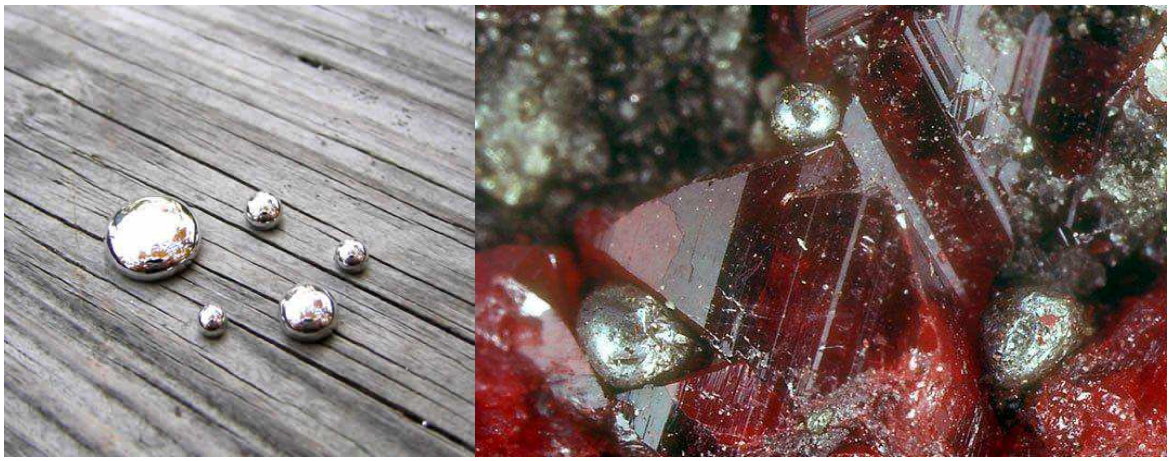

Fig. 2-1: Left: metallic mercury (crfzoraida.blogspot.fr) and right: cinnabar (HgS) from Almadén, Cuidad Real, Spain (http://wwwblogmylcom.blogspot.fr/)

The most important salts are mercuric chloride $HgCl_2$ (corrosive sublimate — a violent poison), mercurous chloride Hg_2Cl_2 (calomel, occasionally still used in medicine), mercury fulminate ($Hg(ONC)_2$), a detonator widely used in explosives, and mercuric sulfide (HgS, vermillion, a high-grade paint pigment). Organic mercury compounds are important. Mercury is a virulent poison and is readily absorbed through the respiratory tract, the gastrointestinal tract, or through unbroken skin. It acts as a cumulative poison and dangerous levels are readily attained in air (Hammond, 2005).

2.1.2 Global Mercury Cycle

The dynamic of mercury in the environment is conditioned by three fundamental properties: *physical* – its volatility at room temperature, *chemical* – by the stability of its bonds with carbon and sulphur and *biological* - by its very strong bioconcentrations and toxicity (Cossa and Ficht, 1999). Mercury can be released in the environment by natural and re-emitted sources or by anthropogenic sources. A schema with the global mercury fluxes is shown in Fig. 2-2 corresponding to actual times (Mason *et al.*, 2012).

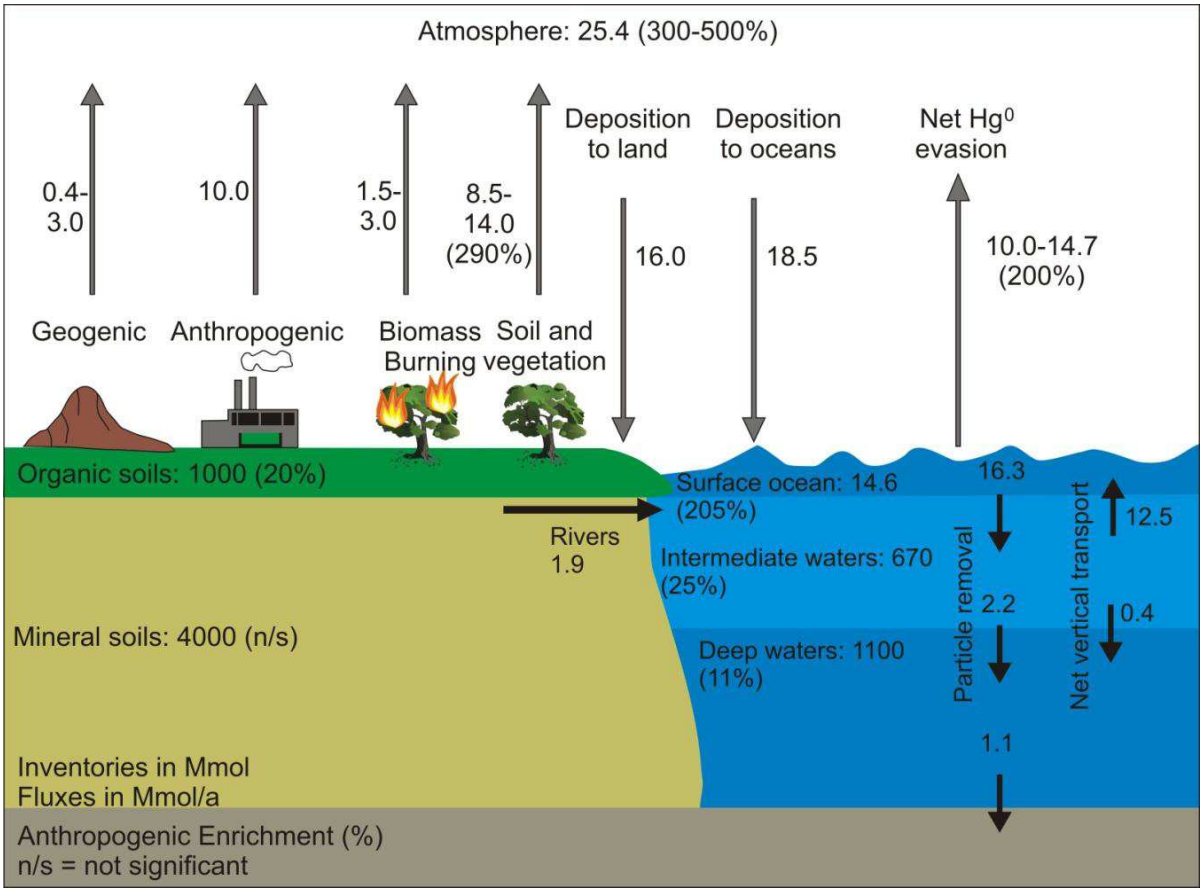

Fig. 2-2: A recent estimate of the fluxes of mercury at the Earth's surface based on simulations using the GEOS-Chem global mercury model. The percentage values in brackets are the estimated increases in concentration and fluxes in the last century due to anthropogenic activities (Mason *et al.*, 2012).

The major natural mercury sources include: degassing from mercury mineral deposits, degassing from mercury contaminated aquatic and terrestrial systems (through reduction of Hg^{2+} to Hg^0), volcanic and geothermal activity and forest fires (Nriagu, 1989; Lindqvist *et al.*, 1991; Nriagu, 1994; Camargo, 2002; Pirrone *et al.*, 2009). Among the main anthropogenic sources, they could be cited: solid waste incineration (municipal and medical wastes), coal and oil combustion, pyrometallurgical processes (iron, lead and zinc) and production of mercury and gold (Pirrone *et al.*, 1996; Pai *et al.*, 2000). The first two account for more than half of the total global emissions (Pirrone *et al.*, 1996). The atmosphere and the oceans play an important role in the distribution and redistribution of mercury at the Earth's surface. Atmospheric mercury deposition to oceans greatly exceeds riverine inputs (Fitzgerald and Lamborg, 2003). A recent study made by Pirrone *et al.*, 2009 estimates that natural sources

release about $5.21x10^3$ tons of mercury per year, part of which represent previously deposited anthropogenic and natural mercury from the atmosphere to ecosystem-receptors due to historic releases and part is a new contribution from natural reservoirs. Current anthropogenic sources, which include a large number of industrial point sources, are estimated to release about 2.91 $x10^3$ tons of mercury on an annual basis, being the fossil fuel-fired power plants ($1.42x10^3$ t y^{-1}) the major contributor. Between natural and anthropogenic emissions they estimate that nearly $8.12x10^3$ tons of mercury are released annually to the global atmosphere. It has been estimated by several authors that current atmospheric deposition is 3 (Von Gunten *et al.*, 1997, Johannessen *et al.*, 2005), 4 (Fitzgerald *et al.*, 1998; Heyvaert *et al.*, 2000; Bindler, 2003), 10 (Bindler, 2003), 16 (Liu *et al.*, 2012) and even 24 times (Heyvaert *et al.*, 2000) higher than pre-industrial flux.

2.1.2.1 Mercury speciation

The speciation of Hg regulates toxicity, transport pathways and residence time within the different compartments of the ecosystem (Lindqvist *et al.*, 1991).

The atmospheric mercury is mainly made up of gaseous Hg (about 95 to 100 %) and the remainder is associated with particles (Lindqvist *et al.*, 1991). The chemical forms of Hg in the atmosphere are still under discussion (Lindqvist *et al.*, 1991; Cossa and Ficht, 1999) but the total predominance of elemental Hg is generally accepted. Besides elemental Hg, methylmercury (MeHg) is present in air but only in minor quantities ~0 to 5 % (Bloom and Fitzgerald, 1988) which increase with altitude (Lindqvist *et al.*, 1991).

In natural waters Hg is often fractionated by their different ability to be reduced to elemental Hg (Lindqvist *et al.*, 1991). Mercury speciation in natural waters has evolved thanks to clean laboratory protocols (Gill and Fitzgerald, 1985; Fitzgerald, 1989) and analytical studies (Bloom and Fitzgerald, 1988; Bloom, 1989). Reactive Hg (Hg_R) consists of Hg species that are readily reduced by $SnC1_2$ under acidic conditions. This fraction is comprised primarily of labile inorganic and organic complexes of Hg(II), and of labile particulate associations. Total Hg (Hg_T) is a measure of the total dissolved and particulate Hg in an unfiltered sample. In dry and wet precipitation, a large part of the Hg_R content is associated with particles (Ferrara *et*

al., 1986; Ahmed *et al.*, 1987; Iverfeldt and Rodhe, 1988) and colloid particles (Brosset and Lord, 1991) and as in the air MeHg species are also present (Ahmed *et al.*, 1987; Lee, 1987; Bloom and Watras, 1989). Precipitations falling through a tree canopy can lead in interactions between Hg and dissolved organic complexes (DOC). The type and amount of compounds associated to canopy will vary to those found in the wet deposition of an open field. The canopy may also act as a sink of Hg in rain due to binding in fixed organic matter and thus, affecting the type and level of Hg species reaching the ground (Lindqvist *et al.*, 1991).

In lake waters, Hg is associated to particles as well with DOC, and the levels of the fractions may vary with seasonal variation. Most of the MeHg is probably associated to DOC. Little is known about the type of complexation between MeHg and other Hg compounds with DOC in water, since DOC is a heterogeneous mixture consisting mainly of fulvic and humic acids (50 to 80 %), carbohydrates, carboxylic acids, amino acids and hydrocarbons. These are capable of forming complexes with many metal ions as a result of the ligand groups present (-COOH, -OH, $-NH_2$ and –RSH) (Lindqvist *et al.*, 1991).

Low but detectable concentrations of dissolved gaseous Hg are usually present in all types of freshwater systems. It is likely that elemental Hg constitutes most of the dissolved gaseous Hg in lakes (Bloom and Watras, 1989; Fitzgerald *et al.*, 1990; Lindqvist *et al.*, 1991) and the evasion of elemental mercury (Hg^0) at the water surface is an important natural flux of Hg to the atmosphere (Vandal *et al.*, 1991).

Concerning sea water, dissolved gaseous Hg concentrations have been found at supersaturated levels in the equatorial region (Kim and Fitzgerald, 1986). The dissolved gaseous Hg consists mainly of elemental Hg, but in sub-surface water also to some degree of dimethyl mercury (DMHg). However, Hg is predominantly (>80 %) in the reactive form in open ocean waters (Gill and Fitzgerald, 1987; Cossa and Noel, 1987).

Hg concentrations in the raw humus layer and the regional variation can be assumed to reflect mainly the atmospheric deposition pattern, integrated over decades or even centuries. Some Hg in the litter has, however, probably also been taken up by the roots and gaseous Hg may have been brought to the surface layer by diffusion from below and, by biological activity, some mineral matter from below may have been mixed into the organic layer. Therefore, to some extent the Hg concentration of raw humus and the regional distribution pattern will also be influenced by the Hg content in parent material and bedrock (Lindqvist *et al.*, 1991).

2.1.3 Dynamics of Hg

2.1.3.1 Redox reactions in the atmosphere

Oceans and coastal seas release Hg to the atmosphere especially in the form of elemental Hg (Hg^0) and some traces of DMHg ($(CH_3)_2Hg^0$) coming from deep waters. MeHg ($(CH_3)_2Hg^+$), decomposed from DMHg, constitutes less than 1 % of Hg in the rain (Cossa and Fitch, 1999). The average residence time could go from hours for some oxidized Hg(II) species to a more than one year for elemental Hg (Fitzgerald, 1989; Slemr, 1992; Cossa and Fitch, 1999; Fitzgerald and Lamborg, 2003).

Many divalent Hg compounds exist as undissociated molecules in water solution as well as in the gaseous phase. Such molecules that may occur in the atmosphere are $HgC1_2$, $HgBr_2$, $Hg(OH)_2$, $Hg(SH)_2$, $Hg(CN)_2$, etc. (Lindqvist *et al.*, 1991).

It is known that elemental Hg reacts with O_3 (P'Yankov, 1949) but it does it as well with Cl_2 (Hall, 1990) in the gas phase.

Some authors have shown that SO_2(g) can reduce HgO at a very slow rate (Zacharewski *et al.*, 1987). Studies concerning photochemical reduction of dissolved divalent Hg were performed in laboratory (Iverfeldt, 1984; Munthe and Linqvist, 1990) and on the field (Brosset, 1987). They showed that $Hg(SO_3)_2^{2-}$ is dissociated thermally while $Hg(OH)_2$ is photodissociated. This can occur because many Hg species (Fig. 2-3) such as complexes with OH^-, HS^-, $C1^-$ and organic ligands can absorb radiation in the highly energetic UV range (270-400 nm) of the solar spectrum (Fujita *et al.*, 1973; Stromberg *et al.*, 1991).

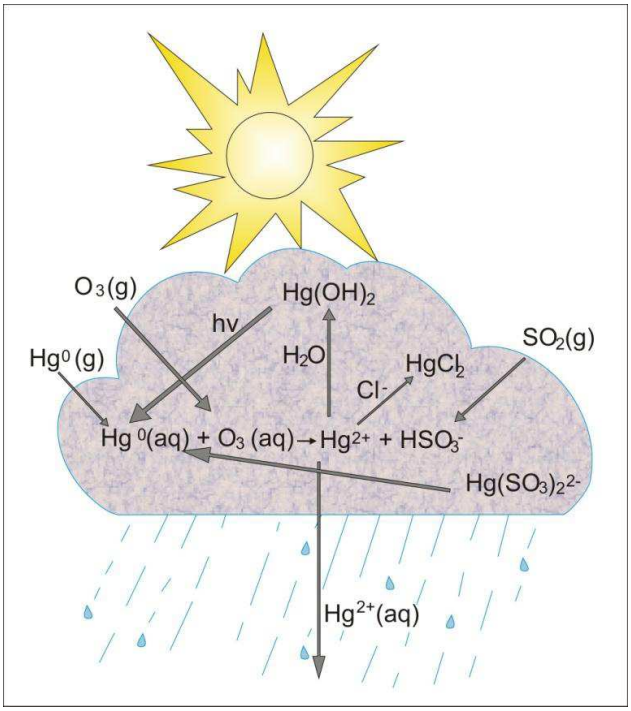

Fig. 2-3: Schema showing the heterogeneous chemistry influencing the wet deposition of Hg. (Modified from Lindqvist *et al.*, 1991)

2.1.3.2 Stable Hg species in natural waters

Hg can exist in three different oxidation states: Hg(0), Hg(I) and Hg(II). The Hg(I) ion, Hg_2^{2+}, is stable in aqueous solution, but the disproportionating reaction (1) will proceed readily to the right if ligands are present that reduce the activity of the mercuric ion (Levason and McAucliffe, 1977).

$$Hg_2^{2+} \leftrightarrow Hg^0\,(aq) + Hg^{2+}\,(aq) \quad (1)$$

Contrary, Hg(II) is stable and form compounds with carbon, nitrogen, halogens but most of all with sulphur and selenium (Mason and Fitzgerald, 1996 ; Cossa and Ficht, 1999). Unlikely other metals, mercury has a strong tendency to form covalent bonds instead of ionic bonds. In the aquatic environment Hg can form chlorine compounds ($HgCl^{+,}$ $HgCl_2$, $HgCl_3^-$), hydroxy compounds ($Hg(OH)^+$, $Hg(OH)_2$) and thiol compounds (HgSR, CH_3HgSR) especially in sea water, and organic compounds (Hg + humic et fulvic acids) in freshwater (Cossa and Ficht,

1999). Hg_2^{2+}, Hg^{2+} and CH_3Hg^+ are soft Lewis acids (Craig, 1986) therefore, in natural waters Hg will preferentially form complexes with soft Lewis bases such as CN-; RHS, RS and others (Lindqvist *et al.*, 1991).

Divalent Hg fraction in aqueous environment constitutes methylation substract. This reaction competes with the organic complexation that usually dominates mercury speciation. In coastal and estuarine environments, methylation is mostly due to sulfate-reducing bacteria existing in sediments and in suboxic environments. Once methylated, mercury becomes very bioaccumulative (Cossa and Ficht, 1999).

2.1.4 Mercury sedimentation

Most of total atmospheric deposition is ruled by the wet deposition especially to water surfaces and land areas. The dry deposition process is more important in areas with forested ecosystems (Iverfeldt, 1991b). In rain the total Hg load is associated with filterable or colloidal particles (Brosset and Lord, 1990; Iverfeldt, 1991a), thus precipitation scavenges particles associated to Hg. But, the source of the Hg-containing particles can be due to direct emissions as primary source or by in-cloud reactions as secondary source (Fig. 2-3). At a local scale, the first process is relevant while at a global scale the second process is the most important. The different transformations that mercury suffers in the ecosystem are summarized in Fig. 2-4. The concentration of Hg measured in a certain place will be influenced by the transport history of the air masses, precipitation events as well as the evaporation/condensation of water droplets in the cloud. Hg level will be also influenced by the type and duration of the precipitation event (Lindqvist *et al.*, 1991).

In aquatic environments the major part of Hg associated to particulate organic matter that sediments in coastal systems is buried almost definitively in sediments as sulfide, selenide and in association with pyrite (Cossa and Ficht, 1999). The Mn and Fe oxides, that enrich the benthic surface layer, could play the role of a barrier to the diffusion of Hg due to their high adsorption capacity (Gobeil and Cossa, 1993). The MeHg found in the epibenthic organisms comes from the absorption of its benthic prays and not from the dissolved MeHg diffused in the overlying water (Cossa and Ficht, 1999).

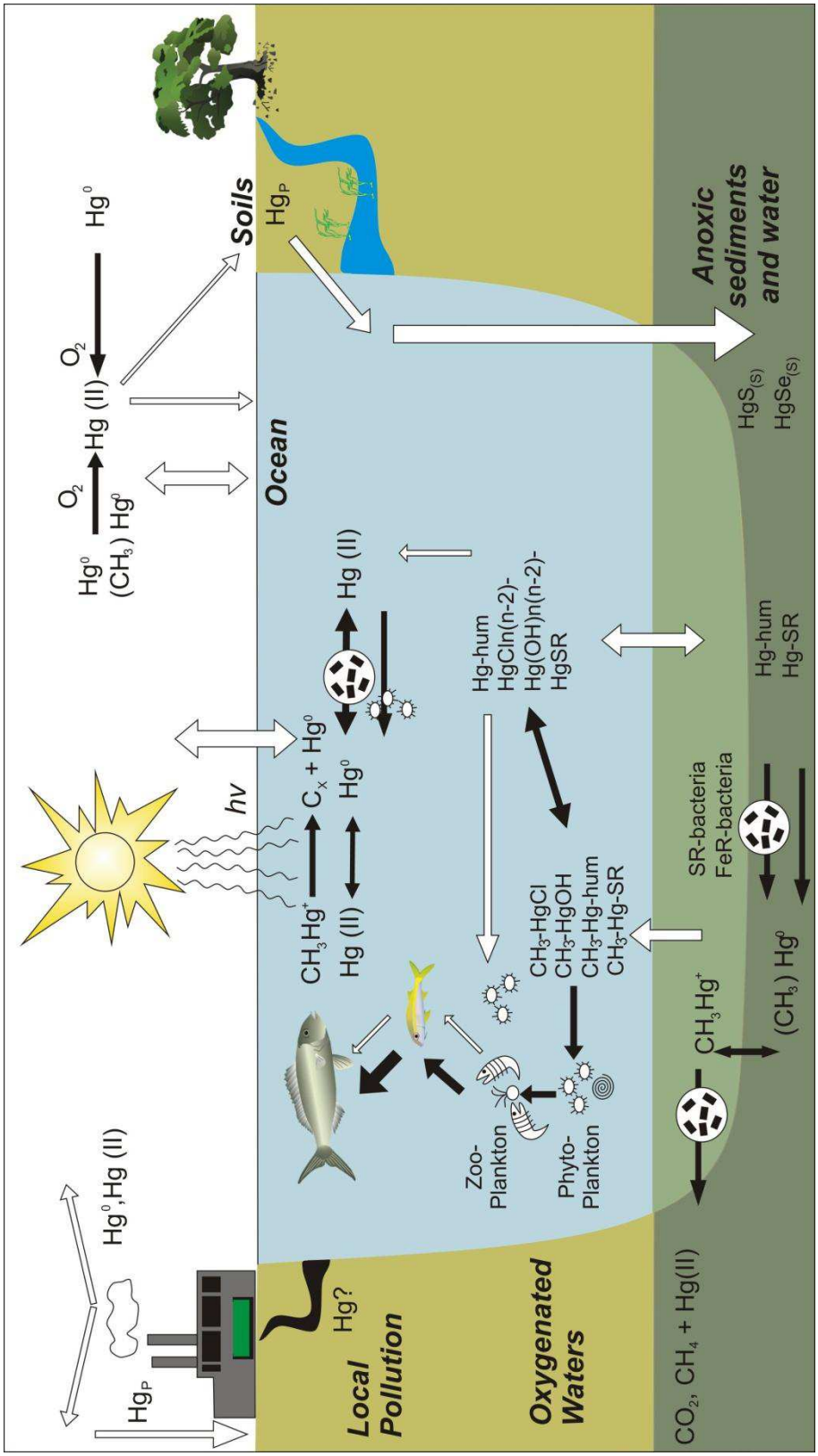

Fig. 2-4: Cycle of Hg. Reactions, transformations and transfers (hum = humic acid; SR-b = sulfate-reducing bacteria; FeR = iron-reducing bacteria). Modified from Castelle, 2008.

2.1.5 Mercury in the world and Argentina

The high mercury concentrations in countries such as Canada, France, Switzerland and China observed at the beginning of the 19th Century were concomitant with the industrial and demographic growth. The periods with the highest concentrations usually coincide with some of the historical times with a marked industrial development such as the "golden age" in 1860, the Second World War (1939-1945), development of uncontrolled mining activities in France and some industrial spill accidents as it is the case in Canada late 1960s. These events were the responsible of liberation and accumulation of large concentrations of this metal in sediments. From half of the 20th Century to nowadays the aim is to reduce the mercury concentrations released to the atmosphere applying clean technologies, amelioration on used and waste waters and the implementation of more severe environmental laws (Von Gunten *et al.*, 1997; Johannessen *et al.*, 2005; Castelle *et al.*, 2007; Liu *et al.*, 2012).

Estimations made by Pirrone *et al.* (1996) and Pacyna *et al.* (2003, 2006) for the years 1990-1992, 1995 and 2000 respectively, indicate that North America and Europe have reduced its global anthropogenic emissions to the atmosphere to less than 20 %. On the other hand, Asia and Africa increased from less than 50 % to about 70 % of global emissions in ten years; this increase is due to the fast economic development. Around 36 % of the total global emissions correspond to anthropogenic sources and the major source corresponds to the combustion of fossil fuels that vary between 15 and 18 % in Europe, North America and Asia (Pirrone *et al.*, 2009).

In the Southern Hemisphere, mercury concentrations are associated mainly to gold mining. In countries such as Brazil, Colombia, Bolivia, Peru, French Guyana, among others, high Hg levels were found in river and lake sediments, soils, fishes and human hairs in towns near the mining areas. Hg is used for separation of gold particles through amalgamation. During this process, a good amount of metallic Hg is also lost to rivers and soils through handling under rough field conditions and to volatilization. After amalgamation, the Au-Hg complex is burned in retorts but in most areas, this operation is done in open air, releasing Hg vapour to the atmosphere. Furthermore, Hg rich tailings are left in most mining sites (Diaz, 2000; Lacerda *et al.*, 2004). In Brazil the gold mining boom was developed from 1979 to 1995 but even nowadays high mercury levels are detected. This is due to the remobilization of sediments and changes in land use such as conversion of forests to pasture (Olivero *et al.*, 2002; Rodrigues Bastos *et al.*, 2006; Huguet *et al.*, 2010). Sediments from de la Plata River in

the Uruguayan coast were analyzed showing high concentrations of Hg and other heavy metals that are related to municipal effluents, industrial waste, oil refinery among others (Muñiz *et al.*, 2004).

In lakes Guanaco, LP and Stuart M. located in the austral Patagonia of Chile, mercury accumulation seem to be fairly constant during the 19th Century and the variations in Hg concentrations in the sediments of these lakes are driven by changes in local precipitation rates as well as leaching of Hg organic complexes from the catchment soils (Hermanns and Biester, 2013).

Argentina in particular, the occurrence of Hg in sediments accumulated in freshwater systems are scarce (i.e., Amin *et al.*, 1996; Hudson-Edwards *et al.*, 2001; Ronco *et al.*, 2001; Marcovecchio *et al.*, 2001; Ribeiro Guevara *et al.*, 2002, 2004, 2005, 2009, 2010; Arribére *et al.*, 2003; De Marco *et al.*, 2006; Botté *et al.*, 2010). Most of these studies are concentrated in the Patagonia region and in coastal areas of the Buenos Aires province. For example, three estuarine systems on the shores of Buenos Aires were studied and total Hg concentrations in sediments and biota were analyzed between 1980 and 2005. The presence of Hg is mainly of anthropogenic origin due that in the region, ports, towns and several industries exist. The results indicate that total Hg values decreased significantly ($p<0.001$) in the last 25 years attributing this tendency to the improvement in the industry practices of the region (De Marco *et al.*, 2006). In the Argentina's Patagonia, the historical record of Hg was analyzed in two sedimentary cores retrieved from lakes Tonček and Moreno in the Nahuel Huapi National Park (Ribeiro Guevara *et al.*, 2005, 2010). These authors found that recent Hg concentrations are around 2.5 times higher than those registered in pre-industrial times. However, high Hg concentrations were also measured in sediments of pre-industrial times that could be related to ancient extended fires and volcanic activity. It is well known that volcanoes represent a potentially important natural source of mercury in the atmosphere (Nriagu and Becker, 2003) and especially this region that is located in the Southern Volcanic Zone (SVZ) that extends from 33 to 46°S (Stern, 2004; Kratzmann *et al.*, 2010) and has shown some eruptive activity in the last two decades (e.g. Matthews *et al.*, 1997). Typical Hg concentrations in rocks, soils and sediments around the world are listed in Table 2-1.

Rock/sediment/soil	Hg concentration average or range ($\mu g\ kg^{-1}$)	References
Rocks		
Basaltic rocks	90	Fitzgerald and Lamborg, 2003
Granites	80	
Shales	40	
Sandstones	30	
Carbonates	40	
Suspended Matter (France)	1000	Schäfer *et al.*, 2004
Contaminated soils		
Italy (Etna)*	40-7500	Kabata-Pendias, 2010
France**	2600-2900	
U.S.A.**	8200-40000	
Lake sediments		
Chile	28-123	Hermans and Biester, 2013
Southern Argentina*	50-500	Ribeiro Guevara *et al.*, 2010
Uruguay	630	Muniz *et al.*, 2004
Maximum Natural Total Particulate Mercury in sediments	150	Schäfer *et al.*, 2006

Table 2-1: Typical Hg concentrations in rocks, soils and sediments around the world.
* Volcanic Influence, ** Mining influenced.

2.2 Arsenic

2.2.1 Arsenic in the environment

Arsenic is a chemical element with symbol As. It has an atomic mass of 74.92 and an atomic number of 33. Its valences are valence –3, 0, +3 or +5. Elemental arsenic occurs in two solid modifications: yellow, and gray or metallic, with specific gravities of 1.97, and 5.73, respectively. It is found native, in the sulfides *realgar* and *orpiment*, as arsenides and sulfarsenides of heavy metals, as the oxide, and as arsenates. Arsenopyrite, (FeSAs –Fig. 2-5) is the most common mineral, from which on heating the arsenic sublimes leaving ferrous sulfide. The element is a steel gray, very brittle, crystalline, semimetallic solid; it tarnishes in air, and when heated is rapidly oxidized to arsenous oxide (As_2O_3) with the odour of garlic. Arsenic and its compounds are poisonous. The most important compounds are white arsenic (As_2O_3), the sulfide, Paris green $3Cu(AsO_2)_2 \cdot Cu(C_2H_3O_2)_2$, calcium arsenate, and lead arsenate; the last three have been used as agricultural insecticides and poisons (Hammond, 2005).

Fig. 2-5: Arsenic minerals. Left image, Arsenopyrite - FeAsS (http://wisconsingeologicalsurvey.org), middle image, Orpiment - As_2S_3 (www.volcanol.fr) and right image, Realgar – AsS (http://webmineral.com).

Arsenic can occur in the environment from natural and anthropogenic sources. Among the natural ones could be cited wind erosion, sea-salt spray, forest fires, low temperature volatilization, volcanoes. Being the latter one of the most important sources emitting around 1.72×10^4 tonnes of As per year compared to the 1.98×10^3 t y^{-1} of wind erosion or the 1.25×10^2 t y^{-1} of forest fires (Chilvers and Peterson, 1988). The greater amount of anthropogenic emissions comes from the smelter production of copper, lead, zinc, steel, wood

fuel, clearance of land crops, arsenic chemical productions, waste incineration, generating in total an estimate burden of 2.81 $x10^4$ t y^{-1} of arsenic emissions to the atmosphere. These authors estimate that 40 % of the atmospheric As emissions correspond to anthropogenic inputs of which more than 40 % answer to copper smelting. In the other hand, 60 % of the total atmospheric As emissions derive from natural sources with nearly 60 % of the total natural flux coming from low temperature volatilization from soils and most of the remainder from volcanoes.

2.2.2 Sources of Arsenic

2.2.2.1 Minerals

Arsenic is present in more than 200 minerals as major constituent. The range goes from elemental As, arsenides, sulphides, oxides, arsenates As(V) and arsenites As(III) but the greatest concentrations occur in mineralised ores associated to Cd, Pb, Ag, Au, Sb, P, W and Mo. Arsenopyrite (FeAsS) is the most abundant As ore (Smedley and Kinniburgh, 2002), although arsenian (As-rich) pyrite ($Fe(S,As)_2$) could be more abundant in ore zones (Nordstrom, 2000). Due to the similar chemistry between As and S, the former can be present in sulphide minerals such as pyrite, substituting S in the crystal structure. Pyrite is present in the sediments of rivers, lakes, oceans and many aquifers. It commonly forms in zones of intense reduction and it is likely some of the soluble As will be incorporated. This mineral is not stable in aerobic systems and oxidizes to Fe oxides with the release of large amounts of SO_4, acidity and associated trace constituents, including As (Smedley and Kinniburgh, 2002).
Arsenic could be found as well as a part of the mineral structure or as sorbed species in many oxide minerals and hydrous metal oxides. Adsorption of arsenate to hydrous Fe oxides is particularly strong and if hydrous Mn and Al oxides are present in quantity could also be important (Peterson and Carpenter, 1983; Goldberg, 1986; Brannon and Patrick, 1987; Manning and Goldberg, 1996; Hiemstra and van Riemsdijk, 1996). Arsenic could be as well sorbed to the edges of clays and on the surface of calcite (Goldberg and Glaubig, 1988). Anyways, As could be present in many others rock-forming minerals due that can substitute Si^{4+}, Al^{3+}, Fe^{3+} and Ti^{4+} in many mineral structures (Smedley and Kinniburgh, 2002).

2.2.2.2 Rocks, soils and sediments

Rocks

The average concentration of As in igneous rocks is around 1.5 mg kg^{-1}. It could be higher depending on the silica content but usually it is less than 5 mg.kg^{-1}. Volcanic glasses have an As content that ranges from 6.83 to 10.4 mg kg^{-1} and especially ashes are often implicated in the generation of high-As waters (Nicolli *et al.*, 1989; Smedley *et al.*, 2002; García *et al.*, 2006; Nicolli *et al.*, 2012). Metamorphic rocks contain around 5 mg kg^{-1} of As or less but pelitic rocks can reach concentrations of 18 mg kg^{-1} (Smedley and Kinniburgh, 2002). On the other hand, the average As concentration in sedimentary rocks is between 5 and 10 mg kg^{-1} (Webster, 1999) being sands and sandstones the ones with the lowest concentrations (4 mg kg^{-1}). Argillaceous deposits have higher As concentrations than sandstones with an average value of 13 mg kg^{-1} reflecting larger proportions of sulphide minerals, oxides, organic matter and clays (Ure and Berrow, 1982). Marine shales tend to have high S concentrations and high As concentrations have been determined. Coal and bituminous deposits have variable concentrations but usually high (100-900 mg kg^{-1}) (Riedel and Eikmann, 1986). Carbonate rocks usually have low concentrations with an average of 3 mg kg^{-1} reflecting the low concentrations of the constituent mineral (Smedley and Kinniburgh, 2002).

Soils

Levels of arsenic in soils vary considerably depending on the geographic region and the kind of parent rock which plays a fundamental role (Mandal and Suzuki, 2002). Baseline concentrations of As in soils are generally from 5 to 10 mg kg^{-1} but peats and bogs soils are considerable higher (average 13 mg kg^{-1}) mainly because of increased prevalence of sulphide mineral phases under the reduced conditions. Even if the main source of As is geological, additional input may be derived locally from anthropogenic activities (Smedley and Kinniburgh, 2002).

Sediments

Arsenic concentrations in unconsolidated sediments are variable and usually the values range from 3 to 10 mg kg^{-1} depending on the texture and mineralogy. For example, alluvial sands and riverbed sediments in Bangladesh vary from 1.0 to 14.7 mg kg^{-1}, lake sediments in United States from 0.5 to 44.0 mg kg^{-1}, loess silts from Argentina from 5.8 to 18.0 mg kg^{-1}. The presence of pyrite or Fe oxides could be reflected by the elevated concentrations of As

(Smedley and Kinniburgh, 2002 and references therein). Discrete Fe-rich or clay-rich bands in sediments may contain higher As concentrations (Smedley *et al.*, 2005).

2.2.3 Arsenic in natural waters

Arsenic can occur in the environment in several oxidation states (-3, 0, +3 and +5) but in natural waters is mostly found in inorganic form as oxyanions of trivalent arsenite As(III) or pentavalent arsenate As(V). It mobilizes at pH values 6.5-8.3 typically found in groundwaters and under both oxidising and reducing conditions (Smedley and Kinniburgh, 2002). Arsenate, among other oxyanions, tend to become less sorbed as the pH increases (Dzombak and Morel, 1990). Under some conditions at least, these anions can persist in solution at relatively high concentrations (tens of $\mu g\ L^{-1}$) even at near-neutral pH values. Therefore the oxyanion-forming element such as Cr, As, U and Se are some of the most common trace contaminants in groundwaters. Arsenic has the particularity of being mobile over a wide range of redox conditions (Smedley and Kinniburgh, 2002).

The factors that control As speciation are mainly the redox potential (Eh) and the pH. Under oxidizing conditions, $H_2AsO_4^-$ is dominant at low pH (less than about pH 6.9), whilst at higher pH $HAsO_4^{2-}$ becomes dominant (H_3AsO_40 and AsO_4^{3-} may be present in extremely acidic and alkaline conditions respectively). Under reducing conditions at pH less than about pH 9.2, the uncharged arsenite species $H_3AsO_3^0$ will predominate (Brookins, 1988; Yan *et al.*, 2000).

Many studies attempted to discriminate the presence of inorganic As species into As(III) and As(V). In rainwater the source will determine the oxidation states of As. When derived from smelters, coal burning and volcanic sources $As(III)_2O_3$ seems to be dominantly. Although organic species may be derived by volatilization from soils, arsine ($As(-III)H_3$) may derive from landfills and reducing soils such as peats, and arsenates may be derived from marine aerosols. The O_2 in the atmosphere will oxidate the reduced forms and reactions with atmospheric SO_2 and O_3 could occur (Cullen and Reimer, 1989).

2.2.3.1 Abundance and distribution

Freshwater

Arsenic concentrations in freshwater varies greatly geographically. It depends mainly of the available amount and the local geochemical environment. The highest and widest concentration range under natural conditions are found in groundwaters due to the influences of rock-water interactions and the physical and geochemical conditions of aquifers to be favourable in the mobilization and accumulation of As. Strongly reducing or oxidising high-pH conditions (under which desorption of As from, or dissolution of metal oxides is favoured) are "young sediments" (Smedley and Kinniburgh, 2002). Sedimentary aquifers from the Quaternary seem to be the most affected by high As concentrations, probably because these sediments contain newly formed and reactive minerals, in contrast to older aquifers that have changed and have been flushed large groundwater volumes since deposition (Smedley *et al.*, 2005).

Atmosphere

Arsenic enters in the atmosphere trough inputs from wind erosion, low-temperature volatilization from soils, marine aerosols, volcanic emissions and pollution. When these last two happen, concentrations are higher (Smedley and Kinniburgh, 2002). Although the speciation is complicated by the fact that most of the arsenic in the atmosphere is in the form of particulate matter, the As appears to consist of mainly $As(III)_2O_3$ dust particles. (Cullen and Reimer, 1989). As is returned to the Earth's surface by wet and dry deposition. Its baselines concentrations in rainfall and snow measured in rural areas are less than 0.03 $\mu g\ L^{-1}$ (Smedley and Kinniburgh, 2002).

River waters

Concentrations of arsenic depend on the composition of the surface recharge, contribution from the baseflow and bedrock lithology. Because of this, a wide range of values have been found around the world. The baseline concentrations of As in river waters are from 0.1 to 0.8 $\mu g\ L^{-1}$ but can reach up to 2 $\mu g\ L^{-1}$. Some authors (Cáceres *et al.*, 1992; Lerda and Prósperi, 1996; Sancha, 1999 among others) have found concentrations over 100 $\mu g\ L^{-1}$ in rivers with influence of high-As groundwaters in northern Chile and central Argentina to name a few. Other reason that can throw high values of naturally-occurring arsenic is the presence of geothermal sources with typical values around 10-70 $\mu g\ L^{-1}$ such is the case in

Sierra Nevada, USA, Waikato in New Zealand or different areas in Iceland (Benson and Spencer, 1983; McLaren and Kim, 1995; Kaasalainen and Stefánsson, 2012). High arsenic concentrations may also occur as result of pollution from mine wastes, mill tailings, industrial or sewage effluents (Smedley and Kinniburgh, 2002).

Lake water

Baseline concentrations for As were found in Canada with values <1 µg L^{-1} but typically they present values close to or lower to those found in river waters. Alkaline closed-basin lakes could present high As concentrations due to an extreme evaporation and/or geothermal inputs (Azcue *et al.,* 1994; Smedley and Kinniburgh, 2002).

Seawater and estuaries

Average concentrations of arsenic in open seawater show little variation and present values around 1.5 µg L^{-1}. Instead, estuarine waters have variable concentrations due to the different river inputs and salinity or redox gradiants. Usually concentrations under natural conditions are less than 4 µg L^{-1} (Smedley and Kinniburgh, 2002).

Groundwater

There are numerous authors that have addressed arsenic concentrations in groundwater and the health risks that a prolonged intake could lead to (e.g.: Smedley *et al.*, 2002; Smedley and Kinniburgh, 2002; Smedley *et al.*, 2005; Francisca and Carro Perez, 2009; Bundschuh *et al.*, 2012). Background concentrations of As in most countries are less than 10 µg L^{-1}. However, in many published work values range from 0.5-5000 µg L^{-1} all under natural conditions and under a variety of environments. Recently Raychowdhury *et al.* (2013) have measured concentrations up to 7500 µg L^{-1} in the Chaco-Pampean Plain (Argentina) with a median of 76 µg L^{-1} As. It has been observed as well that evaporation can play in important role in increasing As values considerably (Smedley and Kinniburgh, 2002; Nicolli *et al.,* 2012).

Brines

There are not many works done in brines but some published data suggest that As concentrations may be very high. White *et al.* (1963) reported concentrations of 5.80 mg L^{-1} As in Hungary in a Na-Cl-dominated brine and up to 243 mg L^{-1} in brines of Searles Lake, USA. In more recent work carried out by Goldstein *et al.* (2007) in the saline groundwater beneath Franklin Lake Playa (California, U.S.A.), they found concentrations of As of

16 mg L^{-1}. They also measured the As concentration on water extractable salts located in the Mojave Desert in the Death Valley between 5 to 15 km upgradiant of Franklin Lake Playa, founding values as high as 600 mg L^{-1} As.

2.2.4 Arsenic in the world and in Argentina

Several countries have identified problems with arsenic in drinking water, where concentrations largely exceed the WHO (2004) guideline value of 10 µg L^{-1}. The ones that required a special attention due to the As-occurrence are Argentina, Bangladesh, Chile, China, Hungary, India, Mexico, Romania, Taiwan, Vietnam and many parts of USA (in particular the SW) (Smedley and Kinniburgh, 2002). Some other countries reflect high As concentrations due to the proximity to geothermal waters and hot springs such is the case of some areas in Argentina, Japan, New Zealand, Chile, Kamchatka, Iceland, France and Dominica (Smedley and Kinniburgh, 2002; Kaasalainen and Stefánsson, 2012; Mitsunobu *et al.*, 2013). Fig. 2-6 shows the distribution of arsenic in the most affected countries and the source of which this element is related to and Table 2-2 shows some of their concentrations. Arnórsson (2003) showed that As concentrations increase with temperature in these areas. As previously mentioned, high arsenic concentrations are also related to areas where sulphide-mining activities are prevalent. This element is released from sulphide minerals as they are oxidised as result of mining operations (Smedley and Kinniburgh, 2002).

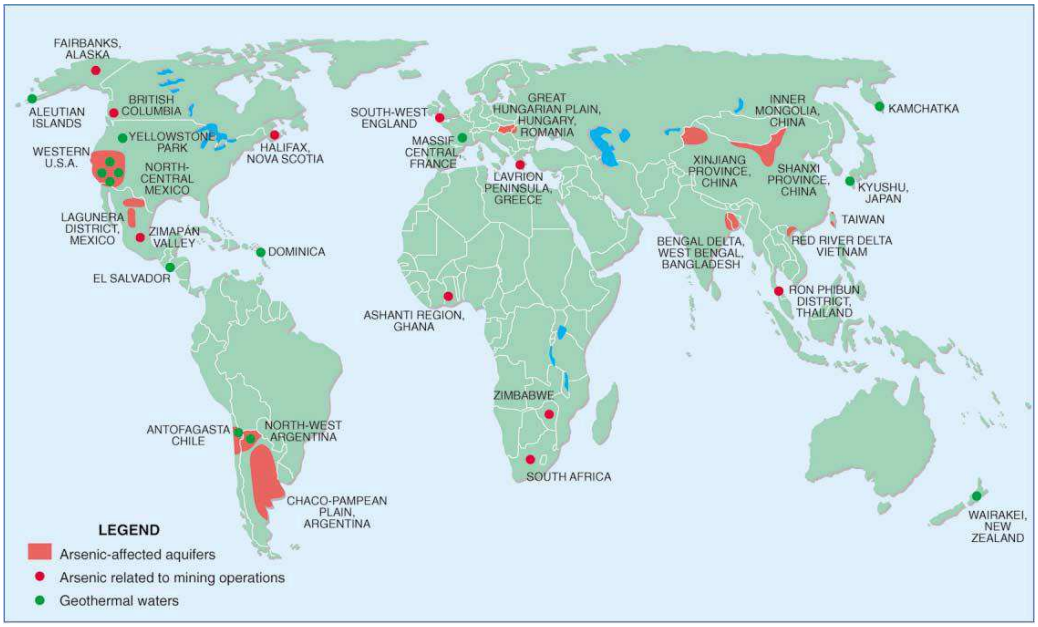

Fig. 2-6: Arsenic distribution of documented world problems whether they are related to aquifers or mining (red dots) and geothermal (green dots) sources (Smedley and Kinniburgh, 2002).

Typical As concentrations in natural waters		**Typical As concentrations in rocks, sediments, soils and other surficial deposits**	
Water body and location	As concentration average or range ($\mu g.l^{-1}$)	Rock/sediment type	As concentration average or range ($mg\ kg^{-1}$)
Rain water		*Igneous rocks*	
Terrestrial rain	0.46	Ultrabasic rocks	1.5 (0.03–15.8)
River water		Basic rocks (basalt)	2.3 (0.18–113)
Norway	0.25 (<0.02–1.1)	Intermediate (diorite, granodiorite, syenite)	1.0 (0.09–13.4)
Dordogne, France	0.7	Acidic rocks (rhyolite)	4.3 (3.2–5.4)
South-east USA	0.15–0.45	Volcanic glasses	5.9 (2.2–12.2)
Córdoba, Argentina*	7–114		
Northern Chile*	190–21800	*Metamorphic rocks*	
Waikato, New Zealand**	32 (28–36)	Quartzite	5.5 (2.2–7.6)
Ron Phibun, Thailand***	218 (4.8–583)	Phyllite/slate	18 (0.5–143)
Lake water			
Japan	0.38–1.9	*Sedimentary rocks*	
Sweden	0.06–1.2	Marine shale/mudstone	3–15 (up to 490)
Western USA**	0.38–1000	Non-marine shale/mudstone	3.0–12
Ontario, Canada***	35–100	Iron formations and Fe-rich sediment	1–2900
Estuarine water		Evaporites (gypsum/anhydrite)	3.5 (0.1–10)
Oslofjord, Norway	0.7–2.0		
Rhône Estuary, France	2.2 (1.1–3.8)	*Unconsolidated sediments*	
Loire Estuary, France***	up to 16	Alluvial mud/clay (Bangladesh)	6.5 (2.7–14.7)
Seawater		River bed sediments (Bangladesh)	1.2–5.9
Deep Pacific and Atlantic	1.0–1.8	Lake sediments, Lake Superior	2.0 (0.5–8.0)
Coastal Malaysia	1.0 (0.7–1.8)	World average river sediments	5
Groundwater		Loess silts, Argentina	5.4–18
As-rich provinces (e.g. Bengal Basin, Argentina, Mexico, northern China, Taiwan, Hungary)	10–5000		
Mining-contaminated	50–10000		
Geothermal water	<10–50000		
Mine drainage			
Various, USA	<1–34000		
Iron Mountain	up to 850000		

Table 2-2: Typical As concentrations in natural waters, rocks and sediments around the world (Smedley and Kinniburgh, 2002). * Groundwater influenced, ** Geothermal influenced, *** Mining influenced.

The case in Argentina

In Argentina, numerous studies have been carried out concerning the presence of arsenic in groundwater and the risk that it could present to human health. The Chaco Pampean Plain that includes the provinces of Córdoba, La Pampa, Santa Fe, Buenos Aires and Tucumán in particular, is one of the largest regions in the world (around $1x10^6$ km^2) that presents As issues (Smedley and Kinniburgh, 2002; Nicolli *et al.*, 2012). Such is the case that the permissible drinking water intake was lowered from 50 to 10 $\mu g\ L^{-1}$ As in 2007 (CAA) to coincide with that one stipulated by the WHO.

Aquifers in the Chaco Pampean Plain are included in sequences of several hundred meters composed of clastic sediments that form a system of interconnected multilayer aquifers that overlie the crystalline basement. Usually this basement presents a faulted system with ascending and descending blocks of granites, metamorphic rocks and basalts that act as aquifuge. The hydrogeological system is composed in the base by thick marine pelitic sediments (green clays from Miocene with very low permeability - aquiclude), hosting very saline Na-sulfate-chloride type waters. Above this and at a regional scale, lies a very thick sequence of heterogeneous deposits of aeolian loess and loess-like sediments from the Pampa Formation (PlioPleistocene) (Nicolli *et al.*, 2012).

During the Pleistocene there was a cold, arid environment that reigned in the Argentina Cordillera that allowed efficient production of fine silt by periglacial processes (Smedley *et al.*, 2002). These fine sediments were transported by the dominant winds from the WSW (Zárate, 2003). Some authors (Raychowdhuy *et al.*, 2013 and references therein) have studied the composition of the Pampean loess concluding that they present mainly plagioclase and orthoclase feldspars, volcanic glass shards, quartz, and muscovite and the coarser fraction contains fragments of metamorphic and acid plutonic rocks mirroring the composition of the Andean rocks (Gaiero, 2007; Maher *et al.*, 2010). Francisca and Carro Perez (2009) have shown that especially the sand and silt fractions present a very high content of volcanic glass (Fig. 2-7). Nevertheless, in the loess of the Chaco-Pampean Plain the silt fraction prevails over the clay fraction.

In the Holocene the loess deposits have been substantially reworked by aeolian and fluvial processes. There is also evidence of post-depositional alteration with formation of carbonate cementation, secondary Mn oxide (as nodules and cement) and soil-forming processes. Thus evidencing significant climatic variations during the Quaternary in the region (Kröhling and Iriondo, 1999; Smedley *et al.*, 2002).

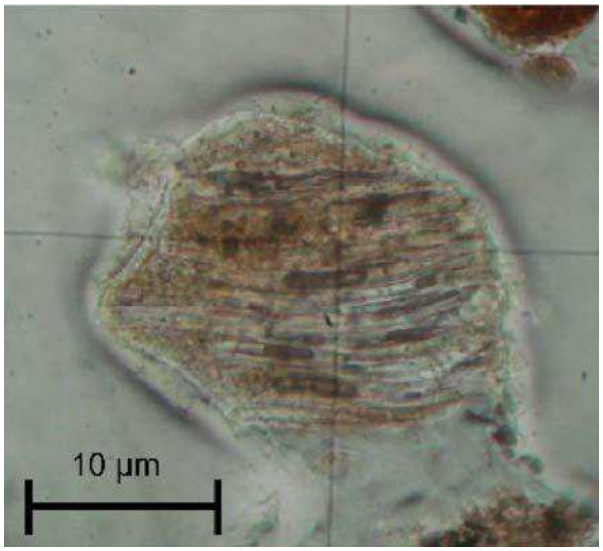

Fig. 2-7: Picture of the volcanic glass typically found in the Chaco-Pampean Plain loess (Francisca and Carro Perez, 2009).

Some authors (Bundschuh *et al.*, 2004; Bhattacharya *et al.*, 2006) have found that the volcanic ash that is present in the loess, contains between 6.83 to 10.40 $mg.kg^{-1}$ of As while the loess itself presents concentrations of 5.81 to 37.30 $mg.kg^{-1}$ (Nicolli *et al.*, 2012). Volcanic glass shards represents usually 25-50 % and exceptionally up to 63 % of the light fraction in the loess. The average chemical composition of the loess-type sediments usually corresponds to that of a dacite, or an andesite, or a trachyandesite (Nicolli *et al.*, 2010). Bundschuh *et al.* (2004) and Bhattacharya *et al.*, (2006) conclude as well that this type of sediment is the principal source of arsenic. This As was dissolved in geological time spans, under favourable conditions and precipitated or adsorbed onto Fe, Al, Mn oxyhydroxides from where desorption can occur as a fast process, according to changing geochemical conditions in time and space. Such changing conditions results in a very patchy distribution of concentrations of dissolved As on short distance with so called "hotspots" (Bundschuh *et al.*, 2012).

Nicolli *et al.* (2010) have summarized the mobility of arsenic in oxidizing groundwaters from loess-type sediments in arid and semi arid dry climates taking as example the Chaco-Pampean Plain, in particular the Salí River Basin as the most representative of the whole region. Groundwaters are oxidizing, highly mineralized in some areas, and highly alkaline. It is usual to find As associated to V, U, B, Sb and Mo in solution. Concentrations of sulphate and chloride increase due to the evaporation and the agricultural activities. Potassium concentrations are high and may increase as well as result of evaporation and contamination. Bicarbonate concentrations are variable and since carbonate minerals are present in the

sediments, carbonate reactions strongly controls the groundwater chemistry. SiO_2 concentrations vary in a wide range reflecting the presence of silicate minerals and the highly soluble amorphous volcanic glass. High pH groundwaters respond to the reaction of silicate minerals. In the Córdoba area, high grade of special variability in groundwater chemistry and minor/trace element concentrations over short distances, indicate groundwater flow with poor mixing (Nicolli *et al.*, 1989). High pH values favour the dissolution of volcanic glass and leaching of volcanic-origin material in loess-type aquifer sediments. As is likely adsorbed under circum-neutral pH conditions on Fe/Mn (hydr)oxides, which are hosted as cement or as coatings on lithic fragments in the loess sediments. Mobilization by desorption is produced under high pH conditions when As, V, U, F and B anions or oxyanions are released. Those groundwaters are mostly of the bicarbonate type and their chemical characteristics are highly controlled by carbonate equilibria

The mineralogical composition of loess is represented by K-mica, clay minerals (kaolinite, Ca-montmorillonite, illite and chlorite) and frequent Fe- and Al oxides and oxi-hydroxides (hematite, goethite, $Fe(OH)_3$(a), gibbsite) forming thing coatings over silicate grains.

3. Materials and methods

3.1 Sampling campaigns and samples treatment

Samples were collected during different field trips with the aim of determining the sources and mobility of Hg and As in the Laguna del Plata's basin within the past ~80 years. For this, three sampling campaigns were performed that allowed to collect water samples along the Suquía River and its collectors, Laguna del Plata and Laguna Mar Chiquita as well as riverbed and lakes bottom sediments. In addition, a 120 cm sediment core was retrieved from Laguna del Plata at 1.5 m water depth in order to span the variation of Hg and As in time. The Fig. 3-1 shows the location of sampling points in the study area. The first field trip was performed on June 2010 and samples were collected along the Suquía River before and after crossing the city of Córdoba and after the sewage treatment plant, places that could be affected by anthropic activities. Samples were collected as well in the lower part of the basin where the river crosses the loessic plain where an intense agriculture exists.

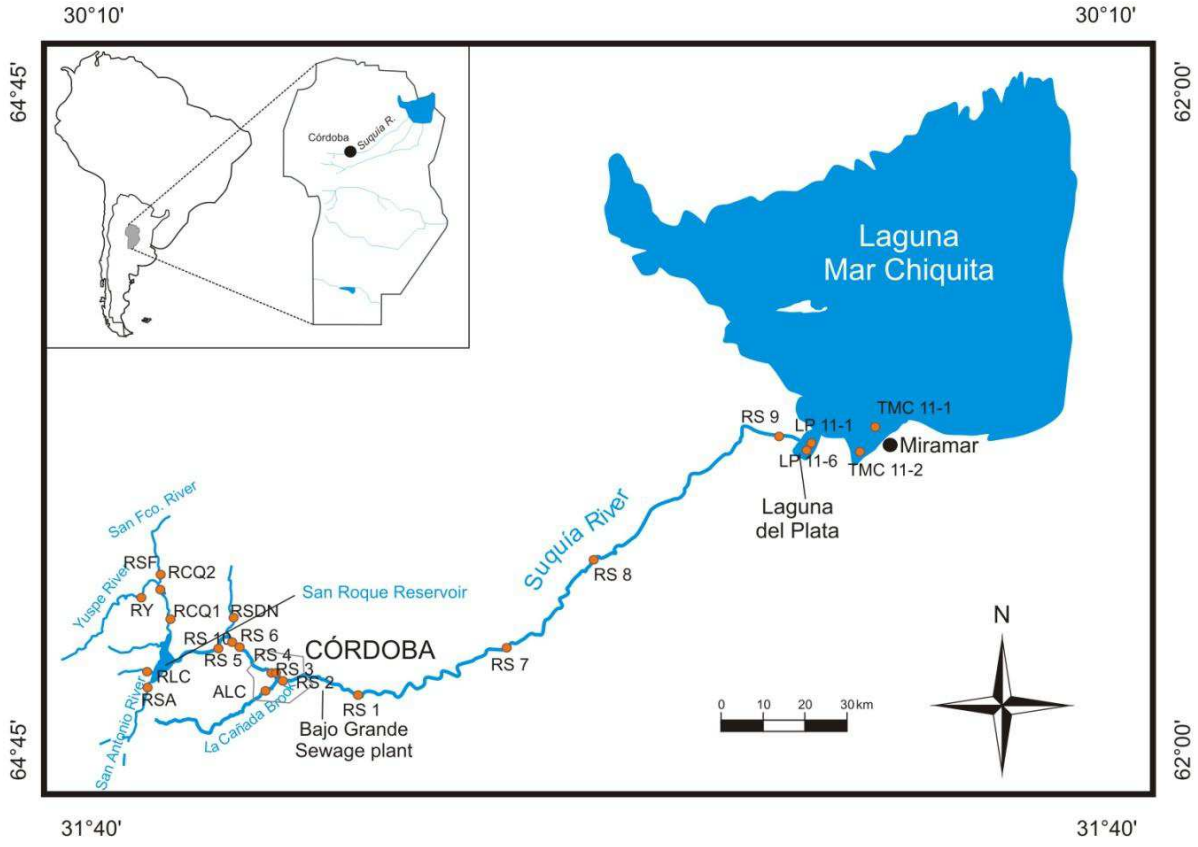

Fig. 3-1: Sampling points on the Suquía River and its catchment area and lakes Laguna del Plata and Laguna Mar Chiquita.

The second field trip was carried out on April 2011 and the aim of this campaign was to collect samples from the Laguna del Plata and Laguna Mar Chiquita as well as the sedimentary core retrieved at the point LP 11-1. Many studies are carried out at Laguna Mar Chiquita but those at Laguna del Plata are fewer.

The last field trip was performed on December 2011 so as to sample the Suquía River collectors located in the Sierras Pampeanas Range in pristine areas.

The whole group of samples is composed by: 22 water samples where 15 correspond to river water and 7 to lake water; 18 sediments samples where 14 were collected from the riverbed and 4 from both lake bottom and 1 sedimentary core from Laguna del Plata.

3.1.1 Water and sediment samples

Previous to the field trip, 1 litre flasks as well as 50 ml polystyrene flasks and 17 ml centrifuge tubes were cleaned with a 5 % v/v Nitric Acid (HNO_3) solution for 36 hours and then washed three times with ultrapure water (Milli-Q® system).

Water and riverbed sediments were collected along the Suquía River and its main tributaries in the basin's catchments (Fig. 3-2a). Besides, water samples from the lakes were collected using a Van Dorn bottle (Fig. 3-2b) that allowed to retrieve samples from different depths. Field determinations consisted of pH, electrical conductivity (EC), total dissolved solids (TDS), temperature, and alkalinity. Determinations were performed using standardized solutions (Hach Co.). All samples were filtered through 0.22 µm cellulose acetate membrane filters (Millipore Corp.) and divided into two aliquots. The filtration equipment was repeatedly rinsed with sample water prior to filtration. Aliquots used for trace elements and major cations (20 ml) were acidified to pH < 2 with ultrapure HNO_3 (~99.999 %, redistilled, Aldrich Chemical) and stored in pre-cleaned polyethylene bottles. The remaining 20 ml aliquot was stored in polyethylene bottles, without acidifying, at 4ºC for the determination of anions.

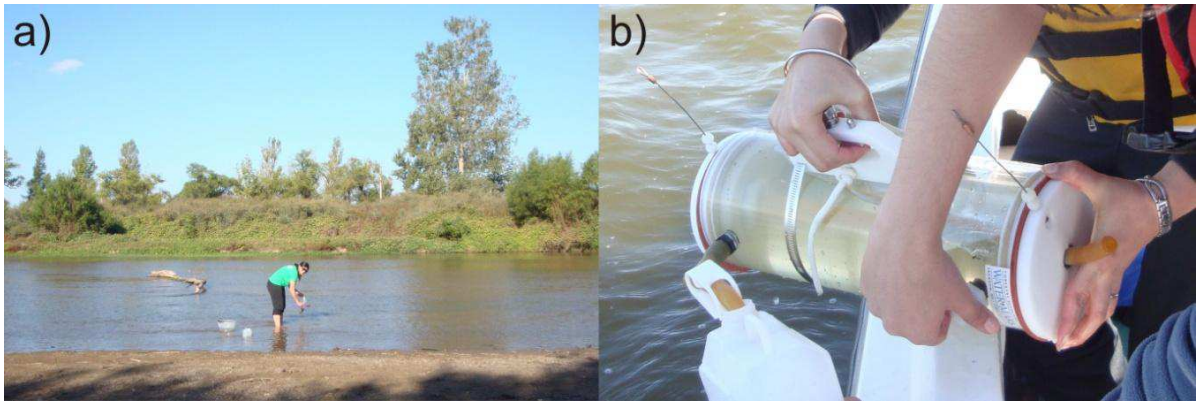

Fig. 3-2: Water and sediment sampling – a) Collecting samples from the river, b) Collecting samples from the lakes using a Van Dorn bottle.

Sediment samples were collected and stored in plastic bags. No samples were collected from the Suquía River stretch that crosses the city, due that in this area the river is channelled. In the laboratory, samples were dried at room temperature and then in oven at 50°C during 7 days.

Once samples were dried, they were sieved with a Retsch® Horizontal Sieve Shaker (AS 400 control) in a circular motion at 200 rpm through 2 different size sieves: 6 and 230 corresponding to 3360 µ and 62 µ mesh size respectively. From now onwards they will be referred as sandy and silty fractions. Sandy fraction samples were grind in Agate mortar for later analysis. All samples were stored in plastic bags.

Sediments from the bottom of the lakes were collected using a Ekman dredge. The obtained samples were stored and dried following the procedure described above for riverbed sediments. Finally, they were grind in agate mortar and stored in plastic bags.

Pluviometric captor sample

One single pluviometric sample (RI 99) was obtained from Dr. Eduardo Piovano that he had collected in one of his many field trips to the Mar Chiquita area. The sample corresponds to the year 1999 and the pluviometric captor is located in Miramar town located in the southern coast of Laguna Mar Chiquita (Fig. 3-1).

3.1.2 Sediment core

One sediment core was retrieved from Laguna del Plata (LP 11-1, Lat. 30°54'48.4"S; Long. 62°51'16.4"W), using a Eijkelkamp core sampler type Beeker (Fig. 3-3a,b) , and a PVC tube of 65 mm diameter and 120 cm long. After extraction the core was stored at 4°C. Right after the opening the core was sliced longitudinally in two. One of the parts was photographed and a high-resolution 256 grey-level image was acquired with the X-ray imaging system SCOPIX; the other half of the core was sampled every 5 mm (Fig. 3-3c,d).

An average of 7.6 g of sample were placed in previously weighted acrylic boxes (1.8 cm^3) and dried in the oven at 50°C until constant weight was obtained. All samples were grind in agate mortar and stored in plastic flasks for its later analysis.

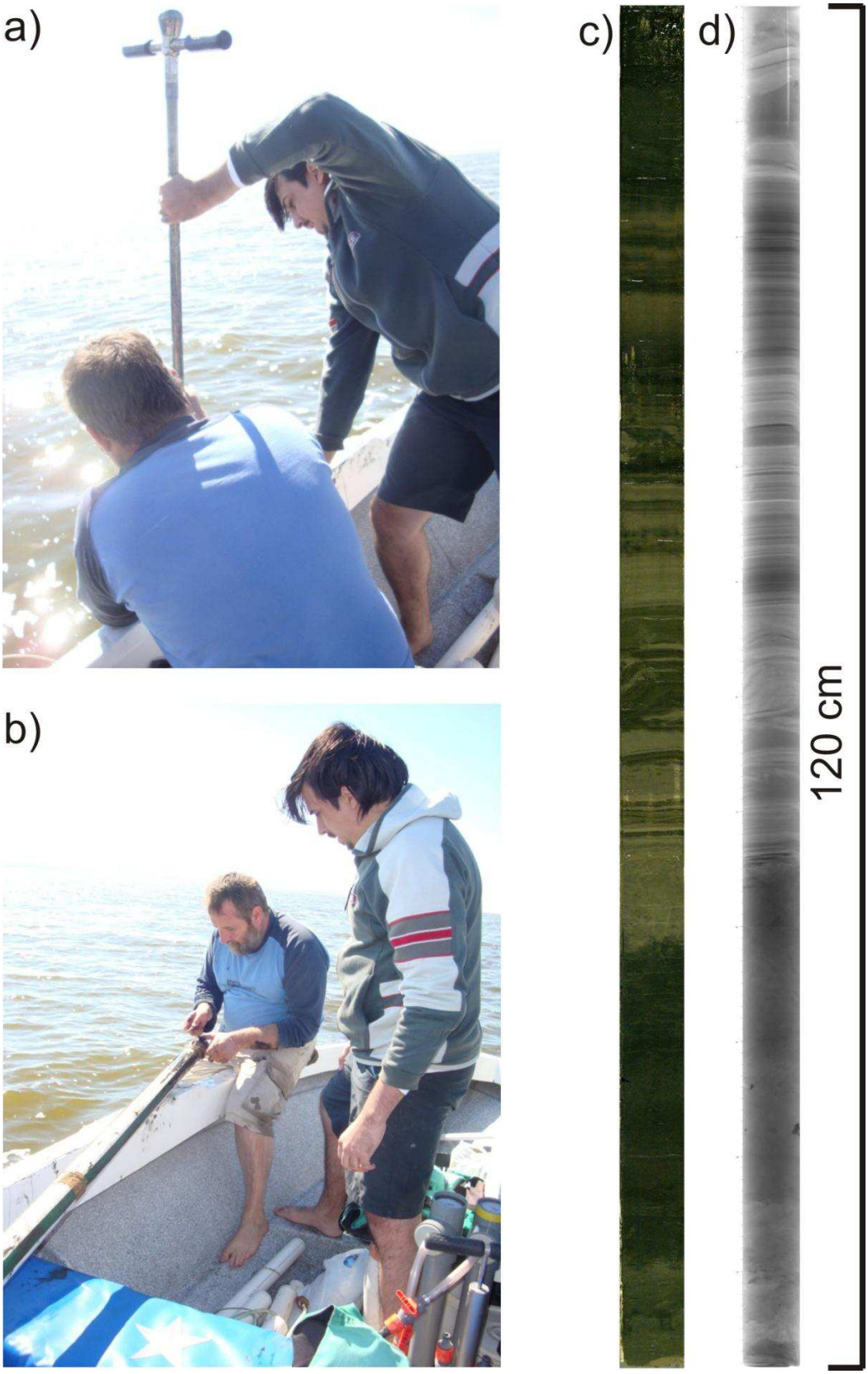

Fig. 3-3: LP Core – a and b) Extraction of the sediment core using a manual Eijkelkamp core sampler type Beeker, c) Core photograph, d) X-ray SCOPIX High-resolution image.

3.2 Analytical Methods

3.2.1 Core dating – Radionuclides

Dating technique using ^{210}Pb was first employed in 1973 by Koide *et al.* (1973) and widely spread since for marine and lacustrine sediments. The ^{210}Pb ($T_{1/2}$ = 22.3 years) is a naturally occurring radionuclide delivered continuously to the landscape by atmospheric fallout (Saari *et al.*, 2010) and becomes rapidly and strongly bound to particulate matter. This atmospherically derived ^{210}Pb scavenged by particles, is referred to ^{210}Pb in excess ($^{210}Pb_{xs}$) of that supported within particles by the decay of its parent isotope, ^{226}Ra. Another radionuclide, the ^{232}Th, occurs naturally and usually is associated to the detrital fraction (van der Klooster *et al.*, 2011), therefore a change in its activity could indicate different lithological sources or proportions. On the other hand, ^{137}Cs ($T_{1/2}$ = 30 years) is an artificial radionuclide resulting from the atmospheric fallout of the nuclear weapon tests during 1953-1963 and the Chernobyl reactor fire in 1986 (United Nations Scientific Committee on the Effects of Atomic Radiation, 2000; Appleby, 2001). As ^{210}Pb is present in all environments (Ivanovich and Harmon, 1992), it has been used as an environmental radiotracer of many processes, such as ocean biogeochemistry, atmospheric deposition and contamination, sedimentary processes and sediment radiochronology (Sánchez-Cabeza and Ruiz-Fernández, 2012 and references therein) in recent sediments of a century or so where there is not an equilibrium between ^{210}Pb and ^{226}Ra (Koide *et al.*, 1973; Sánchez-Cabeza and Ruiz-Fernández, 2012). In systems that have remained closed for sufficient time (>150 years), supported ^{210}Pb is in equilibrium with its parent radionuclide ^{226}Ra ($T_{1/2}$ = 1600 years) (Sánchez-Cabeza and Ruiz-Fernández, 2012). As most of the superficial sediment is under mixing due to physical or biological processes, many authors (Robbins and Edgington, 1975; Carroll *et al.*, 1999; Appleby, 2001; Smith, 2001, Oguri *et al.*, 2012) suggest that it is important to validate ^{210}Pb dates using an independent time marker as ^{137}Cs that can provide an unambiguous time-stratigraphic horizon. For this purpose ^{210}Pb, ^{232}Th, ^{226}Ra and ^{137}Cs activities were measured using a low background, high efficiency, well-shaped γ detector (CANBERRA) (Schmidt et al, 2009). The γ detector was calibrated using certified reference materials (IAEA-RGU-1; IAEA-RGTh; SOIL-6). Activities were expressed in mBq g^{-1} and errors are based on 1 SD counting

statistics. Excess ^{210}Pb ($^{210}Pb_{xs}$) was calculated by subtracting the activity supported by its parent isotope, ^{226}Ra, from the total ^{210}Pb activity in the sediment.

Several models exist in order to obtain an age model, section/layer age as a function of the depth, accumulation rates or estimate sediment mixing rates. Sánchez-Cabeza and Ruiz-Fernández (2012) have summarized the existing models in:

Constant Activity model (CA – Former Constant Initial Concentration CIC). The hypothesis is based that the $^{210}Pb_{xs}$ concentration when the section *i* is formed is constant with a value denoted as $C_{0:}$

$$C_i\,(t = 0) = k \equiv C_0 \quad \text{(Eq. 2)}$$

Where k = $\frac{f_i}{r_i}$.

With f_i is the main flux to sediment surface;

r is the mass accumulation rate (MAR).

Constant Sedimentation model (CS). It is based on the hypothesis that the mass accumulation rate r is constant (both for sections and layers). It can be only used if the values of fluxes to the sediments surface f_i are known during a period of about 100 years. With the radioactive decay and m_i as the dry mass of the section, the equation could be written as:

$$C_i = \frac{f_i}{r}\, e^{-\lambda m_i / r} \quad \text{(Eq. 3)}$$

Constant Flux model (CF). Widely known as Constant Rate of Supply model (CRS) has its fundamental hypothesis in that the $^{210}Pb_{xs}$ flux to the sediment surface is constant ($f_i = f_{(i)} = k$). Where $f_{(i)}$ is the flux to the sediment surface when layer *(i)* is formed.

Constant Flux Constant Sedimentation model (CFCS). This model incorporates simultaneously the CF model hypothesis of constant flux to the sediment surface ($f_i = f_{(i)} = f$) and the CS model of constant mass accumulation rate ($r_i = r_{(i)} = r$):

$$C_i = \frac{f_i}{r}\, e^{-\lambda m_i / r} = C_0\, e^{-\lambda m_i / r} \quad \text{(Eq. 4)}$$

When the CFCS hypotheses are met, a purely exponential decrease of C_i with the depth should be observed. Finally, the equation can be solved through a linear regression between the logarithm of $^{210}Pb_{xs}$ concentration (ln C_i) and the mass depth m_i:

$$ln\ C_i = ln\ C_0 - \frac{\lambda}{r} m_i \quad \text{(Eq. 5)}$$

3.2.2 Selective extractions

It is widely known that the toxicity and mobility of pollutants depend strongly on their specific chemical forms and on their binding states (Gleyzes at al., 2002). Therefore, the identification of the main binding sites and phase associations of trace elements in soils helps to understand the geochemical processes in order to evaluate the remobilization potential and risks induced (Sutherland *et al.*, 2000)

Selective extractions are commonly used in order to determine trace elements distribution in different solid phases (soils and sediments) based on the rational use of a series of more or less selective reagents chosen to solubilise successively the different mineralogical fractions thought to be the responsible for retaining the larger part of the trace metals. The objective is to simulate various possible natural and anthropogenic modifications of environmental conditions (Gleyzes *et al.*, 2002 and references therein).

A very well defined protocol was done by Tessier *et al.* (1979) where the same sample is treated with the different reagents and the amount of the extracted metal is measured on the extractant reagent. Another method is the parallel extraction schemes (e.g. Audry *et al.* 2005) which is the one applied in this study. It consists of assessing the Hg distribution by 3 parallel or single chemical extractions, *i.e* using each reagent on a different sample aliquot (Farrah and Pickering, 1993; Alborés *et al.*, 2000). Using this second technique, some limitations are avoided such as (i) metal transfer from one phase to the another (Bemond, 1992), (ii) multiple risks of sample contamination from successive reagents used (Quevauviller, 1998), (iii) possible changes in elemental speciation during the successive extraction steps and (iv) changes or losses of elemental species during the residue washing step (Rosenberg and Ariese, 2001). Besides, this method shows no risk for sample losses and an error occurred during one extraction does not compromise the entire schema (Tack *et al.*, 1996).

Before the extraction, all solutions were prepared with analytical reagent grade chemicals and purified water (Milli-Q® system). Labware in contact with the samples was acid clean (soaked in 10 % HCl during 3 days, rinsed 3 times with Milli-Q® water and dried under a laminar flow hood). Once that the extraction was done, the solid residue was washed three times with Milli-Q® water, tubes were centrifugated for 15 minutes at 3000 rpm to collect the residual sediment that afterwards they was dried on stove at 50°C, grind in Agate mortar weighted and analyzed.

3.2.2.1 Ascorbate extraction

This reducing single extraction removes trace elements associated with Mn oxides and the most reactive Fe oxide fraction (i.e. amorphous oxides; Kostka and Luther III, 1994; Audry *et al.*, 2006), using a 0.11 M ascorbate reagent (5:5:2 sodium citrate/sodium-bicarbonate/ascorbic-acid mixture; J.T. Baker, Baker analyzed/J.T. Baker, Baker analyzed/Acrôs Organics). For this extraction, 12.5 ml of ascorbate solution and 200 mg of dry sediment were added into a 50 ml previously HCl cleaned Teflon® centrifuge tubes and were placed for 24 h in a rotary shaker at 12 rpm.

3.2.2.2 H_2O_2 extraction

The oxidizing single extraction using hydrogen peroxide (H_2O_2) typically attacks organic matter but sulphides are also partially oxidized during this step (Tessier *et al.*, 1979). This work utilises a modified Tessier protocol (Ma and Uren, 1995, Audry *et al.*, 2006), previously applied for Hg solid speciation (Castelle *et al.* 2007).

For this, 8 ml of 30 % H_2O_2 (J.T. Baker, Baker analyzed), buffered to pH 5 with NaOH (J.T. Baker, Baker analyzed), were added to 250 mg of dry sediment in 50 ml Teflon® centrifuge tubes (Nalgene, Oak-Ridge). The tubes were then placed in an oven at 85°C for 5 h with manual agitation every 10 min and 3 ml of 30 % H_2O_2 and 5 ml of 5 M ammonium acetate (complexing agent, J.T. Baker, Baker analyzed) were added after 3 h. Then, the tubes were shaken for 30 min (Sahuquillo *et al.*, 2003; Castelle *et al.* 2007).

3.2.2.3 HCl extraction

The so-called reactive (HCl 1N acid-soluble) fraction comprises metals associated with amorphous and crystalline Mn and Fe oxides, carbonates, hydrous Al silicates (Huerta-Diaz and Morse 1990, 1992) and acid volatile sulphides (AVS) not including the oxidation products of Fe monosulphides (goethite and hematite; Raiswell *et al.*, 1994). The acid-soluble fraction was also empirically designated to extract most of the potentially bioavailable trace metals (Bryan and Langston, 1992; Langston *et al.*, 1999). For this, 200 mg of dry sediment and 12.5 ml of HCl 1N were placed in previously HCl cleaned Teflon® centrifuge tubes and then placed in a rotary shaker for 24 h at 12 rpm (Castelle *et al.*, 2007). Once the extraction was finished, the pH of the supernatant was measured.

3.2.2.4 Total attack

In this attack, the crystalline matrix of the suspended matter is digested with acid leaving metals in the solution for analysis. This procedure was carried out in three stages and in this occasion the material was previously cleaned with HNO_3 10 % during three days, washed three times with Milli-Q water and dried in hood under laminar flux.

Stage 1: Attack

Grounded samples were weighted and 30 mg were placed on attack tubes. To this, 750 µl of suprapur® HNO_3, 1.5 ml of suprapur® HCl and 2.5 ml of suprapur® HF were added. The tubes were covered with watch glasses and placed in a hot plate at 110°C for 2 h.

Stage 2: Evaporation

After samples cooled, the watch glass was removed and rinsed with Milli-Q water. The tubes were replaced on the hot plate at 110°C for 6 h to evaporate the water and the acids.

Stage 3: Recovery

In this step, 250 µl of suprapur® HNO_3 and 5 ml of Milli-Q water were added to the evaporation residue. The tubes were closed and replaced on the hot plate at 65°C for 30 mn to

accelerate the dissolution. Once the solution cooled, 3.5 ml of supernatant and 6.4 ml of Milli-Q water were placed on a 10 ml tubes and stored for later analysis.

From these attacks two kind of samples were obtained: the solid residue (reducible fraction - Hg_{asc}, oxidisable fraction - $Hg_{H_2O_2}$and acid-soluble/reactive fraction - Hg_{HCl}) and the supernatants fractions (ascorbate, HCl and total). All of them were stored and kept for further analyses.

3.2.3 Mineral characterization

3.2.3.1 Granulometry

Sample sizes determinations were performed with a laser granulometer Malvern Mastersizer S (Fig. 3-4) in the EPOC laboratory (Université de Bordeaux 1).

The particles to be measured were diluted in a beaker of 0.6 to 1 litre and then put into circulation in traversed cell crossed by parallel laser beam. Particles illuminated by the laser deviate the light from its main axis. The amount of deflected light and the extent of the deflection of the angle allow to measure the particle size. Thus, larger particles sizes deviate significant amounts of light on low angles while small particles deviate tiny amounts of light but on wider angles. Intensities received at different angles by the detector are digitized and analyzed by calculation using the Mie theory (Mie, 1908). This mathematical theory, interpreting the light scattered by a particle, is modelled for solid spheres. That is to say that the particles are treated as equivalent spheres. The calculation result is shown as a distribution curve of particles (http://lecob.obs-banyuls.fr). Laser micro-granulometry gives a distribution of particle volume. The analytical range varies approximately between 0.05µm - 900µm.

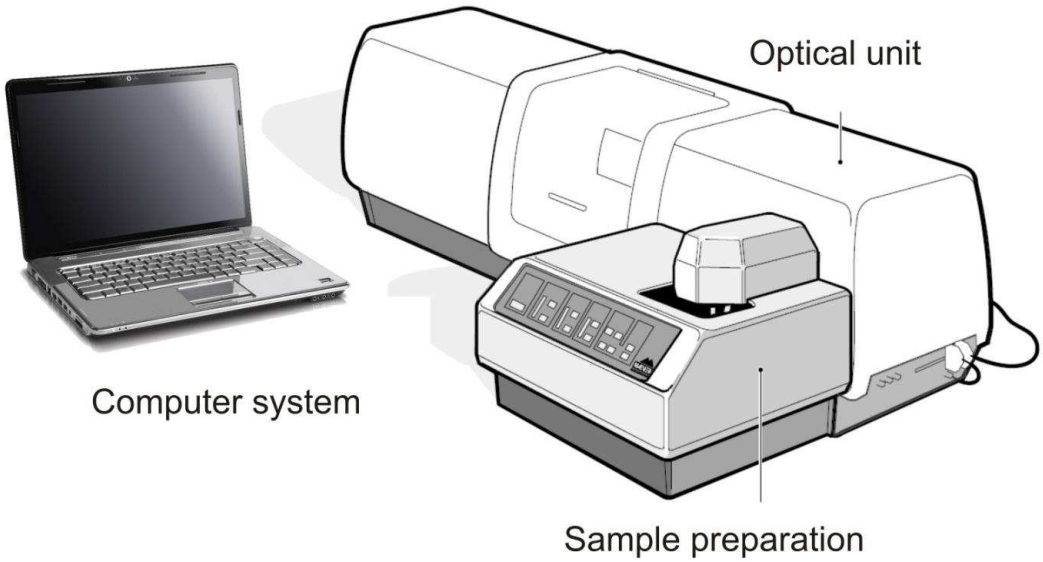

Fig. 3-4: Laser granulometer equipment. Malvern Mastersizer S (Malvern Mastersizer, 1997).

3.2.3.2 X-Ray Diffractometry (XRD) Analysis

The mineral composition was determined on sediments with a SIEMENS D500 X-ray diffractometer (XRD) that has a theta/2theta goniometer and works with a Cu anode (Cu Kalpha= 1.5406 Å). The X-ray diffraction results from the interaction between X-rays and the electrons of atoms. Depending on the atomic arrangement, interferences between the scattered rays are constructive when the path difference between two diffracted rays differ by an integral number of waveleghts. This selective condition is described by the Bragg equation, also called "Bragg's law" (Will, 2006):

$$2d_H \sin \Theta_H = n\lambda \quad \text{(Eq. 6)}$$

Where λ is the wavelength;

d_H the d-spacing and Θ_H the Bragg angle, which is half the angle between incident and reflected beam;

H describes the Miller indices triple *hkl* of each lattice plane.

This method provides information such as types and nature of crystalline phases present or structural make-up of phases. It consists in irradiating a material with a parallel beam of monochromatic X-rays. The atomic lattice of the sample acts as a three dimensional diffraction grating causing the X-ray beam to be diffracted to specific angles. The diffraction pattern, that includes position (angles) and intensities of the diffracted beam, provides information about the sample. In case of pure phase, the diffractogram obtained is always the same and can be described by Miller indices (Warren, 1969; Klug and Alexander, 1974). The diffraction spectrum consists of a plot that reflects intensities in the y axis and the 2Θ detector angle in the x axis.

Samples were previously dried and were not orientated. The analysis was performed between 4 and 90° of 2Θ with a scan step of 0.02° and a step duration of 2 seconds.

3.2.3.3 X-Ray Fluorescence (XRF) analysis

Some major and minor elements (Al, Si, K, Ti, Fe, Zr, Mn, Sr, S, Cl and Ca) were measured on one of the halves of the core through X-ray fluorescence (XRF) with an Avaatech XRF Core – Scanner with a 1mm resolution. The equipment uses a 58 kV X-ray voltage and an X-ray current of 10 mA. This is a well-established analytical technique for estimating the composition of rocks and sediments (Ramsey *et al.*, 1995; Jenkins, 1999; De Vries and Vrebos, 2002).

The principle of XRF analysis is based on excitation of electrons by incident X-radiation. Ejection of electrons from inner atomic shells creates vacancies which are filled by electrons falling back from the outer shells, whereby surplus energy is emitted as a pulse of secondary X-radiation. Emitted fluorescence energy and wavelength spectra are characteristic for atoms of specific elements, which permit estimation of their relative abundances (Jansen *et al.*, 1998; Wien *et al.*, 2005; Ge *et al.*, 2005; Weltje and Tjallingii, 2008). This is an increasingly accepted method as an effective way of obtaining high-resolution elemental records because of its non-destructive and nearly continuous measurements (Croudace *et al.*, 2006; Jansen *et al.*, 1998; Rothwell and Rack, 2006; Thomson *et al.*, 2006). Environmental changes, diagenetic processes and pollutant inputs can be deduced by elemental variations determined by XRF core scanning, as well as it can assist in sediment correlation and process studies (Rothwell and Rack, 2006). The measurements obtained by XRF reflect the composition of a

thin (sub-mm) layer on top of the sediment surface where the intensities of the different elements are expressed as counts per second (cps). The counts should be proportional to the concentration of the element in the sediment but the signal might be attenuated or enhanced by the presence and concentrations of other elements (Löwemark *et al.*, 2011; Liang *et al.*, 2012). Fluctuations along the core do not necessarily mean that there has been an increase or decrease in the flux of a certain element. Usually these variations are given by the deposition rate of the diluting agent, which in lakes it is often the organic matter. This effect is handled by using a conservative element for normalizing. The use of Al for this purpose allows to address the relative variations in the lithogenic component of the sediment (Löwemark *et al.*, 2011). Water content, surface roughness and grain size variations are other sedimentary factors that have an influence over XRF measurements (Böning *et al.*, 2007, Tjallingii et al, 2007; Weltje and Tjallingi, 2008).

3.2.4 Chemical characterization

3.2.4.1 Measurements of pH

The pH values were measured in 1:10 suspensions prepared with samples collected every 5 mm along the LP core using a multi-parameter analyzer (pH meter Consort C561, previously calibrated).

3.2.4.2 Total and Organic Carbon and sulphur

Total and Organic Carbon (C_{org}) and sulphur were determined on sediments of the LP core using a carbon/sulphur LECO CS 125 analyzer (Fig. 3-5a). For the C_{org} analysis, samples were previously acidified in crucibles (Fig. 3-5b) with 2N HCl to destroy carbonates, and then dried at 60°C for 24 hours to remove inorganic C and most of the remaining acid and water (Etcheber *et al.*, 1999).

During measurement, an almost complete oxidation of compounds occurs by combustion at 850°C in an induction furnace under an oxygen flow. The oxygen stream carries the oxidized compounds (SO_2 and CO) into a first infrared cell where SO_2 is detected. The SO_2 and CO compounds are oxidized again through a catalyst (Cu/Pt). The SO_3 formed from SO_2 is captured by a cellulose trap while the CO_2 formed from CO is carried to a second infrared

detection cell (Cauwet *et al.*, 1990). Quality was checked by measuring certified reference materials (e.g. LECO 501–503) and intercalibrations; the accuracy of the measurement is better than 5 % (e.g. King *et al.*, 1998).

Fig. 3-5: Total and Organic Carbon analysis – a) Treated samples with HCl and b) LECO device

3.2.4.3 Determination of major ions

Major ions (except for HCO_3^-) were measured in the laboratory of EA 4592 Géoressources & Environnement, ENSEGID with ion liquid chromatography (Dionex 320 IonPac CS16 for cations and 1100 Dionex IonPac AS11-HC for anions). The quality of the analysis was systematically controlled by calculating the ionic balance. Analyses with a balance greater than 10 % were rejected.

3.2.4.4 Inductively Coupled Plasma (ICP)

- ***Mass Spectroscopy (MS)***

Inductively coupled plasma Mass Spectrometry allows nearly simultaneous measurement of different isotopes of one or more elements. Conventionally, the solution sample is introduced with a peristaltic pump into a steam chamber (fog) where it is transformed into a mist of very fine droplets using argon gas. The formed aerosol is sent in an argon plasma held in a quartz torch at high temperatures (between 6000 and 10000°C), sufficient to completely ionize most

elements. Less than 10 % of the formed ions pass through a differential pumping chamber through the opening of an interface in nickel (1 mm "sampler" cone) and then move into the area of high vacuum (up to 10^{-6} Pa) by a second orifice ("skimmer" cone). In the high vacuum zone, a plurality of electrostatic lenses extracts the positively charged ions and transports them to the quadrupole mass spectrometer. This mass filter transmits only the ions having a particular mass to charge (m/z) determined by the magnetic field applied to the quadrupole. The separated ions are then transmitted to the detector and the signal is transformed into number of pulses (Castelle, 2008).

Samples were sent to the Actlabs laboratory (Canada) to determine trace elements. Samples were previously acidified with nitric acid and analyzed by Perkin Elmer Sciex ELAN 9000 ICP-MS, Perkin Elmer Nexion, Thermo icapQ or Agilent 7700. A blank and two water standards were run at the beginning and end of each group of 32 samples. A reagent blank was run at the beginning of group and every 10^{th} sample was run in duplicate. Detection limits range from 0.001 to 700 μg L^{-1}depending on the element that was analyzed.

- ***Optical Emission Spectrometry (OES)***

The OES also receives a portion of the photons emitted by the ICP and here is where the detection difference with MS is based. A portion of these emitted photons are collected with a lens or a concave mirror. This focusing optic forms an image of the ICP on the entrance aperture of a wavelength selection device such as a monochromator. The particular wavelength exiting the monochromator is converted to an electrical signal by a photodetector. The signal is amplified and processed by the electronic detectors, then displayed and stored by a personal computer (Hou and Jones, 2000).

Samples were analyzed in the laboratory of the EA 4592 Géoressources & Environnement, ENSEGID with a Thermo Scientific iCAP 6000 Series ICP Emission Spectrometer. Two blanks and two standards were measured along with the other samples.

3.2.4.5 Cold Vapour Atomic Absorption Spectrometry (CV-AAS)

Mercury concentrations were determined by Cold Vapour Atomic Absorption Spectrometry (CV-AAS) after incineration with O_2 flux (Fig. 3-6) in ~70-100 mg grind, dry sediment samples. In the atomic absorption, the amount of energy absorbed by the Hg atoms when they

are excited is determined. This absorbance (A_λ) depends on the amount of Hg present (q). According to Beer-Lambert law:

$$A_\lambda = \log \frac{I_0}{I_t} = \varepsilon_\lambda \times l \times q \quad \text{(Eq. 7)}$$

Where ε_λ is the molar absorption coefficient;

l is the optical path length;

I_0 is the initial intensity of the light source (reference radiation);

I_t is the transmitted intensity after passing through the sample.

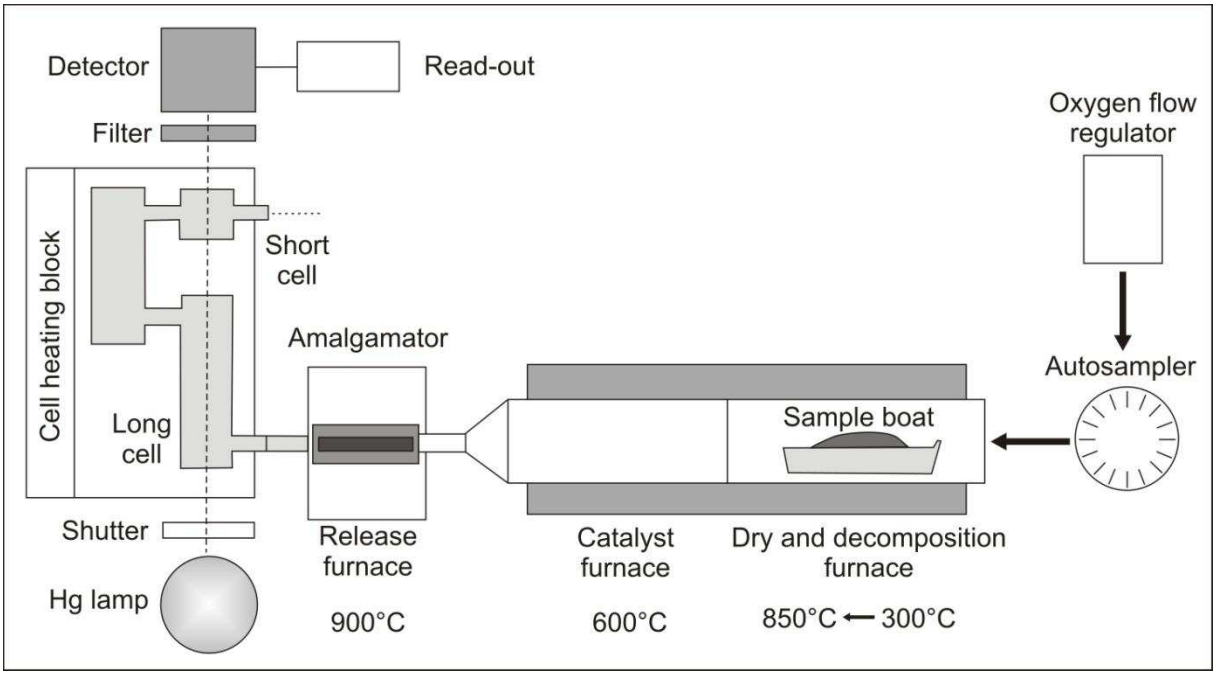

Fig. 3-6: Schematic sampling processing system of DMA equipment (adapted from http://www.milestonesrl.com).

The equipment used for the analysis is the MILESTONE, Direct Mercury Analyzer 80 (Fig. 3-7) in the EPOC laboratory (Université de Bordeaux 1). Firstly, the weighted sample is dried and then thermally decomposed at high temperatures (first 300°C and then 850°C) in an oxygen flow. Combustion products are carried to another furnace at 600 °C containing a catalytic tube that allows gas decomposition and reduction of mercury in Hg^0. Mercury

vapours are trapped on a gold amalgamator and subsequently desorbed for quantitation. The mercury content is determined using atomic absorption spectrophotometry at 254 nm. All this steps are handled automatically by the same device, which also has the advantage of performing the analysis directly from the grind sample, avoiding contamination by the addition of chemical reactive. The quality of the analytical results was systematically checked analyzing international certified sediment reference materials (LKSD-4, IAEA 433, 1646a) every set of 5 samples and concentrations were expressed in μg kg^{-1} dry weight. The detection limit (3 times the standard deviation of 5 blank values) varied daily from 1 to 2 μg kg^{-1}.

Fig. 3-7: Direct Mercury Analyzer (DMA) 80 MILESTONE – a) Analyzer device, b) Auto-sampler tray, c) Read-out terminal.

3.2.4.6 Flow Injection Analysis System (AAS - FIAS)

Determinations of the arsenic concentrations were carried out in the EPOC laboratory with an atomic absorption spectrophotometer (Perkin-Elmer – AAnalyst 300) coupled to a flow injection analysis system (FIAS), an autosampler and an arsenic electrodeless discharge lamp (EDL). Samples were pre-reduced with a solution of KI and Ascorbic acid. Two solutions were prepared that served one as reductant (0.5 g of NaOH and 5 g of $NaBH_4$ in 1000 ml of MilliQ water) and the other one as a carrier (solution of HCl 10 %). There is an hydride formation when the As(III) reacts in an acidic solution with $NaBH_4$ according to the reaction (McCleskey *et al.*, 2003):

$$3NaBH_4 + 4H_3AsO_3 \rightarrow 4AsH_3\,(g) + 3H_3BO_3 + 3NaOH$$

The reaction mixture is purged with a stream of argon through a gas/liquid separator. The liquid is pumped to waste and the argon flow carries the arsenic hydride to a heated quartz absorption cell for measurement by atomic absorption spectrophotometry (Fig. 3-8).

3.2.4.7 Flame Atomic Absorption Spectrometry (FAAS)

Another technique that was used in the EPOC laboratory is the flame atomic absorption spectrometry (FAAS; Perkin Elmer AAnalyst 300). The principle is based on the absorption of light energy by atoms. The sample is nebulised and atomized (thermal dissociation into free atom) in a flame (FAAS). An electrode lamp emits a radiation (specific to the element that is going to be analyzed) through the flame. The atoms absorb the energy emitted to remain in an excited state.

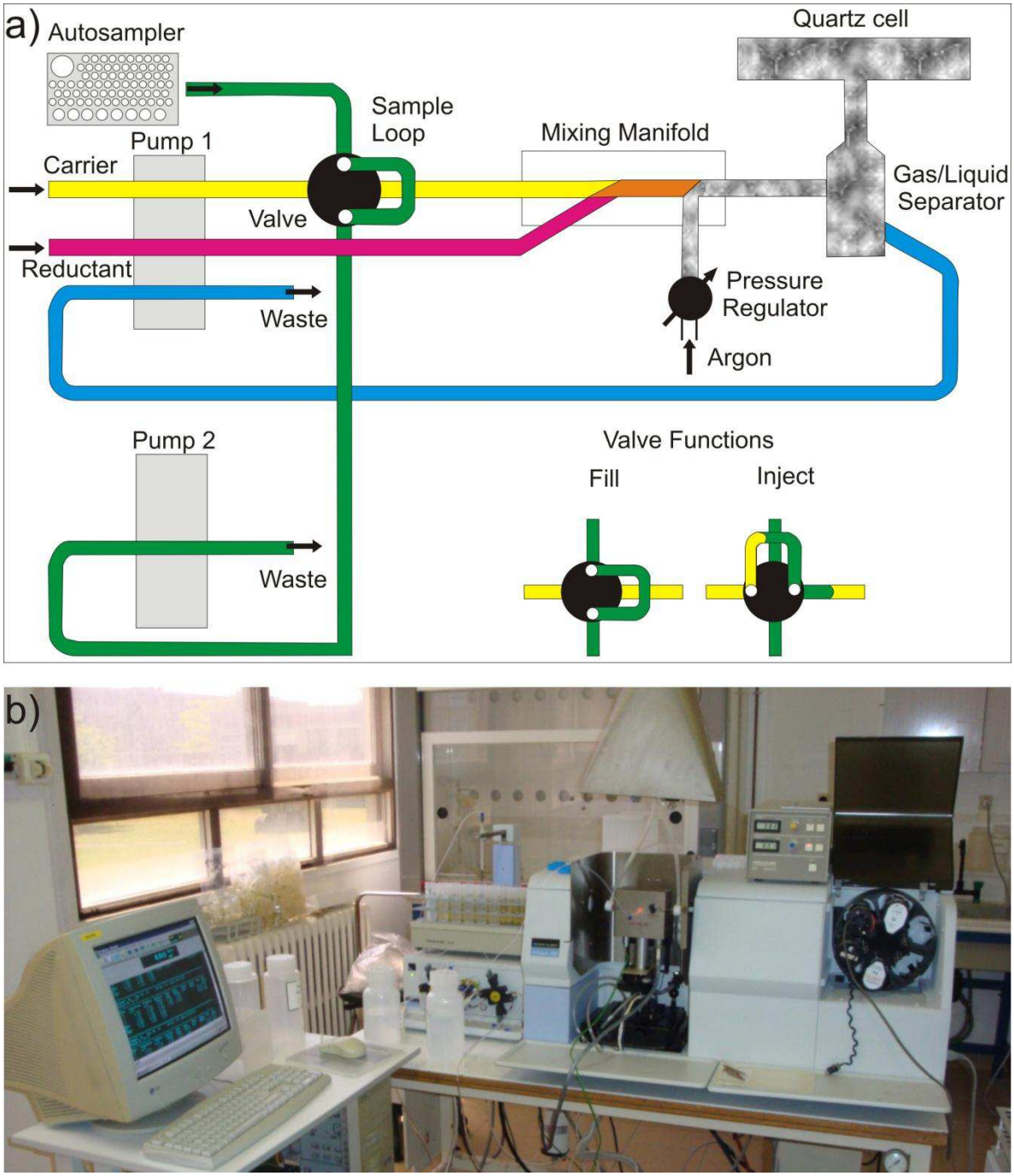

Fig. 3-8: Flow Injection Atomic Absorption Spectrophotometry, a) Schematic operation diagram of FIAS 300 (modified from Hineman, 2011) b) Measurement equipment at EPOC laboratory.

3.2.5 Summary

A wide series of analysis have been performed to different kind of samples, either solid or liquid and after the extraction processes. A list summarizing the sample type, analysis and method used is presented in Table 3-1.

Sample Type	Analysis	Method
Riverbed sediments LP core	Mineralogical	XRD
LP core	Mineralogical	XRF
LP core	Granulometry	Laser granulometry
LP core	Carbon and Sulphur	Complete Oxidation
River and lake water samples	Major Ions	Chromatography
River and lake water samples	Major and Minor Elements	ICP-MS
Total supernatant	As Fe and Mn	ICP-OES FAAS
Ascorbate and HCl Supernatants	As	AAS-FIAS
Hg_{asc}, Hg_{H2O2} and Hg_{HCl} fractions	Hg	CV-AAS
Ascorbate and HCl Supernatants	Fe and Mn	FAAS

Table 3-1: List of sample type, analysis and method used for this work.

3.3 Satellite Image treatment

3.3.1 Contributions of satellite images

It is well known that the entire Mar Chiquita system suffers changes in its size due to the climate changes that originates in South America, as Piovano *et al.* (2002, 2004a) described this area as a "sensitive climate indicator". Beyond that, records that quantify the surface occupation of this system are scarce. In order to study this change in size satellite images from Landsat 5 TM (Thematic Mapper), Landsat 7 ETM+ (Enhanced Thematic Mapper Plus) and the recently launched Landsat 8 LDCM (Landsat Data Continuity Mission - February 11, 2013) images were analyzed with the software ArcGIS version 10.1 (©ESRI 1999-2013). ArcGIS is a comprehensive system that allows people to collect, organize, manage, analyze, communicate, and distribute geographic information (http://resources.arcgis.com).

Remote sensing uses the properties of emission and/or reflexion of radiation. These rays are electromagnetic waves, carrying energy, which propagate without attenuation in the void but are more or less absorbed in different environments. Solar radiation is the external energy input to the Earth. A body whose temperature is greater than 0K emits electromagnetic radiation. It plays the role of source transforming part of the thermal energy into radiant energy. The fraction of absorbed radiation serves for changing the internal energy of the body which will result in an emission in another wavelength. There are several Remote Sensing Systems that register these emissions depending on the wavelength (Fig. 3-9), Girard and Girard (2010).

The Landsat Program is a serie of Earth-observing satellite missions jointly managed by NASA and the U.S. Geological Survey (http://landsat.gsfc.nasa.gov/) that started in 1972. Landsat 5 images are taken with a Thematic Mapper (TM) sensor. These images have data files that consist of seven spectral bands with a resolution of 30 meters. The Landsat 7 images were acquired with an Enhanced Thematic Mapper Plus (ETM+) sensor. These images consist of eight spectral bands with a spatial resolution of 30 meters for bands 1 to 7. The panchromatic band 8 has a resolution of 15 meters. Landsat 8 is the latest satellite sent and the one that covers wider spectra. Table 3-2 shows the characteristics for each band and for the three satellites (5, 7 and 8). All satellites have a 16-day repeat cycle, the approximate scene

size is 170 km north-south by 183 km east-west. The map projection is given in the geodetic system WGS 84 and UTM (Universal Transverse Mercator) projection.

Landsat uses as well the Worldwide Reference System (WRS) where each scene is designated by a path and a row. Sequential path numbers are from east to west to 233 nominal satellite orbital tracks, starting with number 001 for the first track which crosses the equator at 64.60 degrees west longitude. Row refers to the latitudinal centre line of a frame of imagery. As the satellite moves along its path, the observatory instruments are continuously scanning the terrain below with a 5 per cent overlapping. The combination of a Path number and a Row number uniquely identifies a nominal scene centre. The study area is covered by the Path 228 and 229 and the Row 081. Images corresponding to the Path 229 that include the westernmost part of Laguna Mar Chiquita have line gaps hence only images on the path 228 were analyzed. Images were downloaded with free access from http://landsatlook.usgs.gov/, spanning a period from 1986 to 2013. Previous satellite images are not available in free access. Among all the satellite images available, only those who were georeferenced and had a maximum of cloud cover of 20 % were chosen, making a total of 14 satellite images to analyze.

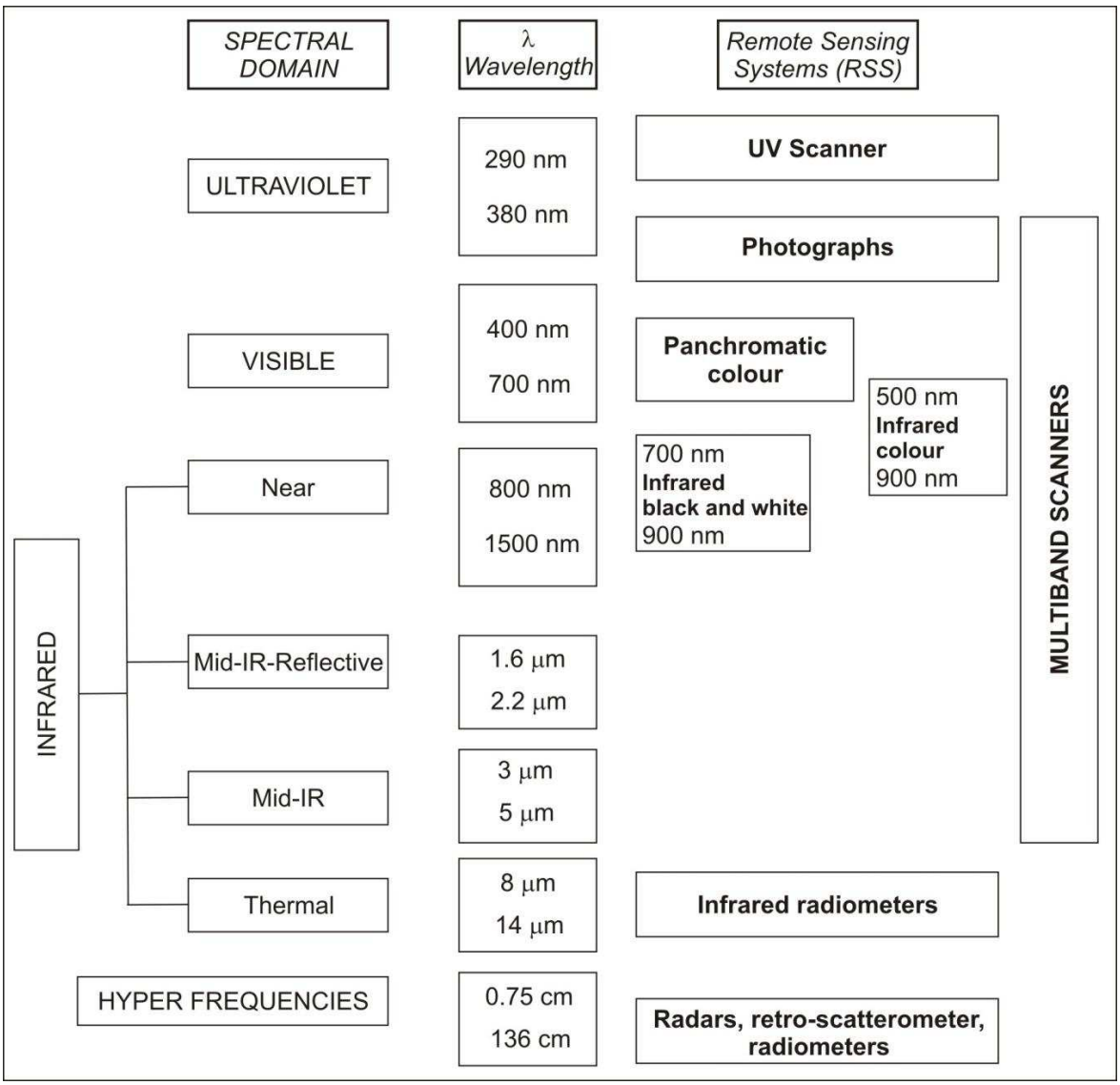

Fig. 3-9: Electromagnetic spectra and Remote Sensing System adapted from Girard and Girard (2010).

LANDSAT						
	5 - TM	7 - ETM+	8 - LDCM	5 - TM	7 - ETM+	8 - LDCM
Band	Wavelength (µm)			Resolution (m)		
1	0.45-0.52		0.43 - 0.45	30		
2	0.52-0.60		0.450 - 0.51	30		
3	0.63-0.69		0.53 - 0.59	30		
4	0.76-0.90	0.77-0.90	0.64 - 0.67	30		
5	1.55-1.75		0.85 - 0.88	30		
6	10.40-12.50		1.57 - 1.65	120* (30)	60** (30)	30
7	2.08-2.35	2.09-2.35	2.11 - 2.29	30		
8		0.52-0.90	0.50 - 0.68	15		
9***			1.36 - 1.38			30
10***			10.6 - 11.19			100
11***			11.5-12.51			100

Table 3-2: Main characteristics for Landsat 5, 7 and 8 bands. * TM Band 6 was acquired at 120-meter resolution, but products processed before February 25, 2010 are resampled to 60-meter pixels. Products processed after February 25, 2010 are resampled to 30-meter pixels. ** ETM+ Band 6 is acquired at 60-meter resolution. Products processed after February 25, 2010 are resampled to 30-meter pixels. ***Information that corresponds to Landsat 8 (http://landsat.usgs.gov).

Images in this study area show mainly water bodies and agricultural lands. As the aim of this remote sensing work was to delimitate the size variation of the lakes, the analysis was based on this criteria. In the near and middle infrared portion of the electromagnetic spectrum, water bodies absorb almost all incident radiant flux while the land surface reflects significant amount of near and middle infrared energy (Bagli and Soille, 2004), thus it exist a marked contrast between them. Landsat bands 3 and 5 are shown in Fig. 3-10 a and b respectively. Band 3 is sometimes called the chlorophyll absorption band because vegetation absorbs nearly all red light so this band can be useful for distinguishing between vegetation and soil and in monitoring vegetation health (http://gif.berkeley.edu). On the other hand, this figure shows the high contrast existing between land and water bodies in band 5. Different studies (Johnston and Barson, 1993; Frazier and Page, 2000; Bagli and Soille, 2004) were done using the band 5 for classification and delimitation of water bodies. Bands 4 and 7 are also on the infrared spectrum and useful for locating water bodies but tend to include more errors of

commission (Frazier and Page, 2000). That is the reason why the delimitation of water bodies, especially for Laguna del Plata, was based on the band 5.

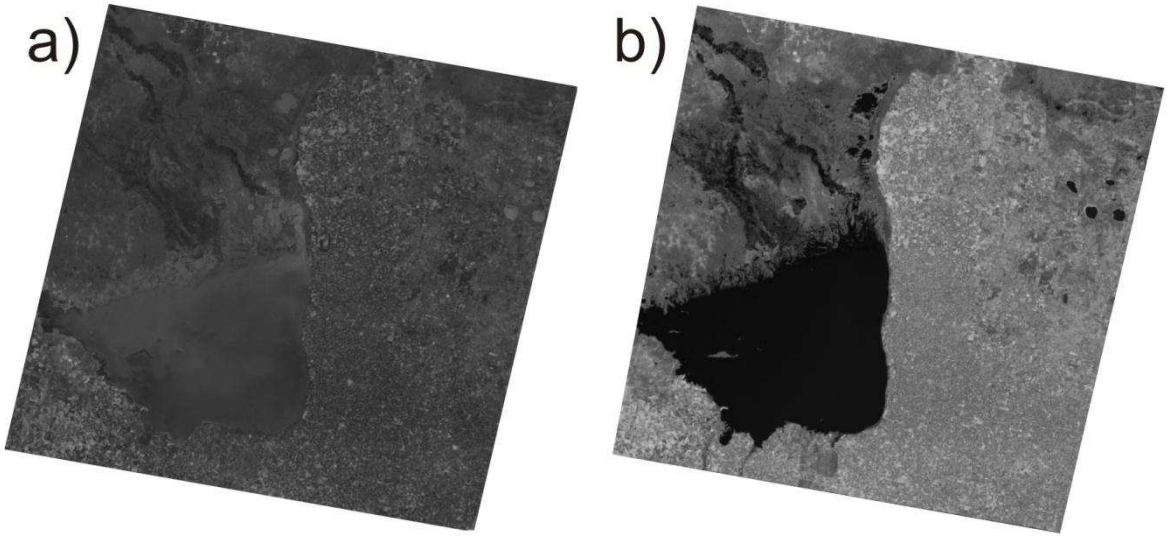

Fig. 3-10: Differences in contrast between bands 3 (a) and 5 (b) of a same satellite image from December 25th, 2000.

3.3.2 Image treatment with ArcGIS

With the aim of analyzing the size variation in Mar Chiquita system a comparison method was performed using separate classification of images (always band 5 of each image) acquired at different times and quantifying the different sizes between those time intervals. ArcGIS is an useful tool that allows to make a *Supervised Classification* which is used mostly for the quantitative analysis of remote sensing data. It uses suitable algorithms to label the pixels in an image as representing particular ground cover types, or classes. There are some practical steps for the classification that include (Richards and Jia, 2006):

- Decide the set of ground cover types into which the image is going to be segmented. They could be cloud, water, croplands, etc.

- Choose a representative or prototype pixels from each of the desired classes (*training data*). Often, training pixels for a given class lie in a common region enclosed by a border. This region is called *training field*.

The Maximum Likelihood Classification is the most common supervised classification method used with remote sensing image data (Richards and Jia, 2006) and is based on the assumption that training areas datasets have a normal distribution, which involves the construction of probability contours (Gibson and Power, 2000).

When working on the image (raster data), several training fields are designed. As it was mentioned before, the purpose was to separate water and land therefore the training fields are constructed having this idea as a base (Fig. 3-11a). So as to perform the classification, these training fields have to be reorganised in their classes which are going to be "water" mainly for the lake area, and the rest is going to be "land" (Fig. 3-11b). No classification is going to be taken into account for the area that corresponds to wetlands.

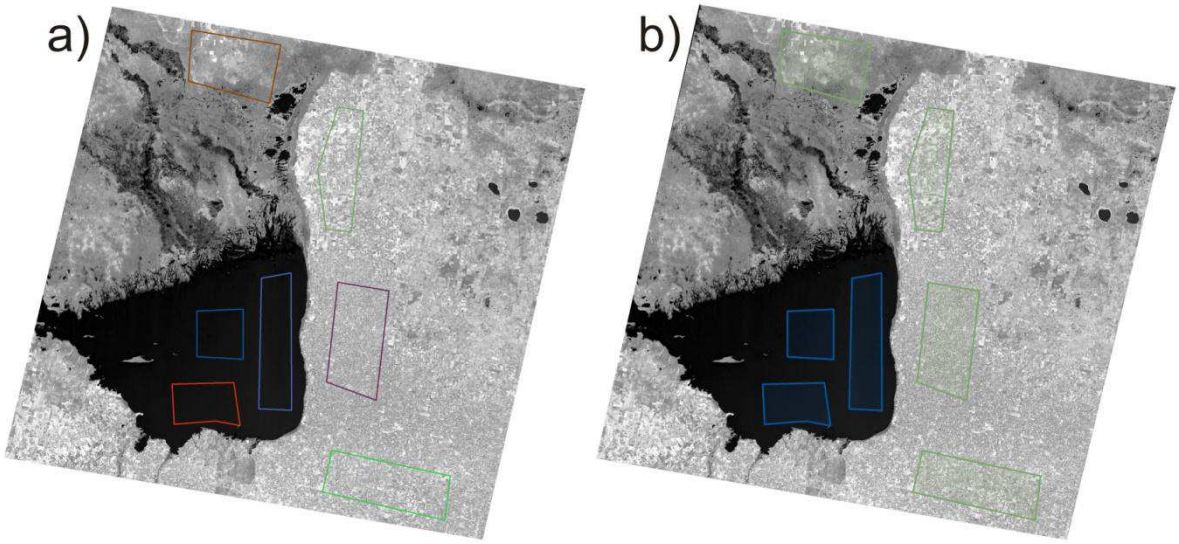

Fig. 3-11: Raster of band 5 showing the training fields (a) and (b) shows training fields already classified. Class "water" corresponds to the polygons in blue and "land" ones those in green.

Once this classification is done, the Maximum Likelihood Classification is run, providing a new raster in which two colours corresponding to the imposed classes are shown (Fig. 3-12a). From this raster is possible to transform both classes into polygons and thus obtaining the quantification of the area for the lake. As it is possible to see in the Fig. 3-12a, the water classification includes not only the lake extension but the wetlands located North from Mar Chiquita. These polygons corresponding to the wetlands were not included into the calculation area. The polygon taken into account was the biggest one that includes the main water body. The final polygon corresponding to this band and on which it is possible to calculate the area is shown in Fig. 3-12b.

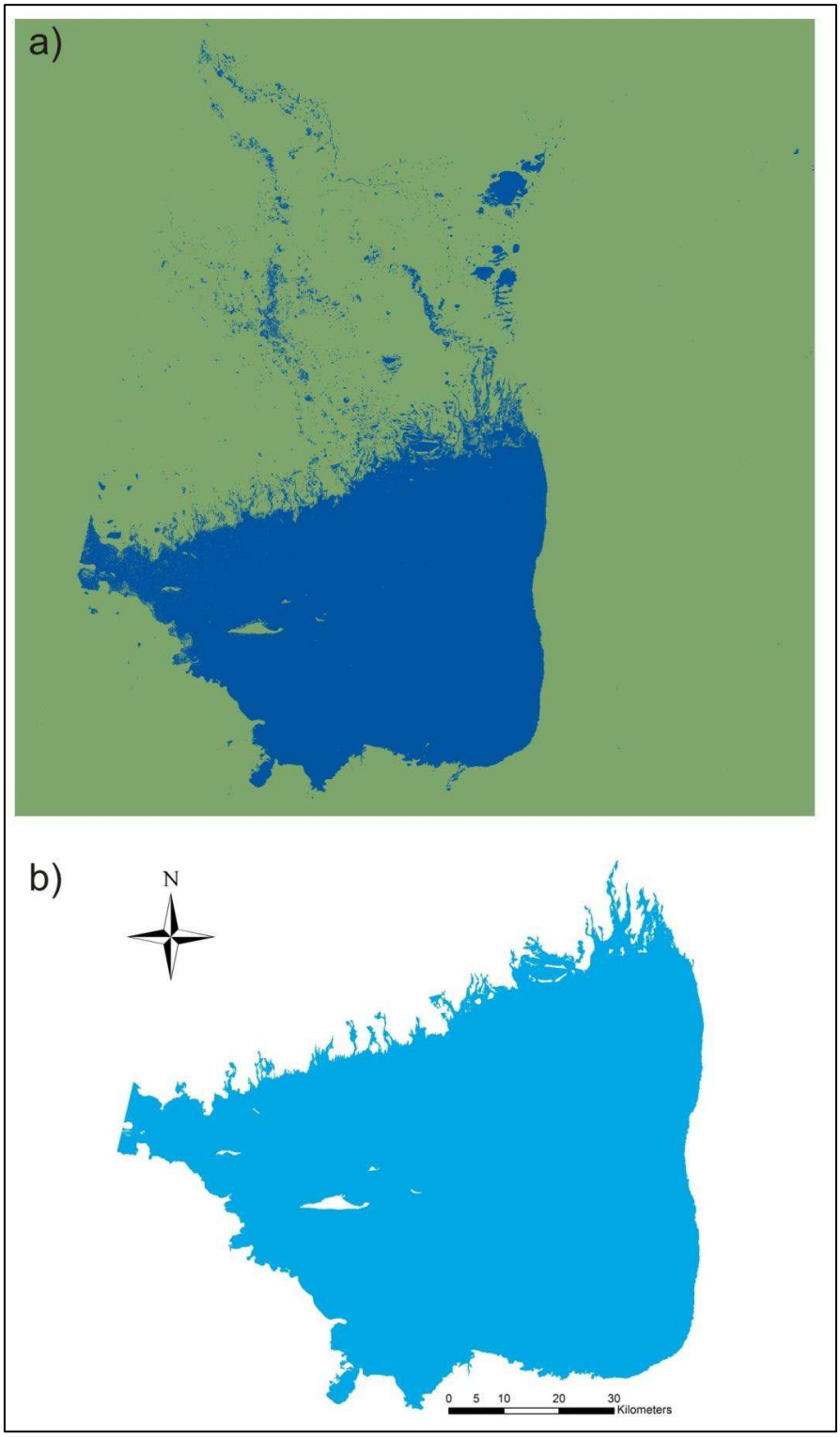

Fig. 3-12: a) Thematic map produced by Maximum Likelihood classification. Blue represents water and green represents land that includes the "rest" besides water; b) Final image showing the main polygon that contains Laguna Mar Chiquita.

For the analysis of Laguna del Plata (LP), a *mask* (a dataset that defines which locations in the inputs will be considered in the execution of the tool - http://resources.arcgis.com) was created in order to use only the part of the raster that includes this lake (Fig. 3-13a). The criteria to create the mask were taking into account the maximum and minimum extensions during this studied period of 26 years. Once that the mask was selected, a new raster is created englobing only the LP lake (Fig. 3-13b). The rest of the analysis was preceded in the same way as with Laguna Mar Chiquita until obtaining the final polygon (Fig. 3-13c).

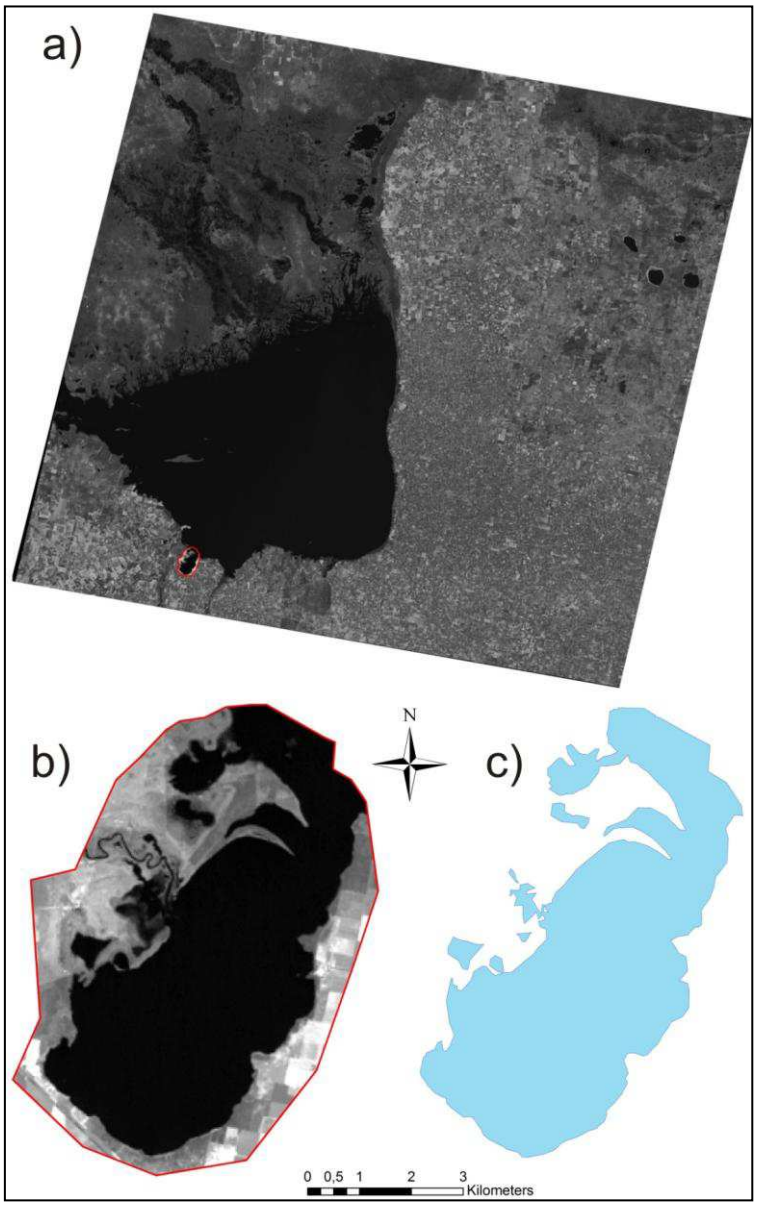

Fig. 3-13: Image a) shows the location of LP and its respective mask in red, b) is the crop of the raster generated by the mask and c) is the final polygon obtained for LP after the Maximum Likelihood Classification.

4. Results

4.1 Geochemical characterization of the basin

The sources of major dissolved ions (Ca^{2+}, Mg^{2+}, Na^{+}, K^{+}, Cl^{-}, SO_4^{2-}; HCO_3^{-}) are multiple such as rainfall inputs, weathering, dissolution of evaporitic minerals or leached during rainstorms (Garrels and Mackenzie, 1971; Drever, 1988; Stallard, 1995a,b). The deposition places or sinks are also multiple like lakes or river beds during their drying stage (Gibbs, 1970; Meybeck, 2003) and there is a growing evidence of active recycling of most of major elements which suggests that each element may have manifold natural sources and sinks (Likens *et al.*, 1977; Meybeck, 2003). Among the factors that control major ions are climate, water runoff (that increases weathering), higher lake residence times, tectonic (especially in recent mountain ranges, rift and/or volcanic regions) (Meybeck, 2003) and lithology, being this one an essential factor in determining river chemistry (Garrels and Mackenzie, 1971; Drever, 1988). Human activities in particular mining, chemical industries, urbanization and agriculture (through the use of fertilizers) have also altered the river chemistry (Meybeck *et al.*, 1989; Flintrop *et al.*, 1996). Comparisons of regular surveys done from the 1960s with those of hundred years ago reveal a worldwide increase in Na^{+}, Cl^{-} and SO_4^{2-} concentrations due to the anthropogenic impact, whereas Ca^{2+}, Mg^{2+} and HCO_3^{-} concentrations are more stable (Meybeck *et al.*, 1989; Kimstach *et al.*, 1998). It is widely known that SO_4^{2-} is a parameter highly sensitive to anthropic influence.

4.1.1 Aquatic geochemistry

With the aim to evaluate if physicochemical changes occur in the Suquía River basin and the lakes major ions as well as conductivity, total dissolved solids (TDS), temperature, pH and dissolved oxygen (DO) were measured. These parameters for the river and lake water samples are presented in

Table 4-1. A clear geochemical gradient is observed from the catchments to the mouth of the river. River waters at the basin catchments are diluted and slightly saline near the river mouth (43 to 1340 $\mu S\ cm^{-1}$). In the lake, waters are highly saline, showing conductivity values that range from 78100 to 126300 $\mu S\ cm^{-1}$. This trend is also noticeably for the pH values: neutral pH values predominate in the catchments and they become increasing alkaline downflow,

ranging from 7.20 to 8.47. Lake waters are markedly alkaline, with pH values ranging from 8.27 to 9.25 (
Table 4-1and Fig. 3-1).
A chemical gradient was also observed in lake water samples for those located near the surface and in depth. Surface samples were collected at ~20 cm from the surface and those in depth were collected at ~4 m for samples corresponding to Laguna Mar Chiquita and at ~1.4 m for samples gathered in Laguna del Plata (they are marked with S or D after the sample name –
Table 4-1). Deeper waters present higher values in conductivity and Total Dissolved Solids (TDS) for both lakes. In LP, deeper waters present lower pH values and cooler temperatures that in surface. Dissolved Oxygen also shows lower concentrations in deeper waters near to the bottom of the lake. Furthermore, major ions present higher concentrations in depth than in surface except for NH^{4+}.

Following the Piper classification (Fig. 4-1), waters in the basin's catchments are of the Ca^{2+}-HCO_3^- type and they evolve downflow to Na^+-Cl^--SO_4^{2-} type. Major ion compositions for 14 samples were also represented on Stiff diagrams (Fig. 4-2) in order to depict the geographical distribution of these different water types. Before entering to the city of Córdoba, river waters are of the calcium-bicarbonate-type (RS5 and RS6). Once in the urban area they change their composition from calcium-sulphate into sodium-sulphate type (RS4, ALC, RS3, RS2 and RS1) and in the lower part of the basin, waters are clearly of the sodium-sulphate type with an increment of Na^+ and Cl^- in samples RS7 and RS8. Concerning lake waters they are saline to brine waters of a clearly marked sodium-chlorided type.

	Sample	Date	Cond. $\mu S\ cm^{-1}$	TDS $g\ L^{-1}$	T°C	pH	Na^{+} $meq\ L^{-1}$	K^{+} $meq\ L^{-1}$	Ca^{2+} $meq\ L^{-1}$	Mg^{2+} $meq\ L^{-1}$	NH^{4+} $meq\ L^{-1}$	F- $meq\ L^{-1}$	HCO_3^{-} $meq\ L^{-1}$	Cl^{-} $meq\ L^{-1}$	SO_4^{2-} $meq\ L^{-1}$	NO_3^{-} $meq\ L^{-1}$	DO $mg\ L^{-1}$
River samples	RCQ1	13/12/2011	72	0.04	23.2	7.61	0.33	0.03	0.31	0.09	*nd*	*nd*	*nd*	*nd*	*nd*	*nd*	*nd*
	RCQ2	13/12/2011	88	0.04	22.4	7.63	0.42	0.05	0.32	0.12	*nd*	*nd*	*nd*	*nd*	*nd*	*nd*	*nd*
	RSA	13/12/2011	43	0.02	22.1	7.20	0.14	0.02	0.18	0.05	*nd*	*nd*	*nd*	*nd*	*nd*	*nd*	*nd*
	RS10	13/12/2011	294	0.15	22.7	7.95	1.11	0.08	1.06	0.31	*nd*	*nd*	*nd*	*nd*	*nd*	*nd*	*nd*
	RSDN	13/12/2011	866	0.43	21.6	8.30	3.27	0.25	3.98	1.70	*nd*	*nd*	*nd*	*nd*	*nd*	*nd*	*nd*
	RS6	01/07/2010	310	0.15	11.7	8.47	1.30	0.09	1.80	0.60	0.05	0.04	2.88	0.26	0.71	0.16	*nd*
	RS5	01/07/2010	320	0.15	11.1	8.17	1.42	0.09	1.84	0.61	0.02	0.01	2.62	0.18	0.84	0.22	*nd*
	RS4	01/07/2010	530	0.27	11.6	8.25	3.12	0.13	2.80	1.06	0.02	0.03	2.12	0.92	5.26	0.17	*nd*
	ALC1	01/07/2010	1070	0.54	9.2	7.67	6.62	0.44	3.43	0.98	0.73	0.03	3.86	1.46	5.16	1.61	*nd*
	RS3	01/07/2010	770	0.39	11.3	8.10	5.14	0.18	3.20	1.99	0.04	0.03	2.16	0.18	10.23	0.37	*nd*
	RS2	01/07/2010	690	0.34	10.7	8.08	4.26	0.16	3.06	1.89	0.09	0.04	2.24	1.39	7.59	0.35	*nd*
	RS1	01/07/2010	1080	0.52	11.4	7.55	5.56	0.28	4.46	1.54	0.65	0.02	3.83	1.56	7.28	0.04	*nd*
	RS7	14/12/2011	1340	0.67	22.7	7.67	7.40	0.62	4.63	1.84	1.02	0.02	2.90	4.80	6.93	0.65	*nd*
	RS8	14/12/2011	1250	0.62	23.6	8.35	5.69	0.47	2.65	1.04	0.94	0.02	2.84	2.84	6.38	0.57	7.5
	RS9	14/12/2011	1240	0.62	22	8.34	3.11	1.06	4.28	1.30	2.53	0.02	3.60	1.50	6.28	0.40	7.9
Lake samples	LP11-6S	27/04/2011	90000	45.00	21.8	9.14	617.27	3.92	12.48	26.56	1.44	0.35	3.60	553.39	155.86	32.28	2.5
	LP11-1S	27/04/2011	78100	39.05	21.9	9.20	322.44	2.62	7.65	12.73	10.35	0.16	3.74	291.98	77.45	23.54	7.4
	LP11-1D	27/04/2011	82500	41.25	20.9	8.35	423.17	2.31	9.50	17.55	1.79	0.22	3.82	389.64	107.09	*nd*	2.5
	TMC 11-1S	27/04/2011	116700	58.30	21.4	8.27	455.25	2.44	10.28	19.08	1.32	0.08	3.60	397.13	108.89	21.16	3.1
	TMC 11-1D	27/04/2011	124100	62.00	21.9	9.25	494.18	2.56	10.01	20.66	5.49	1.21	3.24	474.42	126.55	19.56	0.6
	TMC 11-2S	27/04/2011	121900	60.90	21.2	8.44	756.33	22.60	35.52	53.43	3.20	1.02	2.74	739.62	192.99	*nd*	0.9
	TMC 11-2D	27/04/2011	126300	63.20	21.5	8.38	563.72	3.21	9.22	18.82	2.88	0.52	3.40	558.58	153.00	23.43	1.0

Table 4-1: Physicochemical parameters of river and lake water samples. Cond. – Conductivity, TDS – Total Dissolved Solids. Concentrations of major ions are expressed in meq L^{-1}. IB: Ionic Balance, DO: dissolved Oxigen *nd*: not determined.

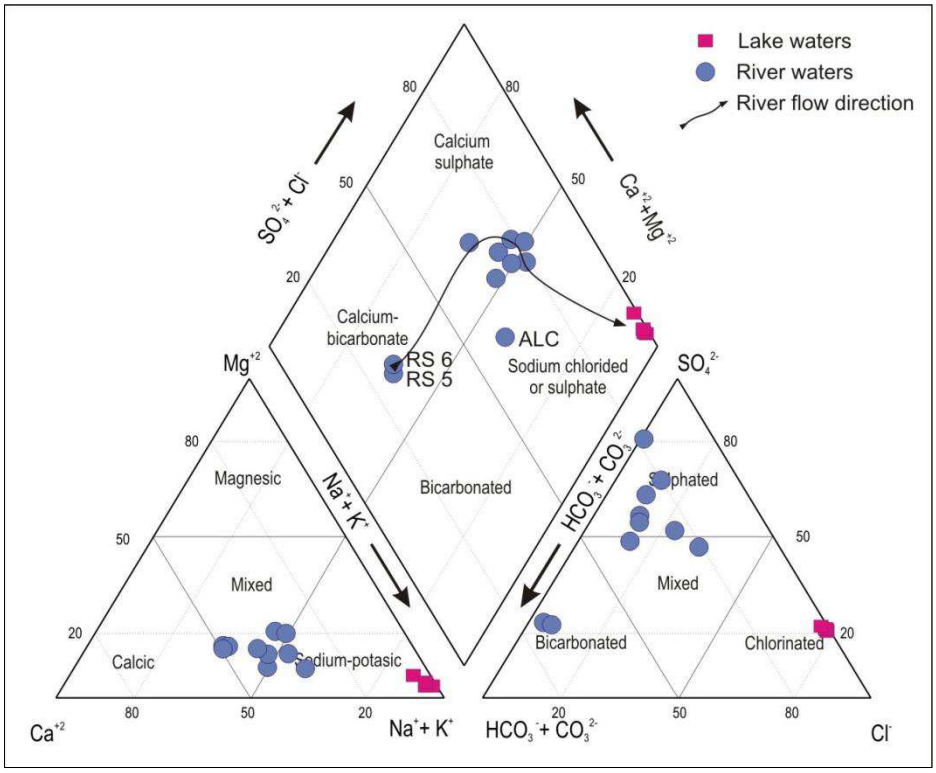

Fig. 4-1: Piper diagrams showing the chemical evolution of Suquía River waters and both lake waters.

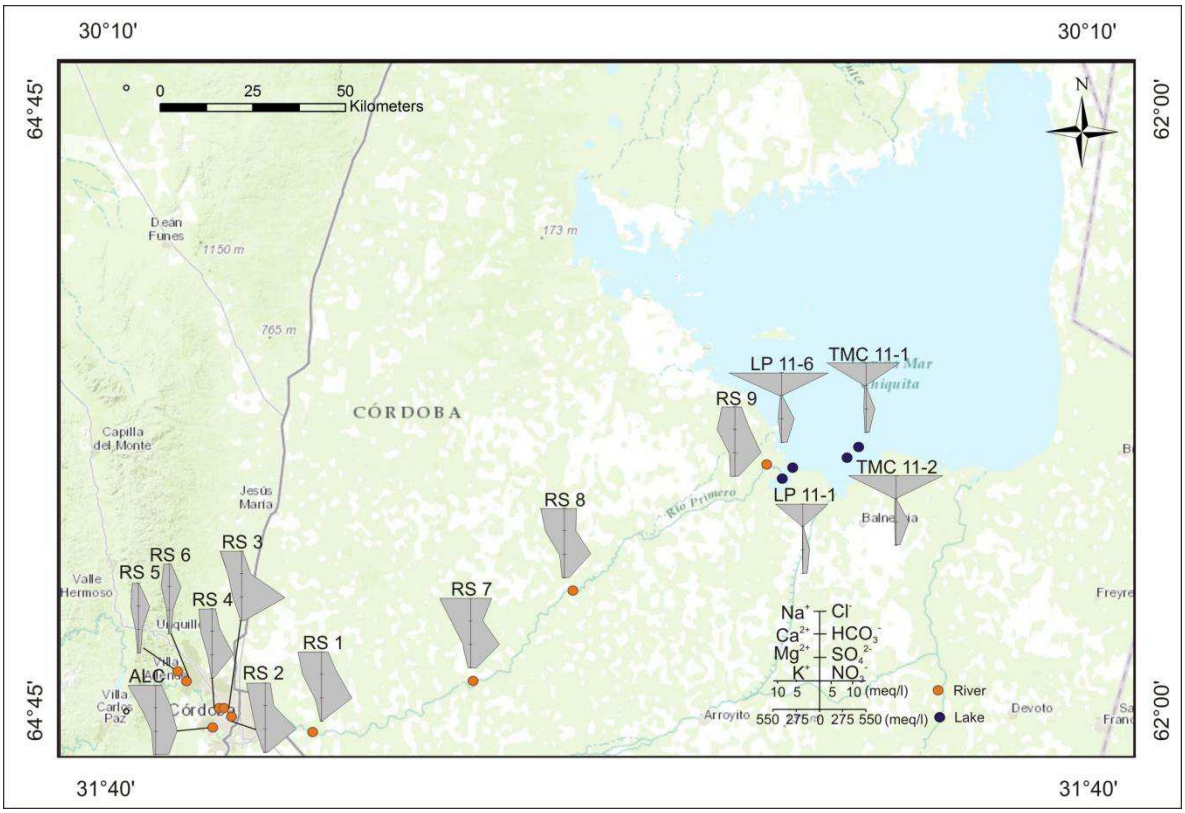

Fig. 4-2: Stiff diagrams showing the major chemical composition of water samples in the Suquía River and in the lakes. Notice that the concentration scale in the X-axis is different for river and lake waters.

Saturation indexes were calculated to state the saturation of water samples with respect to minerals using the geochemical software PHREEQC (Parkhurst and Appelo, 1999) the following the equation (Eq. 8):

$$SI = \log\left(\frac{IAP}{K}\right) \quad \text{(Eq. 8)}$$

Where: *SI* is the saturation index;

*IA*P is the Ion Activity Product;

K is the solubility product.

When $SI = 0$, there is equilibrium between the mineral and the solution, $SI < 0$ reflects subsaturation and $SI > 0$ supersaturation (Appelo and Postma, 2005). The values obtained for the Suquía River, Laguna Mar Chiquita and Laguna del Plata (Table 4-2) show that halite and anhydrite are always subsaturated. Gypsum and fluorite with values clearly < 0 are always subsaturated in river waters but lake waters present mild supersaturation with respect to gypsum and a stronger supersaturation with respect to fluorite. Dolomite and aragonite are almost always supersaturated with the exception, in both cases, in samples ALC and RS1. On the other hand, calcite with values > 0 is supersaturated in all samples. The general tendency shows that the *SI* values become increasingly positive from the upper part of the basin to the lake area.

	Sample	Halite NaCl	Anhydrite $CaSO_4$	Gypsum $CaSO_4{\cdot}2H_2O$	Fluorite CaF_2	Dolomite $CaMg(CO_3)_2$	Aragonite $CaCO_3$	Calcite $CaCO_3$
River samples	RS6	-8.09	-2.51	-2.26	-1.41	**0.86**	**0.54**	**0.69**
	RS5	-8.22	-2.43	-2.17	-3.06	**0.19**	**0.21**	**0.36**
	RS4	-7.19	-1.6	-1.34	-1.49	**0.39**	**0.28**	**0.43**
	ALC	-6.68	-1.59	-1.33	-1.52	-0.37	-0.02	**0.13**
	RS3	-7.71	-1.36	-1.11	-1.64	**0.27**	**0.11**	**0.26**
	RS2	-6.89	-1.47	-1.21	-1.27	**0.26**	**0.11**	**0.27**
	RS1	-6.73	-1.35	-1.1	-1.74	-0.23	-0.01	**0.14**
	RS7	-6.15	-1.39	-1.16	-1.82	**0.32**	**0.16**	**0.30**
	RS8	-6.49	-1.61	-1.38	-2.04	**1.19**	**0.59**	**0.73**
	RS9	-7.02	-1.43	-1.2	-1.82	**1.58**	**0.85**	**1.00**
Lake samples	LP11-6S	-2.38	-0.64	-0.43	**0.17**	**3.32**	**1.28**	**1.43**
	LP11-1S	-2.92	-0.97	-0.75	-0.53	**2.18**	**0.77**	**0.91**
	LP11-1D	-2.68	-0.81	-0.59	-0.24	**2.09**	**0.71**	**0.85**
	TMC 11-1S	-2.65	-0.79	-0.57	-1.15	**2.02**	**0.66**	**0.81**
	TMC 11-1D	-2.54	-0.77	-0.56	**1.22**	**2.93**	**1.1**	**1.24**
	TMC 11-2S	-2.16	-0.17	**0.04**	**1.47**	**3.04**	**1.21**	**1.36**
	TMC 11-2D	-2.41	-0.76	-0.55	**0.44**	**2.04**	**0.65**	**0.80**

Table 4-2: Saturation indices calculated for water samples with PHREEQC.

4.1.2 Trace metal concentrations

Table 4-3 shows the concentrations of trace metals in solution in the Suquía River water samples. These elements were chosen as they are usually related to As. Emphasis was made on this element in the aqueous phase due that concentrations in the solid phase are going to be analyzed later on. The concentrations of As for water samples in the Suquía River basin are shown in Table 4-4. Furthermore, the correlations of all elements measured with the ICP-MS for all rivers water samples are expressed in the correlation matrix (Table 4-5). Here the statistically significant correlations (0>0.5 and 0<-0.5) are highlighted. Those who have a positive correlation are marked in pale gray and those with negative correlation in dark gray. The matrix shows a good correlation between As and Li, Mg, Si, Ca, V, Br, Sr, and Mo. The table shows as well, as good correlation with TDS.

Measures of the Hg concentrations in waters by ICP-MS are not appropriated and therefore these data were not used in the present analysis.

Element	Unit	River waters		
		Min.	Max.	Mean
As	µg L^{-1}	0.54	21.50	5.16
V	µg L^{-1}	1.00	37.70	10.54
U	µg L^{-1}	0.53	21.10	8.02
Se	µg L^{-1}	0.30	2.80	1.25
Sb	µg L^{-1}	0.03	0.49	0.15
Mo	µg L^{-1}	0.20	7.60	2.74
Al	µg L^{-1}	8.00	229.00	67.56
Mn	µg L^{-1}	1.70	295.00	38.26
Li	µg L^{-1}	4.00	25.00	13.48
F	mg L^{-1}	0.10	0.75	0.47

Table 4-3: Statistical summary for some selected trace elements in the Suquía River basin

Sample	As (µg L^{-1})
4RCQ1	1.17
4RCQ2	1.14
4RSA	0.54
4RS10	2.71
4RSDN	6.34
RS6	5.72
RS5	3.13
RS4	4.84
ALC1	9.07
RS3	8.80
RS2	8.12
RS1	3.20
RS7	4.68
RS8	6.41
RS9	21.50

Table 4-4: Arsenic concentrations on water samples in the Suquía River basin

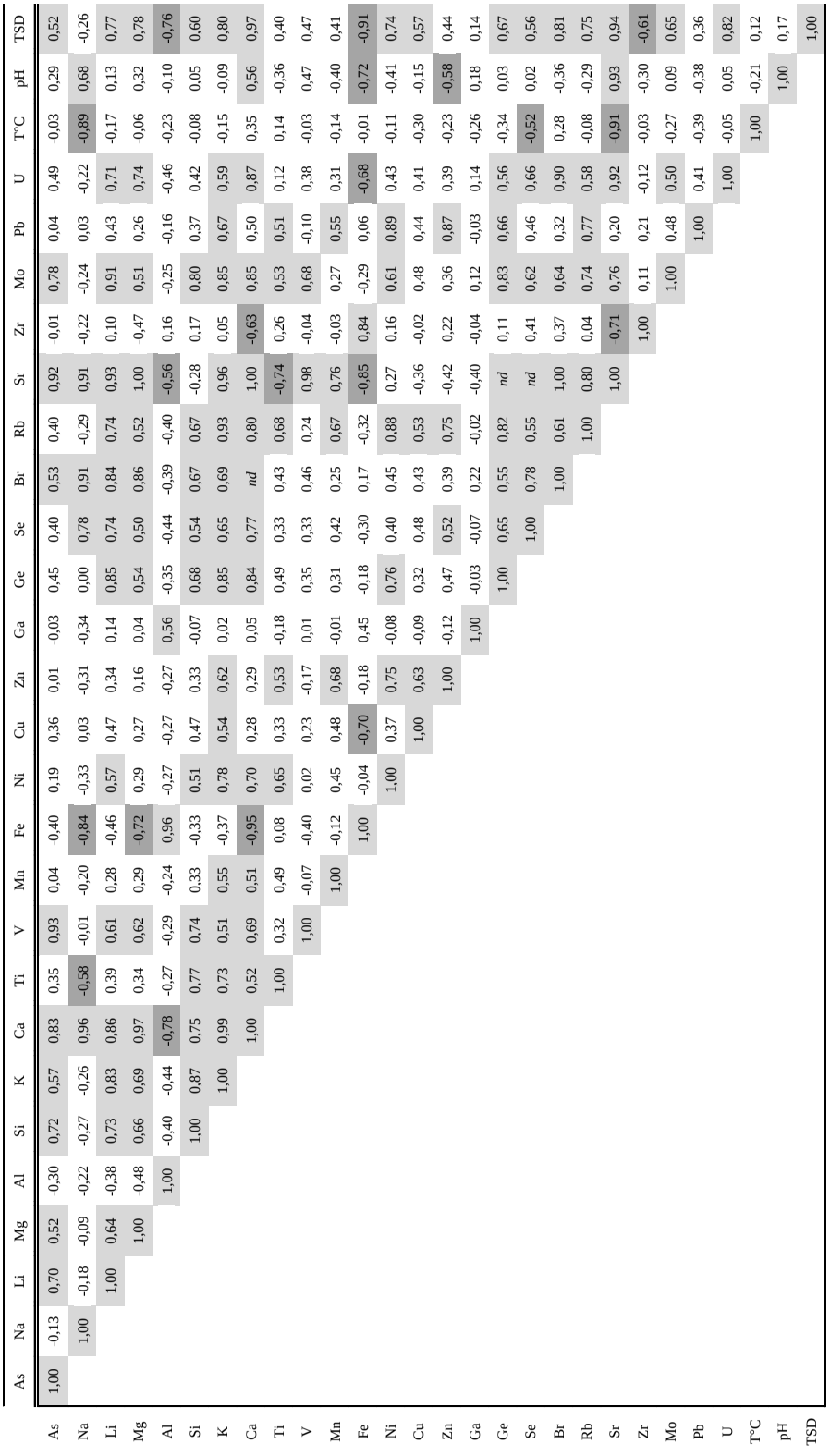

	As	Na	Li	Mg	Al	Si	K	Ca	Ti	V	Mn	Fe	Ni	Cu	Zn	Ga	Ge	Se	Br	Rb	Sr	Zr	Mo	Pb	U	T°C	pH	TSD
As	1,00	-0,13	0,70	0,52	-0,30	0,72	0,57	0,83	0,35	0,93	0,04	-0,40	0,19	0,36	0,01	-0,03	0,45	0,40	0,53	0,40	0,92	-0,01	0,78	0,04	0,49	-0,03	0,29	0,52
Na		1,00	-0,18	-0,09	-0,22	-0,27	-0,26	0,96	-0,58	-0,01	-0,20	-0,84	-0,33	0,03	-0,31	-0,34	0,00	0,78	0,91	-0,29	0,91	-0,22	-0,24	0,03	-0,22	-0,89	0,68	-0,26
Li			1,00	0,64	-0,38	0,73	0,83	0,86	0,39	0,61	0,28	-0,46	0,57	0,47	0,34	0,14	0,85	0,74	0,84	0,74	0,93	0,10	0,91	0,43	0,71	-0,17	0,13	0,77
Mg				1,00	-0,48	0,66	0,69	0,97	0,34	0,62	0,29	-0,72	0,29	0,27	0,16	0,04	0,54	0,50	0,86	0,52	1,00	-0,47	0,51	0,26	0,74	-0,06	0,32	0,78
Al					1,00	-0,40	-0,44	-0,78	-0,27	-0,29	-0,24	0,96	-0,27	-0,27	-0,27	0,56	-0,35	-0,44	-0,39	-0,40	-0,56	0,16	-0,25	-0,16	-0,46	-0,23	-0,10	-0,76
Si						1,00	0,87	0,75	0,77	0,74	0,33	-0,33	0,51	0,47	0,33	-0,07	0,68	0,54	0,67	0,67	-0,28	0,17	0,80	0,37	0,42	-0,08	0,05	0,60
K							1,00	0,99	0,73	0,51	0,55	-0,37	0,78	0,54	0,62	0,02	0,85	0,65	0,69	0,93	0,96	0,05	0,85	0,67	0,59	-0,15	-0,09	0,80
Ca								1,00	0,52	0,69	0,51	-0,95	0,70	0,28	0,29	0,05	0,84	0,77	*nd*	0,80	1,00	-0,63	0,85	0,50	0,87	0,35	0,56	0,97
Ti									1,00	0,32	0,49	0,08	0,65	0,33	0,53	-0,18	0,49	0,33	0,43	0,68	-0,74	0,26	0,53	0,51	0,12	0,14	-0,36	0,40
V										1,00	-0,07	-0,40	0,02	0,23	-0,17	0,01	0,35	0,33	0,46	0,24	0,98	-0,04	0,68	-0,10	0,38	-0,03	0,47	0,47
Mn											1,00	-0,12	0,45	0,48	0,68	-0,01	0,31	0,42	0,25	0,67	0,76	-0,03	0,27	0,55	0,31	-0,14	-0,40	0,41
Fe												1,00	-0,04	-0,70	-0,18	0,45	-0,18	-0,30	0,17	-0,32	-0,85	0,84	-0,29	0,06	-0,68	-0,01	-0,72	-0,91
Ni													1,00	0,37	0,75	-0,08	0,76	0,40	0,45	0,88	0,27	0,16	0,61	0,89	0,43	-0,11	-0,41	0,74
Cu														1,00	0,63	-0,09	0,32	0,48	0,43	0,53	-0,36	-0,02	0,48	0,44	0,41	-0,30	-0,15	0,57
Zn															1,00	-0,12	0,47	0,52	0,39	0,75	-0,42	0,22	0,36	0,87	0,39	-0,23	-0,58	0,44
Ga																1,00	-0,03	-0,07	0,22	-0,02	-0,40	-0,04	0,12	-0,03	0,14	-0,26	0,18	0,14
Ge																	1,00	0,65	0,55	0,82	*nd*	0,11	0,83	0,66	0,56	-0,34	0,03	0,67
Se																		1,00	0,78	0,55	*nd*	0,41	0,62	0,46	0,66	-0,52	0,02	0,56
Br																			1,00	0,61	1,00	0,37	0,64	0,32	0,90	0,28	-0,36	0,81
Rb																				1,00	0,80	0,04	0,74	0,77	0,58	-0,08	-0,29	0,75
Sr																					1,00	-0,71	0,76	0,20	0,92	-0,91	0,93	0,94
Zr																						1,00	0,11	0,21	-0,12	-0,03	-0,30	-0,61
Mo																							1,00	0,48	0,50	-0,27	0,09	0,65
Pb																								1,00	0,41	-0,39	-0,38	0,36
U																									1,00	-0,05	0,05	0,82
T°C																										1,00	-0,21	0,12
pH																											1,00	0,17
TSD																												1,00

Table 4-5: Correlation matrix. Values>0.5 are in pale gray and those <-0.5 in dark gray; TDS: Total Dissolved Solids; *nd*: not determined.

4.1.3 Aquatic geochemistry of As

In shallow and deep groundwater from the Chaco Pampean region of central Argentina, As concentrations exceed the World Health Organization (WHO) requirements for drinking waters (10 µg L^{-1}, Nicolli *et al.*, 2012). Previous works performed in the region (i.e., Nicolli *et al.*, 2010, 2012; Smedley *et al.*, 2002, 2005) suggest that the source of this element is hosted in the loess sediments that blanket the entire basin.

There are almost no references about As concentrations in surface waters in Argentina (Paoloni *et al.*, 2009; Rosso *et al.*, 2011, 2013; Bugueño *et al.*, 2014), neither in saline waters from the lake system that extend with a N-S direction in the eastern part of the Chaco Pampean Plain.

As concentrations measured in water samples from the Suquía River basin (Table 4-4) vary from 0.54 to 21.50 µg L^{-1} and only one sample (RS9) exceeds WHO recommendation for drinking water. Fig. 4-3 shows the aqueous As concentrations from the river catchments to the lower basin and their position in the basin. Samples in the left part of the figure correspond to those located on the crystalline rocks and in the right (from RS1 to RS9) those located in loessic plain. It is possible to see that a concentration gradient exist between samples located in the upper part of the basin to those in the lower part.

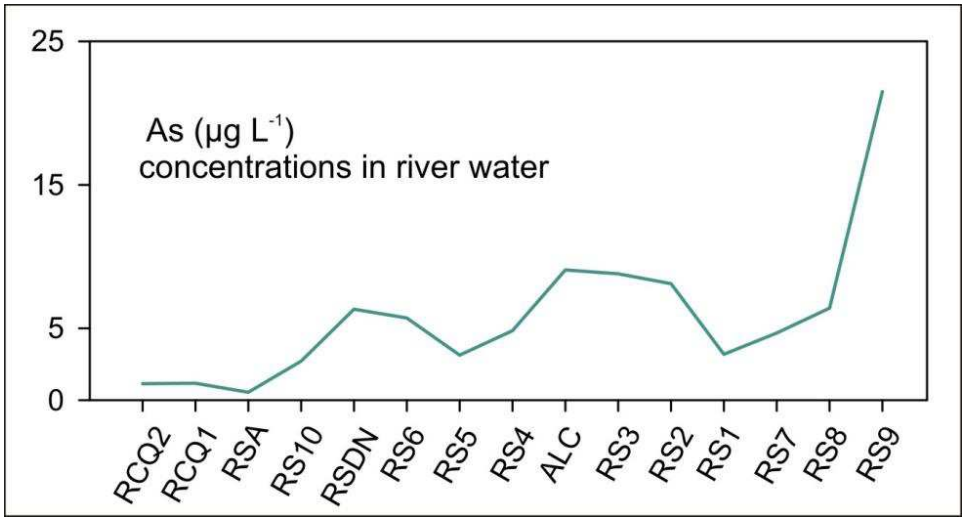

Fig. 4-3: Arsenic concentrations in river waters with respect to the geographical position in the basin (RCQ2 to RSAcorrespond to headwaters).

4.1.4 Mineralogy of sediments and lake bottom sediments

Sediment samples collected in stations RS-7 and RS-8 were analyzed by XRD (Fig. 4-4) following the methodology described in section 3.2.3.2. These sediments are mainly composed of Quartz (Qtz – SiO_2), Albite (Ab - $NaAlSi_3O_8$), Illite (Ill - $(K,H_3O)(Al,Mg,Fe)_2(Si,Al)_4O_{10}[(OH)_2,(H_2O)]$) and Microcline (Mc - $KAlSi_3O_8$). Perovskite (Prv – TiO_3Ca) and Pyrite (Py – FeS_2) were also found as minoritary minerals.

Besides, lake bottom sediment samples were collected in Laguna del Plata (LP 11-6) and Laguna Mar Chiquita (TMC 11-1). The identified primary minerals are Quartz, Albite, Muscovite (Ms – $KAl3Si_3O_{10}(OH)_2$) and Biotite (Bt – $K(MgFeAlTi)_3[(AlSi)_3O_{10}](OHFCl)_2$). Calcite (Cal – $CaCO_3$) and Halite (Hl – NaCl) are also found. In TMC 11-1, Halite crusts are dominant due to precipitation from interstitial water.

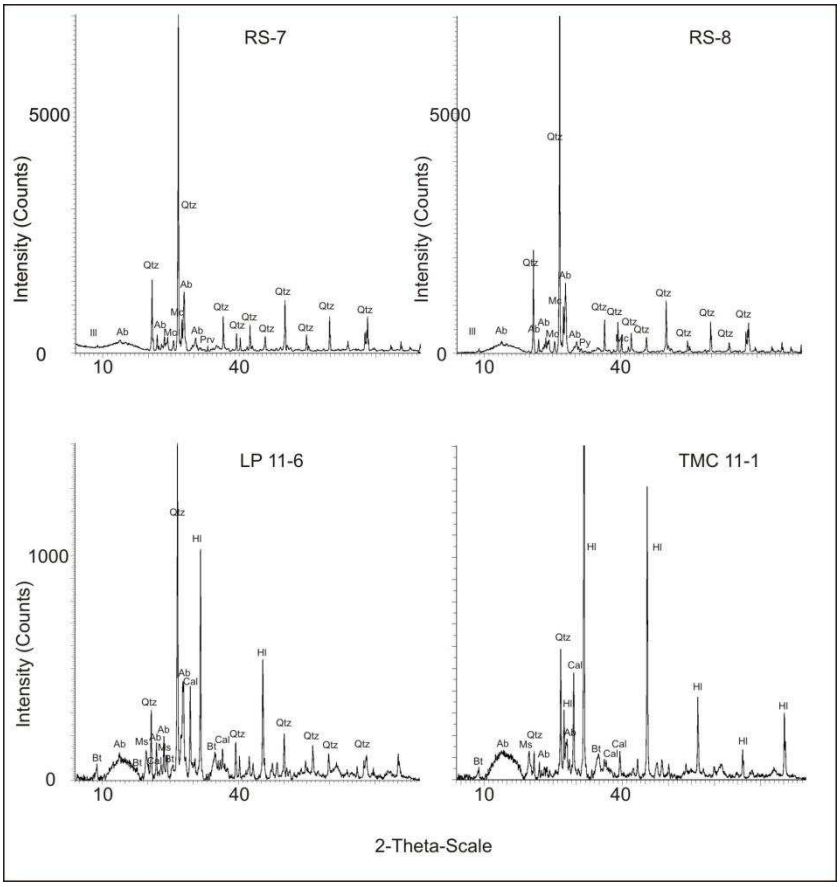

Fig. 4-4: XRD diffractograms for Suquía riverbed sediments (RS-7 and RS-8) and for Laguna del Plata (LP 11-6) and Laguna Mar Chiquita (TMC 11-1) bottom sediments. Ill: Illite, Ab: Albite, Qtz: Quartz, Mc: Microcline, Prv: Perovskite, Py: Pyrite, Cal: Calcite, Hl: Halite, Bt: Biotite.

4.1.5 Hg in riverbed and lake bottom sediments

Hg concentrations were determined in two grain-size fractions of the riverbed sediment samples (Table 4-6). In the coarser sandy fraction, Hg concentrations range from 2.13 to 26.69 μg kg^{-1} while in the silty fraction values are markedly higher and range between 20.42 to 180.9 μg kg^{-1}. Samples collected from the lake bottom correspond to the total fraction of silty granulometry. In these samples the average Hg concentration is 28.88 μg kg^{-1} being the concentrations on Laguna del Plata slightly higher than in Laguna Mar Chiquita. Besides, Hg concentrations were determined in one sample corresponding to atmospheric dry deposition. The sample was collected from a pluviometric captor (sample RI-99) in 1999. The importance of this sample is that it gives a value of the atmospheric Hg input in the basin for the year 1999. The results in Table 4-2 evidence that Hg concentrations are ~7 folds higher in the finest fraction of the basin's sediments.

Sample	Silty fraction	Sandy fraction
RSF	72,41	25,06
RCQ2	62,52	9,61
RCQ1	34,92	7,39
RS10	63,24	10,31
RY	30,57	2,13
RLC	23,18	15,46
RSA	60,49	5,37
RSDN	180,99	10,09
RS6	40,99	17,97
RS5	46,94	26,69
RS1	20,42	9,14
RS7	23,51	2,59
RS8	34,84	2,75
RS9	29,77	11,82
LP11-1	38,89	
LP11-6	38,33	
TMC 11-1	20,69	
TMC 11-2	17,59	
RI - 99	45,15	

Table 4-6: Mercury concentrations on riverbed, lake bottom and pluviometric captor sediment samples expressed in μg kg^{-1}.

The spatial distribution of Hg measured in riverbed and lake bottom sediment is shown in Fig. 4-5. According with this figure, the highest concentrations are located in the basin's catchments while a trend of decreasing Hg concentrations is observed downflow. In the lake area, the highest concentrations are found in samples collected from the bottom Laguna del Plata.

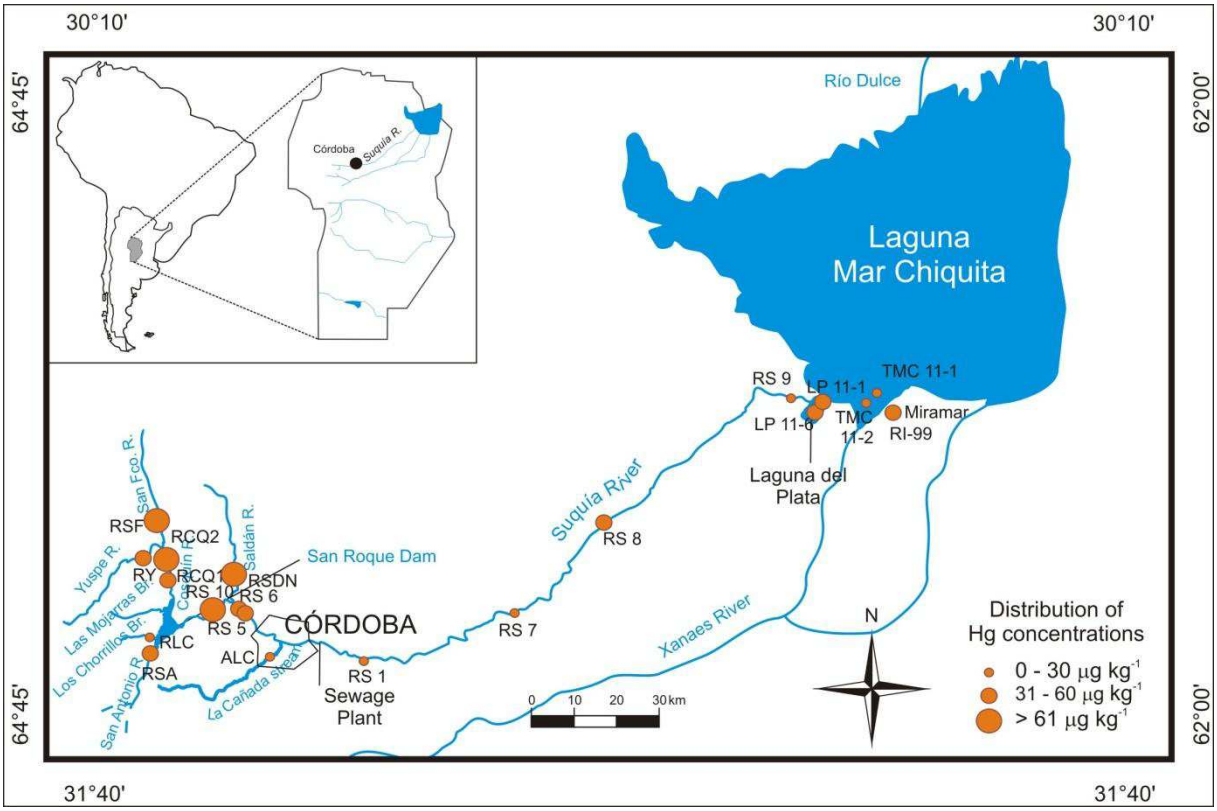

Fig. 4-5: Distribution of Hg concentrations of the silty fraction in the basin. Concentrations are given in µg kg^{-1} and the size of the circle corresponds to the amount of mercury measured at a certain point.

4.2 Geochemical and sedimentological characterization of the sedimentary record in Laguna del Plata

A geo-physicochemical analysis of sediments of the LP core was carried out for the 120 cm sedimentary core. Emphasis was made on Hg and As to understand the carrying phases that these elements are associated to and their behaviour in the basin. These carrying phases were analyzed through selective extractions following the methodology described in section 3.2.2. In the obtained leachates, concentrations of Hg, As, Fe and Mn, were determined.

4.2.1 Textural, physical and chemical properties of the sediments

4.2.1.1 LP core sedimentation – Lamination Indexes

The description performed to the LP core was based on the *Lamination Indexes* (LI) proposed by Piovano *et al.* (2002). These indexes are:

- Continuous laminae: when the layer is up to 2 mm thick are designated by "1";
- Diffuse or discontinuous laminae: 2-4 mm thick by "2";
- Thin banded: 4-10 mm thick by "3" ;
- Thick banded: >10 mm thick by "4";
- Massive: when there is an absence of lamination.

LP core is characterised by an alternance of dark and light lamination which corresponds to greyscale in the SCOPIX X-ray image and olive green scale colour in the photograph (Fig. 4-6a and b). Using these criteria 5 sedimentary units were recognised (Fig. 4-6).

The first one (A) is a massive sequence that extends from the bottom of the core up to 75 cm with a net contact. From the base of the core to the top, this sequence shows different colours on the photograph: light green colour in the deepest part, followed by a dark green olive colour that overlies and a very light green colour on the top of it. In the X-Ray image the colour varies from light gray in the bottom to darker gray in the upper part.

From 75 to 69 cm, it is possible to observe a group of LI2 (B) that is present as an alternance of numerous dark to light colours layers with net contacts between them.

Overlying this small sequence and up to 53 cm there is a group of sedimentary layers (C) that correspond to LI4 that mix with LI2 in the base of the sequence, they show a predominance of a light colour. The intercalations of the LI2 layers are net while the LI4 are quite diffuse or gradual.

From here up to 16 cm a very regular sequence of LI1 and LI2 laminations (D) is present intercalated with a LI3 lamination located between 27-39 cm the contacts between the thinner layers are more net that those corresponding to the thicker ones.

The last 16 cm of the upper part of the core show a LI4 sequence (E) with dark olive green colour in the picture and medium to light grey colour in the X-ray image. In the SCOPIX image, the last 8 cm show a deformation of the sedimentary layers that could also be seen between 58 and 60 cm, this is due to the opening of the core where the sediments moved at the moment of separating both halves.

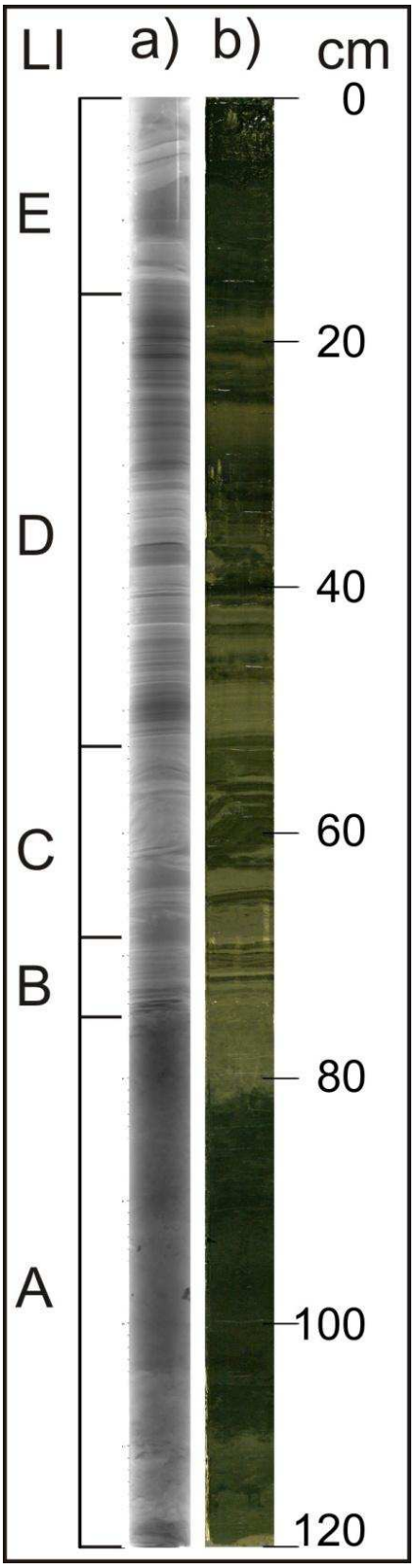

Fig. 4-6: Gray and olive green colour scale corresponding to the SCOPIX X-ray image (a) and the photograph (b). Letters A to E correspond to the Lamination Indexes (LI).

4.2.1.2 Grain size distribution

Samples of the LP core show a grain size distribution that varies from fine to coarse silt (4-62 μm - Fig. 4-7). The mode in the most symmetric curves is placed between 9.5 and 11 μm and changes in the other curves according to the hydrological variations. This mode seems to be finer in the middle and upper part of the core and coarser in the lower part. The size distributions show symmetric curves only in samples at 16.25, 44.25 and 55.75 cm depth and the others curves are asymmetric with a platykurtic kurtosis. Below 80 cm samples revealed a clear bi-modal grain size distribution with two components of 0.3-15 μm and 15-400 μm, probably reflecting two types of transportation process of the clastic materials that were deposited into the lake. In the upper and middle part of the core the grain distribution varies mostly between fine and medium silt (2-20 μm) while in the base of the core it tends to be coarser (20-200 μm). Two fractions are marked: fine and coarse silt and this last one augments in proportion to the first one in depth.

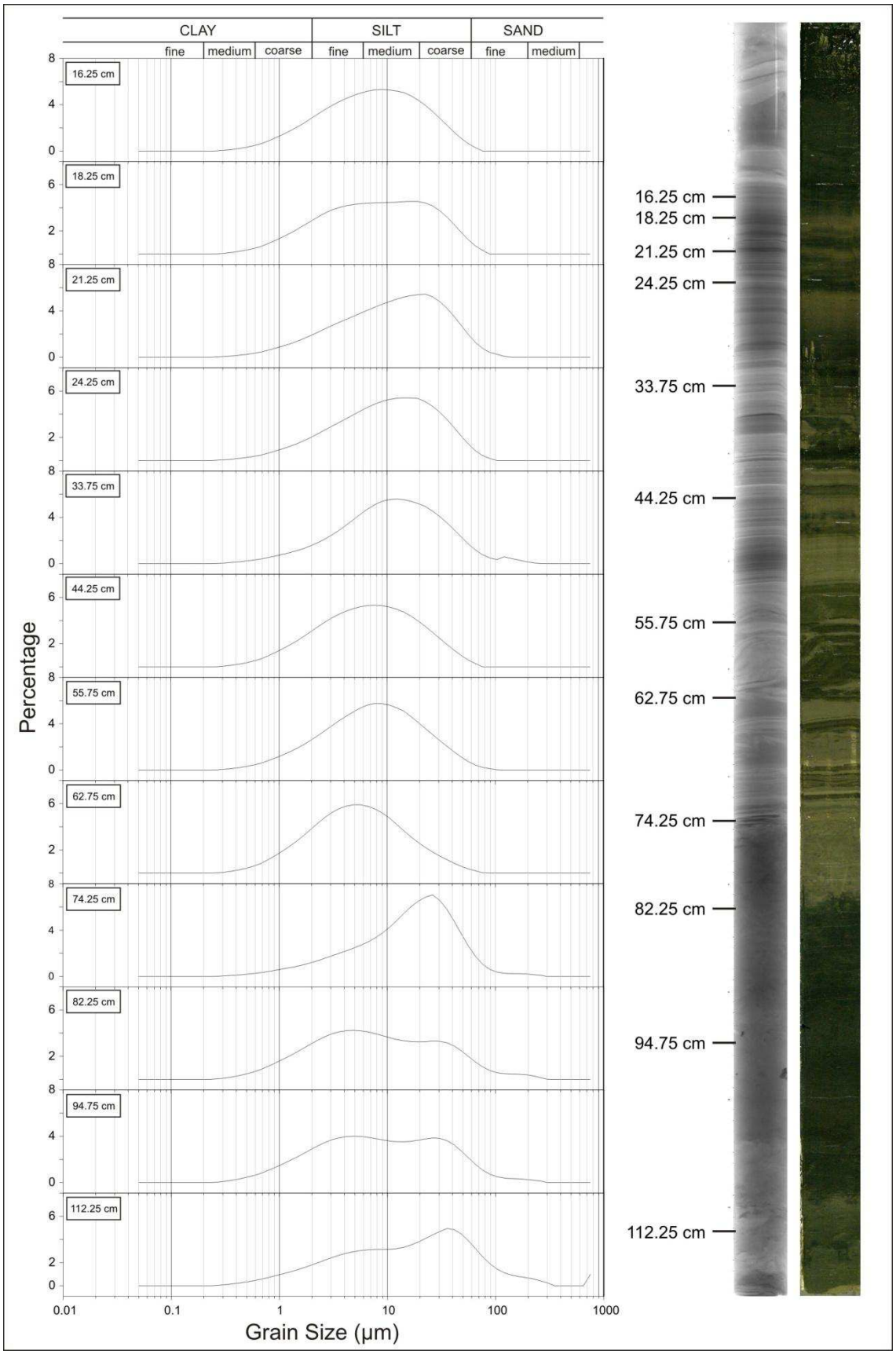

Fig. 4-7: Grain size distribution for LP core samples.

4.2.2 Physicochemical properties

Values of pH showe two different tendencies (Fig. 4-8d): from the bottom of the core up to 65.75 cm, the average is 9.20 while from this level up to the top measures show lower values with an average of 8.51. The lower part corresponds to the period where the lake had low lake-levels (Fig. 4-8c), high salinity and therefore higher pH. The opposite occurs in the upper part of the core: when the lake-level started to rise, a marked diminution on the pH is registered.

Porosity values ranged from 40.0 to 74.5 % (Fig. 4-8e). The lower values occurred near the bottom of the LP core and the higher near the top. These allowed to divide the core into three zones that are delimited in gray dashed lines in Fig. 4-8. In the first zone, that extends from the bottom of the core to 74 cm, the porosity presented average values of 48.4 ± 2.9 %, in the second one (from 74 to 16 cm) porosity raised up to 56.2 ± 6.1 % remaining nearly constant and finally the upper zone that comprises the first 16 cm is represented by an abrupt augmentation of water percentage (from 59.9 to 74.5 %). When regarding the core sedimentation, it is possible to observe a relation with the lamination sections (Fig. 4-6) and the porosity values, where section A corresponds to the lower porosity, B, C and D to the intermediate porosity and E with the highest one.

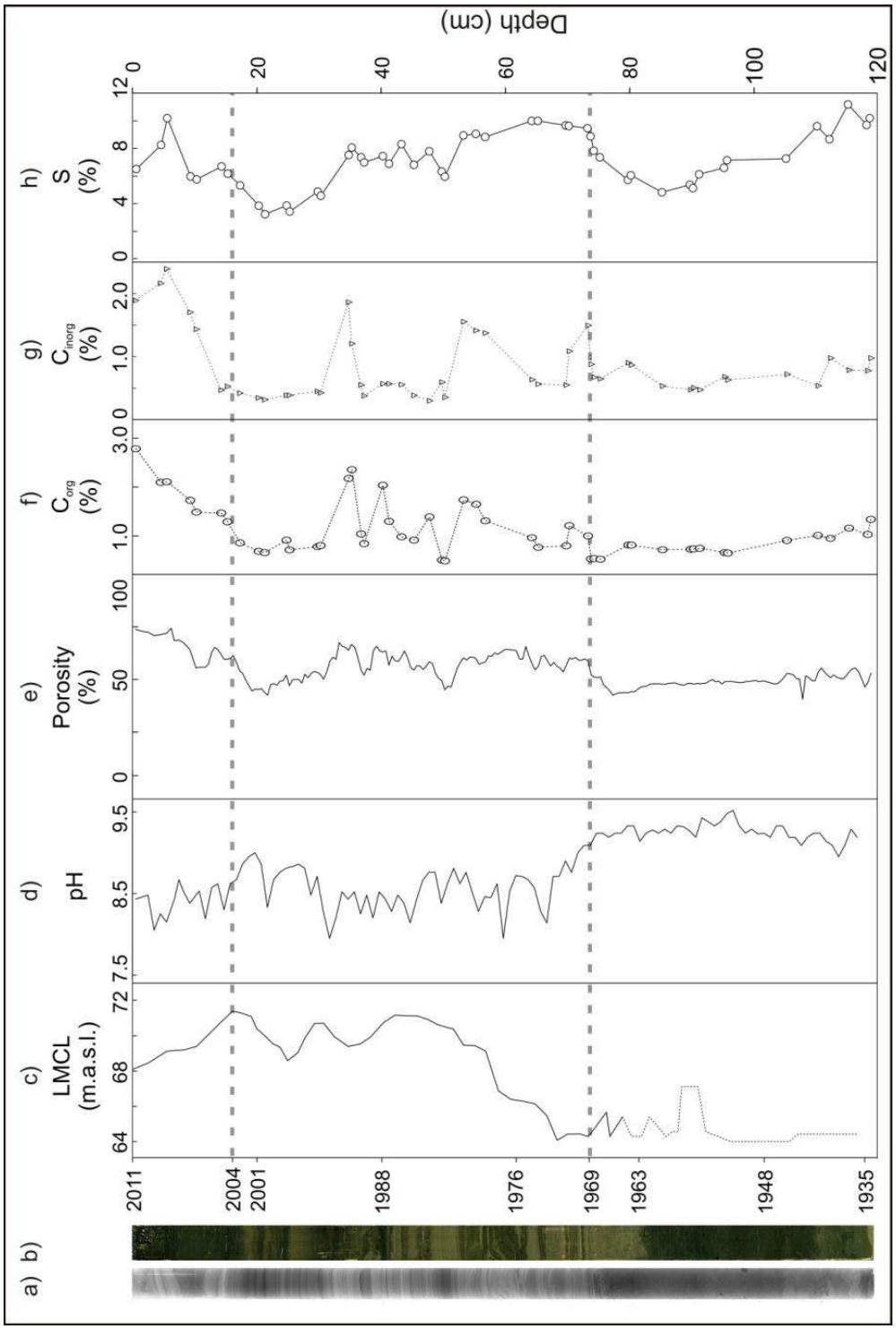

Fig. 4-8: Physical parameters corresponding to LP core plotted next to Laguna Mar Chiquita Lake-level (LMCL) variations, a) sediment core X-ray image, b) sediment core photograph, c) LMCL – Laguna Mar Chiquita Lake-level, the dashed line corresponds to reconstructed data developed in Piovano *et al.*, 2002., d) pH values, e) porosity record expressed in percentage, f) Organic Carbon (C_{org}) content, g) Inorganic Carbon (C_{inorg}) content, h) Sulphur (S) content.

4.2.3 Core dating: age model

The ^{210}Pb ($T_{1/2}$ = 22.3 years) is a naturally occurring radionuclide delivered continuously to the landscape by atmospheric fallout (Saari *et al.*, 2010) and becomes rapidly and strongly bound to particulate matter. This atmospherically derived ^{210}Pb scavenged by particles (Fig. 4-9), is referred to ^{210}Pb in excess ($^{210}Pb_{xs}$) of that supported within particles by the decay of its parent isotope, ^{226}Ra. Once incorporated into the sediment, unsupported ^{210}Pb decays with time in the sediment column according to its half-live, by the following equation:

$$^{210}Pb_{xs(z)} = {}^{210}Pb_{xs(0)}e^{-\lambda t} \quad \text{(Eq. 9)}$$

where $^{210}Pb_{xs(z)}$ and $^{210}Pb_{xs(0)}$ represent the excess ^{210}Pb at the sediment-water interface, or at the base of the mixed layer, and at the depth z, λ is the ^{210}Pb decay constant (0.0311 y^{-1}), and *t* is the age in years.

In LP core, these excess activities range from 5 to 72 mBq g^{-1}. There is a general trend in decreasing $^{210}Pb_{xs}$ as expected due to the decay of the unsupported ^{210}Pb. This decrease presents some irregularities, as observed at about 24 cm where excess is lower when compared to the surrounding layers. The long-lived and naturally occurring ^{232}Th is usually associated with the detrital fraction (van der Klooster *et al.*, 2011), therefore activity changes can be an indication of different lithological sources or proportions. ^{232}Th activities range between 26 and 42 mBq g^{-1}, the lowest values are usually observed in the upper 20 cm. This section presents also the highest total carbon content that is likely to dilute the detrital fraction. It is also noticeable that low $^{210}Pb_{xs}$ at 24 cm is associated with a high ^{232}Th activity. Such a high ^{232}Th is mostly observed in the deepest part of the core, at > 70 cm depth.

To calculate the sedimentation rates and age for the lake based on the CFCS model, two basic assumptions were considered: ^{210}Pb atmospheric deposition and the mass accumulation are constant. The mass accumulation rate (MAR, g cm^{-2} y^{-1}) can be obtained considering the following equation:

$$^{210}Pb_{xs(z)} = {}^{210}Pb_{xs(0)}e^{-m_{(z)}\frac{\lambda}{MAR}} \quad \text{(Eq. 10)}$$

where m(z) is the cumulative dry mass per unit area (g cm^{-2}) at depth z. To compensate the effect of composition changes of sediment, $^{210}Pb_{xs}$ activities were normalized by using ^{232}Th concentrations, measured at the same time through gamma, thus limiting the errors. MAR was

calculated from the slope of the exponential regression of $^{210}Pb^{n}_{xs}$ plotted against cumulative mass (Fig. 4-9A). The average mass accumulation rate is 1.0 g cm^{-2} y^{-1}. The sedimentation rate (in years) has been calculated by dividing the cumulated dry mass per unit area by the mass accumulation rate, allowing to estimate the average sedimentation rates (ASR) (Fig. 4-9B). The expected deposition year for each sediments layer was calculated considering the sampling year (2011) and the water-sediment interface at the uppermost layer as a reference for establishing the chronology.

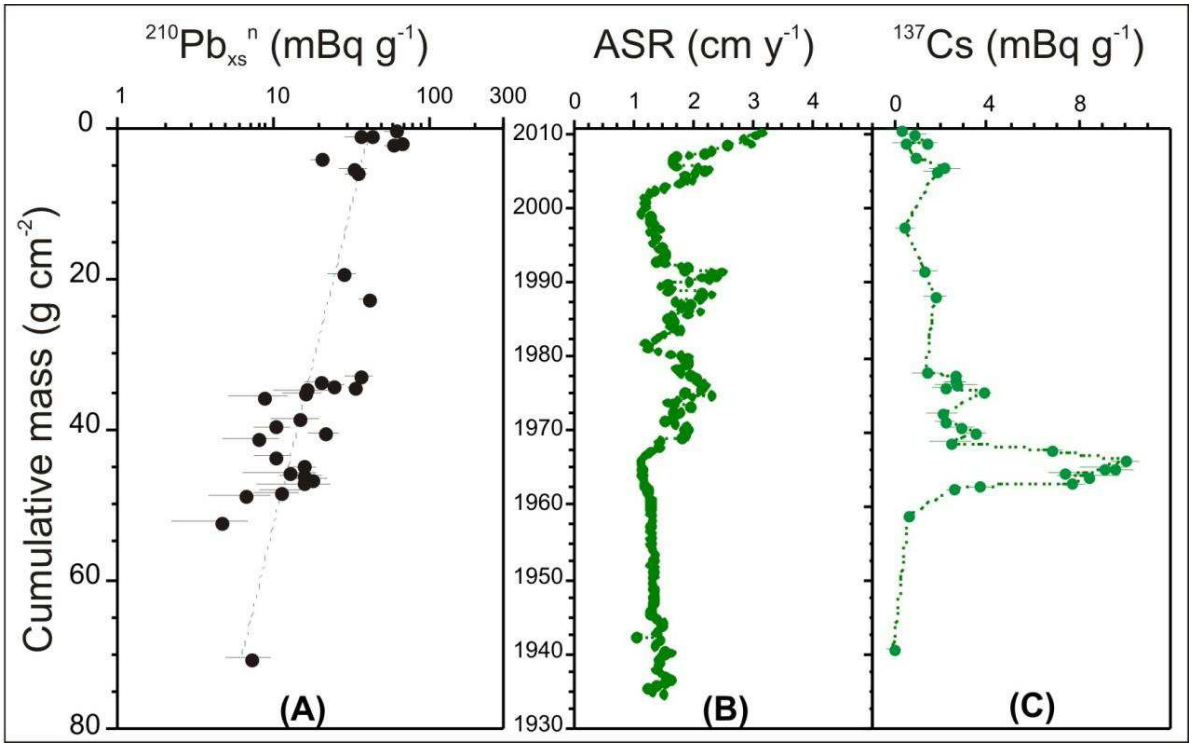

Fig. 4-9: Core dating. (A) Normalized ^{210}Pbxs against cumulative mass: the dashed line corresponds to the exponential regression used to determine Mass Accumulation Rate (MAR). (B) Average Sedimentation Rate (ASR) and (C) ^{137}Cs plotted against calendar ages, based on ^{210}Pb dating.

On the opposite, ^{137}Cs ($T_{1/2}$ = 30 years) is an artificial radionuclide: its occurrence in the environment is primarily the result of the nuclear weapon test fall-out in the early sixties, and in Europe of the Chernobyl accident in 1986 of well-known pulse inputs (UNSCEAR, 2000). Quintana (2011) showed that at present, atmospheric fluxes in Buenos Aires province are almost negligible. Sedimentary profile of ^{137}Cs in core presents the expected shape with a peak in depth and negligible activities in the uppermost section (<1 mBq g^{-1}). The maximum

activities are recorded around 75 – 80 cm, with values up to 26 mBq g^{-1}. Below that peak, ^{137}Cs disappears rapidly to negligible levels below 85 cm. The ^{137}Cs profile was plotted as a function of the time scale based on ^{210}Pb (Fig. 4-9C). It is noticeable that the peak of ^{137}Cs in core LP corresponds to the year 1966, which is in close agreement with the annual atmospheric fallout of ^{137}Cs recorded at Buenos Aires around 1960 (Quintana, 2011). In general the sedimentary ^{137}Cs record mimics rather well the atmospheric fallout, validating the chronology derived from ^{210}Pb and coinciding with the abrupt hydrological changes that the lake system have been through during the decade of 1970's. Sedimentation rates are comprised between 1 and 3 cm y^{-1}, being rather variable with depth. They are less than 2 cm y^{-1} in the deepest part and the highest are located in the uppermost part of the core. What occurs in the lower part of the core is mainly ascribed to sediment compaction and associated with a simultaneous decrease in porosity. During the period covering the early 1970s to the early 1990s, ASR shows strong variability, which may be in relation to environmental changes and the continuous connection of Laguna del Plata to Laguna Mar Chiquita that happened after 1975 during the onset of the last highstand. In the lowermost layers of the core, sedimentation rates display rather constant values, around 1.2-1.5 cm y^{-1}, and are likely to indicate constant sedimentation conditions during lowstand lake scenarios with low fluvial input.

4.2.4 Mineralogical and chemical composition of the LP core sediments

Mineralogy

The mineralogical composition of the LP core sediments through DRX analysis is shown in Fig. 4-10. The identified minerals are Quartz, Albite, Calcite, Muscovite, Biotite and Halite. Clay minerals are Montmorillonite (Mnt – $Si_4O_{10}(OH)_2Al_2$) and Kaolinite (Kln – $Si_4O_{10}(OH)_8Al_4$). Pyrite is present almost all along the sedimentary core except on the samples taken at 20.25 and 100.25 cm.

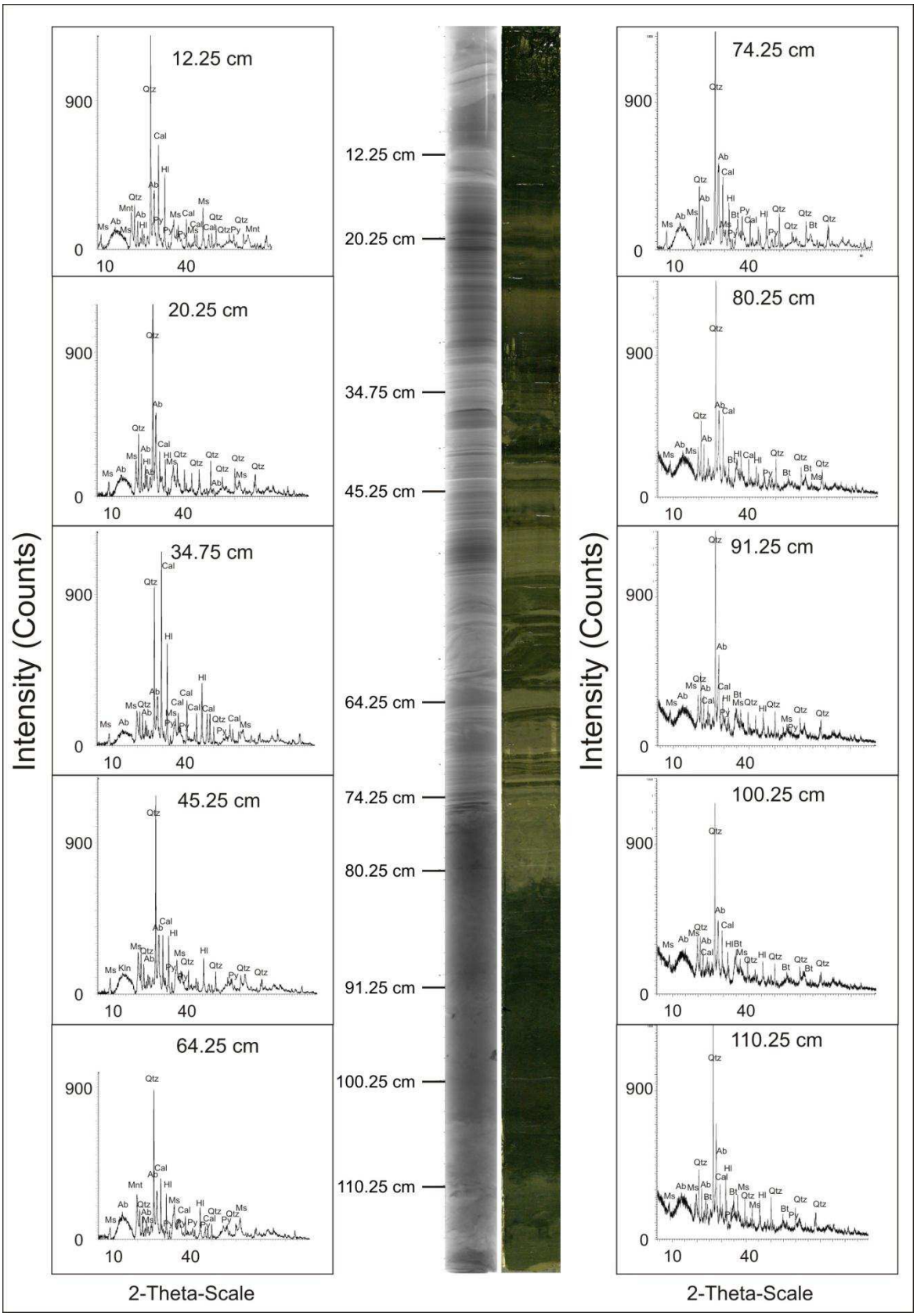

Fig. 4-10: XRD diffractograms LP core sediments. Ms: Muscovite, Bt: Biotite, Kln: Kaolinite, Mnt: Montmorillonite, Ab: Albite, Qtz: Quartz, Cal: Calcite, Hl: Halite, Py: Pyrite.

Chemical composition

Organic carbon (C_{org}) values ranged between 0.49 and 2.79 % and those of inorganic carbon (C_{inorg}) vary from 0.29 to 2.39 %. Regarding C_{org} (Fig. 4-8f), values remained almost constant from 120 to 74 cm (~0.83 % ± 0.22), while they show big fluctuations (between 0.49 to 2.36 %) from 74 up to 30 cm depth that are synchronous with porosity variations. The uppermost centimetres present the highest values reaching a maximum of 2.79 % in the top of the core. C_{inorg} variations are similar to those corresponding to C_{org}. From 120 to 74 cm its average is 0.69 ± 0.17 %, from 74 to 16 cm it is 0.72 ± 0.46 % and in the last 16 cm the average value is 1.51 ± 0.76 % (Fig. 4-8g). C_{inorg} represents the contents of carbonates in the sediments, which range from 2.42 to 19.91 % along the LP core. Carbonate values in Laguna Mar Chiquita span a wider range of concentrations, varying between 0.4 and 25.0 %.

Sulphur (S) concentrations along the sedimentary core oscillate between 3.2 and 11.2 %. The profile shown in Fig. 4-8h evidences three zones in where the maximum S values are registered: underneath 100 cm, between 74 and 35 cm and above 16 cm. These concentrations are assigned to the presence of disseminated sulphides and sulphates along the core. S seems to well correlate with C_{inorg} in the lower part of the core and in the uppermost part, while in the middle part (from 74 to 16 cm) it better correlates with C_{org}. Gypsum is a very common mineral found in sediment cores of the neighbouring Laguna Mar Chiquita (Piovano et al., 2002; Bucher and Bucher, 2006a) especially when the lake presents low lake-levels, but it has not been detected by XRD analysis performed in the LP core.

The contents of some other elements were determined through the core by XRF, depicting mainly three domains (Fig. 4-11). The lower part of the core from the base up to 74 cm is characterised by a signal that remains almost constant except for Zr, S, Sr and Ca that rises in the last centimetres. The second domain shows a high fluctuation visible in all the measured elements that extends in the central part of the core up to 16 cm. From here up to the top Al, Si, K, Ti, Mn, Fe and Zr show a diminution in the signal while for Sr, S, Cl and Ca the opposite occurs.

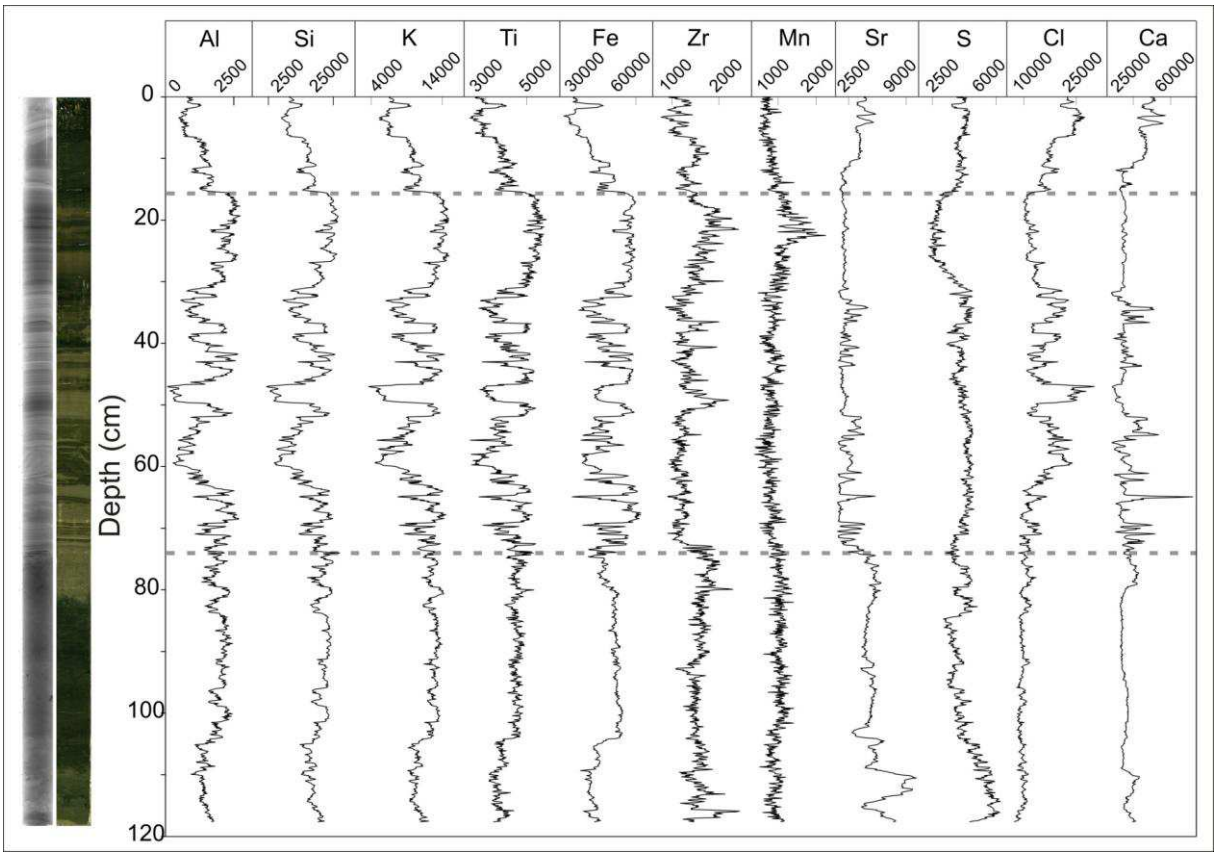

Fig. 4-11: XRF logs from Laguna del Plata. The values are given in counts per second (cps). According to their behaviour, LP core is separated into 3 main zones: from 120 to 74 cm, 74-16 cm and 16-0 cm.

4.2.5 Total Particulate Mercury (Hg_{TP}) and solid speciation

Total Particulate Mercury (Hg_{TP}) concentrations were measured along the LP core and the obtained values varied between ~13 and ~131 μg kg^{-1} (Fig. 4-12a). The profile of Hg_{TP} follows the same trend that porosity, C_{org} and C_{inorg} and trace elements: in the deepest part of the core (from 120 to 74 cm) the lowest and most constant concentrations occurred with an average of 17.24 ± 1.73 μg kg^{-1}; above 74 cm Hg_{TP} concentrations show a significant variability. From 74 cm up to 45 cm the average concentration determined is of 42.38 ± 14.60 μg kg^{-1}, beyond this level and up to 16 cm, the average concentration is 85.26 ± 27.85 μg kg^{-1} with peaks of 89.70, 131.47 and 87.26 μg kg^{-1} at 43.2, 36.7 and 30.2 cm respectively. In the most recent sediments (~16-0 cm), the average Hg_{TP} concentration is 65.61 ± 16.02 μg kg^{-1}.

Due to the observed trends in the elemental distribution along the LP core sediments (relative constant concentrations from the bottom up to 74 cm and rather variable from here to the top), selective extractions were implemented in order to identify the main Hg carrying phases. The analyzed fractions are: reducible (*$Hg_{asc,}$ Ascorbate extraction), oxidisable (*$Hg_{H_2O_2}$, *H_2O_2 extraction)* and acid-soluble/reactive fraction (*$Hg_{HCl,}$ extraction –with HCl).*

Mercury concentrations associated to the reducible fraction were almost undetectable (values ranging from 0 to 0.327 μg kg^{-1} representing less than 1 % Hg_{TP}. Therefore, this fraction was considered negligible throughout the core and is not represented in the figures. On the other hand, Hg in both oxidizable and acid-extracted fractions accounted for the major part of the Hg_{TP} values measured in the sediments. For the first one, Hg concentrations varied from 6.29 to 107.79 μg kg^{-1}, while concentrations of Hg_{HCl} ranged from 0 to 48.19 μg kg^{-1}.

When comparing the extracted fractions with Hg_{TP}, important trends are highlighted. The relative contribution of $Hg_{H_2O_2}$ to Hg_{TP} changed with depth (Fig. 4-12b) showing in average a high value of 76.69 ± 11.02 % in the lower part of the core up to 40 cm. Above this level, the relative contribution of $Hg_{H_2O_2}$ to Hg_{TP} was clearly lower but still important. Similarly, the ratio Hg_{HCl} /Hg_{TP} showed two different patterns (Fig. 4-12c): from the bottom of the core to 74 cm, the ratio was higher revealing that Hg bearing minerals soluble in HCl predominate in these sediments. Above 74 cm to the top, this fraction is remarkably lower.

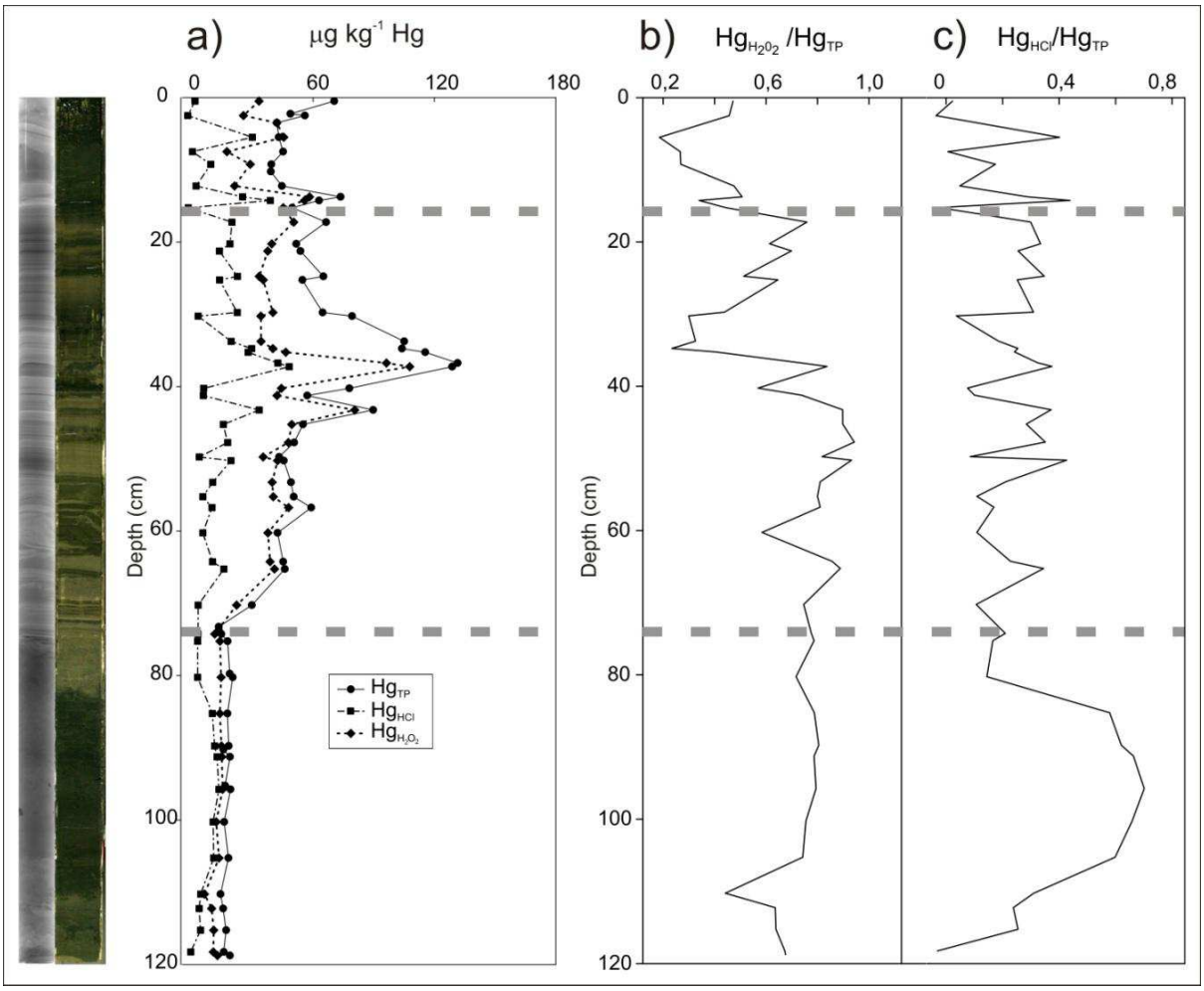

Fig. 4-12: Mercury concentrations. a) Selective extractions corresponding to the concentrations of total particulate (Hg_{TP}), oxidisable ($Hg_{H_2O_2}$) and acid-soluble/reactive (Hg_{HCl}) fractions. Relations between (b) $Hg_{H_2O_2}$ and Hg_{TP} and (c) Hg_{HCl} and Hg_{TP}.

4.2.5.1 Fe and Mn concentrations

Because reducible (Fe and Mn-asc) and acid-soluble/reactive (Fe and Mn-HCl) fractions encompass the dissolution of many Fe and Mn-bearing minerals, these two elements were measured on the corresponding supernatants (Table 3-1). Their profile traces are shown if Fig. 4-13a-b. Fe-total fraction averaged in 30235 mg kg^{-1} in sediments accumulated from the bottom of the core up to 74 cm, 34359 mg kg^{-1} in the central part up to 16 cm, and 28274 2440 mg kg^{-1} in the upper centimeters. The Fe-asc and Fe-HCl fractions, at the same intervals, show average concentrations of 1790, 1259 and 2444 mg kg^{-1}, and 7044, 5247, 6082 mg kg^{-1} respectively. Fe-asc fraction explains in the lower part of the core 4.94 ± 3.43 % of the total

fraction while in the middle and upper part it explains 3.78 ± 2.70 and 8.33 ± 2.74 %. Furthermore, the Fe-HCl fraction explains 22.941 ± 4.495 %, 15.41 ± 3.64 and 21.81 ± 2.48 % of the total respectively.

Regarding Mn at the same depths, the total fraction showed values that averaged 19032, 17734 and 15506 mg kg^{-1} while the concentrations for the Mn-asc and Mn-HCl averaged 1482, 1713 and 1550 mg kg^{-1} and 9211, 5969 and 5571 mg kg^{-1} respectively. Mn-asc concentrations represent 7.78 ± 2.60, 8.98 ± 6.69 and 9.92 ± 1.93 % of the total Mn fraction while Mn-HCl concentrations represent 48.03 ± 10.14, 31.87 ± 12.56 and 36.82 ± 8.02 %. In addition, the HCl extraction seems to react in greater extent in the lower part of the core representing ~1.3 times more than the ascorbate fraction with respect to Fe and ~1.8 times with respect to Mn.

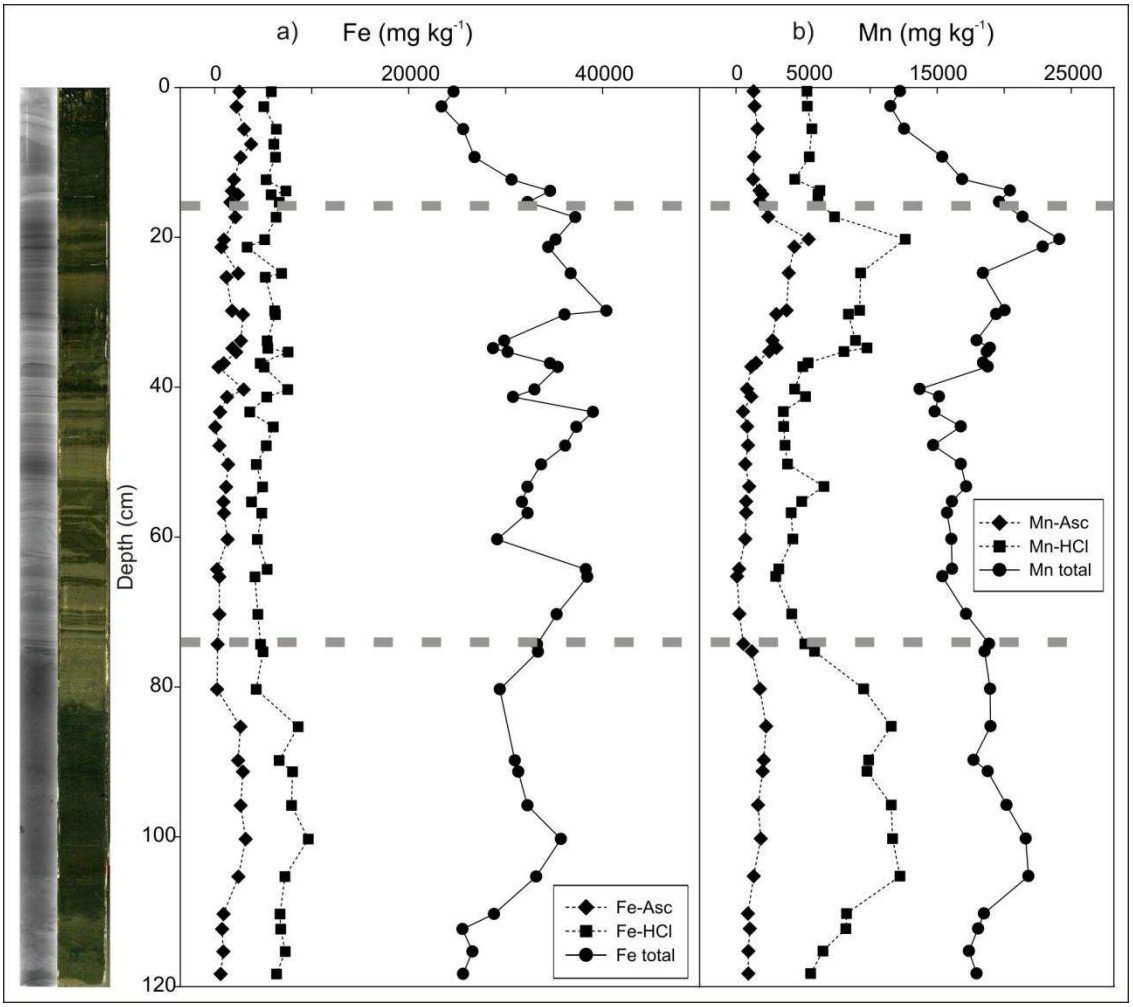

Fig. 4-13: Fe (a) and Mn (b) determinations in the supernatants of HCl and Asc.

4.2.6 Total Particulate arsenic (As_{TP}) and solid speciation

In order to determine the solid speciation of Arsenic, the concentrations determined in leachates obtained in the selective extraction procedures, are analyzed. Results indicate that both, the acid soluble/reactive (As-HCl) and the reducible (As-ascorbate) fractions show the same trend along the core depth. As-HCl concentrations vary from 0 to 25.089 mg kg^{-1} while As-ascorbate contents range between 0.901 and 13.61 mg kg^{-1} (Fig. 4-14a). As-HCl fraction explains most of the total As concentrations along the core, accounting for up to ~78 % (average 35.47 ± 15.82 %) while the As-ascorbate fraction accounts for up to ~46 % (average of 19.66 ± 11.13 %). Using the ratios As-HCl/Astot and As-asc/Astot it is possible to delimitate three zones along the core depth: 1) 120-74 cm; 2) 74-16 cm and 3) 16-0 cm. In each segment, the As-HCl average contributions are 46.58 ± 12.93 %; 27.17 ± 11.06 % and 48.28 ± 17.51 respectively (Fig. 4-14b) While average values determined for the As-ascorbate fraction are 25.11 ± 16.42; 15.28 ± 7.01 % and 27.38 ± 5.12 % respectively (Fig. 4-14c). The highest values for the As-HCl fraction occur in the first 5 cm whereas for the As-ascorbate fraction they occur at about 90 cm depth.

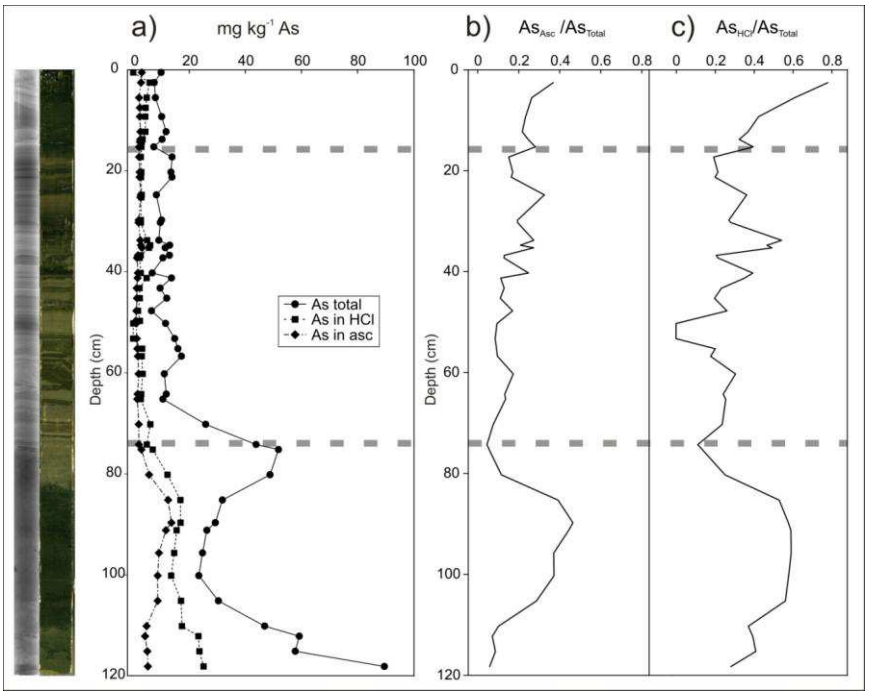

Fig. 4-14: Arsenic profiles along the LP core depth showing a) Total arsenic (As_{total}), reducible (As_{asc}) and acid-soluble/reactive (As_{HCl}) fractions. (b) Ratios of As_{asc}/As_{total} and (c) As_{HCl}/As_{total}.

The HCl extraction is related to the fraction that comprises the elements associated to carbonates and acid volatile sulphides. The profile of figure 4-14a clearly shows that the As-HCl fraction explains an important percentage of As-total. In order to analyze a possible association with carbonates, the As-HCl profile was compared with the one of the C_{inorg} fraction (

Fig. 4-15a, b). This figure shows that peaks of As generally coincide with peaks of C_{inorg} in the upper and middle part of the core, while in the core bottom, constant As-HCl concentrations coincide with rather constant C_{inorg} contents.

Furthermore, the molar ratio calculated for calcium and arsenic is shown in

Fig. 4-15c. Molar ratios in the lower part of the core range from 30.20 to 60.91 while in the middle and upper part of the core they range between 126.71 to 814.55 showing peaks at 53.25, 40.25, 34.75, 15.25 and 5.5 cm coinciding to those showed by the As-HCl fraction and C_{inorg}.

Calcite precipitation is produced when supersaturation is reached, that is, when Ca^{2+} and CO_3^{2-} concentrations in the lake waters are high and when pH conditions are alkaline (because the deprotonated C_{inorg} species predominates). Increasing ionic concentrations in closed lakes such as the Mar Chiquita system are produced during lowstand conditions, enhancing the precipitation of many relatively soluble salts. In consequence, the inverse trend observed between C_{inorg} concentration and lake levels can be explained by calcite precipitation. Arsenic concentrations also show an inverse trend regarding the Laguna Mar Chiquita lake-level (Fig. 4-8), which suggest a probable association of this element with calcite.

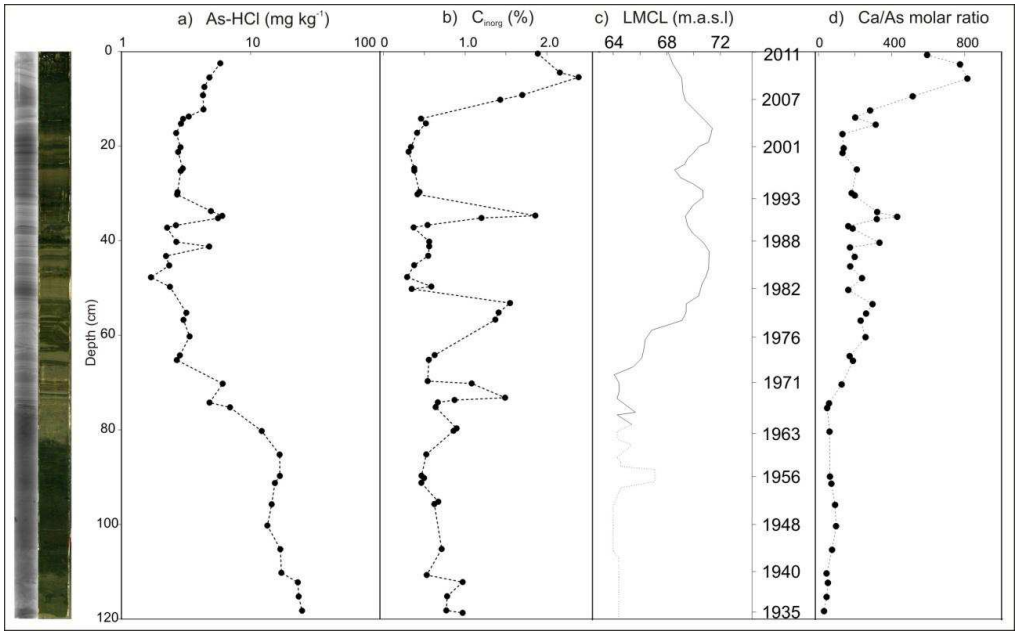

Fig. 4-15: Comparison between a) As-HCl fraction, b) C_{inorg} along the sedimentary core, c) Laguna Mar Chiquita Lake-level variations (LMCL) and d) Ca/As molar ratio.

The relationship between the As, Fe and Mn concentrations measured in the ascorbate fraction are shown in Fig. 4-16. As-asc fraction relates very well with both Fe and Mn-asc fractions mainly in the bottom part of the core (below 74 cm). Moreover, the graphic shows that exists a positive correlation in the middle and upper part of the core (above 74 cm) but it is less significant suggesting another bearing phase.

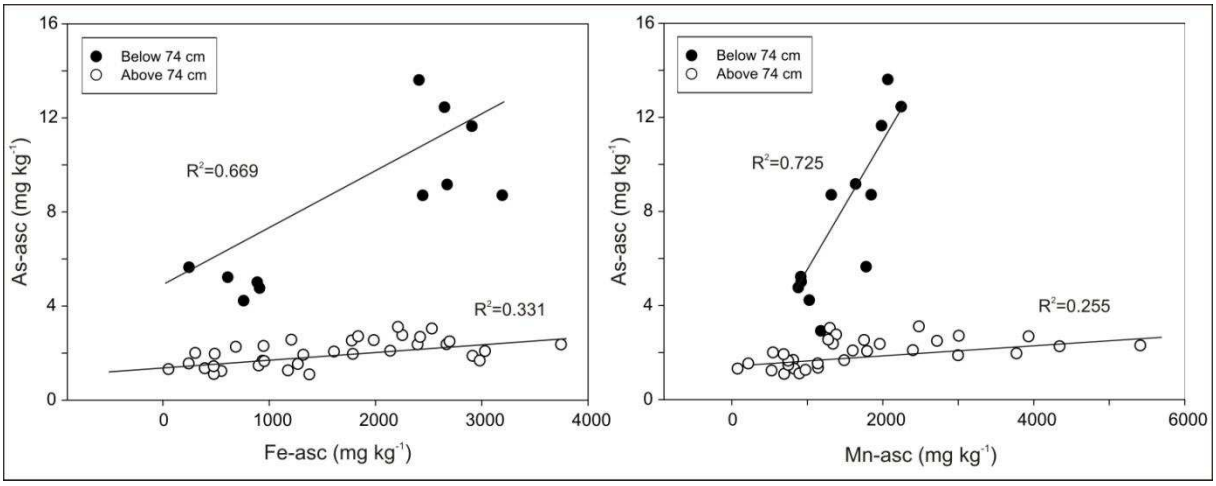

Fig. 4-16: Relationship between Fe and As and Mn and As measured in the ascorbate (asc) fraction.

4.3 Accumulation rates of Hg and As

Accumulation rates of Hg and As were calculated for the LP core, using the Mass Accumulation Rate (MAR) determined previously (see section 4.2.3 – Eq. 9). MAR varied between 0.331 and 1.566 μg cm^{-2} y^{-1} with an average of 1.07 ± 0.225 μg cm^{-2} y^{-1}. Accumulated masses (AM) are calculated using equation (Eq. 11):

$$AM = MAR \times element\ concentration \quad \text{(Eq. 11)}$$

The determined values for the accumulated mass of Hg (Fig. 4-17b) in the lower part of the core are very constant and reach an average value of 0.022 ± 0.003 μg cm^{-2} y^{-1}. Above 75 cm and up to 45 cm, the accumulated mass of Hg increases noticeably reaching an average value of 0.038 ± 0.016 μg cm^{-2} y^{-1} which represents an average increase of 1.7 relative to the rate

determined in the segment right below. This increase is further intensified in sediments deposited between 45 and 16 cm depth, where the accumulated mass of Hg per unit area reaches an average value of 0.078 ± 0.022 μg cm^{-2} y^{-1}, with a peak of 0.135 μg cm^{-2} y^{-1} Hg at 36 cm depth. The most modern sediments, accumulated above 16 cm depth, show an accumulated mass of Hg that in average is ~2 times lower (0.041 ± 0.014 μg cm^{-2} y^{-1} Hg) to the previous period but at the same time is ~2 times higher than the average value at the lower part of the core. These accumulation rate values for Hg are similar to those obtained in a non-polluted area in China (with Hg_{TP} values in the order of those found in the LP core - Xia *et al.*, 2011) where the sedimentations rates are high, that also correspond to the ones measured in this work.

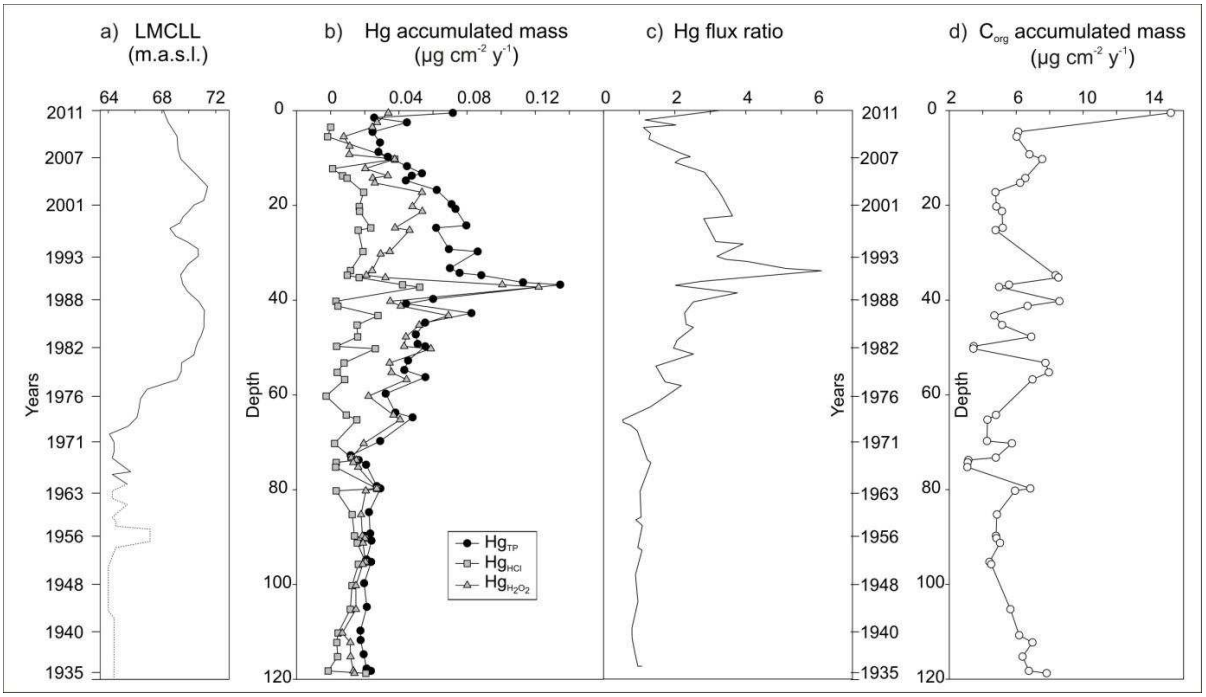

Fig. 4-17: a) LMCLL – Laguna Mar Chiquita Lake-level variations, b) Accumulated mass for Hg for Hg_{TP}, $Hg_{H_2O_2}$ and Hg_{HCl} fractions, c) Hg fluxes and d) Accumulated mass for C_{org}.

The gradual increase of Hg concentrations in modern sediments accumulated in remote regions of the Earth (i.e., Biester *et al.*, 2002; Hermanns and Biester, 2013) was assigned to increasing global atmospheric Hg. To differentiate these inputs from others of geogenic nature, a reference value assigned to non-affected conditions by atmospheric inputs was calculated using the average Hg concentrations on the bottom of the core (sediments

accumulated before 1970). This assumption is based on the constancy of the values registered in this part of the core and the similitude of these values with those measured in sediments of the Suquía River basin (Table 4-6), suggesting that these sediments could have been the main source of Hg to the lake in the years prior to 1970. Fig. 4-17c shows the obtained profile of the ratio between the accumulated mass of Hg and the corresponding background value. It is possible to see a gradual increase in the accumulation rate of Hg from early 1970s, reaching values ~3.5 times higher in sediments accumulated in the year 2011 with respect to those registered in the sediments accumulated before 1970. Despite this marked increase, the maximum accumulation values of Hg occurred between 1990 and 1995, when peaks between ~ 4 and ~ 7 times higher than the background values were registered.

When calculating the accumulated mass per unit area of the two extracted fractions of Hg, it appears that much of the increase in the flux of Hg in sediments accumulated between 75 and 16 cm depth is explained mainly by the contribution of Hg associated with oxidizable fraction (organic matter + sulphide). This fraction explains almost 100 % of the accumulated mass until approximately the year 1990. In the most recent sediments there is an Hg excess that cannot be explained by neither of both fractions (Fig. 4-17b).

Following the same procedure, the accumulated mass of organic carbon (C_{org}) was calculated along the core. The obtained profile (Fig. 4-17d) shows a distribution more or less constant from the bottom of the core until the 16 cm (average accumulated mass 5.55 ± 1.52 μg cm^{-2} y^{-1} C). Above this level, the accumulated mass of C starts to gradually increase reaching an average value of 7.79 ± 3.57 μg cm^{-2} y^{-1} C. This distribution prompts that the organic matter contribution was more or less constant between 1935 and 2003 and that the beginning of the humid period from in the beginning of the 1970s only affected the variability in the organic matter input to the lake, without significantly altering its average accumulated mass. Consequently, increasing Hg associated to the oxidizable phase in the sediments accumulated between 75 and 16 cm depth may be assigned not only to the organic matter but also to the presence of other oxidizable phases in the sediment, probably pyrite since this mineral has been identified through the analysis of X-ray diffraction (Fig. 4-10).

Beyond the predominance of the oxidizable fraction along the entire sedimentary core, the bioavailable fraction also plays an important role in solid speciation of Hg, especially below 74 cm depth (Fig. 4-17b). This fraction represents the Hg that is adsorbed on the surface of Fe and Mn oxides or other minerals, including pyrite.

The distribution of the Fe and Mn concentrations measured in the ascorbate extraction revealed a strong presence of oxides below 80 cm and above 40 cm (Fig. 4-13). Hg extracted in this same fraction is negligible, suggesting that most of the Hg present at these levels is not associated to Fe and Mn-oxide coatings. Accordingly most of the Hg extracted with HCl would be associated to pyrite (total S oscillates between 5 to 10 % in these levels, Fig. 4-8).
As accumulation rates (Fig. 4-18a) were calculated using Eq. 10. In average, rates in the bottom of the core up to 74 cm were 53.54 ± 24.77 μg cm^{-2} y^{-1} As while in the top core, the calculated average value was 11.03 ± 4.42 μg cm^{-2} y^{-1} As. The accumulation rates determined for the As–HCl and As-asc fractions show a clear predominance of the former. In the deeper part of the core, average values for As-HCl fraction were 19.22 ± 6.99 μg cm^{-2} y^{-1} As against 8.88 ± 4.89 μg cm^{-2} y^{-1} corresponding to the accumulation rates of the As-asc fraction. In the upper part of the core, the As-HCl fraction average an accumulation rate of 2.88 ± 1.28 μg cm^{-2} y^{-1} while the As-asc fraction, 1.91 ± 0.685 μg cm^{-2} y^{-1}.

As previously indicated for Hg, As fluxes were calculated for sediments accumulated in the LP core. Fig. 4-14a shows that the most constant values of As were measured in sediments accumulated in the range of depth between 74 cm and the top of the core. The average accumulated mass of As_{TP} for this section was 11.03 ± 4.42 μg cm^{-2} y^{-1}. This value was used as a reference of background conditions. As seen in the profile that shows the As accumulation rates in depth (Fig. 4-18b), under dry conditions, the deposition of As-bearing sediments was ~5 times higher than under humid conditions that prevailed from the beginning of the 1970s. Besides, a marked peak is observed at ~75 cm depth. After this period, As flux show a decreasing pattern. The two analyzed As fractions follow a similar trend, but they cannot explain the total As accumulation rate in the lower part of the core As-HCl counts in average for 41.29 % and As-asc counts for 22.36 % of the total As. All along the lower segment of the core, the As acid-soluble fraction (As-HCl) predominates over the reducible fraction (As-asc), indicating that As is preferentially released from the sediments due to the dissolution of some acid-soluble As-bearing mineral. Some As is also considered to be adsorbed onto Fe and Mn hydr(oxides) in these sediments. In agreement, the Fe and Mn profiles for the reducible fraction (Fig. 4-13) correlates with that of the As. The adsorption of arsenate ions onto Fe (oxy)hydroxides occurs under neutral to acidic conditions; desorption, hence, is favoured at alkaline pH (Hiemstra and Van Riemsdijk, 2000).

The unexplained fraction of As could be assign to oxidizable minerals (mainly secondary sulphides), whose extraction was not performed for the study of As speciation. The presence of pyrite determined through DRX (Fig. 4-10) in the lower part of the core may support this hypothesis.

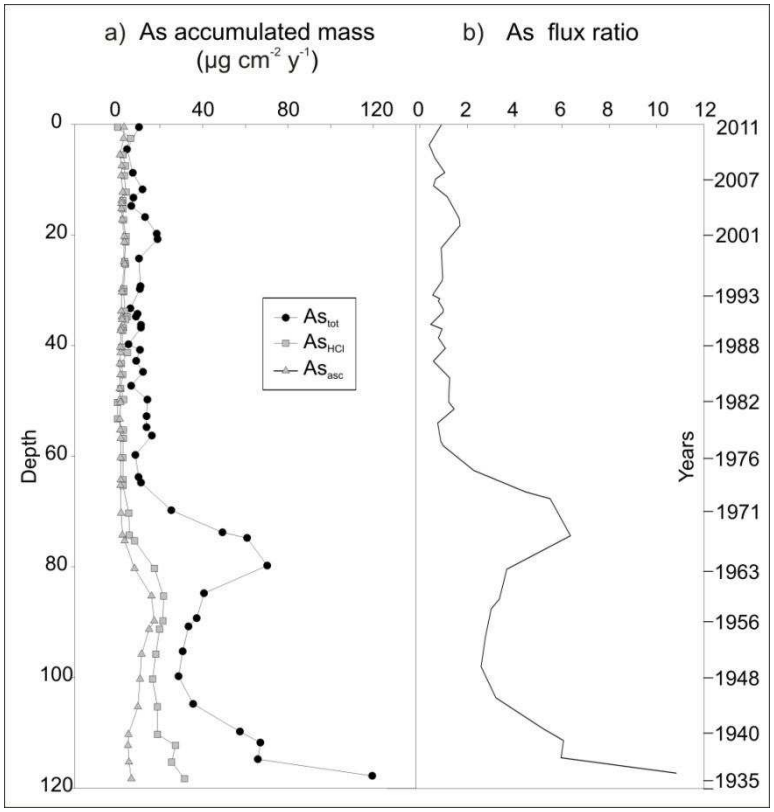

Fig. 4-18: a) Accumulated mass for As for As_{tot}, Hg_{HCl} and Hg_{asc} fractions, b) As fluxes

4.4 Quantification of the size variation of Laguna Mar Chiquita and Laguna del Plata Lake system

The Mar Chiquita system is a vast and important ecosystem (Bucher *et al.*, 2006) and as Piovano *et al.*, (2002, 2004a) mentioned, it is a sensitive climate indicator along with other lakes located in the Chaco Pampean Plain (Piovano *et al.*, 2009). Estimations of its size change are given in the bibliography (e.g., Piovano *et al.*, 2004b). Nevertheless, there are no

existing records of a detailed size change for Laguna del Plata. This section aims to quantify this variation for Laguna del Plata as well to estimate the size of Laguna Mar Chiquita nowadays. In order to perform the calculations, Landsat satellite images and the software ArcGIS were used. The treatment procedure is explained in section 3.3. Unfortunately the Path 229 of Landsat images have some line gaps that do not allow to treat the images properly, therefore only the images that correspond to Path 228 and Row 081 were used.

4.4.1 Laguna Mar Chiquita

Laguna Mar Chiquita size variation is very impressing. Due to its wide extension, Laguna Mar Chiquita occupies two paths of the satellite images (the 228 and 229). Because of the line gaps in path 229 the size of Laguna Mar Chiquita, especially for the highstand periods, was not able to be fully calculated. The part of the lake that is located on the Path 229 was estimated around 130 km^2 in periods of intermediate lake levels (~2002). In the Fig. 4-19 it is possible to see the change suffered by the major part of Laguna Mar Chiquita. The black line on the left of the lake marks the limit between the Path 228 and the Path 229. The images are placed according to the size variation and not chronologically. Even with a missing part, the area measurements were performed for 14 satellite images that covered a period from 1986 to 2013. During these twenty-seven years, the greater extension was reached in the satellite image dating May 8th, 2003 (referenced as 2003.05.08) with an area of 6537.39 km^2 and the smaller was reached not long ago, on June 12st, 2013 with 2219.64 km^2. Taking into account these calculations, nowadays Laguna Mar Chiquita has reduce its size over 60 %. Due to this reduction, the extension of the lake in 2012 and 2013 fits in the Path 228 and Row 081 and the area can be well determined. Hence, it is important to highlight that the size that LMC presents in the satellite images in 2013 is its real size.

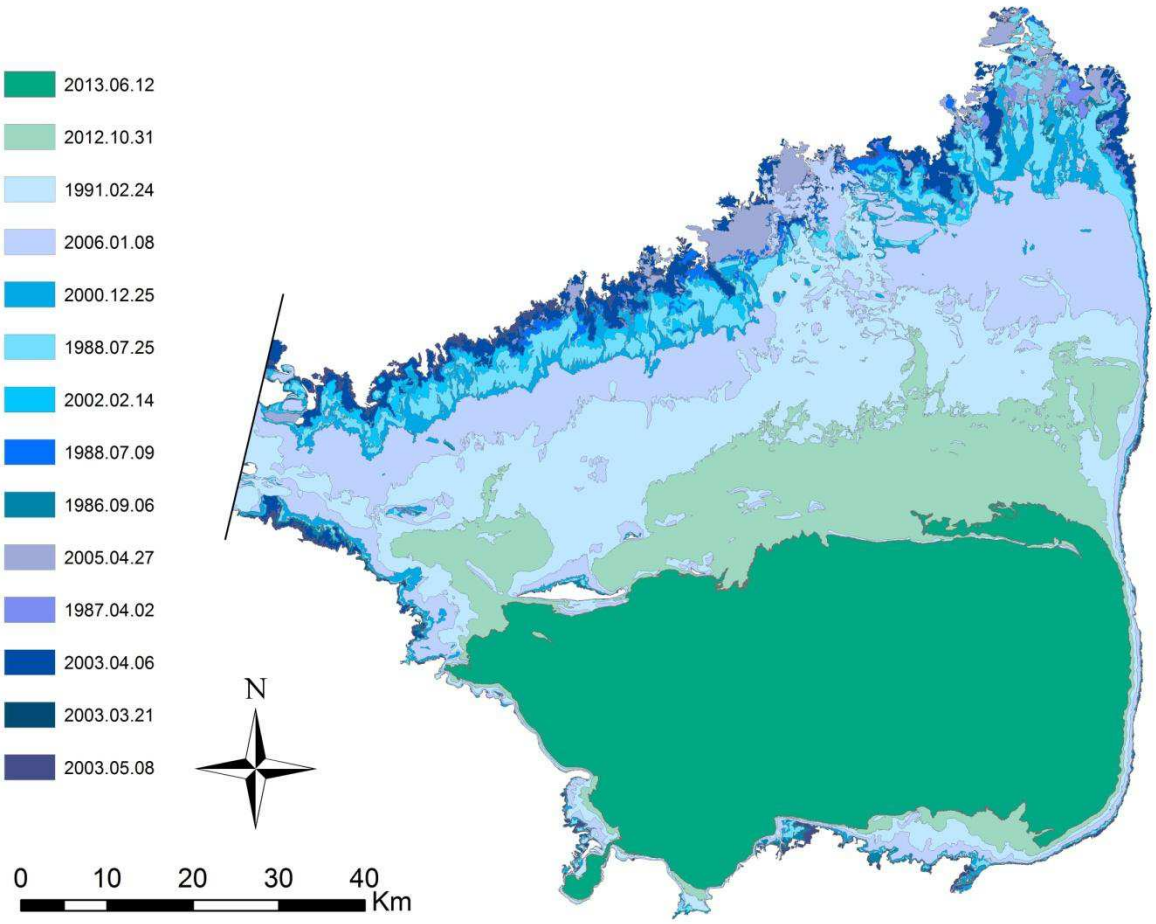

Fig. 4-19: Size variation of Laguna Mar Chiquita. The biggest size corresponds to the year 2003 while the smallest one to 2013 in the period that spans from September 1988 to June 2013.

4.4.2 Laguna de Plata

The reduction in the size of Laguna del Plata is as impressive as Laguna Mar Chiquita. This smaller lake is entirely situated in the Path 228 and Row 081 allowing to measure its extension in a fairly way. Fig. 4-20 shows clearly this variation through the studied period. The maximum size was calculated in the image corresponding to May 8th, 2003 (referenced as 2003.05.08) with an area of 28.86 km^2, while the minimum size was registered on June 12th, 2013 showing an extension of 13.81 km^2. Taking into account these values, LP presents nowadays a reduction so far of 53.6 % compared to the biggest measured size. The percentage of reduction for all images was compared to the maximum extension that occurred in the year 2003 and they are presented in Table 4-7 .

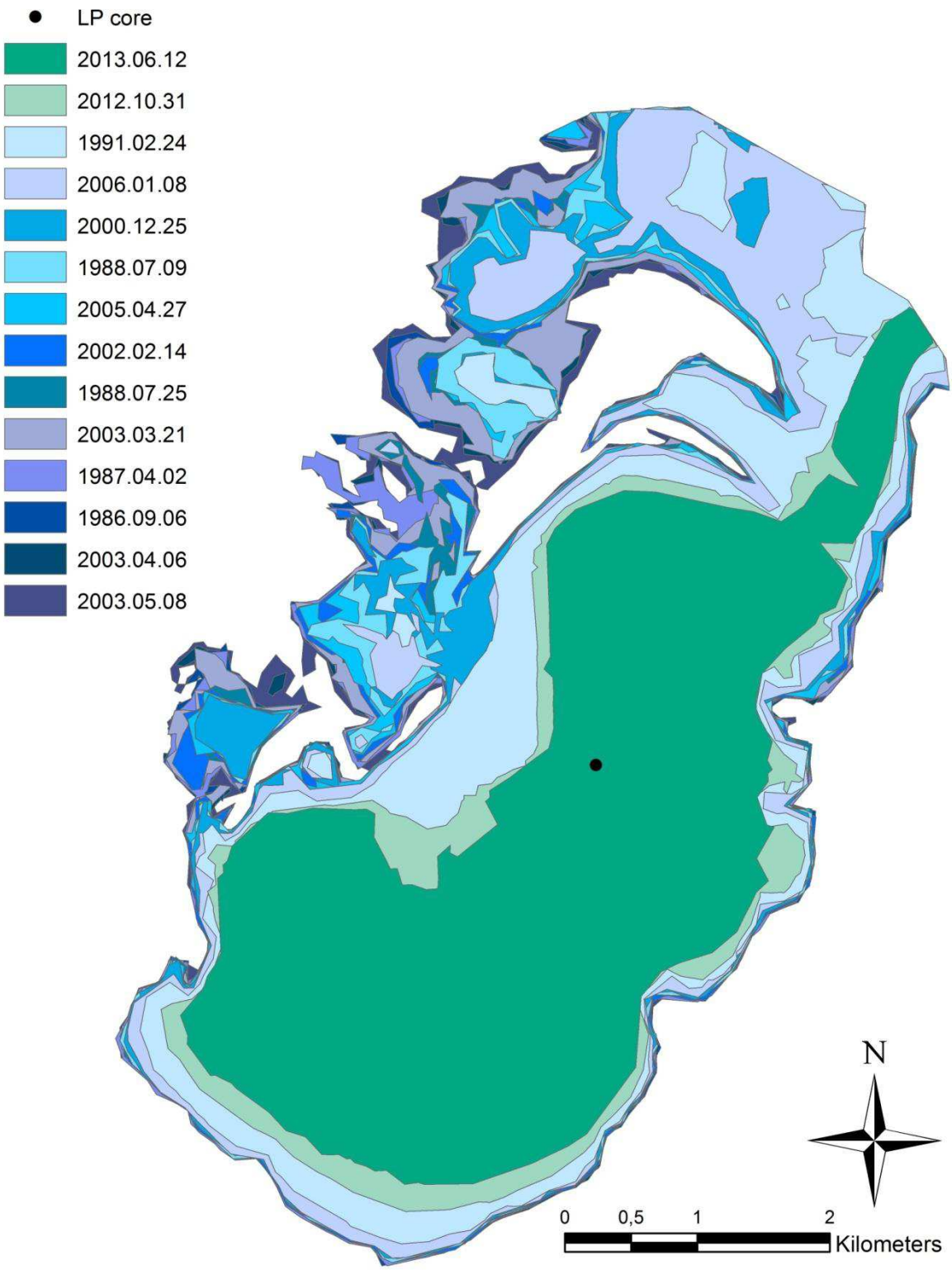

Fig. 4-20: Size variation of Laguna de Plata The biggest size corresponds to the year 2003 while the smallest one to 2013 in the period that spans from September 1988 to June 2013. The black dot corresponds to the emplacement of LP core.

Image name	Date	Referenced as	Calculated size km^2	Reduction %
LT52280811986297CUB00	1986-09-06	1986.09.06	28.6	4.1
LT52280811987092CUB03	1987-04-02	1987.04.02	28.5	4.4
LT52280811988191CUB00	1988-07-09	1988.07.09	25.9	13.3
LT52280811988207CUB00	1988-07-25	1988.07.25	26.9	10.0
LT52280811991055CUB00	1991-02-24	1991.02.04	20.1	32.7
LE72280812000360AGS00	2000-12-25	2000.12.25	24.8	16.9
LE72280812002045AGS00	2002-02-14	2002.02.14	26.6	10.9
LE72280812003080EDC00	2003-03-21	2003.03.21	28.4	4.9
LE72280812003096EDC00	2003-04-06	2003.04.06	28.9	3.2
LE72280812003128ASN00	**2003-05-08**	**2003.05.08**	**29.9**	**0.0**
L71228081_08120050427	2005-04-27	2005.04.27	26.2	12.1
L71228081_08120060108	2006-01-08	2006.01.08	23.2	22.4
LT52280812011270CUB01	2012-10-31	2012.10.31	15.8	47.2
LC82280812013163LGN00	2013-06-12	2013.06.12	13.8	53.6

Table 4-7: Satellite images information and the calculated size and reduction. Satellite image in black correspond to the maximum extension.

Fig. 4-20 shows the size variation for LP and as with LMC, they are represented according to their decreasing size where the maximum extension corresponds to the year 2003. As it was mentioned before, the hydrological variations in Laguna Mar Chiquita have a strong influence over Laguna del Plata, especially during high-stands when both lakes are connected. Chronological size fluctuations are illustrated in Fig. 4-21 as well as the LMC lake-level variations and the precipitations measured in the Miramar town. The rise in the water level of LMC as well and the increment in precipitation registered at Miramar town reflect the beginning of the humid period early in 1970s. Unfortunately satellite images corresponding to this period were not available to measure the size of the lake at that time but important contrasts are given between humid and dry periods. The most humid periods like those that occurred in 2003 or 1986 show the biggest sizes while the important droughts that took place in 1991 or the ones that are happening nowadays have left an imprint of a very reduced lake. Laguna Mar Chiquita lake-level has reached so far 67.45 m.a.s.l. and keeps on decreasing what could be traduced in an even smaller size of Laguna del Plata.

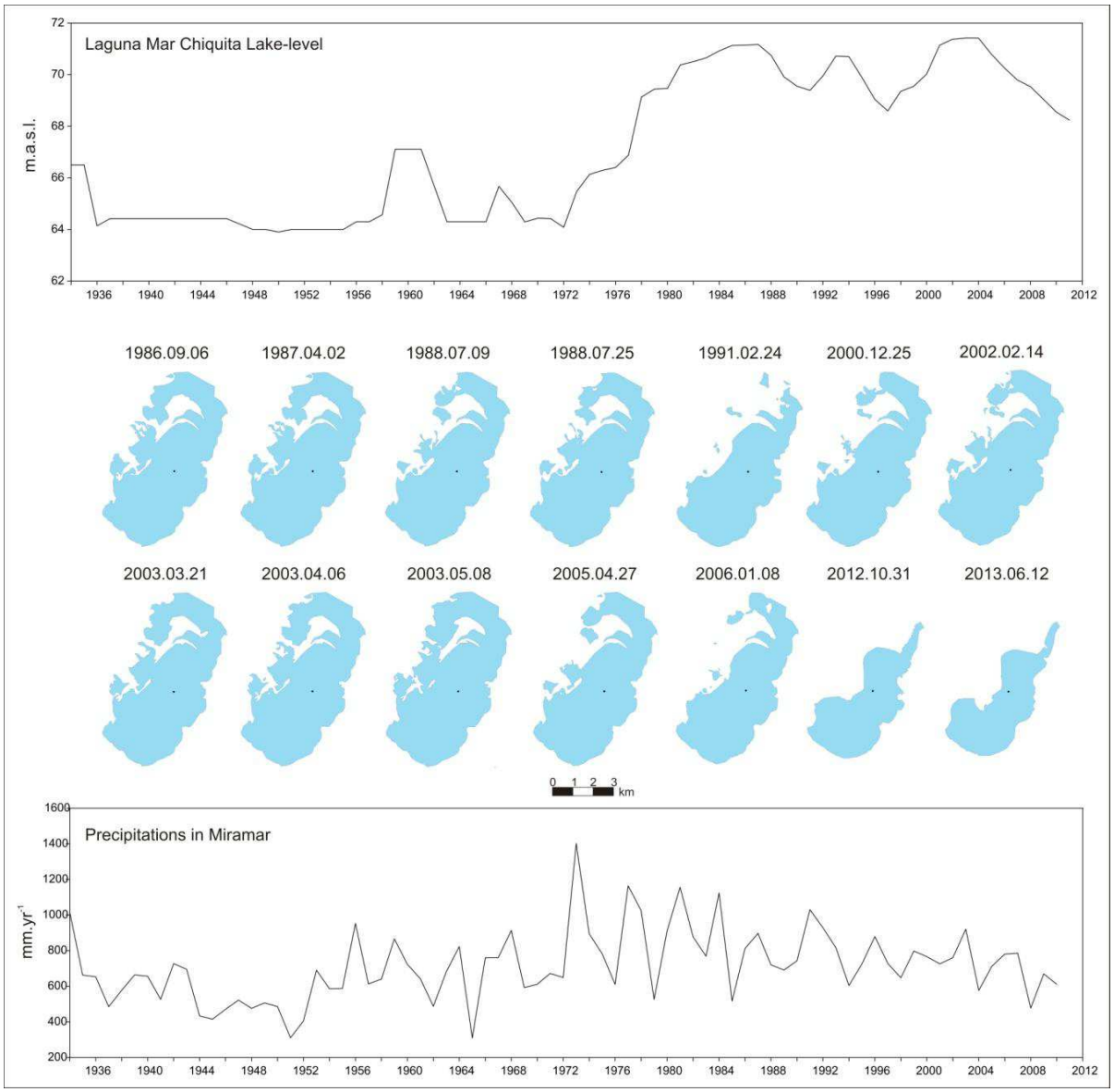

Fig. 4-21: Chronological size variation of Laguna del Plata compared to the variation of the lake-level of Laguna Mar Chiquita and the precipitation record of the Miramar town.

4.5 Summary

Finally, the main results could be synthesized as follow:

Geochemical characterization of the Suquía River basin:

- The Suquía River waters show a physicochemical gradient from the headwaters to downwaters until arriving to the Mar Chiquita system. Waters change from calcium-sulphate to sodium-chlorided type.
- Saturation indexes for halite, anhydrite, gypsum, fluorite, dolomite, aragonite and calcite become increasingly positive from headwaters to the lake.
- Soluble As concentrations have a good correlation with Li, Mg, Si, Ca, V, Br, Sr, and Mo.
- As concentrations in river water show an increasing gradient from the upper basin (crystalline rocks) to the lower basin (loessic sediments).
- Total particulate Hg concentrations measured in riverbed sediments collected from tributaries and from the Suquía River higher at the basin's catchments. Besides, HgTP concentrations are ~7 times higher in the finer fraction (<63 µm) of the riverbed sediments.
- Riverbed sediments are composed of quartz, albite, illite, microcline, perovskite and pyrite, while in lake bottom sediments, evaporite salts such as halite and calcite are identified along with quartz, albite, muscovite, and biotite.

Geochemical and sedimentological characterization of the sedimentary core

- Core dating allows to have a chronology for the last ~80 years.
- Mainly 3 zones in the core (corresponding to the years 1953 to 1969, 1969 to 2004 and 2004 to 2011 at the depth of 120 to 75, 75 to 16 and 16 to 0 cm respectively), are identified based on marked variations of porosity, pH, C_{org}, C_{inorg}, sulphur as well as of major and trace element concentrations.
- Minerals identified along the core are quartz, albite, calcite, muscovite, biotite and halite as well as the clay minerals: montmorillonite and kaolinite. Pyrite is also present as an accesory mineral.

- Significant differences from 1970s until present are traduced in abrupt changes in the grain-size distribution and elemental concentrations, particularly in total particulate Hg and As as well as in their corresponding solid species.
- Hg associated with the oxidizable fraction (OM and sulphides) mostly explain the Hg_{TP} concentration measured along the core, especially in the sediments accumulated after 1970. Before this date, the acid-soluble Hg fraction is as important as the oxidizable one. The concentration of Hg associated with the reducible fraction (Hg-ascorbate) is neglible all along the core.
- There is an important Hg peak at ~35 cm depth that cannot be explained by the fractions analyzed through selective extractions, suggesting than another Hg-bearing phase is present.
- As associated with the acid soluble fraction (As-HCl) is as important as the As associated with the reducible fraction (As-ascorbate). However, none of them may completely explain the concentrations of total particulate As along the core.
- There is an important As peak at ~75 cm depth that coincides with a rise in Cinorg and S concentrations.
- Increasing Hg accumulation rates are determined from 1970. Conversely, the As accumulation rates show a decreasing trend in the same period.
- Laguna del Plata has reduced its size in over 50 % in the last 10 years.

5. Discussion

The Laguna Mar Chiquita system has been widely studied as a whole but not many studies have been performed in the small lake of Laguna del Plata. The sedimentary record of this highly size-changing small lake helps to understand the hydrodynamics of its affluent (the Suquía River), as well as the environmental and geochemical evolution of the basin with time. Furthermore, the elemental proxies obtained in this hyper-saline lake serve as a comparative means for lakes with similar characteristics.

5.1 The hydrogeochemistry of the Suquía River basin

The Suquía River plays an important role of carrying sediments and solutes from the headwaters until it reaches the Laguna del Plata. Donwnflow, its chemical and physicochemical composition changes due to the impact of the city of Córdoba, industries located nearby and also due to the intensive agriculture activities. However, both lithology and hydrology seem to be the most important factors controlling the geochemical evolution of the river. Chemical alteration described in the river waters and sediments are linked with the organic nature of the urban effluents that produce a marked consumption of dissolved oxygen that originates anaerobic conditions inmediatly downflow the city of Córdoba (i.e., Pesce and Wunderlin, 2000; Wunderlin *et al.,* 2001; Monferrán *et al.,* 2011; Merlo *et al.,* 2011).

Besides the mentioned anthropogenic influence, a natural gradient represented by increasing conductivity, TDS and pH values is observed downflow. Values of pH are close to neutral in the headwaters while downflow it becomes more alkaline until reaching values of ~9.5 in lake waters. The mentioned trend is more likely attributed to the lithology that also controls the major chemical composition of waters in the basin. At the basin's catchment, where igneous and metamorphic rocks prevail, waters are of the calcium-bicarbonate-type and change to the sulphate type in the middle stretch of the river after crossing the city of Córdoba where lithology is dominated by loessic deposits. Near to the lake area, waters show their maximum concentrations in TDS and the highest conductivities in the basin changing from fresh water to saline water (30-50 g L^{-1}) in the Laguna Mar Chiquita and into brines (>50 g L^{-1}). The interaction with lithology also controls the saturation of the water in the basin with respect to different minerals. Piovano *et al.,* (2009) indicate that drier conditions predominate in the region from 2003. The Mar Chiquita systems reduced its size considerably and these changes can be seen in figures Fig. 4-19 and Fig. 4-20. Laguna del Plata has reduced its size at least 50 % in the last 10 years. These changes are in agreement with the precipitation record (Fig.

4-21) measured in Miramar town that shows a humid trend early 1970s and a reduction in precipitations early 2000s. The changes in water input carried a consequent increase in salinity and precipitation of salts. This climatic trend gives high probability to reach supersaturation conditions to allow precipitation of minerals like dolomite, aragonite and calcite (Table 4-2) as it found in river water samples and that increase in these minerals while closer to the lake. Dissolution of salts such as halite could occur in the basin and even if saturation for this mineral is not reached, values tend to be less negative downflow.
The physicochemical gradient that was observed in lake waters with depth can be explained by the existence of a microbial mat that covers the bottom of the lake. This mat corresponds to the contact zone between the water and the bottom of the lake (Bucher and Abril, 2006). In salt lakes, this zone favours the development of a rich community of bacteria, algae and microscopic animals (Jonkers *et al.,* 2003) and it is where an important amount of primary productivity occurs (Hammer, 1986). Even if the water column in both lakes is well oxygenated as cause of the dominant winds, the diminution of dissolved oxygen (
Table 4-1) between water in the surface and in the bottom of the lake proves its existence.

Soluble trace metals were also determined in waters of the basin. Focus was made on As and some other elements usually associated with it in groundwaters in contact with loessic sediments accumulated in the Chaco Pampean Plain (see section 2.2.4). In waters of the Suquía River basin, As concentrations are below the WHO drinking water guideline (10 μg L^{-1}) in most of the sampling points located in the catchments. Nevertheless, As concentrations reach values that exceed over 2 times the drinking water guideline (22.4 μg L^{-1}) in the lower part of the basin (RS9). Especially in the middle and lower part of the basin, higher As concentrations are assigned to a longer water-rock interaction but also to the presence of loessic sediments. As concentrations measured in surface waters are markedly lower than those measured in groundwaters (i.e. Nicolli *et al.,* 2012 and references therein) due to the shorter time of contact between water and sediments. The source of As in surface waters is likely associated with the loessic sediments, as suggested by the high correlation values that exist between As and some other trace elements such as Li, V and Mo (Table 4-5). The good correlation between As and this elements has also been reported in groundwaters of the Chaco Pampean Plain, and this behaviour was atributted to the dissolution of volcanic glass grains spread in the loess matrix (Nicolli *et al.,* 2010, 2012).

5.2 The geochemistry of riverbed sediments in the Suquía basin

Sediments play an important role as sinks of trace metals and therefore they constitute excellent archives of past contamination (Castelle *et al.,* 2007). Besides, they may act as secondary sources, releasing them again into solution under suitable environmental conditions (Schäfer *et al.,* 2010). The concentration of trace metals in sediments is also linked to the particle size; generally it increases with decreasing particle size (Brook and Moore, 1988). Mineralogical composition of riverbed sediments (Fig. 4-4) reveals the presence of quartz, albite, illite, microcline, and accessory minerals such as perovskite and pyrite. All these minerals are former components of the crystalline rocks of the Sierras Pampeanas Range located in the western margin of the study area, thus reflecting the weathered materials that are transported downstream. Minerals identified in the lake bottom sediments are mostly the same but some secondary minerals such as calcite and halite are also identified. These minerals formed by precipitation from the supersaturated lake waters (Table 4-2)

Both, silty and sandy fractions show that the higher Hg concentrations are located in the upper part of the basin where values are over 61 μg kg^{-1} while in the middle stretch of the Suquía River and lower part of the basin, Hg concentrations remain low (<61 μg kg^{-1}). Even if higher Hg concentrations are located in the upper part of the basin, values are among those considered within the limits of natural total particulate Hg in sediments (150 μg kg^{-1}, Schäfer *et al.,* 2006). The upper part of the basin is located in the Sierras Pampeanas Range where exists the presence of sulphur mineralization (Mutti *et al.,* 2005) and could be the source of this Hg. Besides, part of the sediment carried by the river and that contains Hg, could be deposited in the San Roque Dam and stop the transport downflow. Furthermore, the industries and city input in the middle stretch and lower part of the Suquía River seems to be negligible due to that Hg concentrations are more or less constant before and after crossing the city of Córdoba until the river mouth in Laguna de Plata.

The geochemistry of sediments is marked by the imprint of the dominant rocks in the area. Hg concentrations are below the limit of natural values. Nevertheless, higher concentrations occur in the mountainous area associated to sulphur mineralization but punctual anthropogenic source was not detected.

5.3 Chronology and sediment deposition of the sedimentary core

The sedimentary core taken in Laguna del Plata (LP) where the Suquía River mouths allows to understand more about the sedimentation processes that took place in this lake.

The Mar Chiquita system has suffered dramatic hydrological changes. Piovano *et al.* (2009) calculated that Laguna Mar Chiquita (LMC) had ~1000 km^2 prior to the 1970s and that it increased its size up to ~6000 km^2 in the wettest periods (like in 2003). Nowadays, Laguna Mar Chiquita covers an extension of ~2000 km^2. Concerning Laguna del Plata, reconstructions of the size of the lake have not been previously calculated. However, the climatic changes that affected the region have transformed the physiognomy of this lake reducing its size in more than 50 % (from 29.9 to 13.8 km^2) in the last 10 years (section 4.4.2). These changes are also registered in the sediments, thus the chronology was determined along the sedimentary core for better identify the events. The core dating estimates a sedimentary succession of ~80 years. Furthermore, it evidences an average sedimentation rate of 1 cm y^{-1} but in general two different sedimentation rates are noticed. One with values around 1.2-1.5 cm y^{-1} that occur before the year 1975 (up to 65 cm depth) and the other one with values up to 3 cm y^{-1} determined in the upper part of the core. The latter is in agreement with the negative hydrological conditions that prevailed in the region since 2003. Before 1975 Laguna Mar Chiquita and Laguna del Plata did not have a hydrological connexion. However, Laguna del Plata continued receiving the sedimentary input from the Suquía River. Regarding the water balance, main contributions to the lake were from the Suquía River and groundwater discharges (Troin *et al.*, 2010). In contrast and due to its larger extension, Laguna Mar Chiquita sedimentation rates are much lower and vary between 0.25-0.34 cm y^{-1} during lowstands and between 0.77-1.12 cm y^{-1} during highstands (Piovano *et al.*, 2002; 2006). These differences in sedimentations could be due to the position of the sedimentary core taken at LP11-1 sampling station. This location faces the entrance of the river to the lake and the contribution of sediment could be important.

In the early 1970s the climatic conditions started to change, and the dry period was replaced by a humid period (Troin *et al.*, 2010) that lead to an augmentation in the Mar Chiquita lake-level. Near the year 1975 alternating re-connections and disconnections between both lakes alternated may have occurred which are evidenced in the sedimentary record by the alternance of light and dark laminations at the depth of 70 cm (Fig. 4-6). Since 1976 there was a total reconnection between LP and LMC that persist until nowadays. However, since 2003 the

water budget started to decrease (Piovano *et al*,.2004, 2009) leaving a small channel that connects both lakes and that gets increasingly narrow (Fig. 4-20).

When comparing the grain-size distribution in sediments accumulated in Laguna del Plata with the historical LMC lake-level variation (Fig. 4-8c) it is possible to deduce that predominating fine silt correspond to periods where the lake-level was stable for a short period of time. Medium to coarse silt fractions are related to periods were the lake-level started to rise, either if it was after a long or a short dry period. This clearly represents an enhanced transport of larger particles from the basin due to the higher water energy and higher runoff. Different water input budgets are traduced as well in the porosity values (Fig. 4-8e). The lower part of the core is represented by almost constant porosity values but from the beginning of the wet period they increase. Higher water budget generated an increase in primary production that it is traduced in higher C_{org} inputs that may additionally control the porosity values. C_{org} values registered in the lower part of the core are almost constant (~0.83 % ± 0.22) and in addition they are concomitant to the scarce precipitations and the high water salinity. These values are markedly lower than those previously reported for some Patagonian lakes. In Northern Patagonia, C_{org} oscillated between 6 and 8 % (i.e. Ribeiro Guevara *et al.*, 2010) while in the South, values varied between 12 and 15 % (Hermanns and Biester, 2013). C_{org} values are important indicators of Hg input from soil erosion in the upper watershed of lakes due to the high affinity of this element for organic matter (Driscoll *et al.*, 1995; Rydberg *et al.*, 2010; Teisserenc *et al.*, 2010).

The bottom part of the core represents the period that spans the years between 1935 and 1975. According to Cioccale (1999) present climate conditions in Argentina started around the middle 19th Century after the end of the Little Ice Age which was characterized by cold and arid episodes alternated with short humid events. In this arid period great amount of loess (from 45 to 145 g m^{-2} y^{-1}) were transported from the Andes to the Chaco Pampean Plain (Zárate, 2003; Maher *et al.*, 2010) and could have influenced the input of larger particles into the lake. Furthermore, Martínez *et al.* (1994) and Kröhling and Iriondo (1999) identified that the west part of the Mar Chiquita system is composed by aeolian sands (Fig. 1-8).

Recent studies performed by Gaiero *et al.* (2013) show that sediments with origin in the Puna-Altiplano region (north of Argentina) can be transported for long distances thanks to the dominant air masses movements in South America. Two dusts events were monitored in 2009 and 2010 and even if their plumes were reduced ~50 % along its trajectories, their signals were registered 24 h after the beginning of the event in places located ~1300 km SE from the

source. The plumes were also registered in Marcos Juarez (located between Miramar and Buenos Aires) and the shape of the granulometric curves obtained for the atmospheric dust samples are identical to the grain-size distribution determined in top soil samples collected from the Puna-Altiplano region. In Laguna del Plata, granulometric distributions located below 80 cm are clearly bimodal which reflect the inputs from two different sources: 1) fluvial sediments transported to the lake by the Suquía River and 2) aeolian sediments that reach the lake as dust storms probably originated in northern Argentina. The latter is more evident during drier periods.

A clear example of this aeolian contribution was recently observed in the study area. On September 15th, 2013, high speed winds deflate the salt crusts and bare soils formed in the northern coast of Mar Chiquita and formed a thick plume over the region, as seen in the NASA satellite image shown in Fig. 5-1.

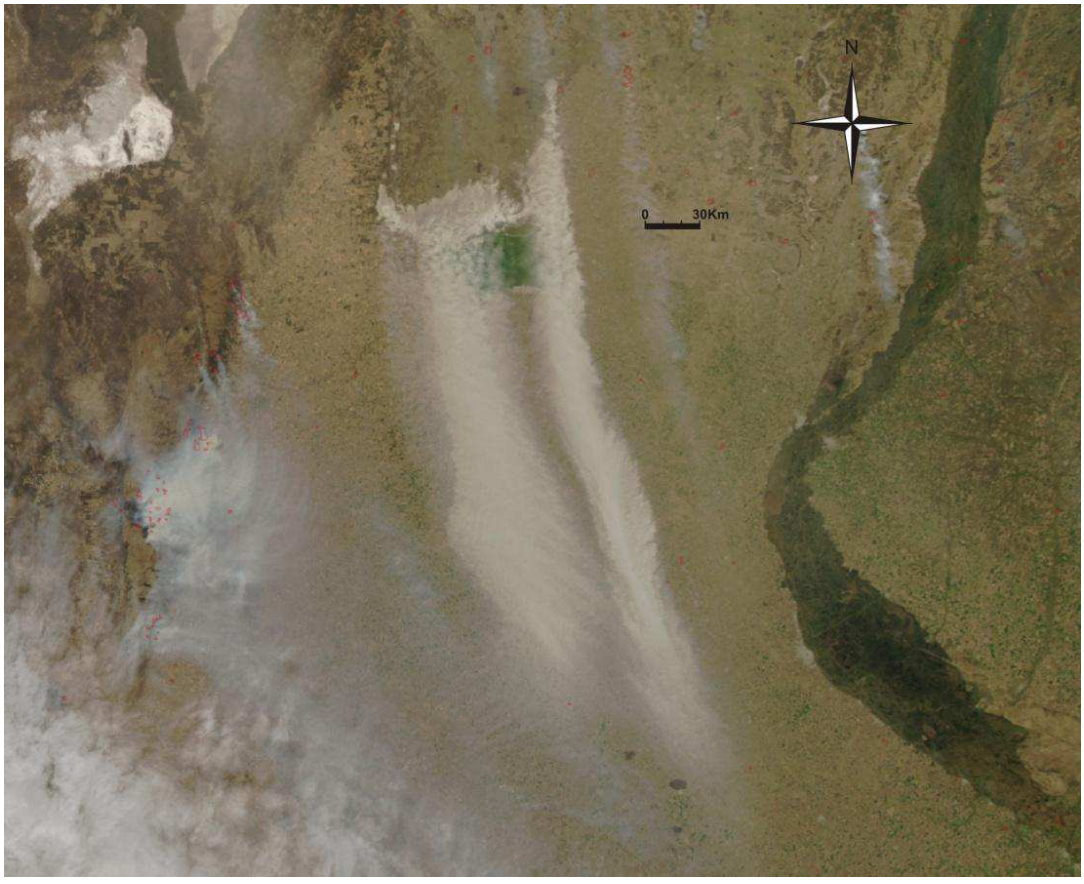

Fig. 5-1: Salt storm over Mar Chiquita System on September 15th, 2013 (NASA).

Using XRF data, Piovano *et al.* (2004b) conclude that the elemental variations along the sedimentary record of both, Laguna del Plata and Mar Chiquita seem to be controlled by well-

known hydrological fluctuations that affected the region during the 20th Century. Sediments accumulated in the bottom part of the LP core up to 74 cm represent the sedimentation before 1970s when LP was completely isolated from LMC and the inputs were mainly from the Suquía River. In agreement with these data, XRF signals measured in the core retrieved for this study (Fig. 4-11) reflect this single contribution to the sedimentary record. The augmentation of the regional precipitations that allowed the LMC lake-level to rise driving the re-connection of both lakes around 1976, generated a change in the sedimentation pattern overall the Laguna Mar Chiquita system (Piovano *et al.*, 2002; 2004a). Rising lake-level likely triggered the strong variations in Al, Si, K, Ti, Fe, and Zr concentrations measured in the LP core between 74 to 16 cm depth, reflecting a higher contribution from detrital input due to soil or fluvial-bank erosion in the basin's catchments. Several authors (Rothwell and Rack, 2006; Böning *et al.*, 2007; Moreno *et al.*, 2007; Löwemark *et al.*, 2011) coincide that variations of terrigenous elements such as Al, Si, K, Fe, and Ti are likely the consequence of inputs of allocthonous materials. The evaporitic signal can be inferred from Cl and Ca signals, which show constant profiles in the lower part of the core. An increment in the water budget could have contributed to the dissolution of salt crusts that are usually formed on top of the muddy sediments in drier periods next to the lake rising the signal of these elements, such is the case around 70 cm depth. The profiles of both elements in the upper part on the core (last 16 cm) show an augmentation of the signal toward the top. At the same time, these last 16 cm correspond to the period that spans from 2003-2004 to date. LMC lake-levels started to continuously decrease from 71.80 to 67.45 m.a.s.l. (Troin *et al.*, 2010) and rising the salinity from 27.0 g L^{-1} (Bucher and Bucher, 2006b) to 67.3 g L^{-1} (Biglia *et al.*, 2013) that could suggest a concentration of these elements in the sediments in LP.

Finally, the analysis of the sedimentary core showed to have a relation between sedimentation rates, grain-size distribution and chemical variations with changes of hydrological conditions through ~80 years:

- Until early 1970s dry and arid conditions prevailed and LP and LMC were hydrologically disconnected,
- From ~1976 to 2003-2004 wet conditions predominated and a lake-level followed with the consequent reconnection of both lakes,
- From 2003 until now, a new dry period started with the decrease in both lake-levels. LP and LMC are still connected through a narrow channel.

5.4 The historical record of Hg and As in sediments accumulated in Laguna del Plata during the last ~80 years

In connection with the hydrological variations previously identified and lithological context of the study area, changes in concentrations of Hg and As in the core are analyzed, as well as their souces and carrying phases.

5.4.1 Mercury

Using the sedimentological features, mineralogical composition, dating and selective extraction procedures, it was possible to reconstruct the historical record of Hg in the Suquía River basin and analyze the results on the context of the hydrological change.

Sediments accumulated in the lake before the 1970s show rather constant and very low Hg_{TP} concentrations (Fig. 4-12). During this period of high aridity and low lake levels, particles transported by the Suquía River exclusively settled in the Laguna del Plata due to the absence of hydraulic links between the latter and Laguna Mar Chiquita. The values of Hg registered in the lower part of the core are low compared with those measured in the upper part. However, they are similar to the concentrations measured in the riverbed sediment samples collected along the Suquía River watershed and also in a sample of atmospheric dry deposition collected in a pluviometric captor located near the lake.

According with selective extraction results, the main Hg carrying phases in sediments accumulated before 1970, are probably secondary sulphides, especially in the 105-85 cm depth range (Fig. 4-12). This is consistent with X-Ray Difractometry data that shows the presence of pyrite in the base of the core (Fig. 4-10), indicating that the precipitation of authigenic sulphides occurred under dominant anoxic conditions, likely produced by bacterial activity at the water-sediment interface. Similar conditions were found in different lakes around the world, for example Green Lake in United States (Suits and Wilkin, 1998), Baptiste Lake, Canada (Manning *et al.*, 1999), Qinghai Lake, China (Sugimori *et al.*, 2007) or Lake Kinneret, Israel (Nowaczyk, 2011).

Bucher and Bucher (2006b) studied the bottom lake muddy sediments from Laguna Mar Chiquita and they attributed the typical black colour of the sediments to the presence of bacteria that live in the microbial mat of the bottom of the lake. These bacteria include not only the bacteria (Cyanobacteria) *sensu strict* but the other two fundamental domains:

Archaea (single-celled microorganisms) and Eukaryote (cells containing a nucleus) (Bucher and Abril, 2006).

Hg can be bound to sulphides -mostly pyrite-, by adsorption (e.g., Bostick and Fendorf, 2003; Doyle *et al.*, 2004; Borah and Senapati, 2006; Ozverdi and Erdem, 2006) in a wide pH range (Behra *et al.*, 2001) forming Hg-Cl and Hg-OH complexes (Behra *et al.*, 2001; Bower *et al.*, 2008) and this process is favoured by the high water salinity and alkalinity (Bower *et al.*, 2008). Elevated salinity (380 g L^{-1}; Piovano *et al.*, 2004a) and alkaline chloride–sulphate sodium type waters (Martínez 1991) represent the geochemical conditions predominating during lake lowstands. Mercury associated with the residual fraction not extracted by the single extraction approach, attributed to the non-reactive crystalline matrix, was very low (close to zero) in the sediments accumulated before the 1970s, indicating that nearly all Hg deposited during that period was potentially bioavailable.

In sediments accumulated after the 1970s, the Hg_{TP} concentrations (Fig. 4-12) are clearly higher than downcore (almost ~4 times in average). This coincides with the beginning of an increasingly humid period in the region, and a concomitant rise in the lake system levels. During this period increased erosion and riverborne particle transport in the Suquía River watershed also occurred. The values in this section of the core are within the range measured in lakes of the Argentinean Patagonia and in other remote regions of the world that are not directly affected by human activity (e.g. Ribeiro Guevara *et al.*, 2010; Yang *et al.*, 2010; Conaway *et al.*, 2012; Hermanns and Biester, 2013).

In the 74-40 cm depth range, Hg is predominantly associated with sedimentary organic matter. Within this depth range, the C_{org} values are highly variable, but higher in average than the values measured in the bottom of the core. This trend reflects increasing Hg concentrations related to increased lake primary productivity but also to increased soil erosion and transport rates of riverborne particles in the Suquía River (Piovano *et al.*, 2009). The latter is also manifested through the presence of a major proportion of Hg associated with Mn and Fe oxy-hydroxides. Amorphous or poorly crystalline oxides are known as sinks for metal contaminants owing to their large surface area and/or microporous structure (Axe and Trivedi, 2002). For example, ferruginous nodules, formed during the lateritic weathering process, used to contain elevated Hg contents (Roulet and Lucotte, 1995; Roulet et al., 1998; De Oliveira et al., 2001; Brabo et al., 2003). The adsorption of Hg onto Fe oxides has been widely reported, and it is preferentially produced under alkaline conditions (e.g., Schuster, 1991; Tiffreau et al., 1995).

Hydrochemical conditions in the lake during highstands corresponded to alkaline chloride–sulphate sodium type waters, supersaturated in calcite and occasionally in gypsum (Martínez *et al*., 1994) as it was found in Laguna Mar Chiquita (Piovano *et al.*, 2004b). Martínez (1991) and Piovano *et al.* (2002) conclude that calcite disseminated in sediments accumulated in the Laguna del Mar Chiquita is authigenic and formed by precipitation from calcite supersaturated lake waters, conditions that predominate even during the most dilute stages of the lake. In the case of Laguna del Plata, gypsum was not found in the sediment. This is probably due to the diluting effect that Suquía River exerts on LP waters that prevents arriving to the necessary concentrations to form gypsum. Durigneux (1978) indicated the presence of sodium sulphates in LMC but the specific salts were not specified. However, due to the recent retraction of the lake water, muddy sediments from the bottom of the lake are exposed. The analysis of these sediments showed the presence of sodium sulphate minerals that appear as efflorescences Biglia *et al.* (2013). These minerals are Thenardite ($NaSO_4$) and Mirabilite ($NaSO_4 \cdot 10H_2O$), that, although frequent in saline lakes were unknown in LP until now.

Mercury profile show maximum Hg_{TP} at ~38 cm, i.e. in the depth range roughly attributed to records of the years 1990-1995. The residual Hg fraction shows maximum levels (>50% of Hg_{TP}) at ~35 cm depth, suggesting an episode with major transport and deposition of non-reactive Hg-bearing phases during the 1990s just after the episode responsible of the Hg_{TP} maximum. Accordingly, the maximum Hg_{TP} levels together with minimum Hg_{H202}/Hg_{TP} and relatively low Hg_{HCl}/Hg_{TP} suggest dominance of Hg-bearing phases not accessible to the used selective extractions. Among the different Hg sources described in natural systems, volcanic emissions are a major issue (i.e., Fitzgerald and Lamborg, 2003, Selin, 2009). Due to the proximity to the Andean volcanic system and its well known influence on the study area (e.g. Gaiero *et al.*, 2007; Osores *et al.*, 2011) volcanic eruptions could account for this observation. In fact, the eruption record of the past 100 years indicates that the observed peak could reflect Hg inputs from the eruption of the Chilean Hudson and Láscar volcanoes located in Chile. The first one is situated at 45°54'S - 72°58'W and erupted in two phases in August 1991, producing 4.3 km^3 of pyroclastic material during one of the major eruptions of the 20th Century (Wilson *et al.*, 2011). The second one is located at 23°22'S – 67°44'W and started its activity in 1984 culminating with a major explosive eruption in April 1993. This last eruption generated a column between 5 and 25 km above the volcano (Matthews *et al.*, 1997). In both cases, the respective ash plumes were documented to have reached the Laguna del Plata region thus the Hg associated to volcano-clastic particles could have settled as wet or dry

deposition in the Suquía River watershed. This could explain the peak of Hg_{TP} observed in the core (between 37.2 and 30.2 cm) and its preferential association with non-reactive particles in the sediments accumulated in the years following the eruption.

5.4.2 Arsenic

In what concerns to As, it shows an opposite behaviour with respect to Hg. The higher concentrations are located in the lower part of the core that corresponds to dry climate periods and higher pH values. As it was previously mentioned, the sediments of the lower part of the core have two provenances fluvial and aeolian. In this dry period most of the As contributions could be attributed to the input of the Chaco Pampean Plain loess that was transported to Laguna del Plata by winds from nearby regions. The average As-tot concentration measured in the core is 20.953 ± 18.006 mg kg^{-1}, which is consistent with the As concentrations reported in loessic sediments of the Chacopampean Plain (Nicolli et al., 2012 and references therein), This value results more than 4 times higher than the As concentrations reported in some other lakes of the world (i.e., Cook *et al.*, 1995; Smedley and Kinniburgh, 2002 and references therein)

It is possible as well that a small part of the As deposited in the salt crusts around the lake was blown away and re deposited on the lake or re entered in solution. In the other hand, lower As concentrations occur in the middle and upper part of the core when the hydrological conditions started to change. Part of the As retained in the salt crusts formed around the lake could be wash-out during the first precipitation events and also at increasing lake-levels.

The results of the As-asc and As-HCl extractions (Fig. 4-14) explain up to ~46 and ~78 % respectively of the As-tot. This suggests that As seems to be adsorbed onto reactive Fe and Mn hydr(oxides) all along the sedimentary core. Nevertheless, the relationships found between As, Fe and Mn extracted from the ascorbate fraction (Fig. 4-16), show that As correlates better in the lower part of the core. Moreover, there is a difference between As-asc and HCl fractions in the lower part of the core where As-asc explains in average 5.83 ± 16.42 % and As-HCl 59.04 ± 12.93 % of the As-tot. It is possible to think that due to the presence of pyrite and the high sulphur concentrations (Fig. 4-8) at this depth, part of the As is associated to sulphides. Several authors have reported the association between As and

pyrite (Bostick and Fendorf, 2003; Doyle *et al.*, 2004; Rickard and Morse, 2005; Özverdi and Erdem, 2006; Charlet *et al.*, 2011), wich is enhanced under anoxic conditions that usually prevail in the mat located at the bottom lakes (Couture *et al.*, 2013). The presence of sulphur reducing bacteria also play an important role in controlling the soluble trace metal concentrations, as they promote the precipitation of secondary sulphides Rittle *et al*, (1995), Oremland *et al.*, (2000), Kirk *et al.*, (2004).

With the increase of water budget in the humid period, fluctuations in C_{org} and C_{inorg} contents are noticed (Fig. 4-8f-g) around 74 cm. Moreover, a decrease of the Fe and Mn acid soluble and reducible fractions (Fig. 4-13) is registered. It has been demonstrated (e.g: Cheng *et al.*, 1999; Fernández-Martínez *et al.*, 2006; Román-Ross *et al.*, 2006) that As may co-precipitate along with calcite and gypsum. Furthermore, some authors (Moon *et al.*, 2004; Di Benedetto *et al.*, 2006) showed that when Ca/As molar ratio is >1 favours the association of As with calcite or kaolinite minerals. When regarding the chemistry and mineralogy of the water and sediments of the lake, gypsum is not found and, at least in Laguna del Plata, water is subsaturated in this mineral (Table 4-2). Nevertheless, water is always superaturated (Table 4-2) in calcite and this mineral is frequent in the sediments (Fig. 4-10). Clay minerals such as illite or kaolinite were also found in sediments of the basin and in the lake. Some authors indicate that calcite-coated clays, such as illite, may adsorb arsenate ions under alkaline conditions (Bugueño *et al.*, 2014).
The As acid-soluble fraction show a peak that is coincident with another peak of C_{inorg} (
Fig. 4-15a), strongly suggesting that part of the As may be immobilized by co-precipitation with calcite.

Although the As-HCl fraction can explain over 75 % of the total As (Fig. 4-14) there is part of residual As (i.e., crystalline lattice) that could not be explained neither to As-HCl nor As-asc. Rickard and Morse (2005) showed that pyrite partially dissolves when treated with HCl. Thus, it could exist part of As adsorbed onto the un-dissolved pyrite fraction that is not released in the extraction.

6. Conclusion

This work has led to the study of behavior and the origin of mercury and arsenic, two trace elements present in the Mar Chiquita system. Based on the results previously discussed, an hydro-geochemical model concerning the functioning of Mar Chiquita system can be proposed (

Fig. 6-1). This is a modification of the original model proposed by Piovano *et al.* (2004a,b) and was adjusted in Stupar *et al.* (2013) that aims to include the main Hg and As bearing phases identified previously in the area and.

Precipitation (P) and evaporation (E) are represented with arrows, whose relative lengths are proportional to their volume. The higher river runoff, which occurred after the 1970s, is indicated by a solid arrow, whereas dotted arrow indicate comparatively low inputs that prevailed in the dry period. The thickness of the arrows associated with different Hg and As-bearing phases recognized in the studied area is proportional to their respective importance. During the dry conditions and low lake-levels that predominated in the study area before the 1970s, inputs of Hg to the lake corresponded mainly to contributions from natural sources such as Hg-bearing particles (particularly sulphides) that were transported to the lake from the Suquía River upper basin and atmospheric Hg (dry deposition). Under high stand conditions (after 1970s), these two sources increased their contributions due to increasing precipitation (wet deposition) and higher soil erosion in the catchments, but also to increasing global Hg flux. The more humid conditions lead to increased lake primary productivity and hence, a higher affinity of Hg for organic matter particle is found in sediments accumulated during this period.

Arsenic instead is mainly associated to Mn and Fe (hydr)oxides in the aquatic phase favoured by the high pH conditions of the lake during low and high stands. Furthermore, under more arid conditions, the As input to the lake was enhanced by the prevailing winds that carried As-rich loess particles. Under more humid conditions the As input from the atmosphere is less important and it is mostly introduced into the lake associated with riverborne particles. Besides being bounded to Mn and Fe, As is associated to pyrite in the lower part of the core and to calcite in the middle and upper parts. The residual As that could not be explained by the selective extractions may be attached onto non reactive pyrite.

The sources of Hg and As in the Laguna del Plata sediments are mostly assigned to natural sources. In the case of Hg a contribution from global inputs should be considered, as well as from some other local anthropogenic sources, that became increasingly important after the 1970s when an incipient industrial development started in the region. The volcanic activity occurred early 1990s could have increased the signal of Hg. Regarding As, the main input is

clearly associated with increasing contribution of loessic particles during the dry period that predominated in the region before the 1970's.

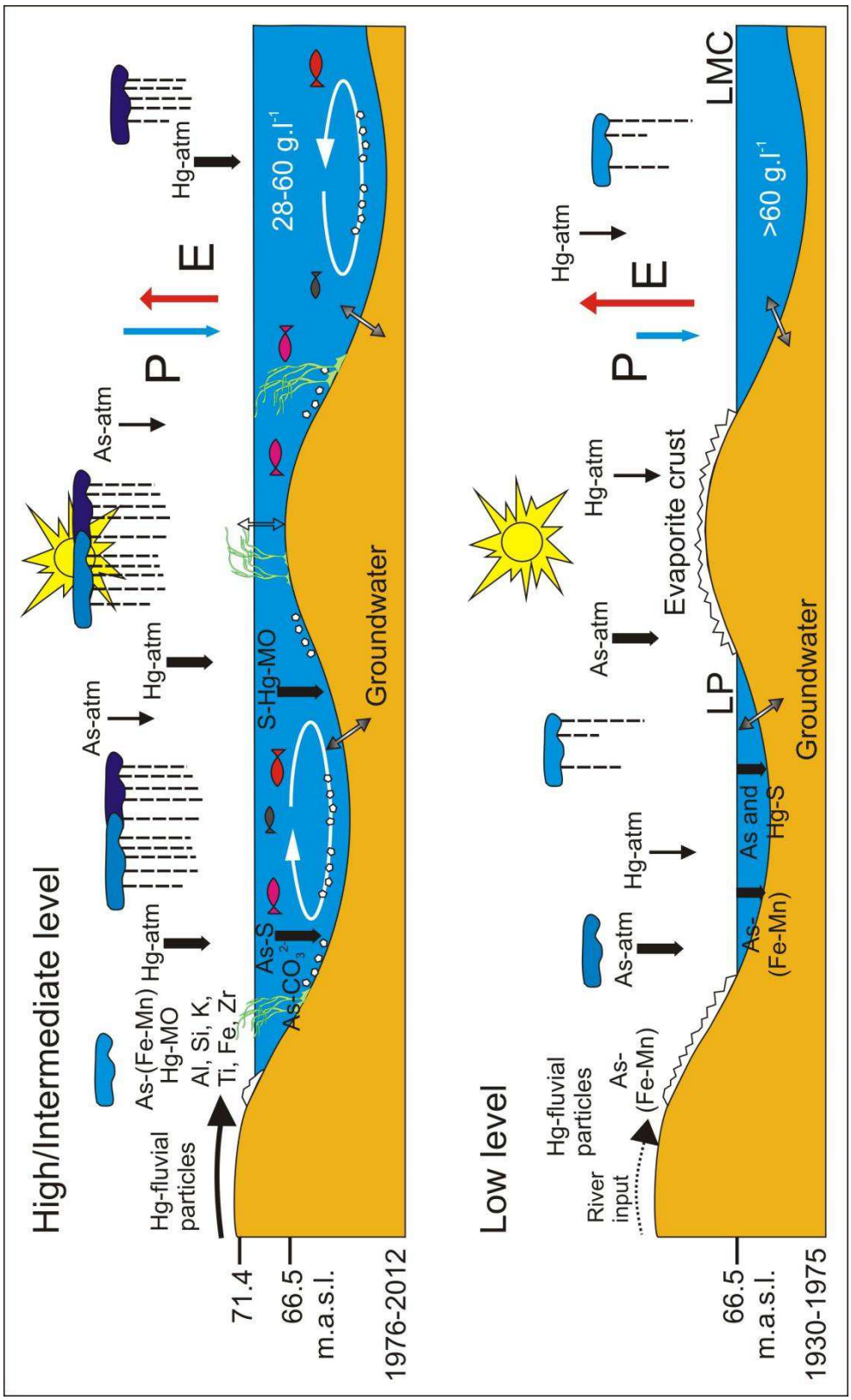

Fig. 6-1: Main mineralogical inputs related to hydrological variations in Laguna del Plata. Modified from Piovano *et al.* (2002).

This study allowed to have a global understanding of the sources and dynamic of Hg and As in Laguna del Plata. As well as the important role that climate and hydrological balance exert controlling the behaviour of these two elements. This study also enabled to identify the main Hg and As bearing phases through the utilization of selective extractions, finding that sulphurs and pyrite in special, is a key mineral that acts as a trap. With these results, this work clearly contributes to better interpret the functioning of this small salt lake.

The work carried out in this thesis has allowed to submit two articles in indexed journals that are added as annexes:

Annexe A: 1st article: **Stupar, Y.V.,** Schäfer, J., García, M.G., Schmidt, S., Piovano, E., Blanc, G., Huneau, F., and Le Coutumer, P. Historical mercury trends recorded in sediments from the Laguna del Plata, Córdoba, Argentina. Journal: Chemie der Erde / Geochemistry. Status: accepted for publication, http://dx.doi.org/10.1016/j.chemer.2013.11.002.

Annexe B: 2nd article: **Stupar, Y.V.,** García, M.G., Schäfer, J., Schmidt, S., Piovano, E., Blanc, G., Huneau, F., and Le Coutumer, P. Identificación de fases portadoras y flujos de mercurio en el registro sedimentario de la Laguna del Plata, región central de Argentina. Journal: Revista Mexicana de Ciencias Geológicas. Status: accepted for publication.

6.1 Perspectives

In terms of the perspectives of this work, the modalities of operation of this hydro-geochemical model could be improved by answering the following questions:

- What is the role of organic matter in the speciation of As and Hg?
- What is the contribution of As from atmospheric dust and the loessic formations?
- What are the mechanisms that determine the speciation of As in highly saline environments?
- What is the role of pH and ionic strength in the aqueous and solid phases of these two elements?

However, this work constitutes a first approach in the study of the origin of these trace metals in the Laguna del Plata and the associated Suquía River system. The question regarding their evolution is still a matter of study. Nevertheless, understand the (bio)geochemical processes involved in the reactivity, fate and toxicity of Hg and As could lead to answer it.

Bibliography

A

Aceituno, P., 1988. On the functioning of the Southern Oscillation in the South American sector. Part I: surface climate. Monthly Weather Review. 116, 505–524.

Aceñolaza, F.G. and Toselli, A., 1976. Consideraciones estratigráficas y tectónicas sobre el Paleozoico inferior del Noroeste Argentino. 2° Congreso Latinoamericano de Geología, Actas 2: 755-763, Caracas.

Ahmed, R., May, K. and Stoeppler, M., 1987. Ultratrace analysis of mercury and methylmercury (MM) in rainwater using cold vapour atomic absorption spectroscopy. Fresenius Z. Analytical Chemistry. 326, 510-516.

Alborés, A.F., Cid, B.P., Gómez, E.F. and López, E.F., 2000. Comparison between sequential extraction procedures and single extractions for metal partitioning in sewage sludge samples. Analyst. 125, 1353-1357.

Amin, O., Ferrer, L. and Marcovecchio, J., 1996. Heavy metal concentrations in litteral sediments from the Beagle Channel, Tierra del Fuego, Argentina. Environmental Monitoring and Assessment 41 (3), 219-231.

Arnórsson, S., 2003. Arsenic in surface- and up to 90°C ground waters in a basalt area, N-Iceland: Processes controlling its mobility. Applied Geochemistry. 18 (9), 1297-1312.

Appelo, C.A.J. and Postma, D., 2005. Geochemistry, Groundwater and Pollution, Second Edition. Taylor & Francis. The Netherlands. pp.649.

Appleby, P.G., 2001. Chronostratigraphic techniques in recent sediments. W. M. Last & J. P. Smol (eds.).Tracking Environmental Change Using Lake Sediments. Volume 1: Basin Analysis, Coring, and Chronological Techniques. Kluwer Academic Publishers, Dordrecht, The Netherlands.

Arribére, M.A., Ribeiro Guevara, S., Sánchez, R.S., Gil, M.I., Román Ross, G., Daurade, L.E., Fajon, V., Horvat, M., Alcalde, R. and Kestelman, A.J., 2003. Heavy metals in the vicinity of a chlor-alkali factory in the upper Negro River ecosystem, Northern Patagonia, Argentina. Science of the Total Environment. 301 (1-3), 187-203.

Audry, S., Blanc, G. and Schäfer, J., 2005. The impact of sulphide oxidation on dissolved metal (Cd, Zn, Cu, Cr, Co, Ni, U) inputs into the Lot-Garonne fluvial system (France). Applied Geochemistry 20 (5), 919-931.

Audry, S., Blanc, G., Schäfer, J., 2006. Solid state partitioning of trace metals in suspended particulate matter from a river system affected by smelting waste drainage. Science of the Total Environment. 363, 216–236.

Azcue, J.M., Murdoch, A., Rosa, F. and Hall, G.E.M., 1994. Effects of abandoned gold mine tailings on the arsenic concentrations in water and sediments of Jack of Clubs Lake, BC. Environmental Technology. 15, 669–678.

Axe, L. and Trivedi, P., 2002. Intraparticle Surface Diffusion of Metal Contaminants and their Attenuation in Microporous Amorphous Al, Fe, and Mn Oxides. Journal of Colloid and Interface Science. 247 (2), 259-265.

B

Bagli, S. and Soille, P., 2004. Automatic delineation of shoreline and lake boundaries from Landsat satellite images. Proceedings of initial ECO-IMAGINE GI and GIS for Integrated Coastal Management, Seville 13th–15th May 2004.

Behra, P., Bonnissel-Gissinger, P., Alnot, M., Revel, R. and Ehrhardt, J.J., 2001. XPS and XAS study of the sorption of Hg(II) onto pyrite. Langmuir 17, 3970-3979.

Benson, L.V. and Spencer, R.J., 1983. A Hydrochemical Reconnaissance Study of the Walker River Basin, California and Nevada. USGS Open File Repport, 83–740. United States Geological Survey, Denver.

Berbery, E.H. and Collini, A., 2000. Springtime precipitation and water vapour flux over southeastern South America. Monthly Weather Review. 128, 1328-1346.

Berbery, E.H. and Barros, V., 2002. The hydrologic cycle of the La Plata basin in South America. Journal of Hydrometeorology. 3, 630-645.

Bermond, A.P., 1992. Thermodynamics applied to the study of the limits of sequential extraction procedures used for the speciation of trace elements in sediments and soils. Environmental Technology. 13 (12), 1175-1179.

Bertoldi de Pomar, H., 1953. El origen de la Laguna Mar Chiquita. Doctoral Tesis. Unpublished. Universidad Nacional de Córdoba.

Bhattacharya, P., Claesson, M., Bundschuh, J., Sracek, O., Fagerberg, J., Jacks, G., Martin, R.A., Storniolo, A.R. and Thir, J.M., 2006. Distribution and mobility of arsenic in the Río Dulce alluvial aquifers in Santiago del Estero Province, Argentina. Science of the Total Environment. 358, 97-120.

Biester, H., Kilian, R., Franzen, C., Woda, C., Mangini, A. and Schöler, H.F., 2002. Elevated mercury accumulation in a peat bog of the Magellanic Moorlands, Chile (53°S) - an anthropogenic signal from the Southern Hemisphere. Earth and Planetary Science Letters. 201 - 609-620.

Biglia, H.O., Colombo, F., Piovano, E. and Córdoba, F., 2013. Thénardita y Mirabilita en precipitados químicos litorales de la Laguna Mar Chiquita, Córdoba (Argentina). XI Congreso de mineralogía y metalogenia. 16-19 de Octubre, 2013. San Juan, Argenitna (en prensa).

Bindler, R., 2003. Estimating the natural background atmospheric deposition rate of mercury utilizing ombrotrophic bogs in southern Sweden. Environmental Science and Technology. 37, 40-46.

Bloom, N.S., 1989. Determination of picogram levels of methylmercury by aqueous phase ethylation, followed by cryogenic gas chromatography with atomic fluorescence detection. Canadian Journal of Fisheries and Aquatic Sciences. 46, 1131-1140.

Bloom, N.S. and Fitzgerald W.F., 1988. Determination of volative mercury species at the picogram level by low-temperature gas chromatography with cold-vapor atomic fluorescence detection. - Analytica Chimica Acta. 208, 151-161.

Bloom, N.S. and Watras, C.J., 1989. Seasonal and vertical variability in the mercury speciation of an acidified Wisconsin lake. In: Heavy Metals in the Environment, 349-352, Vernet D.P. (Ed.) CEP Consultants, Edinburgh, UK.

Böning, P., Bard, E. and Rose, J., 2007. Toward direct, micron-scale XRF elemental maps and quantitative profiles of wet marine sediments. Geochemistry, Geophysics, Geosystems. 8 (5), doi:10.1029/2006GC001480.

Borah, D. and Senapati, K., 2006. Adsorption of Cd(II) from aqueous solution onto pyrite. Fuel. 85, 1929-1934.

Bostick, B.C. and Fendorf, S., 2003. Arsenite sorption on troilite (FeS) and pyrite (FeS_2). Geochimica et Cosmochimica Acta. 67, 909-921.

Botté, S.E., Freije, R.H. and Marcovecchio, J.E., 2010. Distribution of Several Heavy Metals in Tidal Flats Sediments within Bahía Blanca Estuary (Argentina). Water Air Soil Pollution. 210, 371–388. DOI 10.1007/s11270-009-0260-0.

Boulanger, J-P., Leloup, J., Penalba, O., Rusticucci, M., Lafon, F. and Vargas, W., 2005. Observed precipitation in the Paraná-Plata hydrological basin: long-term trends, extreme conditions and ENSO teleconnections. Climate Dynamics. 24, 393-413.

Bower, J., Savage K.S., Weinman B., Barnett M.O., Hamilton W.P. and Harper W.F., 2008. Immobilization of mercury by pyrite (FeS2). Environmental Pollution. 156, 504-514.

Brannon, J.M. and Patrick, W.H., 1987. Fixation, transformation, and mobilization of arsenic in sediments. Environmental Sciences and Technology. 21, 450–459.

Brabo, E.S., Angélica, R.S., Silva, A.P., Faial, K.R.F., Mascarenhas, A.F.S. and Santos, E.C.O., 2003. Assessment of mercury levels in soils, waters, bottomsediments and fishes of acre state in Brazilian Amazon.Water Air and Soil Pollution. 147(1), 61–77.

Brook, E.J. and Moore, J.N., 1988. Particle-size and chemical control of As, Cd, Cu, Fe, Mn, Ni, Pb, and Zn in bed sediment from the Clark Fork River, Montana (U.S.A.). Science of The Total Environment. 76 (2-3), 247-266.

Brookins, D.G., 1988. Eh-pH Diagrams for Geochemistry. Springer-Verlag, Berlin.

Brosset, C., 1987. The behavior of mercury in the physical environment. Water, Air and Soil Pollution. 34, 145-166.

Brosset, C. and Lord, E., 1991. Hg in precipitation and ambient air. Water, Air, and Soil Pollution. 56, 493-506.

Brunetto, E. and Iriondo, M.H., 2007. Neotectónica en la Pampa Norte (Argentina). Revista de la Sociedad Geológica de España, 20 (1-2), 17-29.

Bryan, G.W. and Langston, W.J., 1992. Bioavailability, accumulation and effects of heavy metals in sediments with special reference to United Kingdom estuaries: a review. Environmental Pollution. 76 (2), 89– 131.

Bucher, E.H., Gavier Pizarro, G. and Curto, E.D., 2006. Cap. 1. Síntesis geográfica. En: Bañados del Río Dulce y Mar Chiquita (Córdoba, Argentina) (ed. Bucher E.H), pp. 15-27. Academia Nacional de Ciencias (Córdoba, Argentina).

Bucher, E.H. and Bucher, A.E., 2006a. Cap. 5. Limnología física y química. En: Bañados del Río Dulce y Mar Chiquita (Córdoba, Argentina) (ed. Bucher E.H), pp. 79-101. Academia Nacional de Ciencias (Córdoba, Argentina).

Bucher, E.H. and Abril, A.B., 2006. Cap. 7. Limnología biológica. En: Bañados del Río Dulce y Mar Chiquita (Córdoba, Argentina) (ed. Bucher E.H), pp. 117-137. Academia Nacional de Ciencias (Córdoba, Argentina).

Bucher, E.H. and Bucher, A.E., 2006b. Cap. 8. Síntesis funcional. En: Bañados del Río Dulce y Mar Chiquita (Córdoba, Argentina) (ed. Bucher E.H), pp. 139-159. Academia Nacional de Ciencias (Córdoba, Argentina).

Bugueño, M.P., Acevedo, S.E., Bonilla, C.A., Pizarro, G.E., Pasten, P.A., 2014. Differential arsenic binding in the sediments of two sites in Chile's lower Loa River basin. Science of the Total Environment. 466-467, 387-396.

Bundschuh, J., Litter, M.I., Parvez, F., Román-Ross, G., Nicolli, H.B., Jean, J.-S., Liu, C.-W., López, D., Armienta, M.A., Guilherme, L.R.G., Cuevas, A.G., Cornejo, L., Cumbal, L. and Toujaguez, R., 2012. One century of arsenic exposure in Latin America: A review of history and occurrence from 14 countries. Science of the Total Environment. 429, 2-35.

Bundschuh, J., Farias, B., Martin, R., Storniolo, A., Bhattacharya, P., Cortes, J, Bonorino, G., Albouy, R., 2004. Groundwater arsenic in the Chaco-Pampean Plain, Argentina: case study from Robles county, Santiago del Estero Province. Applied Geochemistry. 19 (2), 231-243.

C

CAA - Código Alimentario Argentino, 2012. Bebidas hídricas, agua y agua gasificada. Capítulo XII. Ley 18284. Actualizado, Octubre, 2012.

Camargo, J.A., 2002. Contribution of Spanish American silver mines (1570-1820) to the present high mercury concentrations in the global environment: a review. Chemosphere. 48, 51-57.

Cardich, A., 1980. El fenómeno de las fluctuaciones de los límites superiores del cultivo en los Andes: Su importancia. Relaciones de la Sociedad Argentina de Antropología. XIV, 1 (N.S.), 7-31.

Carignano, C., 1997. Caracterización y Evolución, durante el Cuaternario Superior, de los ambientes geomorfológicos en el noroeste de la provincia de Córdoba. Tesis Doctoral. Unpublished.

Carroll, J., Williamson, M., Lerche, I., Karabanov, E. and Williams, D.E., 1999. Geochronology of Lake Baikal from ^{210}Pb and ^{137}Cs radioisotopes. Applied Radiation and Isotopes. 50, 1105-1119.

Cáceres, L., Gruttner, V.E. and Contreras, R., 1992. Water recycling in arid regions: Chilean case. Ambio. 21 (2), 138–144.

Castellanos, A., 1959. Posibles desplazamientos morfológicos en el pasado de las redes potamográficas en la llanura cordobesa. Separata del Boletín de Estudios Geográficos, Córdoba 19, 29–63.

Castelle, S., Schäfer, J., Blanc, G., Audry, S., Etcheber, H. and Lissalde, J-P., 2007. 50-year record and solid state speciation of mercury in natural and contaminated reservoir sediment. Applied Geochemistry. 22, 1359–1370.

Castelle, S., 2008. Spéciation et réactivité du mercure dans le système fluvio-estuarien girondin. Doctoral Thesis. Université de Bordeaux 1.

Cauwet, G., Gadel, F., De Souza Sierra, M.M., Donard, O. and Ewald, M., 1990. Contribution of the Rhône River to org. C inputs to the Northwestern Mediterranean Sea. Continental Shelf Research. 10, 1025-1037.

Charlet, L., Morin, G., Rose, J., Wang, Y., Auffan, M., Burnol, A. and Fernandez-Martinez, A., 2011. Réactivité aux interfaces nano(particule)-solution, processus redox et transport de l'arsenic dans l'environnement | [Reactivity at (nano)particle-water interfaces, redox processes, and arsenic transport in the environment]. Comptes Rendus - Geoscience. 343 (2-3), 123-139.

Cheng, L., Fenter, P., Sturchio, N.C., Zhong, Z., and Bedzyk, M.J., 1999. X-ray standing wave study of arsenite incorporation at the calcite surface. Geochimica et Cosmochimica Acta. 63, 3153–3157.

Chilvers, D.C. and Peterson, P.J., 1988. Clobal Cycling of Arsenic, chapter 17. In Lead, Mercury, Cadmium and Arsenic in the Environment. Edited by T.C. Hutchinson and K.M. Meema. John Wiley and Sons Ltd. 605 Third Ave., New York, NY 10158. 279-301.

Cioccale, M.A., 1999. Climatic fluctuations in the Central Region of Argentina in the last 1000 years. Quaternary International. 62, 35-47.

Conaway, C.H., Swarzenski, P.W., Cohen, A.S., 2012. Recent paleorecords document rising mercury contamination in Lake Tanganyika. Applied Geochemistry. 27 (1), 352–359.

Cook, S.J., Levson, V.M., Giles, T.R. and Jackaman, W., 1995. A comparison of regional lake sediment and till geochemistry surveys—a case-study from the Fawnie Creek area, Central British Columbia. Exploration and Mining Geology. 4, 93–110.

Corral, M., Pozzi C., Plencovich, G., Hillman, G., Pagot, M., Rodríguez, A., Oroná, C., 2006. Modelación hidrodinámica de experimento con trazadores en la laguna del Plara, Córdoba, Argentina. Asociación Argentina de Mecánica Computacional http://www.amcaonline.org.ar.

Cossa, D. and Noel, J., 1987. Concentrations of mercury in near shore surface waters on the Bay of Biscay and in the Gironde Estuary. Marine Chemistry. 20 (4), 389-396.

Cossa, D. and Ficht, A., 1999. La dynamique du mercure. Programme scientifique Seine-Aval, Editions Ifremer, ISBN 2-84433-028-2, 23 pp.

Costa, C., 1999. Tectónica cuaternaria en las Sierras Pampeanas. Geología Argentina. Anales 29. Subsecretaría de Minería de la Nación. Servicio Geológico Minero Argentino. Instituto de Geología y Recursos Minerales. Buenos Aires.

Couture, R.-M., Wallschläger, D., Rose, J. and Van Cappellen, P., 2013. Arsenic binding to organic and inorganic sulfur species during microbial sulfate reduction: A sediment flow-through reactor experiment. Environmental Chemistry. 10 (4), 285-294.

Craig P.J., 1986. In: Comprehensive organometallic chemistry, 979, Wilkinson G., Stone F.G.A. and Abel E.W. (Eds.), Pergamon Press, New York.

Croudace, I.W., Rindby, A. and Rothwell, R.G., 2006. ITRAX: description and evaluation of a new multi-function X-ray core scanner. In: Rothwell, R.G. (Ed.), New Techniques in Sediment Core Analysis. Special Publication, vol. 267. Geological Society, London, pp. 51–63.

Cullen, W.R. and Reimer, K.J., 1989. Arsenic speciation in the environment. Chemical Reviews. 89 (4), 713–764.

D

Dapeña, C; Panarello, H. and Nicolli, H., 1997. South American Symposium on Isotope Geology - Brazil, June 1997.

Dapeña, C. and Panarello, H., 2001. Isotopic study of the "Laguna Mar Chiquita", Córdoba, Argentina and its hydrogeological and Paleoclimatical implications. Use of isotope techniques in lake dynamics investigations, IAEA, Vienna, 2001, IAEA-TECDOC-1206.

De Marco, S.G., Botté, S.E. and Marcovecchio, J.E., 2006. Mercury distribution in abiotic and biological compartments within several estuarine systems from Argentina: 1980–2005 period. Chemosphere. 65, 213–223.

De Oliveira, S.M.B., Melfi, A.J., Fostier, A.H., Forti, M.C., Favaro,D.I.T. and Boulet, R., 2001. Soils as an important sink for mercury inthe Amazon. Water, Air, and Soil Pollution. 26, 321-337.

Depetris, P.J., Kempe, S., Latif, M. and Mook, W.G., 1996. ENSO controlled flooding in the Paraná River (1904-1991). Naturwissenschaften. 83, 127–129.

De Vries, J.L. and Vrebos, B.A.R., 2002. Quantification of infinitely thick specimens by XRF analysis, In: van Grieken, R.E., Markovicz, A.A. (Eds.), Handbook of X-Ray Spectrometry, Second Edition. Marcel Dekker, New York, pp. 341–405.

Diaz, E., 2000. Mercury pollution at gold mining sites in the Amazon environment. Principles of Environmental Toxicology. University of Idaho. pp. 24.

Di Benedetto, F., Costagliola, P., Benvenutti, M., Lattanzi, P., Romanelli, M. and Tanelli., G., 2006. Arsenic incorporation in natural calcite lattice: evidence from electron spin echo spectroscopy. Earth Planetary Science Letters. 246, 458-465.

Doyle, M. and Barros, V.R., 2002. Mid summer low-level circulation and precipitation in subtropical South America and related sea surface temperature anomalies in the South Atlantic. Journal of Climate. 15, 3394-3410.

Doyle, C.S., Kendelewicz, T., Bostick, B.C. and Brown, G.E., 2004. Soft X-ray spectroscopic studies of the reaction of fractured pyrite surfaces with Cr(Vl)-containing aqueous solutions. Geochimica et Cosmochimica Acta. 68, 4287-4299.

Drever, J.I., 1988. The Geochemistry of Natural Waters, 2nd edn. Prentice Hall, Englewood Cliff, NJ, 437 pp.

Driscoll, C.T., Blette, V., Yan, C., Schofield, C.L., Munson, R. and Holsapple, J., 1995. The role of dissolved organic carbon in the chemistry and bioavailability of mercury in remote Adirondack lakes. Water Air and Soil Pollutution. 80, 499–508.

Durigneux, J., 1978. Composición química de las Aguas y Barros de la Laguna Mar Chiquita en la Provincia de Córdoba. Miscelánea, Academia Nacional de Ciencias (Córdoba, Argentina). 59, 3-12.

Dzombak, D.A., Morel, F.M.M., 1990. Surface Complexation Modelling- Hydrous Ferric Oxide. John Wiley, New York.

E

Etcheber, H., Relexans, J-C., Beliard, M., Weber, O., Buscail, R. and Heussner, S., 1999. Distribution and quality of sedimentary organic matter on the Aquitanian margin (Bay of Biscay). Deep-Sea Research II. 46, 2249-2288.

F

Farrah, H. and Pickering W.F., 1993. Factors influencing the potential mobility and bioavailability of metals in dried lake sediments. Chemical Speciation and Bioavailability. 5 (3), 81-96.

Fernández-Martínez, A., Román-Ross, G., Cuello, G.J., Turrillas, X., Charlet, L., Johnson, M.R. and Bardelli, F., 2006. Arsenic uptake by gypsum and calcite: Modelling and probing by neutron and X-ray scattering. Physica B: Condensed Matter 385-386, 935-937.

Ferrara, R., Maseri, B. and Petrosino, A., 1986. Mercury levels in the Atlantic and Mediterranean waters in the Strait of the Tyrrhenian Sea. - In: Rapp. Proces-Verb. Reunions, XXX Congr. (Mallorca), Abstract C-17, 35, Monaco, CIESM.

Fitzgerald, W.F., 1989. Atmospheric and Oceanic Cycling of Mercury. In Chemical Oceanography Vol. 10, Riley, J.P. and Chester, R. (Eds.), Academic Press, London pp. 151-186.

Fitzgerald, W.F., Mason, R.P. and Vandal, G.M., 1990. Atmospheric cycling and air-water exchange of mercury over mid-continental lacustrine regions. Water, Air and Soil Pollution. 56 (1), 745-767.

Fitzgerald, W.F. and Mason, R.P., 1997. Biogeochemical cycling of mercury in the marine environment. In: Sigel, H., Sigel, A. (Eds.), Metal Ions in Biological Systems, Mercury and its Effects on Environment and Biological Systems, vol. 34. Marcel Dekker Inc., New York, pp. 3–110.

Fitzgerald, W.F., Engstrom, D.R., Mason, R.P. and Nater, E.A., 1998. The case for atmospheric mercury contamination in remote areas. Environmental Science and Technology. 32, 1-7.

Fitzgerald, W.F. and Lamborg C.H., 2003. Geochemistry of Mercury in the Environment. In: In: Holland, H.D. and Turekian, K.K. (Eds), Treatise on Geochemistry, ed. BS Lollar, pp. 107-148. New York: Elsevier.

Flintrop, C., Hohlmann, B., Jasper, T., Korte, C., Podlaha, O.G., Sheele, S., and Veizer, J.,1996. Anatomy of pollution: rivers of North Rhine-Westphalia, Germany. American Journal of Science. 296, 58–98.

Francisca, F.M. and Carro Perez, M.E., 2009. Assesment of natural arsenic in groundwater in Córdoba Province, Argentina. Environmental Geochemical Health. 31, 673-682.

Frank, H., 1915. Contribución al conocimiento de las Salinas Grandes y la Mar Chiquita de la Provincia de Córdoba. Revista del Centro de Estudiantes de Ingienería, 3:91-107.

Fujita, S., Horii, H. and Taniguchi, S., 1973. Pulse radiolysis of mercuric ion in aqueous solutions. The Journal of Physical Chemistry. 77 (24), 2868-2871.

G

Gaiero D.M., Roman Ross, G., Depetris, P.J. and Kempe, S. 1997. Spatial and temporal variability of total non-residual heavy metals content in stream sediments from the Suquía river system, Córdooba, Argentina. Water, Air and Soil pollution. 93, 303-319.

Gaiero, D.M., 2007. Dust provenance in Antarctic ice during glacial periods: From where in southern South America? Geophysical Research Letters. 34, L17707.

Gaiero D.M., Brunet, F., Probst, J-L. and Depetris, P.J., 2007. A uniform isotopic and chemical signature of dust exported from Patagonia: Rock sources and occurrence in southern environments. Chemical Geology. 238 (1-2), 107-120.

Gaiero, D.M., Simonella, L., Gassó, S. Gili, S., Stein, A.F., Sosa, P., Becchio, R., Arce, J. and Marelli, H., 2013. Ground/satellite observations and atmospheric modeling of dust storms originating in the high Puna-Altiplano deserts (South America): Implications for the interpretation of paleo-climatic archives. Journal of Geophysical Research: Atmospheres. 118, 1-15. doi:10.1002/jgrd.50036.

García, M.G., Moreno, C., Galindo, M.C., Hidalgo, M.V., Fernández, D.S. and Šráček, O., 2006. Intermediate to high levels of arsenic and fluoride in deep geothermal aquifers from the northwestern Chacopampean plain, Argentina. In Natural Arsenic in Groundwaters of Latin America. Mexico City, Mexico: UNAM, 2006. s. 32.

Garreaud, R.D., Vuille, M., Compagnucci, R. and Marengo, J., 2009. Present-day Souh American Climate (LOTRED South America). Palaeogeography, Palaeoclimatology, Palaeoecology. 281, 180–195.

Garreaud, R.D., 2009. The Andes climate and weather. Advances in Geosciences. 22, 3–11.

Garrels, R.M. and Mackenzie, F.T., 1971. The Evolution of Sedimentary Rocks. W. W. Norton, New York.

Ge, L.Q., Lai, W.C. and Lin, Y.C., 2005. Influence of and correction for moisture in rocks, soils and sediments on in situ XRF analysis. X-Ray Spectrometry. 34, 28–34.

Gibbs, R.J., 1970. Mechanism controlling world water chemistry. Science. 170, 1088–1090.

Gibson, P.J. and Power, C.H., 2000. Introductory Remote Sensing: Digital image processing and Applications. Routledge, pp. 249.

Gill, G.A. and Fitzgerald, W. F., 1985. Mercury sampling of open ocean waters at the picomolar level. Deep Sea Research. 32, 287-297.

Gill, G.A. and Fitzgerald, W.F., 1987. Picomolar mercury measurements in seawater and other materials using stannous chloride reduction and two-stage gold amalgamation with gas phase detection. - Marine Chemistry. 20, 227-243.

Gilli A., Anselmetti F.S. and Ariztegui D., 2005. Seismic stratigraphy, buried beach ridges and contourite drifts: The Late Quaternary history of the closed Lago Cardiel basin, Argentina (49°S). Sedimentology. 51, 1–23.

Girard, M-C. and Girard C-M., 2010. Traitement des données de télédétection - 2ème édition - Environnement et ressources naturelles. Série : Environnement et Sécurité. Editeur: Dunod, 553 pp.

Gleyzes, C., Tellier, S. and Astruc, M., 2002. Fractionation studies of trace elements in contaminated soils and sediments, a review of sequential extraction procedures. Trends in Analytical Chemistry. 21 (6-7), 451–467.

Gobeil, C. and Cossa, D., 1993. Mercury in sediments and sediment pore waters in the Laurentian trough. Canadian Journal of Fisheries and Aquatic Sciences. 50, 1794-1800.

Goldberg, S., 1986. Chemical modeling of arsenate adsorption on aluminum and iron oxide minerals. Soil Science Society of America Journal. 50, 1154–1157.

Goldberg, S. and Glaubig, R.A., 1988. Anion sorption on a calcareous, montmorillonitic soil—arsenic. Soil Science Society of America Journal. 52, 1297–1300.

Goldstein, H.L., Breit, G.N, Yount, J.C. and Reynolds, R.L., 2007. Trace metal accumulation in brines and salts of Franklin Lake Playa and the ash meadows area of Nevada and California. GSA (Geological Society of America) Denver Annual Meeting. 28–31 October 2007.

González Bonorino, F., 1966. Soil clay mineralogy of the Pampa plains, Argentina. Journal of Sedimentary Petrology. 36 (4), 1026–1035.

Gorgas, J.A. and Tassile, J.L., 2003. Recursos Naturales de la Provincia de Córdoba. Los suelos. Nivel de reconocimiento. Escala 1:5000000. Agencia Córdoba D.A.C. y T.S.E.M. Dirección Ambiente e Instituto de Tecnología Agropecuaria INTA - Manfredi. Córdoba.

Goyenechea, M., 1917. Sobre la nueva enfermedad descubierta en Bell-Ville. Revista Médica de Rosario. (7), 485.

H

Hall, B., Lindqvist, O. and Ljungström, E., 1990. Mercury chemistry in simulated flue gases related to waste incineration conditions. Environmental Science and Technology. 24 (1), 108-111.

Hammer, U.T., 1986. Saline Lakes Ecosystems of the World. Dr. W. Junk Publishers, Boston. 619 pp.

Hammond, C.R., 2005. The elements in Lide, D. R., ed. CRC Handbook of Chemistry and Physics (86th ed.). Boca Raton (FL): CRC Press.

Hermanns, Y.M. and Biester, H., 2013. Anthropogenic mercury signals in lake sediments from southernmost Patagonia, Chile. Science of the Total Environment. 445-446, 126-135.

Heyvaert, A.C., Reuter, J.E., Slotton, D.G. and Goldman, C.R., 2000. Paleolimnological reconstruction of historical atmospheric lead and mercury deposition at Lake Tahoe, California-Nevada. Environmental Science and Technology. 34, 3588-3597.

Hiemstra, T. and van Riemsdijk, W.H., 1999. Surface structural ion adsorption modeling of competitive binding of oxyanions by metal hydroxides. Journal of Colloid and Interface Science. 210, 182–193.

Hiemstra, T. and Van Riemsdijk, W.H., 2000. Fluoride Adsorption on Goethite in Relation to Different Types of Surface Sites.Journal of Colloid and Interface Science. 225 (1), 94-104.

Hineman, A., 2011. Determination of As, Se and Hg in Waters by Hydride Generation/Cold Vapor Atomic Absorption Spectroscopy. Application Note, Atomic Absorption. PerkinElmer, Inc. Ontario, Canada.

Hou, X. and Jones, B.T., 2000. Inductively Coupled Plasma - Optical Emission Spectometry. In Encyclopedia of Analytical Chemistry. R.A. Meyers (Ed.). pp. 9468-9485. John Wiley and Sons Ltd., Chichester.

Hudson-Edwards, K.A., Macklin, M.G., Miller, J.R. and Lechler, P.J., 2001. Sources, distribution and storage of heavy metals in the Río Pilcomayo, Bolivia. Journal of Geochemical Exploration. 72 (3), 229-250.

Huerta-Diaz, M.A. and Morse, J.W., 1990. A quantitative method for determination of trace metal concentrations in sedimentary pyrite. Marine Chemistry. 29, 119–44.

Huerta-Diaz, M.A. and, Morse, J.W., 1992. Pyritization of trace metals in anoxic marine sediments. Geochimica et Cosmochimica Acta. 56 (7), 2681–702.

Huguet, L., Castelle, S., Schäfer, J., Blanc, G., Maury-Brachet, R., Reynouard, C. and Jorand, F., 2010. Mercury methylation rates of biofilm and plankton microorganisms from a hydroelectric reservoir in French Guiana. Science of the Total Environment. 408, 1338–1348.

I

Imbellone, P.A., Giménez, J.E., Mormeneo, M.L. and Cuberes, M.G., 2012. Suelos loéssicos influenciados por depósitos de conchilla Pleistocenos de la Formación Pascua, noreste de la provincia de Buenos Aires, Argentina | [Loessial soils influenced by Pleistocene shell deposits of the Pascua Formation, northeastern Buenos Aires province, Argentina]. Latin American Journal of Sedimentology and Basin Analysis. 19 (2), 67-88.

Imbodem, D.M., 1990. Mixing and Transport in lakes. In: Large Lakes: Ecological Structure amd Function (eds. Tilzer, M.M. and Serruya, C.) pp. 150-222. Springer Verlag, Berlin.

Iriondo, M.H.,1989. Major fractures of the Chaco-Pampa plain. In: Mörner, N. (Ed.), Bullettin of the INQUA, Neotectonics Comission, NA, pp. 12–42.

Iriondo, M.H., 1997. Models of deposition of loess and loessoids in the Upper Quaternary of South America. Journal of South American Earth Sciences. 10, 71–79.

Ivanovich M. and Harmon H.S., 1992. Uranium Series Disequilibrium: Applications to Environmental Problems. Clarendon Press, Oxford, pp. 571.

Iverfeldt, Å., 1984. Structural, thermodynamic and kinetic studies of mercury compounds; applications within the environmental cycle. - Ph.D. thesis, Dept of Inorganic Chem., CTH, S-412 96, GSteborg, Sweden.

Iverfeldt, Å., 1991a. Mercury in canopy throughfall water and its relation to atmospheric dry deposition. Water, Air and Soil Pollution. 56 (1), 553-564.

Iverfeldt, Å., 1991b. Occurrence and turnover of atmospheric mercury over the Nordic countries. Water, Air and Soil Pollution. 56 (1), 251-265.

Iverfeldt, Å. and Rodhe, H., 1988. Atmospheric Transport and Deposition of Mercury in the Nordic Countries. Report for the Nordic Council of Ministers, L87/285, 1-22, Swedish Environmental Research Institute, Box 47086, 402 58 Grteborg, Sweden.

J

Jansen, J.H.F., Van der Gaast, S.J., Koster, B. and Vaars, A.J., 1998. CORTEX, a shipboard XRF scanner for element analyses in split sediment cores. Marine Geology. 151 (1-4), 143–153.

Jenkins, R., 1999. X-Ray Fluorescence Spectroscopy, Second Edition. Wiley & Sons, New York. 207 pp.

Johannessen S.C., Macdonald, R.W. and Eek, K.M., 2005. Historical trends in mercury sedimentation and mixing in the strait of Georgia, Canada. Environmental Science and Technology. 39, 4361-4368.

Jonkers, H.M., Ludwig, R., Wit, R., Pringault, O., Muyzer, G., Niemann, H., Finke, N. and Beer, D., 2003. Structural and functional analysis of a microbial mat ecosystem from a unique permanent hypersaline inland lake: 'La Salada de Chiprana' (NE Spain). FEMS Microbiology Ecology. 44, 175-189

K

Kaasalainen, H. and Stefánsson, A., 2012. The chemistry of trace elements in surface geothermal waters and steam, Iceland. Chemical Geology. 330–331, 60–85.

Kabata-Pendias, A., 2010. Trace Elements in Soils and Plants, Fourth Edition. CRC Press 2010. 548 pp.

Kim, J. P. and Fitzgerald, W. F., 1986. Sea-air partitioning of mercury in the equatorial Pacific Ocean. Science. 231, 1131-1133.

Kimstach, V., Meybeck, M., and Baroudy, E., (eds.) 1998. A Water Quality Assessment of the Former Soviet Union. E and FN Spon, London.

King, P., Kennedy, H., Newton, P.P., Jickells, T.D., Brand, T., Calvert, S., Cauwet, G., Etcheber, H., Head, B., Khripounoff, A., Manighetti, B. and Miquel, J.C., 1998. Analysis of total and organic carbon and total nitrogen in settling oceanic particles and a marine sediment: an interlaboratory comparison. Marine Chemistry. 60, 203–216.

Kirk, M.F., Holm, T.R., Par, J., Jin, Q., Sandford, R.A., Fouke, B.W. and Bethke, C.M., 2004. Bacterial sulfate reduction limits natural arsenic contamination in groundwater. Geology. 32 (11), 953-956.

Klug, H.P. and Alexander, L.E., 1974. X-ray diffraction procedures: for polycrystalline and amorphous materials. X-Ray Diffraction Procedures: For Polycrystalline and Amorphous

Materials, 2nd Edition, by Harold P. Klug, Leroy E. Alexander, pp. 992. ISBN 0-471-49369-4. Wiley-VCH, May 1974., vol. 1.

Koide, M., Bruland, K.W. and Goldberg, E.D., 1973. Th-228/Th-232 and Pb-210 geochronologies in marine and lake sediments. Geochimica et Cosmochimica Acta. 37, 1171-1187.

Kostka, J.E. and Luther III, G.W., 1994. Partitioning and speciation of solid phase iron in saltmarsh sediments. Geochimica et Cosmochimica Acta. 58 (7), 1701–1710.

Kraemer, P.E., Escayola, M.P. and Martino, R.D., 1995. Hipótesis sobre la evolución tectónica neoproterozoica de las Sierras Pampeanas de Córdoba (30°40'-32°40'), Argentina. Revista de la Asociación Geológica Argentina, 50 (1-4), 47-59, Buenos Aires.

Kratzmann, D.J., Carey, S.N., Fero, J., Scasso, R.A. and Naranjo, J.A., 2010. Simulations of tephra dispersal from the 1991 explosive eruptions of Hudson volcano, Chile. Journal of Volcanology and Geothermal Research. 190, 337–352.

Kröhling, D. and Iriondo, M., 1999. Upper Quaternary Palaeoclimates of the Mar Chiquita area, North Pampa, Argentina. Quaternary International. 57/58, 149-163.

L

Labraga, J.C., Frumento, O. and López, M., 2000. The atmospheric water vapor cycle in South America and the tropospheric circulation. Journal of Climate. 13,1899-1915.

Lacerda, L.D., De Souza, M. and Ribeiro, M.G., 2004. The effects of land use change on mercury distribution in soils of Alta Floresta, Southern Amazon. Environmental Pollution. 129, 247-255.

Langston, W.J., Burt, G.R. and, Pope, N.D., 1999. Bioavailability of metals in sediments of the Dogger Bank (central North Sea): a mesocosm study. Estuarine, Coastal and Shelf Science. 48 (5), 519– 540.

Lee, Y.H., 1987. Determination of methyl- and ethyl-mercury in natural waters at sub-nanogram per litre levels using SCF-adsorbent procedure. International Journal of Environmental Analytical Chemistry. 29, 263-267.

Lerda, D.E. and Prosperi, C.H., 1996. Water mutagenicity and toxicology in Rio Tercero, Cordoba, Argentina. Water Research. 30, 819–824.

Leroy, S.A.G., Warny S., Lahijani, H., Piovano, E.L., Fanetti, D., Berger, A.R., 2010. The Role of Geosciences in the Mitigation of Natural Disasters: Five Case Studies. Geophysical Hazards. International Year of Planet Earth, 115-147 pp.

Levason, W. and McAucliffe, C.A., 1977. The coordination chemistry of mercury. In: The chemistry of mercury, 49-138, McMillan of Canada.

Liang, L., Sun, Y., Yao, Z., Liu, Z. and Wu, F., 2012. Evaluation of high-resolution elemental analyses of Chinese loess deposits measured by X-ray fluorescence core scanner. Catena. 92, 75–82.

Likens, G.E., Bormann, F.H., Pierce, R.S., Eaton, J.S. and Johnson, N.M., 1977. Biogeochemistry of a Forested Ecosystem. Springer, Berlin. 146 pp.

Linares, E., Haller, M.J. and Ostera, H.A., 2002. Los ciclos magmáticos de la República Argentina: Revisión sobre la base de las edades radimétricas al año 2000. Actas del XV Congrso Geológico Argentino, El Calafate.

Lindqvist, O., Johansson, K., Aastrup, M., Adersson, A., Bringmark, L., Hovsenius, G., Hankanson, L., Iverfeldt, A., Meili, M., Timm, B., 1991. Mercury in the Swedish environment: recent research on causes, consequences and corrective methods. Water, Air, and Soil Pollution. 55, 1-261.

Liu, X., Xu, L., Chen, Q., Sun, L., Wang, Y., Yan, H., Liu, Y., Luo, Y. and Huang, J., 2012. Historical change of mercury pollution in remote Yongle archipelago, South China Sea. Chemosphere. 87, 549–556.

Löwemark, L., Chen, H.F., Yang, T.N., Kylander, M., Yu, E.F., Hsu, Y.W., Lee, T.Q., Song, S.R. and Jarvis, S., 2011. Normalizing XRF-scanner data: A cautionary note on the interpretation of high-resolution records from organic-rich lakes. Journal Of Asian Earth Sciences. 40, 1250–1256.

Luyten, P.J., Jones, J.E., Proctor, R., Tabor, A., Tett, P. and Wild-Allen, K., 1999. COHERENS - A coupled Hydrodynamical-Ecological Model for Regional and Shelf Seas. User Documentation. MUMM (Management Unit of the Mathematicals Models of the Noth Sea). Bruxells.

M

Ma, Y. and Uren, N.C., 1995. Application of a new fractionation scheme for heavy metals in soils. Communications in Soil Science and Plant Analysis. 26 (19-20), 3291-3303.

Maher, B.A., Prospero, J.M., Mackie, D., Gaiero, D., Hesse, P.P. and Balkanski, Y., 2010. Global connections between aeolian dust, climate and ocean biogeochemistry at the present day and at the last glacial maximum. Earth-Science Reviews. 99 (1-2), 61-97.

Malvern Mastersizer, 1997. Mastersizer S and X. Getting started. Manual 0101, Issue 1.3

Mandal, B.K. and Suzuki, K.T., 2002. Arsenic round the world: a review. Talanta. 58, 201-235.

Manning, B.A., Goldberg, S., 1996. Modeling competitive adsorption of arsenate with phosphate and molybdate on oxide minerals. Soil Science Society of America Journal. 60, 121–131.

Manning, P.G., Prepas, E.E. and Serediak, M.S., 1999. Pyrite and vivianite intervals in the bottom sediments of eutrophic Baptiste Lake, Alberta, Canada. The Canadian Mineralogist. 37, 593-601.

Marcovecchio, J.E., Andrade, S., Ferrer, L.D., Asteasuain, R.O., De Marco, S.G., Gavio, M.A., Scarlato, N., Freije, R.H. and Pucci, A.E., 2001. Mercury distribution in estuarine environments

from Argentina: The detoxification and recovery of salt marshes after 15 years. Wetlands Ecology and Management. 9 (4), 317-322.

Marengo, J.A. and Rogers, J.C., 2001. Polar air outbreaks in the Americas: assessments and impacts during modern and past climates. In: Interhemispheric Climate Linkages. V. Markgraf, Ed., Adademic Press, San Diego, 17-51.

Markgraf, V., 1998. Past climate of South America. In: Hobbs JE, Lindesay JA, Bridgman HA (eds) Climate of the southern continents: Present, past and future. John Wiley & Sons Ltd, Hoboken, NJ.

Martínez, D.E., 1991. Caracterización geoquímica de las aguas de la Laguna Mar Chiquita, Provincia de Córdoba. Universidad Nacional de Córdoba –Facultad de Ciencias Exactas Físicas y Naturales – Doctoral Thesis, 284 pp.

Martínez, D.E., Gómez Peral, M.A. and Maggi, J., 1994. Caracterización geoquímica y sedimentológica de los fangos de la laguna Mar Chiquita, Provincia de Córdoba: aplicación del análisis multivariante. Revista de la Asociación Geológica Argentina. 49 (1-2), 25-38.

Mason, R.P., Fitzgerald, W.F., 1996. Sources, sinks and biogeochemical cycling of mercury in the ocean. In: Baeyens, W., *et al.* (Eds.), Global and Regional Mercury Cycles: Sources, Fluxes and Mass Balances. Kluwer Academic, Netherlands, pp. 249-272.

Mason, R.P., Choi, A.L., Fitzgerald, W.F., Hammerschmidt, C.R., Lamborg, C.H., Soerensen, A.L., Sunderland, E.M., 2012. Mercury biogeochemical cycling in the ocean and policy implications. Environmental Research. 119, 101-117.

Matthews, S.J., Gardeweg, M.C. and Sparks, R.S.J., 1997. The 1984 to 1996 cyclic activity of Lascar Volcano, northern Chile: cycles of dome growth, dome subsidence, degassing and explosive eruptions. Bulletin of Volcanology. 59 (1), 72–82.

McCleskey, R.B., Nordstrom, D.K. and Ball, J.W., 2003. Metal Interferences and their Removal Prior to the Determination of As(T) and As(III) in Acid Mine Waters by Hydride Generation Atomic Absorption Spectrometry. USGS, Water Resources Investigations Report 03-4117.

McLaren, S.J. and Kim, N.D., 1995. Evidence for a seasonal fluctuation of arsenic in New Zealand's longest river and the effect of treatment on concentrations in drinking water. Environmental Pollution. 90, 67–73.

Menghi, M., Del Sueldo, R. and Carelli, H., 2001. Relación entre la diversidad y biomasa en comunidades herbáceas del valle de inundación del Río Dulce (Argentina Central). Importancia para su manejo. Pastos. XXXI (2), 217-232.

Menghi, M., 2006. Vegetación. En: Bañados del Río Dulce y Mar Chiquita (Córdoba, Argentina) (ed. Bucher), pp. 15-27. Academia Nacional de Ciencias (Córdoba, Argentina).

Merlo, C., Abril, A., Amé, M.V., Argüello, G.A., Carreras, H.A., Chiappero, M.S., Hued, A.C., Wannaz, E., Galanti, L.N., Monferrán, M.V., González, C.M. and Solís. V.M., 2011. Integral

assessment of pollution in the Suquía River (Córdoba, Argentina) as a contribution to lotic ecosystem restoration programs. Science of the Total Environment. 409, 5034–5045.

Meybeck, M., Chapman, D., and Helmer, R. (eds.), 1989. Global Fresh Water Quality: A First Assessment. Basil Blackwell, Oxford, 307pp.

Meybeck, M., 2003. Global Occurrence of Major Elements in Rivers. In: Holland, H.D and Turekian, K.K. (eds) - Treatise on Geochemistry. Elsevier-Pergamon, Oxford. Vol. 5, pp. 207-223.

Mie, G., 1908. Beiträge zur Optik trüber Medien, speziell kolloidaler Metallösungen. (Contributions to the optic of turbid media, particularly of colloidal metal solutions). Leipzig. Annalen der Physik. 25 (3), 377–445.

Mitsunobu, S., Hamanura, N., Kataoka, T. and Shiraishi, F., 2013. Arsenic attenuation in geothermal streamwater coupled with biogenic arsenic(III) oxidation. Applied Geochemistry. 35, 154-160.

Mon, R. and Gutiérrez, A., 2009. The Mar Chiquita Lake: An indicator of intraplate deformation in the central plain of Argentina. Geomorphology. 111, 111–122.

Monferrán, M.V., Galanti, L.N., Bonansea, R.I., Amé, M.V. and Wunderlin, D.A., 2011. Integrated survey of water pollution in the Suquía River basin (Córdoba, Argentina). Journal of Environmental Monitoring. 13, 398–409.

Moon, D.H., Dematas, D. and Menounou, N., 2004. Arsenic immobilization by calcium-arsenic precipitates in lime treated soils. Science of the Total Environment. 330, 171-185.

Moreno, A., Giralt, S., Valero-Garcés, B., Sáez, A., Bao, R., Prego, R., Pueyo, J.J., González-Sampériz, P. and Taberner, C., 2007. A 14 kyr record of the tropical Andes: The Lago Chungara sequence, 18 S, northern Chilean Altiplano. Quaternary International. 161,4–21.

Munthe, J. and Lindqvist, O., 1990. The aqueous atmospheric chemistry of mercury. Proceedings, Nordic Symposium on Atmospheric Chemistry. December 6-8, 1989. Stockholm - Helsinki.

Muñiz, P., Danulat, E., Yannicelli, B., García-Alonso, J., Medina, G. and Bícego, M.C., 2004. Assesment of contamination by heavy metals and petroleum hydrocarbons in sediments of Montevideo Harbour (Uruguay). Environmental International. 29, 1019-1028.

Mutti D., Tourn, S., Caccaglio, O., Herrmann, C., Geuna, S., Di Marco, A., and Gonzalez Chiozza, S., 2005. Evolución metalogenética de las Sierras Pampeanas de Córdoba y sur de Santiago del Estero: Ciclos famatiniano, gondwánico y ándico. Revista de la Asociación Geol Argentina. 60 (3), 467–485.

N

Nicolli, H.B., Suriano, J.M., Gómez Peral, M.A., Ferpozzi, L.H. and Baleani, O.A., 1989. Groundwater contamination with arsenic and other trace elements in an area of the Pampa, Province of Córdoba, Argentina. Environmental Geology and Water Sciences. 14 (1), 3-16.

Nicolli, H.B., Bundschuh, J., García, J.W., Falcón, C.M. and Jean J-S., 2010. Sources and controls for the mobility of arsenic in oxidizing groundwaters from loess-type sediments in arid/semi-arid dry climates—evidence from the Chaco–Pampean plain (Argentina). Water Research. 44 (19), 5589–604.

Nicolli, H.B., Bundschuh, J., Blanco, M.C., Tujchneider, O.C., Panarello, H.O., Dapeña, C. and Rusansky, J.E., 2012. Arsenic and associated trace-elements in groundwater from the Chaco-Pampean plain, Argentina: Results from 100 years of research. Science of the Total Environment. 429, 36–56.

Nogues-Paegle, J. and Mo, K.C.,1997. Alternating wet and dry conditions over South America during summer. Monthly Weather Review. 125, 279–291.

Nordstrom, D.K., 2000. An overview of arsenic mass poisoning in Bangladesh and West Bengal, India. In: Young, C. (Ed.), Minor Elements 2000: Processing and Environmental Aspects of As, Sb, Se, Te, and Bi. Society for Mining, Metallurgy and Exploration, pp. 21–30.

Nowaczyk, N.R., 2011. Dissolution of titanomagnetite and sulphidization in sediments from Lake Kinneret, Israel. Geophysical Journal International. 187 (1), 34-44.

Nriagu J.O., 1989. A global assessment of natural sources of atmospheric trace metals. Nature. 338, 47–49.

Nriagu, J.O., 1994. Mechanistic steps in the photoreduction of mercury in natural waters. The Science of the Total Environment. 154, 1-8.

Nriagu, J. and Becker, C., 2003. Volcanic emissions of mercury to the atmosphere: global and regional inventories. The Science of the Total Environment 304, 3–12.

O

Oguri, K., Harada, N. and Tadai, O., 2012. Excess ^{210}Pb and ^{137}Cs concentrations, mass accumulation rates and sedimentary processes on the Bearing Sea continental shelf. Deep-Sea Research II. 61-64, 193-204.

Oldfield, F. and Appleby, P.G., 1984, Empirical testing of ^{210}Pb-dating models for lake sediments, in Lake Sediments and Environmental History (ed. Haworth, E.Y., and Lund, J.W.G.), pp. 93-124, University of Minnesota, Minneapolis.

Olivero, J., Johnson, B. and Arguello, E., 2002. Human exposure to mercury in San Jorge river basin, Colombia (South America). The Science of the Total Environment. 289, 41-47.

Oremland, R.S., Dowdle, P.R., Hoeft, S., Sharp, J.O., Schaeffer, J.K., Miller, L.G., Switzer Blum, J., Smith, R.L., Bloom, N.S. and Wallschlaeger, D., 2000. Bacterial dissimilatory reduction of arsenate and sulfate in meromictic Mono Lake, California. Geochimica et Cosmochimica Acta. 64 (18), 3073–3084.

Oroná, C., Carranza, P.M, Rodríguez, M.I., Larrosa, N., Pozzi, C. and Rodríguez, A., 2010. Evaluación Limnológica de la Laguna del Plata-Mar Chiquita, Córdoba. Ciencia. 5 (20), 63-73.

Osores M.S., Pujol, G., Collini, E. and Folch, A., 2011. Análisis de la dispersión y depósito de ceniza volcánica mediante el modelo fall3d para la erupción del volcán Hudson en 1991. Trabajo para el Servicio de Hidrografía Naval y el Servicio Meteorológico Nacional.

Özverdi, A. and Erdem, M., 2006. Cu^{2+}, Cd^{2+} and Pb^{2+} adsorption from aqueous solutions by pyrite and synthetic iron sulphide. Journal of Hazardous Materials. 137, 626-632.

P

Pacyna, J.M., Pacyna, E.G., Steenhuisen, F. and Wilson, S., 2003 . Mapping 1995 global anthropogenic emissions of mercury. Atmospheric Environment. 37 (S1), S109 – S117.

Pacyna, E.G., Pacyna, J.M., Steenhuise, F. and Wilson, S., 2006. Global anthropogenic mercury emission inventory for 2000. Atmospheric Environment. 40, 4048 – 4063.

Parkhurst, D. and Appelo, C., 1999. User's guide to PHREEQC (version 2). A computer program for speciation, batch-reaction, one-dimensional transport, and inverse geochemical calculations : U.S. Geological Survey Water-Resources Investigations Report 99-4259, 312 p.

Pai, P., Niemi, D., Powers, B., 2000. A North Amercian inventory of anthropogenic mercury emissions. Fuel Processing Technology. 65-66, 101-115.

Paoloni, J.D., Sequeira, M.E., Espósito, M.E., Fiorentino, C.E., and Blanco, M.C., 2009. Arsenic in water resources of the Southern Pampa Plains, Argentina. Journal of Environmental and Public Health.

Pasquini, A.I., Lecomte, K.L., Piovano, E.L. and Depetris, P.J., 2006. Recent rainfall and runoff variability in central Argentina. Quaternary Internacional. 158, 127-139.

Pasquini A.I., Formica, S.M. and Sacchi, G.A., 2011. Hydrochemistry and nutrients dynamic in the Suquía River urban catchment's, Córdoba, Argentina. Environmental Earth Science. DOI 10.1007/s12665-011-0978-z.

Pesce, S.F. and Wunderlin D.A., 2000. Use of water quality indices to verify the impact of Córdoba City, Argentina, on Suquía River. Water Research. 34 (11), 2915-2926.

Peterson, M.L. and Carpenter, R., 1983. Biogeochemical processes affecting total arsenic and arsenic species distributions in an intermittently anoxic Fjord. Marine Chemistry. 12, 295–321.

Piovano, E.L., Ariztegui, D. and Damatto, Moreira, S., 2002. Recent environmental changes in Laguna Mar Chiquita (central Argentina): a sedimentary model for a highly variable saline lake. Sedimentology. 49, 1371–1384.

Piovano, E.L., Ariztegui, D., Bernasconi, S.M. and McKenzie, J.A., 2004a. Stable isotopic record of hydrological changes in subtropical Laguna Mar Chiquita (Argentina) over the last 230 years. The Holocene. 14 (4), 525–535.

Piovano, E.L., Larizzatti, F.E., Fávaro, D.I., Oliveira, S.M.B., Damatto, S.R., Mazzilli, B.P. and Ariztegui, D., 2004b. Geochemical response of a closed-lake basin to 20th century recurring droughts/wet intervals in the subtropical Pampean Plains of South America. Journal of Limnology. 63 (1), 21-32.

Piovano, E.L, Zanor, G.A., and Ariztegui, D., 2006. Historia geológica y registro climático. En: Bañados del río Dulce y laguna Mar Chiquita (Córdoba, Argentina) (ed. Bucher, E.H.), pp. 37-55. Academia Nacional de Ciencias (Córdoba, Argentina).

Piovano, E.L., Ariztegui, D., Córdoba, F., Cioccale and M, Sylvestre, F., 2009. Hydrological Variability in South America Below the Tropic of Capricorn (Pampas and Patagonia, Argentina) During the Last 13.0 Ka, in Vimeux, F., Sylvestre, F., Khodri, M. (eds.), Past Climate Variability in South America and Surrounding Regions, From the Last Glacial Maximum to the Holocene, Volume 14: Springer, 323-351.

Pirrone, N., Keeler, G.J., Nriagu, J.O., 1996. Regional differences in worldwide emissions of mercury to the atmosphere. Atmospheric Environment. 30, 2981-2987.

Pirrone, N., Cinnirella, S., Feng, X., Finkelman, R.B., Friedli, H.R., Leaner, J., Mason, R., Mukherjee, A.B., Stracher, G., Streets, D.G. and Telmer, K., 2009. Global Mercury Emissions to the Atmosphere from Natural and Anthropogenic Sources. In: Mercury Fate and Transport in the Global Atmosphere. Emissions, Measurements and Models. 2009, pp 1-47. Editors: Robert Mason, Nicola Pirrone. ISBN: 978-0-387-93957-5 (Print) 978-0-387-93958-2 (Online). Springer

Pozzi, C.; Plencovich, G.; Hillman, G.; Rodriguez, A.; Caamaño Nelli, G.; Michelutti, P.; Salio, P.; Pagot, M., 2005. Monitoreo hidroambiental de la Laguna Mar Chqiuita, Córdoba. Aplicación al diseño de las defensas costeras de Miramar. XX Congreso Nacional del Agua 2005 y III Simposio de Recursos Hídricos del Cono Sur. Mendoza, Argentina. Mayo 2005.

Pozzi, C.E., Plencovich, G.E., Corral, M., Pagot, M.R., Hillman, G.D., Rodríguez, A., Curto, E.D. and Bucher, E.H., 2006. Circulación de las aguas superficiales en la Laguna Mar Chiquita. En: Bañados del Río Dulce y Mar Chiquita (Córdoba, Argentina) (ed. Bucher E.H), pp. 103-115. Academia Nacional de Ciencias (Córdoba, Argentina).

P'Yankov, V.A., 1949. Kinetics of the reaction between mercury vapor and ozone. Zhurnal Organicheskoi Khimii. (Russian Journal of Organic Chemistry). 6, 224-229.

Q

Quevauviller, P., 1998. Method performance studies for speciation analysis. Cambridge, UK7 Royal Society of Chemistry.

Quintana, E., 2011. Environmental impact of the nuclear tests in Argentina. Comprehensive nuclear-test-ban treaty, science and technology, 8-10 June, 2011. Vienna, Austria.

R

Raiswell, R., Canfield, D.E., and Berner, R.A., 1994. A comparison of iron extraction methods for the determination of degree of pyritization and the recognition of iron-limited pyrite formation. Chemical Geology. 111(1-4), 101–10.

Ramos, V.A., 1988a. Tectonics of the Late Proterozoic-Early Paleozoic: a collisional history of southern South America. Episodes. 11 (3), 168-174, Ottawa.

Ramos, V.A., 1988b. The tectonics of the Central Andes: 30° to 33° S latitude. En: Clark, S. and Burchfiel, D. (Eds.): Processes in Continental Lithospheric Deformation. Geological Society of America, Special Paper 218: 31-54, Boulder.

Ramsey, M.H., Potts, P.J., Webb, P.C., Watkins, P., Watson, J.S. and Coles, B.J., 1995. An objective assessment of analytical method precision: comparison of ICP-AES and XRF for the analysis of silicate rocks. Chemical Geology. 124, 1–19.

Raychowdhury, N., Mukherjee, A., Bhattacharya, P., Johannesson, K., Bundschuh, J., Bejarano Sifuentes, G., Nordberg, E., Martin, R.A. and Storniolo, A.R., 2013. Provenance and fate of arsenic and other solutes in the Chaco-Pampean Plain of the Andean foreland, Argentina: From perspectives of hydrogeochemical modeling and regional tectonic setting. Journal of Hydrology. In press. DOI: http://dx.doi.org/10.1016/j.jhydrol.2013.07.003.

Reati, G.J., Florín, M., Fernández, G.J. and Montes, C., 1997. The Laguna Mar Chiquita (Córdoba, Argentina): a little known, secularly fluctuating, saline lake. International Journal of Salt Lake Research. 5, 187-219.

Ribeiro Guevara, S., Massaferro, J., Villarosa, G., Arribére, M. and Rizzo, A., 2002. Heavy metal contamination in sediments of lake Nahuel Huapi, Nahuel Huapi National Park, Northern Patagonia, Argentina. Water, Air, and Soil Pollution 137 (1-4), 21-44.

Ribeiro Guevara, S., Bubach, D. and Arribére, M., 2004. Mercury in Lichens of Nahuel Huapi National Park, Patagonia, Argentina, Journal of Radioanalytical and Nuclear Chemistry. 261, 679–687.

Ribeiro Guevara, S., Rizzo, A., Sánchez, R. and Arribére, M., 2005. Heavy metal inputs in Northern Patagonia lakes from short sediment core analysis. Journal of Radioanalytical and Nuclear Chemistry. 265 (3), 481–493.

Ribeiro Guevara, S., Catán, S.P. and Marvin-Di Pasquale, M., 2009. Benthic methylmercury production in lacustrine ecosystems of Nahuel Huapi National Park, Patagonia, Argentina. Chemosphere 77 (4), 471-477.

Ribeiro Guevara, S., Meili, M., Rizzo, A., Daga, R. and Arribére, M., 2010. Sediment records of highly variable mercury inputs to mountain lakes in Patagonia during the past millennium. Atmospheric Chemistry and Physics. 10, 3443–3453.

Rich, J, 2002. Great Salt Lake South Arm circulation: current, velocity and influencing factors. En: Great Salt Lake. An overview of change (Ed. Wallace Gwynn J.), pp. 171-183. Utah Geological Survey, Salt Lake City, U.S.A.

Richards, J.A. and Jia, X., 2006. Remote Sensing Digital Image Analysis: An introduction. 4th edition. Springer, 439 pp.

Rickard, D. and Morse, J.W., 2005. Acid volatile sulfide (AVS). Marine Chemistry. 97, 141–197

Riedel, F.N., Eikmann, T., 1986. Natural occurrence of arsenic and its compounds in soils and rocks. Wissenschaft und Umwelt. 3–4, 108–117.

Rittle, K.A., Drever, J.I., Colberg, P.J.S., 1995. Precipitation of arsenic during bacterial sulfate reduction. Geomicrobiology Journal. 13, 1–11.

Robbins, J.A., Edgington, D.N., 1975. Determination of recent sedimentation rates in Lake Michigan. Geochimica et Cosmichimica Acta. 39, 285-304.

Rodrigues Bastos, W., Oliveira Gomes, J.P., Cavalcante Oliveira, R., Almeida, R., Nascimento, E.L., Bernardi, J.V.E., Drude de Lacerda, L., da Silveira, E.G. and Pfeiffer, W.C., 2006. Mercury in the environment and riverside population in the Madeira River Basin, Amazon, Brazil. Science of the Total Environment. 368, 344– 351.

Rodriguez, A., Pozzi, C., Plencovich, G., Hillman, G., Pagot, M. and Caamaño Nelli, G., 2005. Caracterización hidrodinámica preliminar de la Laguna Mar Chiquita, Córdoba, Argentina. Congreso Nacional del Agua, Mendoza, Argentina.

Román-Ross, G., Cuello, G.J., Turrillas, X., Fernández-Martínez, A. and Charlet, L., 2006. Arsenite sorption and co-precipitation with calcite. Chemical Geology. 233 (3-4), 328-336.

Ronco, A., Camilión, C. and Manassero, M., 2001. Geochemistry of heavy metals in bottom sediments from streams of the western coast of the Rio de la Plata Estuary, Argentina. Environmental Geochemistry and Health. 23 (2), 89-103.

Rosenberg, E. and Ariese, F., 2001. Quality control in speciation analysis. In: Ebdon L, Pitts L, Cornelis R, Crews H, Donard OFX, Quevauviller Ph, editors. Trace Element Speciation for Environment, Food and Health. Cambridge, UK, Chap 7, The Royal Society of Chemistry; 2001. p. 17– 50.

Rosso, J.J., Troncoso, J.J. and Fernández Cirelli, A., 2011. Geographic Distribution of Arsenic and Trace Metals in Lotic Ecosystems of the Pampa Plain, Argentina. Bulletin of Environmental Contamination and Toxicology. 86, 129–132.

Rosso, J.J., Schenone, N.F., Pérez Carrera, A. and Fernández Cirelli, A., 2013. Concentration of arsenic in water, sediments and fish species from naturally contaminated rivers. Environmental Geochemistry and Health. 35 (2), 201-214.

Rothwell, R.G. and Rack, F.R., 2006. New techniques in sediment core analysis: an introduction. In: Rothwell, R.G. (Ed.), New techniques in sediment core analysis. Special Publications. Geological Society, London, pp. 1–29.

Roulet, M. and Lucotte, M., 1995. Geochemistry of mercury in pristine and flooded ferralitic soils of a tropical rain forrest in French Guiana, South America. Water, Air and Soil Pollution. 80, 1069-1088.

Roulet, M., Lucotte, M., Saint Aubin, A., Tran, S., Rhéault, I., Farella, N., Jesus Da Silva, E., Dezaencourt, J., Sousa Passos, C.-J., Santos Soares, G., Guimaraes, J.-R.D., Mergler, D. and Amorin, M., 1998. The geochemistry of mercury in central Amazonian soils developed on the Alter-do-Chao formation of the lower Tapajos River Valley, Para state, Brasil. Science of the Total Environment. 223, 1-24.

Rydberg, J., Klaminder, J., Rosén, P. and Bindler, R., 2010. Climate driven release of carbon and mercury from permafrost mires increases mercury loading to sub-arctic lakes. Science of the Total Environment. 408, 4778–83.

S

Saari, H-K., Schmidt, S., Castaing, P., Blanc, G., Sautour, B., Masson, O. and Kirk Cochran, J., 2010. The particulate $^{7}Be/^{210}Pb_{xs}$ and $^{234}Th/^{210}Pb_{xs}$ activity ratios as tracers for tidal-to-seasonal particle dynamics in the Gironde estuary (France): Implications for the budget of particle-associated contaminants. Science of the Total Environment. 408, 4784–4794.

Sahuquillo, A., Rauret, G., Bianchi, M., Rehnert, A. and Muntau, H., 2003. Mercury determination in solid phases from application of the modified BCR-sequential extraction procedure: a valuable tool for assessing its mobility in sediments. Analytical and Bioanalytical Chemistry. 375 (4), 578–583.

Sancha, A.M., 1999. Full-scale application of coagulation processes for arsenic removal in Chile: a successful case study. In: Chappell, W.R., Abernathy, C.O., Calderon, R.L. (Eds.), Arsenic Exposure and Health Effects. Elsevier, Amsterdam, pp. 373–378.

Sanchez-Cabeza, J.A., Ani-Ragolta, I. and Masqué, P., 2000. Some considerations of the ^{210}Pb constant rate of supply (CRS) dating model. Limnology and Oceanography. 45 (4), 990-995.

Sanchez-Cabeza, J.A. and Ruiz-Fernández, A.C., 2012. ^{210}Pb sediment radiochronology: An integrated formulation and classification of dating models. Geochimica et Cosmochimica Acta. 82, 183–200.

Saulo, A.C., Nicolini, M. and Chou, S.C., 2000. Model characterization of the South American low-level flow during the 1997–98 spring–summer season. Climate Dynamics. 16, 867–881.

Schäfer, J., Blanc, G., Audry, S., Coynel, A. and Lissalde, J.P., 2004. Mercury fluxes and sedimentary record in the Lot-Garonne River system (France). Abstract N° 634, 7th International Conference, Mercury as a Global Pollutant, June 27-July 2, 2004, Ljubljana, Slovenia.

Schäfer, J., Blanc, G., Audry, S., Cossa, D. and Bossy, C., 2006. Mercury in the Lot-Garonne River system (France): sources, fluxes and anthropogenic component. Applied Geochemistry. 21, 515–527.

Schäfer J., Castelle S., Blanc G., Dabrin A., Masson M., Lanceleur, L. and Bossy C., 2010. Mercury distribution and methylation potential in sediments of a highly turbid macrotidal estuary (Gironde, France). Estuarine, Coastal and Shelf Science. 90, 80-90.

Schmalzer, P-.A. and Ross Hinkle, C., 1992. Soil dynamics following fire in juncus and spartina marshes. Wetlands. 12 (1), 8-21.

Schmidt, S., Howa, H., Mouret, A., Lombard, F., Anschutz, P. and Labeyrie, L., 2009. Particle fluxes and recent sediment accumulation on the Aquitanian margin of Bay of Biscay. Continental Shelf Research. 29, 1044-1052.

Schuster, E., 1991. The behavior of mercury in the soil withspecial emphasis on complexation and adsorptionprocesses-a review of the literature. Water, Air and Soil Pollution. 56, 667-680.

Selin, N., 2009. Global Biogeochemical Cycling of Mercury: A Review. Annual Review of Environment and Resources. 34, 43–63.

Silvestri, G., 2004. El Niño signal variability in the precipitation over southeastern South America during the austral summer. Geophysical Research Letters. 31, L18206.

Slemr, F. and Langer, E., 1992. Increase in global atmospheric concentrations of mercury inferred from measurements over the Atlantic-Ocean. Nature. 355 (6359), 434-437.

Smedley, P.L and Kinniburgh, D.G., 2002. A review of the source, behaviour and distribution of arsenic in natural waters. Applied Geochemistry. 17, 517-568.

Smedley, P.L., Nicolli, H.B., Macdonald, D.M.J., Barros, A.J. and Tullio, J.O., 2002. Hydrogeochemistry of arsenic and other inorganic constituents in groundwaters from La Pampa, Argentina. Applied Geochemistry. 17, 259–284.

Smedley, P.L., Kinniburgh, D.G, Macdonald, D.M.J., Nicolli, H.B., Barros, A.J., Tullio, J.O., Pearce, J.M. and Alonso, M.S., 2005. Arsenic associations in sediments from the loess aquifer of La Pampa, Argentina. Applied Geochemistry. 20, 989–1016.

Smith, J.N., 2001. Why should we believe ^{210}Pb sediment geochronologies? Journal of Environmental Radioactivity. 55, 121–123.

Stallard, R.F., 1995a. Relating chemical and physical erosion. In Chemical Weathering Rates of Silicate Minerals, Reviews in Mineralogy (eds. A. F. White and S. L. Brantley). Mineralogical Society of America, Washington, DC, pp. 543–562.

Stallard, R.F., 1995b. Tectonic, environmental and human aspects of weathering and erosion: a global review using a steady-state perspective. Annual Review of Earth and Planetary Sciences. 23, 11–39.

Stern, C., 2004. Active Andean volcanism: its geologic and tectonic setting, Revista Geológica de Chile. 31, 161–206.

Stupar, Y.V., Schäfer, J., García, M.G., Schmidt, S., Piovano, E., Blanc, G., Huneau, F. and Le Coustumer, P., (2013). Historical mercury trends recorded in sediments from the Laguna del Plata, Córdoba, Argentina. Chemie Erde - Geochemistry, http://dx.doi.org/10.1016/j.chemer.2013.11.002

Stromberg, D., Stromberg, A. and Wahlgren, U., 1991. Relative quantum calculations on some mercury sulfide molecules. Water, Air and Soil Pollution. 56, 681-695.

Sugimori, K., Matsuo, M., Kuno, A., Wang, Q., Chen, G.J., Horie, M., 2007. Sulfate - Reducing bacterial activity and pyrite formation in sediments from Qinghai Lake in China. Water-Rock Interaction - Proceedings of the 12th International Symposium on Water-Rock Interaction, 12 (2), 1283-1286. Kunming; China; 31 July through 4 August 2007.

Suits, N.S. and Wilkin, R.T., 1998. Pyrite formation in the water column and sediments of a meromictic lake. Geology. 26, 1099-1102.

Sutherland, R.A., Tack, F.M.G., Tolosa, C.A. and Verloo, M.G., 2000. Operationally Defined Metal Fractions in Road Deposited Sediment, Honolulu, Hawaii. Journal of Environmental Quality 2000. 29 (5), 1431-1439.

T

Tack, F.M.G., Vossius, H.A.H., and Verloo, M.G., 1996. A Comparison between Sediment Fractions, Obtained from Sequential Extraction and Estimated from Single Extractions. International Journal of Environmental Analytical Chemistry. 63 (1), 61-66.

Teisserenc, R., Lucotte, M., Houel, S., 2010. Terrestrial organic matter biomarkers as tracers of Hg sources in lake sediments. Biogeochemistry. 103, 235–244.

Tessier, A., Campbell, P.G.C. and Bisson, M., 1979. Sequential extraction procedure for the speciation of particulate trace metals. Analytical Chemistry. 51 (7), 844–51.

Thomson, J., Croudace, I.W. and Rothwell, R.G., 2006. A geochemical application of the ITRAX scanner to a sediment core containing eastern Mediterranean sapropel units. In: Rothwell, R.G. (Ed.), New Techniques in Sediment Core Analysis. Special Publication, vol. 267. Geological Society, London, pp. 65–77.

Tiffreau, C., Lützenkirchen, J. and Behra, P., 1995. Modelling the adsorption of mercury (II) on (hydr)oxides. Journal of Colloid and Interface Science. 172, 82-93.

Tilzer, M.M. and Serruya, C., 1990. Lakes, ecological structure and function. Springer Verlag, Berlin.

Tjallingii, R., Röhl, U., Kölling, M. and Bickert, T., 2007. Influence of the water content on X-ray fluorescence core-scanning measurements in soft marine sediments. Geochemistry, Geophysics, Geosystems. 8 (2). Doi:10.1029/2006GC001393.

Troin, M., Vallet-Coulomb, C., Sylvestre, F. and Piovano, E., 2010. Hydrological modelling of a closed lake (Laguna Mar Chiquita, Argentina) in the context of 20th century climatic changes. Journal of Hydrology. 393, 233–244.

Tsuzuki, M.Y., Aikawa, H., Strussman, C.A. and Takashima, F., 2000. Comparative survival and growth of embryos, larves and juveniles of pejerrey (*Odontesthes bonariensis* and *O. Hatcheri*) at different salinities. Jurnal of Applied Ichthyology. 16, 126-130.

U

United Nations Scientific Committee on the Effects of Atomic Radiation, 2000, Sources and effects of ionizing radiation: UNSCEAR 2000. Report to the General Assembly, with Scientific Annexes, United Nations, New York, 1, 654 pp.

Ure, A., Berrow, M., 1982. The elemental constituents of soils. Chapter 3. In: Bowen, H.J.M. (Ed.), Environmental Chemistry. Royal Society of Chemistry, London, pp. 94–203.

V

Vandal, G.M., Mason, R.P. and Fitzgerald, W.F., 1991. Cycling of volatile mercury in template lakes. Water, Air and Soil Pollution. 56 (1), 791-803.

Van der Klooster, E., van Egmond, F.M. and Sonneveld, M.P.W., 2011. Maping soil clay contents in Dutch marine districts using gamma-ray spectrometry. European Journal of Soil Science. 62, 743-753.

Vázquez,, J., Miatello, M. and Roqué, M., 1979. Geografía física de la Provincia de Córdoba. Editorial Boldt. República Argentina. 464 pp.

Vera, C., Higgins, W., Amador, J., Ambrizzi, T., Garreaud, R., Gochis, D., Gutzler, D., Lettenmaier, D., Marengo, J., Mechoso, C.R., Nogues-Paegle, J., Silva Diaz, P.L. and Zhang, C., 2006. Towards a unified view of the American Monsoon System. Journal of Climate19, 4977–5000.

Von Guten H.R., Strum, M and Moser, R.N., 1997. 200-Year record of metals in Lake sediments and natural backgrounds concentration. Environmental Science and Technology. 31, 2193-2197.

W

Warren, B.E., 1969. X-ray Diffraction. Courier Dover Publications, 381 pp.

Webster, J.G., 1999. Arsenic. In: Marshall, C.P., Fairbridge, R.W. (Eds.), Encyclopaedia of Geochemistry. Chapman Hall, London, pp. 21–22.

Whelan, R.J., 1995. The ecology of fire. Cambridge Studies in Ecology. 360 pp.

White, D.E., Hem, J.D. and Waring, G.A., 1963. Data of Geochemistry, 6th ed. M. Fleischer, (Ed). Chapter F. Chemical Composition of Sub-Surface Waters. US Geol. Surv. Prof. Pap. 440-F.

WHO (World Health Organization), 2004. Guidelines for Drinking-water Quality. Third Edition, Volume 1, Recommendations. Geneva. pp. 540.

Wien, K., Wissmann, D., Kölling, M. and Schulz, H.D., 2005. Fast application of X-ray fluorescence spectrometry aboard ship: how good is the new portable Spectro Xepos analyzer? Geo-Marine Letters. 25, 248–264.

Will, G., 2006. Powder diffraction: the Rietveld Method and the two-stage Method. Springer. 224 pp.

Wilson, T.M., Cole, J.W., Stewart, C., Croning, S.J. and Johnston, D.M., 2011. Ash storms. Impacts of wind-remobilised volcanic ash on rural communities and agriculture following the 1991 Hudson eruption, southern Patagonia, Chile. Bulletin of Vulcanology. 73, 223–239.

Weltje, G.J. and Tjallingii, R., 2008. Calibration of XRF core scanners for quantitative geochemical logging of sediment cores: Theory and application. Earth and Planetary Science Letters. 274, 423–438.

Wunderlin D.A., Díaz, M.P., Amé, M.V., Pesce, S.F., Hued, A.C. and Bistoni, M.A.,. 2001. Pattern recognition techniques for the evaluation of spatial and temporal variations in water quality. A case study: Suquía River Basin (Córboba-Argentina). Water Resources. 12, 2881-2894.

X

Xia, P., Meng, X., Yin, P., Cao, Z., Wang, X., 2011. Eighty-year sedimentary record of heavy metal inputs in the intertidal sediments from the Nanliu River estuary, Beibu Gulf of South China Sea. Environmental Pollution. 159 (1), 92-99.

Y

Yan, X.-P., Kerrich, R. and Hendry, M.J., 2000. Distribution of arsenic(III), arsenic(V) and total inorganic arsenic in porewaters from a thick till and clay-rich aquitard sequence, Saskatchewan, Canada. Geochimica et Cosmochimica Acta. 64, 2637–2648.

Yang, H., Engstrom, D.R., Rose, N.L., 2010. Recent changes in atmospheric mercury deposition recorded in the sediments of remote equatorial lakes in the Rwenzori Mountains, Uganda. Environmental Science and Technology. 44 (17), 6570–6575.

Z

Zacharewski, T. R., Chesniak, E. A. and Schroeder, W. H., 1987. FTIR investigations of the heterogeneous reaction of HgO(s) with SO_2(g) at ambient temperature. Atmospheric environment. 21, 2327-2332.

Zárate, M., 2003. Loess of Southern America. Quaternary Science Reviews. 22, 1987–2006.

Zular, A., Sawakuchi, A.O., Guedes, C.C.F., Mendes, V.R., Nascimiento Jr., D.R., Giannini, P.C.F., Aguilar, V.A.P. and DeWitt, R., 2013. Late Holocene intensification of colds fronts in southern Brazil as indicated by dune development and provenance in the Sao Francisco do Sul coastal barrier. Marine Geology. 335, 64–77.

Annexes

Annexe A : 1st article - Historical mercury trends recorded in sediments from the Laguna del Plata, Córdoba, Argentina

Historical mercury trends recorded in sediments from the Laguna del Plata, Córdoba, Argentina

Chemie Erde - Geochemistry, http://dx.doi.org/10.1016/j.chemer.2013.11.002

Yohana Vanesa Stupar [1, 2], Jörg Schäfer[3, 4], María Gabriela García[2], Sabine Schmidt[3, 4], Eduardo Piovano[2], Gérard Blanc[3,4], Frédéric Huneau[5,6], Philippe Le Coustumer[1]

[1]Université de Bordeaux, EA 4592 Géoressources & Environnement, ENSEGID, 1 allée F. Daguin, F-33607 Pessac, France

[2]Centro de Investigaciones en Ciencias de la Tierra (CICTERRA), CONICET/Universidad Nacional de Córdoba, Av. Vélez Sarsfield 1611, X5016CGA, Córdoba, Argentina.

[3]Université de Bordeaux, EPOC, UMR5805, F-33400 Talence, France

[4]CNRS, EPOC, UMR5805, F-33400 Talence, France

[5]Université de Corse Pascal Paoli, Laboratoire d'Hydrogéologie, Campus Grimaldi, BP 52, F-20250 Corte, France

[6]CNRS, UMR 6134 SPE, BP 52, F-20250 Corte, France

ABSTRACT

The main carrying phases of mercury (Hg) were analyzed in a 120 cm sediment core taken at the Laguna del Plata (LP), a small lake connected to the main water body of Laguna Mar Chiquita (LMC) during highstands. LMC is considered to be one of the largest saline lakes in the world representing a sensitive climatic indicator due to its frequent lake level variations at millennial and interdecadal scale like the last ones that started early in the 1970s and after 2004. Total Particulate Hg (Hg_{TP}) concentrations vary between ~13 and ~131 µg kg^{-1} indicating a system with low pollution. Selective extractions with ascorbate, HCl and H_2O_2 were performed in the sediments and they revealed that Hg is associated mainly to reactive sulfides in the base of the core, while in the middle and upper part the organic matter seems to be the main Hg-bearing phase. The highest and most important peak was found in sediments accumulated between 1991 and 1995. More than a punctual source of pollution, this peak is likely related to two eruptive events occurred in the Andean Cordillera in this period: the eruption of Hudson volcano in southern Patagonia that occurred in 1991 and the one of the Lascar volcano in northern Chile that occurred in 1993. In both cases, the respective ash plumes were documented to have reached the Laguna del Plata region.

Key words: Mercury speciation - *S*elective extractions –hydroclimatic variability – Laguna del Plata – Laguna Mar Chiquita – evaporates – Córdoba – Argentina – metal records in sediments.

1 - Introduction

Mercury (Hg) is mobilized naturally through geological and volcanic activities (Fitzgerald and Lamborg 2003) but due to human activities such as coal burning, industry and mining, the cycle of mercury has been altered increasing long-term particle transport in the atmosphere and making deposition three to five times larger than preindustrial deposition in the northern hemisphere (Selin, 2009). This element can be transported in the atmosphere in three forms: as elemental gaseous mercury Hg(0), divalent mercury Hg(II) in small water droplets or particulate mercury Hg(P). Because divalent and particulate Hg are more soluble in water than elemental Hg, they are the Hg predominant forms deposited in the ecosystem through wet and dry deposition (Fitzgerald and Lamborg, 2003; Selin, 2009). Particulate Hg may account for more than 90% of total Hg in freshwater systems, estuaries or coastal zones (Fitzerald and Mason, 1997; Balcom *et al.*, 2004; Schäfer *et al.*, 2006) and sediments can represent efficient Hg traps and archives of past contamination (Gagnon *et al.*, 1997, Castelle *et al.*, 2007).

In countries such as Canada, France, Switzerland and China, the highest Hg concentrations are observed at the beginning of the XIX century due to the demographic and industrial growth such as "the golden age" (1860), or the Second World War (1935-1945) among others. These events were responsible for the release and accumulation of this metal in sediments, and even with the implementation of clean technologies and more strict environmental laws, concentrations are 2 to 3 folds higher than preindustrial times (i.e., Von Gunten *et al.*, 1997; Johannessen *et al.*, 2005; Castelle *et al.*, 2007). In South America, most of the high Hg concentrations are linked to gold mining in countries such as Colombia, Bolivia and Peru where high Hg levels were found in river and lake sediments, soils, fishes and human hairs in (Olivero *et al.*, 2002; Rodrigues Bastos *et al.*, 2006). Hg is used for separation of gold particles through amalgamation. During this process, a good amount of metallic Hg is also lost to rivers and soils through handling under rough field conditions and to volatilization. After amalgamation, the Au-Hg complex is burned in retorts but in most areas, this operation is done in open air, releasing Hg vapour to the atmosphere. Furthermore, Hg rich tailings are left in most mining sites (Diaz, 2000; Lacerda *et al.*, 2004). In the southernmost part of the continent, where pristine conditions are still conserved, Hg concentrations measured in sediments accumulated in lakes during the last century were attributed to volcanic events, soil erosion and the influence of global Hg fluxes (Ribeiro Guevara *et al.*, 2010; Hermanns and Biester, 2013).

In Argentina in particular, the occurrence of Hg in sediments accumulated in freshwater systems are scarce (i.e., Amin *et al.*, 1996; Hudson-Edwards *et al.*, 2001; Ronco *et al.*, 2001; Marcovecchio *et al.*, 2001; Ribeiro Guevara *et al.*, 2002, 2005, 2009, 2010; Arribére *et al.*, 2003; De Marco *et al.*, 2006; Botté *et al.*, 2010). Most of these studies are concentrated in the Patagonia region and in coastal areas of the Buenos Aires province. For example, De Marco *et al.* (2006) analized total Hg concentrations in sediments and biota in three estuarine systems on the shores of Buenos Aires between the years 1980 and 2005. The results indicate that total Hg values decreased significantly ($p<0.001$) in the last 25 years attributing this trend to the improvement in the industry practices. In the Argentina Patagonia, where the population density is low, Ribeiro Guevara *et al.*, (2010) concluded that the high Hg concentrations measured in lake sediments of pre-industrial time are due to extended fire records and volcanic activity.

Even though aquatic ecosystems are globally exposed to Hg by atmospheric inputs of increasing concern, few studies have been focusing on the sources, fate and history of freshwater systems of the southern hemisphere (Downs et al., 1998; Lamborg et al., 2002; Biester et al., 2007). In this context, the study of Hg accumulation in the sedimentary record in Laguna del Plata (30°55'S, 62°51'W) is a contribution to understand the fluxes of global Hg in a climatic-sensitive region of southern South America (e.g. Piovano et al., 2004a; Piovano et al., 2004b).

Laguna del Plata (30°55'S, 62°51'W) is situated in the SW margin of the Laguna Mar Chiquita system, composed by the Laguna del Plata, linked to the main water body, the Laguna Mar Chiquita itself and the Dulce River wetlands. The area has a rich biodiversity as well paleontological and archeological interest to the point that the lake has been declared as a Ramsar site by the United Nations (Bucher *et al.*, 2006). Laguna del Plata is fed by the Suquía River (200 km length and average discharge of 10 $m^3 s^{-1}$) that reaches the lake from its southern margin. The river headwaters are located in the Sierras Pampeanas de Córdoba (between 29°00' - 33°30'S and 64°00' - 65°30'W) where different mining activities (mainly rock quarries) and land-use have been developed. The San Roque reservoir (643

m.a.s.l.) collects the waters from the catchment's tributaries and is used for flood control and drinking water reservoir. Downflow, the Suquía River crosses from West to East the city of Córdoba which is the second biggest of Argentina (1.3 million inhabitants) after Buenos Aires. Automobile industry, machinery manufacturing, food and paint production are the main economical activities in the city. In its lower stretch, the Suquía river crosses the loessic depression of the Chacopampean plain (Zárate, 2003) which is one of the most important agricultural areas of the country. Some authors (Pesce and Wunderlin, 2000; Wunderlin *et al.*, 2001; Monferrán et al, 2011, Pasquini *et al.*, 2011) observed a decrease in the water quality from pristine regions in the upper fluvial catchments to the proximity of the lake. And even if Gaiero *et al.* (1997) noticed an increase in trace metal concentrations in riverbed sediments downflow attributed to the urban impact, Hg was not included into the studied ones. At present there is no comprehensive data on the long-term change in metal contents of the Suquía river sediment load.

The present study focuses on the sedimentary record of Hg concentrations and its main operationally-defined carrier phases in Laguna del Plata over the past ~80 years. Due to its already documented sensibility to global changes, climatic-driven variability of a typical atmospherically transported element such as Hg, will be clearly recorded in the sediments accumulated in this lake. In consequence, the main objective of this work is to understand if and how global change factors, such as population growth and/or hydroclimatic variability (lake-water level changes) affect lacustrine Hg concentrations and solid state speciation in this part of South America.

2 - Materials and methods

2.1 – Study area

2.1.1 – Background

Laguna Mar Chiquita is the biggest saline lake in South America and one of the largest in the world conserving still a wild and little altered physiognomy (Bucher *et al.*, 2006). Three rivers pour their waters into the lake (Fig. 1a): (i) The Suquía River; (ii) The Xanaes River (total length 340 km and average discharge of 14.5 m^3 s^{-1}); and (iii) The Dulce River (total length of 812 km and an average discharge of 80 m^3 s^{-1}), which is the biggest one, and has its catchments in the North-West region of Argentina.

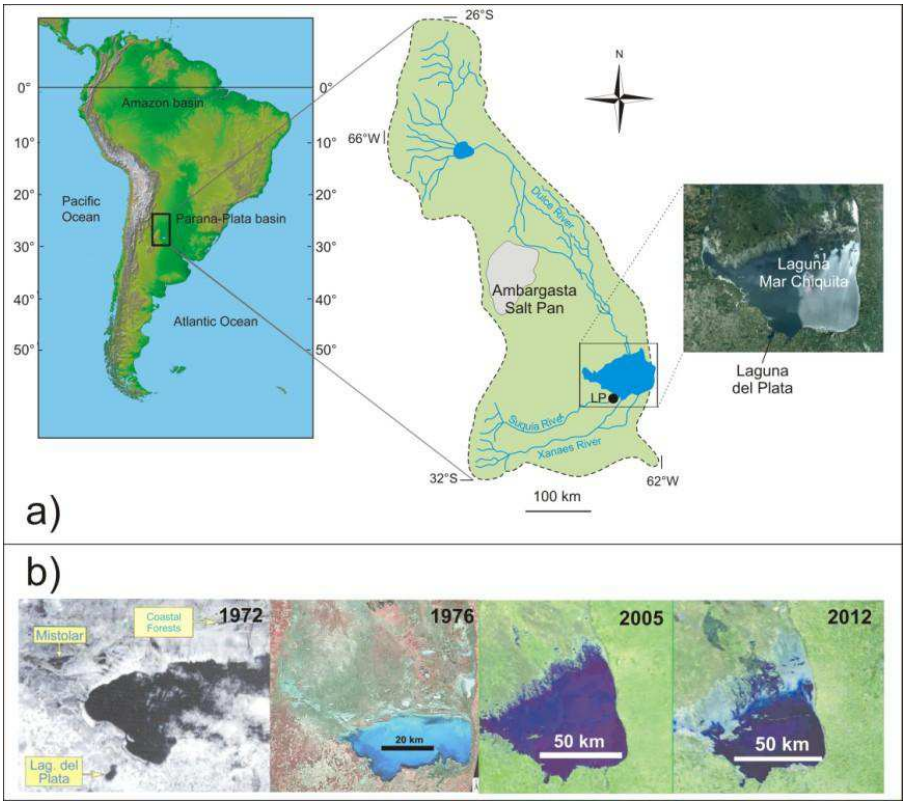

Fig. 1. a) Study area with location of Laguna del Plata sediment core (LP), b) Satellite images that show the size variation in the Laguna Mar Chiquita system.

During the 20th century, laguna Mar Chiquita showed important water-level and surface variations (Fig. 1b). The first 75 years of the 20th century Laguna Mar Chiquita was characterised by low levels but in the decade of 1970s a wet spell started (Piovano *et al.*, 2009) and high levels were registered. From 2003-2004 up to nowadays Mar Chiquita has been showing decreasing lake levels. Low and high water stands were defined as below or above 66.5 m.a.s.l. water altitude (average value) being synchronous with decreasing and increasing average regional precipitation (Piovano *et al.*, 2002). During these stages, water salinities changed from 360 g L^{-1} in 1911 (Frank 1915) to 270 g L^{-1} in 1970 (Martinez 1991) and 35 g L^{-1} in 1989 (Martinez *et al.*, 1994). Even in extreme dry periods with almost non-existent river supply, the lake was never completely desiccated due to groundwater recharge (Piovano *et al.*, 2002, 2004 a,b) but it was disconnected from Laguna del Plata until the early 1970s (see Satellite images Fig. 1b). Accordingly, important differences existed between both systems, with lower water salinity in Laguna del Plata due to the diluting effect of Suquía River (Reati *et al.*, 1997).

2.1.2. – Climatic and geological settings

The Laguna Mar Chiquita system catchment covers an area of around 127,000 km^2, (between 62-66°W and 26-31°S). Austral summer precipitation and dry winters characterize the climate of the region, where the only external sources of water vapour for rainfall are the Atlantic Ocean and the tropical latitudes, which is related to the development of a Monzon-like climatic system (Garreaud *et al.*, 2009). The ENSO (El Niño Southern Oscillation) teleconnections also control precipitation and the hydrology of major riverine systems (Aceituno 1988: Depetris *et al.*, 1996: Silvestri 2004; Boulanger *et al.*, 2005: Pasquini *et al.*, 2006). Based on the studies of long cores (~3 m) retrieved from Mar Chiquita Lake, interpretation of satellite images, drilled cores and fieldwork, Piovano *et al.* (2004a,b, 2009) determined the paleoenvironmental evolution of the area during the late Quaternary (last 13,000 years). The analyzed hydroclimatic record of Laguna Mar Chiquita indicates the onset of a positive hydrological balance at 13.0 cal ka BP (calibrated thousand years Before Present). This period was followed by extremely dry conditions that triggered the precipitation of evaporates and more positive isotope composition of carbonates and organic matter. After 6.8 cal ka BP there was an increase in the temperature gradient as a result of an enhanced influence of the Southeast Pacific anticyclone, larger Antartic sea-ice extend (Gilli *et al.*, 2005) and the effect of changes in insolation (Markgraf 1998) that derived on the strengthening of the Southern Westerlies. The most intense magnitude was dated around 4.7 cal ka BP, this cold and dry phase of the Middle Holocene is consistent with a reduced latitudinal convey of moisture from the tropics to the subtropics as a consequence of a weakened Monsoonal circulation. These conditions extended until the middle of the first millennia when less extreme lowstands can be inferred by 1.5 cal ka BP (Kröhling and Iriondo, 1999). The timing of the droughts for both the first and second millennia are poorly resolved due to the occurrence of several sedimentary hiatuses indicated by gypsum-halite layers. In the middle part of the 18th century (~A.D. 1770), sedimentation became more constant and a good chronology has been established for this latter part of the sequence based on ^{210}Pb dates (Piovano *et al.* 2002). This lowstand has been associated with the last part of the Little Ice Age whereas the lake level remained very low until the last quarter of the 20th century (i.e., decade of 1970's) when a hyperhumid period started.

The landscape in the region is characterized by Plio-Pleistocene alluvial fans progressing from the Sierras Pampeanas to the East (Kröhling and Iriondo, 1999). These sediments are covered by aeolian deposits of loessic sediments made of metamorphic and igneous rocks shards and volcaniclastic material derived from the Andes Cordillera, Sierras Pampeanas, Paraná basin and Uruguayan shield (Zárate, 2003) and transferred by southern winds that formed the Pampean Aeolian System (Brunetto and Iriondo, 2007). The uplift of the San Guillermo High. due to the activation of the Tostado-Selva fault in the Middle Pleistocene (Iriondo 1989, 1997), and the accumulation of the fans of Suquía and Xanaes Rivers against it, closed the Dulce River thus generating the Mar Chiquita impounding (Costa, 1999; Mon and Gutierrez 2009)

2.2 - Sampling methods

The 120 cm sedimentary core LP (30°55'S, 62°51'W) was taken at Laguna del Plata (Fig. 1a), at 1.5 m water depth with an Eijkelkamp hand corer beeker (CICTERRA-UNC). At the EPOC laboratory (France), the core was opened, described, photographed, sliced longitudinally for radiographical study (Fig. 2 a-b) and sampled each 0.5 cm. High-resolution 256 grey-level images were

acquired with the automated X-ray core imaging system SCOPIX (Migeon *et al.*, 1999 and Lofi and Weber 2001). Porosity has been determined from the measure of the weight before and after drying at 50°C for three days until constant weight, using an ultra precise balance (serie 32OXT, Precisa). Dry bulk density (DBD) was then calculated by using wet and dry weight, assuming the density of sediment grains to be 2.65 g cm^{-3}. Subsequently, samples were ground to 4-µm powder for further analysis.

2.3 - Analytical methods

2.3.1 - Total and Organic Carbon, Major and Minor elements

Total carbon and Organic Carbon (C_{org}) concentrations were determined with a LECO CS 125 analyzer by direct combustion in an induction furnace, and quantitative CO_2 detection by infrared absorption using ~50 mg dry sediment sub-samples without additional sample treatment (Total Carbon) or after carbonate elimination (Organic Carbon). For this, sample aliquots were acidified (2N HCl) in ceramic crucibles, then dried at 60°C for 24 hours to remove inorganic carbon and most of the remaining acid and water previous to the combustion (Etcheber *et al.*, 1999). Quality was checked by measuring certified reference materials (e.g. LECO 501–503) and intercalibrations (e.g. King *et al.*, 1998).
Measures of Al, Si, K, Ti, Fe, Zr, Mn, Sr, S, Cl and Ca were performed by XRF using an Avaatech XRF Core – Scanner on one of the halves of the core at 1mm resolution. The measurements were produced using 58 kV X-ray voltage and an X-ray current of 10 mA. The measurements obtained by XRF reflect the composition of a thin (sub-mm) layer on top of the sediment surface where the intensity of the different elements is expressed as counts per second (cps). The use of Al for this purpose allows monitoring and correcting the relative variations in the lithogenic component of the sediment (Löwemark *et al.*, 2011, Liang *et al.*, 2012) and additional sedimentary factors that influence XRF measurements (water content, surface roughness and grain size variations; Böning *et al.*, 2007, Tjallingii et al, 2007; Weltje and Tjallingi, 2008).

2.3.2 - Radionuclides

Activities of ^{210}Pb, ^{232}Th, ^{226}Ra and ^{137}Cs were measured using a low background, high efficiency, well-shaped γ detector (CANBERRA) (Schmidt et al, 2009). Calibration of the γ detector was achieved using certified reference materials (IAEA-RGU-1; IAEA-RGTh; SOIL-6). Activities are expressed in $mBq.g^{-1}$ and errors are based on 1 SD counting statistics. Excess ^{210}Pb ($^{210}Pb_{xs}$) was calculated by subtracting the activity supported by its parent isotope, ^{226}Ra, from the total ^{210}Pb activity in the sediment.

2.3.3 – Total Particulate Hg

Total Particulate Hg (Hg_{TP}) concentration was determined on ~70-100 mg aliquots of dry sediment by cold vapour atomic absorption spectrometry after incineration (O_2 stream) and amalgamation, using a Direct Mercury Analyzer (MILESTONE, DMA 80). The quality of the analytical results was systematically checked analyzing international certified sediment reference materials (LKSD-4, IAEA 433, 1646a) every set of 5 samples and concentrations were expressed in $\mu g\ kg^{-1}$ dry weight.

2.3.4 – Selective extractions

Selective extractions are commonly used in order to determine trace element distribution in different solid phases (soils and sediments) by extracting different operationally-defined fractions following either sequential (Tessier *et al.*, 1979; Sahuquillo *et al.*, 2003) or parallel extraction schemes (Audry *et al.*, 2005). In this study, Hg distribution on different solid carrier phases was operationally assessed by 3 parallel or single chemical extractions, i.e using each reagent on a different sample aliquot (Farrah and Pickering, 1993; Alborés *et al.*, 2000), as described in Castelle *et al.* (2007). Parallel extraction schemes avoid certain limitations such as (i) metal transfer from one phase to the another (Bemond, 1992), (ii) multiple risks of sample contamination from successive reagents used (Quevauviller, 1998), (iii) possible changes in elemental speciation during the successive extraction steps and (iv) changes or losses of elemental species during the residue washing step (Rosenberg and Ariese, 2001). Besides, this method shows no risk for sample losses and an error occurred during one extraction does not compromise the entire schema (Tack et al., 1996). A brief summary with the details of the three different operationally-defined fractions is listed in Table 1.

Fraction	Sample weight (mg)	Reagent	Shaking time, temperature
Ascorbate extraction - reducible fraction	200	12.5 ml of ascorbate solution	24 h, 25 °C
H_2O_2 extraction - oxidizable fraction	250	8 ml of 30 % H_2O_2 + NaOH (pH 5)	5 h, 85 °C
		Then 3 ml of 30 % H_2O_2 + NaOH	3 h, 85 °C
		Then 5 ml of 5 M NH_4OAc + 20 ml H_20 Milli-Q	30 min, 25 °C
HCl extraction - acid-soluble/reactive fraction	200	12.5 ml of 1N HCl	24 h, 25 °C

Table 1: Operating conditions applied for the single extraction procedures

For all the analyses indicated above, solutions prepared with analytical reagent grade chemicals and purified water (Milli-Q® system) were used. Labware in contact with the samples were acid cleaned (soaked in 10% HCl during 3 days, rinsed 3 times with Milli-Q® water and dried under a laminar flow hood) before proceeding with laboratory work.

Ascorbate extraction (reducible fraction)

This reducing single extraction removes trace elements associated with Mn oxides and the most reactive Fe oxide fraction (i.e. amorphous oxides; Kostka and Luther, 1994; Audry *et al.*, 2006), using a 0.11 M ascorbate reagent (5:5:2 sodium citrate/sodium-bicarbonate/ascorbic-acid mixture; J.T. Baker, Baker analyzed/J.T. Baker, Baker analyzed/Acrôs Organics).

H_2O_2 extraction (oxidizable fraction)

The oxidizing single extraction using hydrogen peroxide (H_2O_2) typically extracts organic matter but sulfides are also partially oxidized during this step (Tessier *et al.*, 1979). This work utilises a modified Tessier protocol (Ma and Uren, 1995, Audry *et al.*, 2006), previously applied for Hg solid speciation (Castelle *et al.*, 2007).

HCl extraction (acid-soluble/reactive fraction)

The so-called reactive (1M HCl acid-soluble) fraction comprises metals associated with amorphous and crystalline Mn and Fe oxides, carbonates, hydrous Al silicates and acid volatile sulphides (AVS) (Huerta-Díaz and Morse, 1990, 1992, Nova-López and Huerta-Díaz, 2001) not including the oxidation products of Fe monosulphides (goethite and hematite; Raiswell *et al.*, 1994). Acid volatile sulfide (AVS) is operationally defined as the fraction of sulfides that is extractable by 1 or 6 M cold HCl. The acid-soluble fraction was also empirically designated to extract most of the potentially bioavailable trace metals (Bryan and Langston, 1992; Langston *et al.*, 1999).

In the final step of each individual extraction procedure, the tubes were centrifugated for 15 minutes at 3000 rpm, and the residual sediment was rinsed twice with Milli-Q® water, dried at 50 °C and homogenized in an agate mortar. The residual Hg fraction was measured with the DMA (as described above) and subtracted from the Hg_{TP} to evaluate each extracted Hg fraction.

3 - RESULTS

3.1 - Textural, physical and chemical properties of Laguna del Plata core

Laguna del Plata (LP) sedimentary core is characterised by the alternance of dark and light grey lamination (Fig. 2a). The core description is based on four values of lamination indexes (LI) proposed by Piovano *et al.* (2002). Continuous laminae up to 2 mm thick are designated by "1", diffuse or discontinuous 2-4 mm thick by "2", thin banded 4-10 mm thick by "3" and finally thick banded >10 mm thick by "4". When there is an absence of lamination the sedimentation is called massive. Fig. 2 shows a photograph and X-ray radiograph image of the LP core that summarizes its main sedimentological features. Thus, 5 sedimentary units could be recognised. The first one (A) is a massive sequence that extends from the bottom up to 75 cm with a net contact. From the base of the core to the top this sequence shows different colours on the photograph: light green colour in deepest part, followed by a dark green olive colour that overlies and a very light green colour on the top of it. In the X-Ray image the colour varies from light gray in the bottom to darker gray in the upper part. A small sequence characterised by LI2 (B) from 75 to 69 cm shows lamination due to an alternance of dark to light colours sediments. Overlying this sequence up to 53 cm there is an

alternance of LI4 (C) with a predominance of a light colour. From here up to 16 cm a sequence of LI1 and LI2 laminations (D) are intercalated with a small LI3 lamination located at 27-39 cm. There is an alternance of dark to light gray making more visible the contacts between laminations. The upper part of the core shows a LI4 sequence (E) with a dark olive green colour in the picture (Fig. 2).

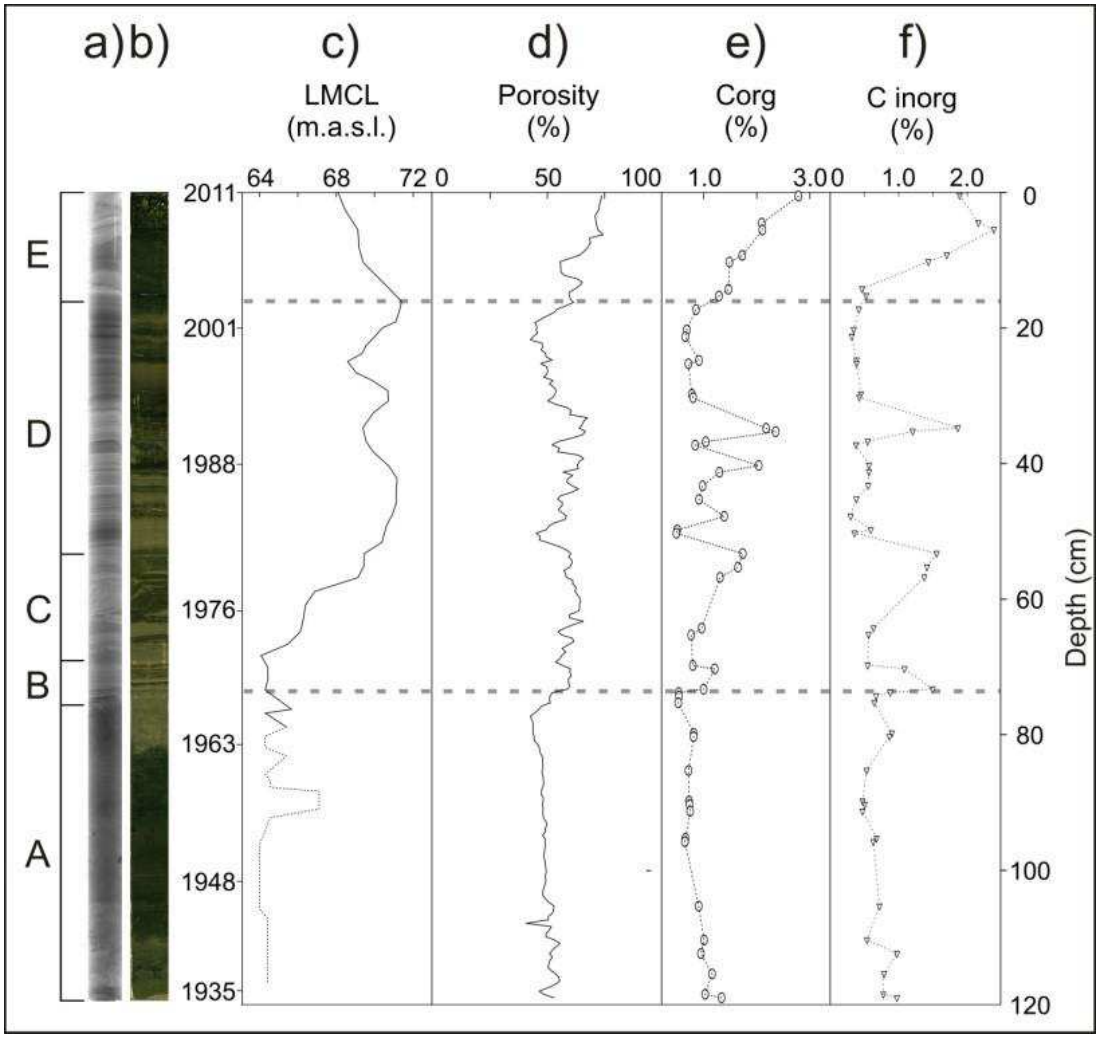

Fig. 2. Sedimentary units A to E where defined on the base of Lamination Indexes (LI). a) sediment core X-ray image, b) sediment core photograph, c) LMCL (Laguna Mar Chiquita Level - The dashed line corresponds to reconstructed data developed in Piovano *et al.*, 2002.), d) porosity record expressed in percentage, e) Organic Carbon (C_{org}) content, f) Inorganic Carbon (C_{inorg}) content.

Some physical and chemical characteristics of the core are shown in the profiles of Fig. 2. The level with the lowest porosity value (40.0 %) occurred near the bottom of the LP core, while the highest (75.5 %) was registered near the top. Thus three zones could be described (light gray dashed lines in Fig. 2): from the bottom to 74 cm the porosity present average values of 48.4 ± 2.9 %, from 74 to 16 cm porosity raised up to 56.2 ± 6.1 % remaining nearly constant and finally the first 16 cm are represented by an abrupt augmentation of water percentage (from 59.9 to 74.5 %). Lamination seems to be related to this change in porosity: section A to the lower porosity, B, C and D to the intermediate porosity and E with the highest one.

Organic carbon (C_{org}) values ranged between ~0.5 and ~2.8 %. This parameter seems to follow the same tendency of porosity. From 120 to 74 cm C_{org} values remained practically constant around ~0.8 % ± 0.2, up to 30 cm values suffered a big fluctuation between 0.5 to 2.4 %, being synchronous with porosity variations. The last centimetres are given by the highest values with its maximum of 2.8 % in the top of the core. Inorganic carbon (C_{inorg}) profile shows a

similar behaviour to C_{org}. Its contents (Fig 2f) vary from 0.3 to 2.4 % along the core. From 120 to 74 cm the average value is 0.7 ± 0.2 %, from 74 to 16 cm it is 0.7 ± 0.5 % and in the last 16 cm the average value is 1.5 ± 0.8 %.

XRF elemental profiles depict mainly three domains (Fig. 3). The lower part of the core from the base up to 74 cm is characterised by a signal that remains almost constant except for Zr, S, Ca and Sr that rises in the last centimetres. The second domain shows a high fluctuation visible in all the measured elements that extends in the central part of the core up to 16 cm. From here up to the top Al, Si, K, Ti, Mn, Fe and Zr show a diminution in the signal while for Sr, S, Cl and Ca the opposite occurs.

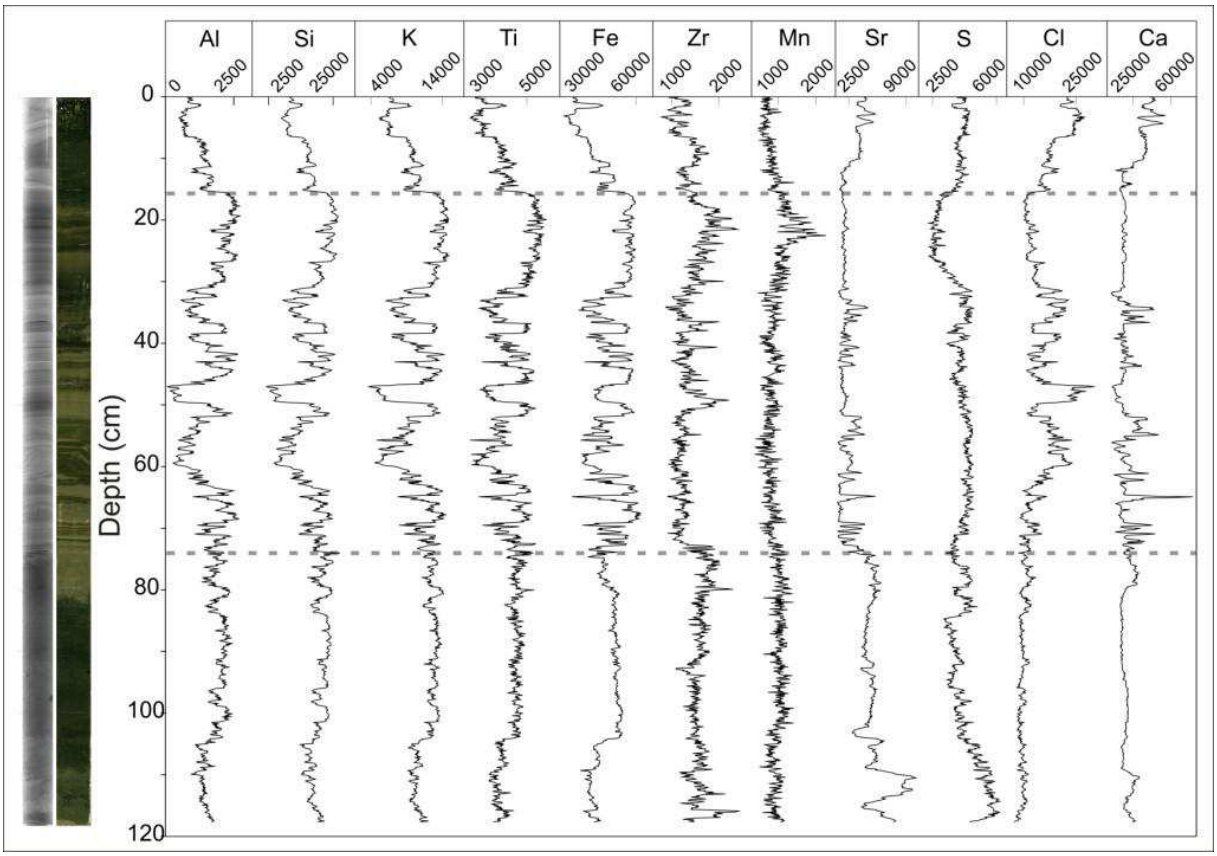

Fig. 3. XRF logs from Laguna del Plata. The values are given in counts per second (cps).

3.2 - Radionuclides

The ^{210}Pb ($T_{1/2}$ = 22.3 years) is a naturally occurring radionuclide delivered continuously to the landscape by atmospheric fallout (Saari *et al.*, 2010) and becomes rapidly and strongly bound to particulate matter. This atmospherically derived ^{210}Pb scavenged by particles (Fig. 4), is referred to ^{210}Pb in excess ($^{210}Pb_{xs}$) of that supported within particles by the decay of its parent isotope, ^{226}Ra. In LP core these excess activities range from 5 to 72 mBq g^{-1}. There is a general trend in decreasing $^{210}Pb_{xs}$ as expected due to the decay of the unsupported ^{210}Pb. This decrease presents some irregularities, as observed at about 24 cm where excess is lower when compared to the surrounding layers. The long-lived and naturally occurring ^{232}Th is usually associated with the detrital fraction (van der Klooster *et al.*, 2011), therefore activity changes can be an indication of different lithological sources or proportions. ^{232}Th activities range between 26 and 42 mBq g^{-1}, the lowest values are usually observed in the upper 20 cm. This section presents also the highest total carbon content that is likely to dilute the detrital fraction. It is also noticeable that low $^{210}Pb_{xs}$ at 24 cm is associated with a high ^{232}Th activity. Such a high ^{232}Th are mostly observed in the deepest part of the core, at > 70 cm depth.

On the opposite, ^{137}Cs ($T_{1/2}$ = 30 years) is an artificial radionuclide: its occurrence in the environment is primarily the result of the nuclear weapon test fall-out in the early sixties, and in Europe of the

Chernobyl accident in 1986 of well-known pulse inputs (UNSCEAR, 2000). At present, atmospheric fluxes are almost negligible (Quintana, 2011). Sedimentary profile of ^{137}Cs in core presents the expected shape with a peak in depth and negligible activities in the uppermost section (<1 mBq g^{-1}). The maximum activities are recorded around 75 – 80 cm, with values up to 26 mBq g^{-1}. Below that peak, ^{137}Cs disappears rapidly to negligible levels below 85 cm.

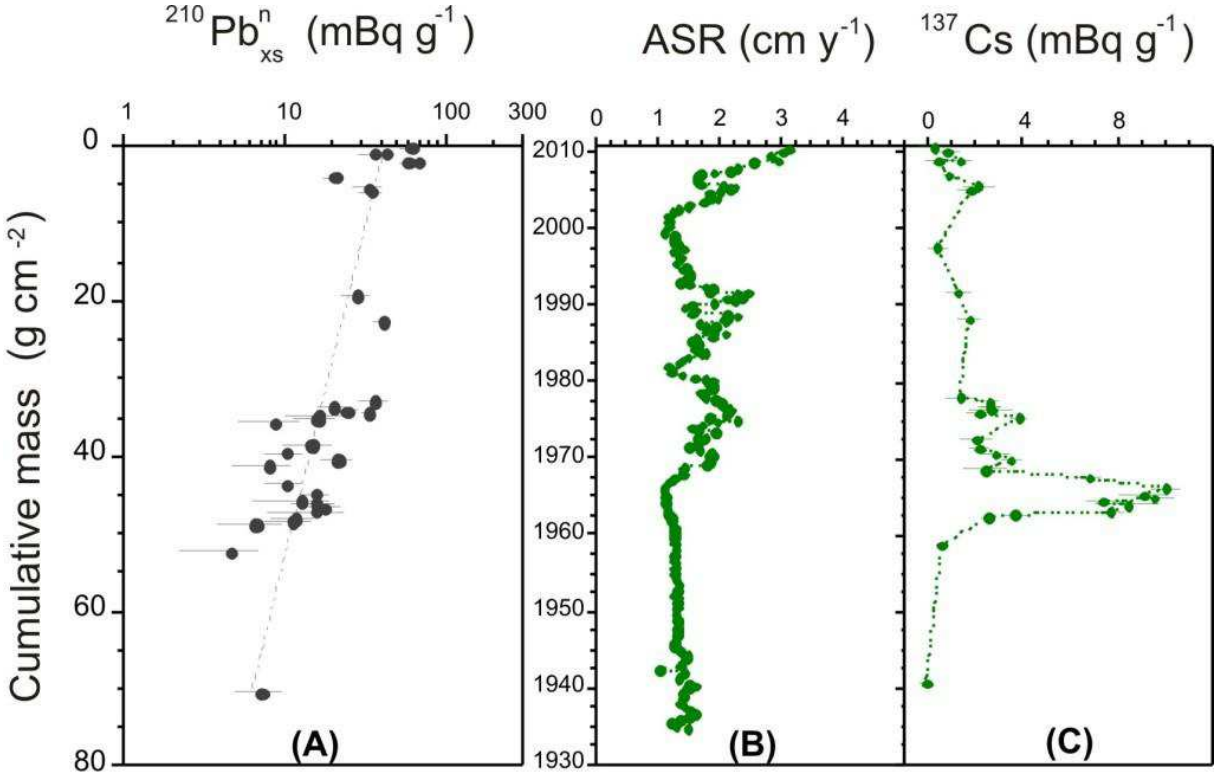

Fig. 4. (A) Normalized ^{210}Pbxs against cumulative mass: the dashed line corresponds to the exponential regression used to determine Mass Accumulation Rate (MAR). (B) Average Sedimentation Rate (ASR) and (C) ^{137}Cs plotted against calendar ages, based on ^{210}Pb dating.

3.3 – Hg concentrations

Total Paticulate Hg (Hg_{TP}) concentrations measured every 0.5 cm interval along the Laguna del Plata core, varied between ~13 and ~131 µg/kg (Fig.5a). In the deepest part of the core (from 120 to 74 cm) the lowest and most constant concentrations occurred (an average of 17.2 ± 1.7 µg kg^{-1}). From this point to the surface Hg_{TP} values are variable. From 74 cm up to 45 cm they show average concentrations of 42.4 ± 14.6 µg kg^{-1}, beyond this level distinct peaks of 89.7, 131.5 and 87.3 µg kg^{-1} are shown at 43.2, 36.7 and 30.2 cm respectively. In most recent sediments (~16-0 cm), the average concentration is 65.6 ± 16.2 µg kg^{-1}.

Hg concentration associated to the reductible fraction was negligible throughout the core, while the Hg in both acid-extracted (1M HCl) and oxidizable fractions accounted for the major part of the Hg_{TP} values measured in the sediments.

The relation between Hg_{HCl} and Hg_{TP} showed two different patterns (Fig. 5b): (i) from the bottom of the core to 74 cm, Hg_{HCl} accounted in average for 42.8 ± 22.3 % of Hg_{TP} and (ii) above 74 cm to the top, Hg_{HCl} represented in average 21.4 ± 13.7 % of $Hg_{TP.}$ Similar to Hg_{HCl}, the relative contribution of Hg_{H2O2} to Hg_{TP} changed with depth (Fig. 5c) showing in average the highest values of 76.4 ± 11.6 % in the lower part of the core up to 40 cm. Above, the relative contribution of Hg_{H2O2} to Hg_{TP} was clearly lower but still represented 47.2 ± 18.5 %.

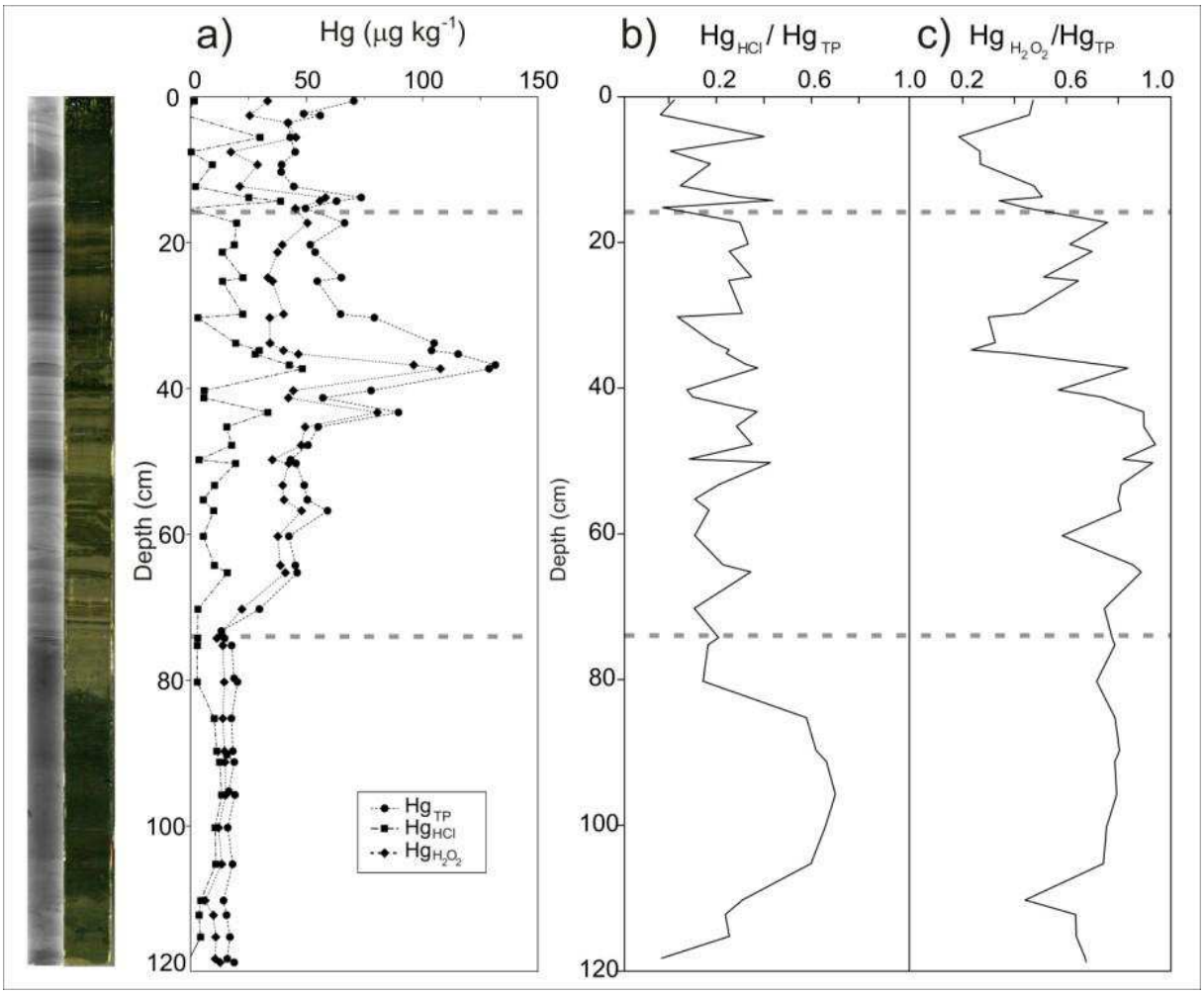

Fig. 5. Mercury concentrations. a) Selective extractions corresponding to the total particulate (Hg_{TP}), oxidiable (Hg_{H2O2}) and acid-soluble/reactive (Hg_{HCl}) fractions.

4 - DISCUSSION

Sediment deposition and chronology

Use of ^{210}Pb has been widely done to calculate short-term (years to decades) sediment accumulation rates in continental and oceanic environment since the last 40 years (Appleby, 2001). Dating is calculated using excess activity of ^{210}Pb ($^{210}Pb_{xs}$) which is incorporated rapidly into the sediment from atmospheric fallout and water column scavenging. Once incorporated into the sediment, unsupported ^{210}Pb decays with time in the sediment column according to its half-live, by the equation (1) :

$$^{210}Pb_{xs(z)} = {}^{210}Pb_{xs(0)}e^{-\lambda t} \quad (1)$$

where $^{210}Pb_{xs(z)}$ and $^{210}Pb_{xs(0)}$ represent the excess ^{210}Pb at the sediment-water interface, or at the base of the mixed layer, and at the depth z, λ is the ^{210}Pb decay constant (0.0311 y^{-1}), and *t* is the age in years. Several models have been developed to calculate an age or accumulation rate (Sanchez-Cabeza and Ruiz-Fernández, 2012, among others): CIC (constant initial concentration); CSR (constant rate of supply); CFCS (constant flux-constant sedimentation). The Constant Initial Concentration (CIC) model in which the sediments have a constant ^{210}Pb concentration regardless the accumulation rates (Appleby, 2001) was left behind due to that Laguna del Plata has suffered alternated connections and disconnections from Laguna Mar Chiquita influencing the amount and nature of the sedimented material (Piovano *et al.*, 2002). Thus the CFCS model was chosen to calculate the sedimentation rates and age for the lake under the two basic assumptions: ^{210}Pb atmospheric deposition and the mass accumulation are constant. The mass accumulation rate (MAR, g cm^{-2} y^{-1}) can be obtained considering the equation (2) :

$$^{210}Pb_{xs(z)} = {}^{210}Pb_{xs(0)}e^{-m_{(z)}\frac{\lambda}{MAR}} \quad (2)$$

where m(z) is the cumulative dry mass per unit area (g cm^{-2}) at depth z. To compensate the effect of

composition changes of sediment, $^{210}Pb_{xs}$ activities were normalized by using ^{232}Th concentrations, measured at the same time through gamma, thus limiting the errors. MAR was calculated from the slope of the exponential regression of $^{210}Pb^{n}_{xs}$ plotted against cumulative mass (Fig. 4A). The average mass accumulation rate is 1.0 g cm^{-2} y^{-1}. The sedimentation rate (in years) has been calculated by dividing the cumulated dry mass per unit area by the mass accumulation rate, allowing to estimate the average sedimentation rates (ASR) (Fig. 4B). The expected deposition year for each sediments layer was calculated considering the sampling year (2011) and the water-sediment interface at the uppermost layer as a reference for establishing the chronology.

Robbins and Eddington (1975) showed that it is necessary to confirm the accuracy of the ^{210}Pb-based model using an independent time-stratigraphic marker, such as fallout ^{137}Cs. The ^{137}Cs profile was plotted as a function of the time scale based on ^{210}Pb (Figure 4C). It is noticeable that the peak of ^{137}Cs in core LP corresponds to the year 1966, which is in close agreement with the annual atmospheric fallout of ^{137}Cs recorded at Buenos Aires around 1960 (Quintana, 2011). In general the sedimentary ^{137}Cs record mimics rather well the atmospheric fallout, validating the chronology derived from ^{210}Pb and coinciding with the abrupt hydrological changes that the lake system have been through during the decade of 1970's.

Sedimentation rates are comprised between 1 and 3 cm y^{-1}, being rather variable with depth. They are less than 2 cm y^{-1} in the deepest part and the highest are located in the uppermost part of the core. What occurs in the lower part of the core is mainly ascribed to sediment compaction and associated with a simultaneous decrease in porosity. During the period covering the early 1970s to the early 1990s, ASR shows strong variability, which may be in relation to environmental changes and the continuous connection of Laguna del Plata to Laguna Mar Chiquita that happened after 1975 during the onset of the last highstand (see Fig. 1b Satellite images). In the lowermost layers of the core, sedimentation rates display rather constant values, around 1.2-1.5 cm y^{-1}, and are likely to indicate constant sedimentation conditions during lowstand lake scenarios with low fluvial input.

Chemical data given by XRF helps to understand the changes that Laguna del Plata sediments composition experienced during the last six decades. In concordance with previous observations performed by Piovano *et al.* (2004b) in cores retrieved from Laguna de Mar Chiquita and Laguna del Plata, the elemental variations described in Fig. 3 seem to be controlled by well-known hydrological fluctuations. For comparison purposes, Mar Chiquita lake level record was considered because there is no a continuous record for Laguna del Plata lake and both are controlled by the same hydrological balance (Troin *et al.*, 2010). The bottom part of the core up to 74 cm corresponds to the sedimentary record before ~1970 where LP was completely isolated from LMC and the inputs were mainly from the Suquía River. The almost constant XRF signals at the lowermost part of the core reflect this single contribution to the sedimentary record (Fig 3). The onset of higher regional precipitations since ~1970, generated the connection of both lakes by 1976 that persist nowadays (Fig. 1b), changing the sedimentation pattern overall the Laguna Mar Chiquita system (Piovano *et al.*, 2002; 2004a). Rising lake level likely triggered the strong variations in Si, K, Ti, Fe, and Zr concentations measured in the core between 74 to 16 cm depth, reflecting a high contribution of detrital input due to soil or fluvial-bank erosion suffered in the catchment. Several authors (Rothwell and Rack, 2006; Böning *et al.*, 2007; Moreno *et al.*, 2007; Löwemark *et al.*, 2011) coincide that variations of terrigenous elements such as Al, Si, K, Fe, and Ti are likely the consequence of inputs of allocthonous materials. In addition, an increase in the lake primary productivity during highstands, marked by changes in the C_{org} % (Fig. 2e), may additionally control the porosity values.

Historical record of Hg and its solid carrier phases in sediments of Laguna del Plata

Hg levels measured in the Laguna del Plata sediments (Fig. 4) were much lower than those typically reported for contaminated freshwater or marine areas (e.g., Streets *et al.*, 2005; Castelle *et al.*, 2007; Larrose *et al.*, 2010, Elbaz-Poulichet *et al.*, 2011). Given the fine-grained nature of the sediment, such Hg_{TP} levels are clearly within the range of those attributed to weakly contaminated systems (e.g., Schäfer *et al.*, 2006).

Like for the other parameters discussed above, the variations of Hg and its main solid carrier phases observed in the Laguna del Plata core are due to both changes in lake hydrology and general atmospheric deposition, rather than pollution point sources in the watershed.

The sediments accumulated in the lake before the 1970s show rather constant and very low Hg_{TP}

concentrations. During this period of high aridity and low lake levels, particles transported by the Suquía River exclusively settled in the Laguna del Plata due to the absence of hydraulic links between the latter and Laguna Mar Chiquita. The high Hg_{HCl} fraction (>40% of Hg_{TP}) combined with the relatively high Hg_{H202} fraction (76.4 ± 11.6 %) shows that most of Hg_{TP} measured in the sediments is associated with secondary sulfides, especially in the 105-85 cm depth range (Fig. 5c). This is consistent with X-Ray Difractometry data that shows the presence of pyrite at the base of the core (data not shown) which indicates that precipitation of autigenic sulfides occurred under dominant anoxic conditions produced by bacterial activity at the water-sediment interface. Elevated salinity (380 g L^{-1}; Piovano *et al.*, 2004a) and alkaline chloride–sulphate sodium type waters (Martínez 1991) represent the geochemical conditions predominating during lake lowstands. Hg associated with the residual fraction not extracted by the single extraction approach, i.e. attributed to the non-reactive crystalline matrix, was very low (close to zero) in the sediments before the 1970s, indicating that nearly all Hg deposited during that period was potentially bioavailable.

In the uppermost part of the core (74-0 cm), i.e. in sediments accumulated from the 1970s, Hg_{TP} concentrations were clearly higher than downcore. This situation coincides with the beginning of an increasingly humid period in the region, and concomitant rise in the lake system levels. Increased erosion and riverborne particle transport in the Suquía River watershed also occurred during this period.

In the 74-40 cm depth range, maximum Hg_{H202} and clearly lower Hg_{HCl} indicate that Hg is mainly associated with sedimentary organic matter, which is consistent with increasing lake primary productivity, (Da Silva *et al.*, 2008) but also with increasing erosion and particle transport in the Suquía river (Piovano *et al.*, 2009). The highly variable Hg_{HCl} relative to Hg_{TP} in the top 74 cm of the core reflects episodes of intense erosion with changing proportions of Hg associated with clay minerals and Mn and Fe oxy-hydroxides transported from the catchments. Hydrochemical conditions in the lake during highstands corresponded to alkaline chloride–sulphate sodium type waters, supersaturated in calcite and occasionally in gypsum (Martínez *et al*., 1994)

Hg profile shows maximum Hg_{TP} at ~38 cm, i.e. in the depth range roughly attributed to records of the years 1990-1995. The residual Hg fraction shows maximum levels (>50% of Hg_{TP}) at ~35 cm depth, suggesting an episode with major transport and deposition of non-reactive Hg-bearing phases during the 1990s just after the episode responsible of the Hg_{TP} maximum. Accordingly, the maximum Hg_{TP} levels together with minimum Hg_{H202}/Hg_{TP} and relatively low Hg_{HCl}/Hg_{TP} indicate dominance of Hg-bearing phases not accessible to the used selective extractions. Among the different Hg sources described in natural systems, volcanic emissions are a major issue (i.e., Fitzgerald and Lamborg, 2003, Selin, 2009). Due to the proximity to the Andean volcanic system and its well known influence on the study area (e.g. Gaiero *et al.*, 2007; Osores *et al.*, 2011) volcanic eruptions could account for this observation. In fact, the eruption record of the past 100 years indicates that the observed peak may reflect Hg inputs from the eruption of the Hudson and Lascar volcanoes occurred in 1991 and 1993 respectively. The Hudson volcano is located in Chile at 45°54'S - 72°58'W. This volcano erupted in two phases in August 1991, producing 4.3 km^3 of pyroclastic material during one of the major eruptions of the 20th century (Wilson *et al.*, 2011). The ashes from the first eruption moved mainly in NNE to NE direction (Kratzmann *et al.*, 2008, 2010) and reaching the Laguna del Plata. Unfortunately it is not possible to define the limits of the plume with certitude due to its low ash content (Constantine *et al.*, 2000). Lascar volcano is located at 23°22'S – 67°44'W and started its activity in 1984 culminating with a major explosive eruption in April 1993. This last eruption generated a column between 5 and 25 km above the volcano and tephra ashes reached Buenos Aires located 1500 km to the southeast (Matthews *et al.*, 1997). With these plumes arriving to the study area, the Hg associated to volcano-clastic particles settled as wet or dry deposition in the Suquía River watershed. This is in agreement with the peak of Hg_{TP} observed in the core (between 37.2 and 30.2 cm) and its preferential association with non-reactive particles in the sediments accumulated in the years following the eruption.

The hydrological model of the Laguna del Plata system proposed by Piovano *et al.* (2004) for the last century, was modified in order to show the inputs of the main Hg-bearing phases identified in the area (Fig. 6). Precipitation (P) and evaporation (E) are represented with arrows, whose relative lengths are proportional to their volume. The higher river runoff, that occurred after the 1970s, is indicated by a solid arrow, whereas dotted arrow indicate comparatively low inputs that prevailed in the dry period. The thickness of the arrows associated with different Hg-

bearing phases recognized in the studied area, is proportional to their respective importance. During the dry conditions that predominated in the study area before the 1970s, inputs of Hg to the lake corresponded mainly to contributions from natural sources such as atmospheric Hg (dry deposition) and Hg-bearing particles (particularly sulphides) that were transported to the lake from the Suquía River upper basin. Under high stand conditions (after 1970s), these two sources increased their contributions due to increasing precipitation (wet deposition) and higher soil erosion in the catchments, but also to increasing global Hg flux. The more humid conditions lead to increased lake primary productivity and hence, a higher affinity of Hg for organic matter particle is found in sediments accumulated during this period.

The sources of Hg in the Laguna del Plata sediments are mostly assigned to natural sources, but also a minor contribution from global Hg inputs should be considered, as well as from some other local anthropogenic sources, that became increasingly important after the 1970s when an incipient industrial development started in the region.

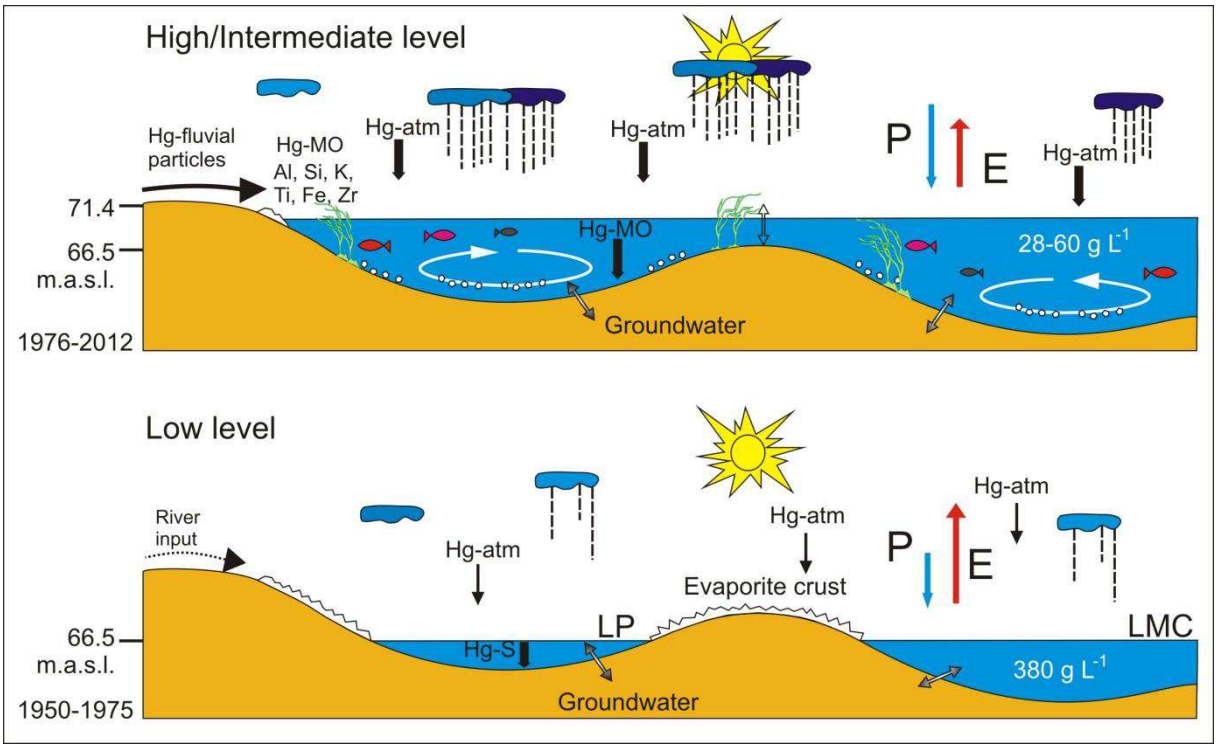

Fig. 6. Schematic section of Laguna del Plata (LP) and Mar Chiquita (LMC) system showing Hg and other elements cycles under different hydrological stages. Modified from Piovano *et al.*, (2004). Length and thickness of the arrows are proportional to the components contribution. Hg-atm: atmospheric Hg; Hg-S: Hg-bearing sulfides, Hg-OM: Hg-bearing organic matter.

CONCLUSIONS

Sedimentary record in Laguna del Plata shows a highly variable sedimentation regime in the last ~76 years, controlled by changes in the regional hydrological balance. These changes also triggered variations in the chemical composition of the sediments. Among the analyzed elements, Hg was used as a potential marker of the natural and atrophic activities.

Before the 1970's, LP was completely isolated from LMC and the inputs of sediments were mainly from the Suquía River. During this period, the occurrence of highly saline waters and anoxic conditions at the water-sediment interface, promoted the precipitation of Hg-bearing sulfides. In the following years, the more humid conditions enhanced primary

productivity in the lake, driving increased organic matter contents in the sediment record. Hg accumulated during this period, was preferentially associated with the organic fraction of the sediments. The upper centimetres of the core show increasing Hg concentrations that are considered to be closely related to the industrial development of the region but also to the increasing influence of global Hg fluxes.

The highest Hg_{TP} values are found at ~35 cm depth (corresponding to the years 1990-1995) where the Hg_{H202}/Hg_{TP} and Hg_{HCl}/Hg_{TP} relations are also relatively low. This suggests a contribution from a Hg-bearing source that is not affected by the applied extraction methods. More than a punctual source of pollution, this peak is likely related to two eruptive events occurred in the Andean Cordillera in this period: the eruption of Hudson volcano in southern Patagonia that occurred in 1991 and the one of the Lascar volcano in northern Chile that occurred in 1993. In both cases, the respective ash plumes were documented to have reached the Laguna del Plata region.

ACKNOWLEDGMENTS

This work is in the frame of a doctoral thesis financed by ERASMUS MUNDUS External Cooperation Window, lot 18 –BAPE – Bolivia, Argentina, Peru and Europe. Field trips were financed with funds from PIP 112-200801-00808 (CONICET-Argentina). The authors want to thank equally to the reviewers and their constructive remarks.

REFERENCES

Aceituno, P., 1988. On the functioning of the Southern Oscillation in the South American sector. Part I: surface climate. Monthly Weather Review. 116, 505–524.

Alborés, A.F., Cid, B.P., Gómez, E.F. and López, E.F., 2000. Comparison between sequential extraction procedures and single extractions for metal partitioning in sewage sludge samples. Analyst. 125, 1353-1357.

Amin, O., Ferrer, L. and Marcovecchio, J., 1996. Heavy metal concentrations in litteral sediments from the Beagle Channel, Tierra del Fuego, Argentina. Environmental Monitoring and Assessment 41 (3), 219-231.

Appleby, P.G., 2001. Chronostratigraphic techniques in recent sediments. W. M. Last & J. P. Smol (eds.).Tracking Environmental Change Using Lake Sediments. Volume 1: Basin Analysis, Coring, and Chronological Techniques. Kluwer Academic Publishers, Dordrecht, The Netherlands.

Arribére, M.A., Ribeiro Guevara, S., Sánchez, R.S., Gil, M.I., Román Ross, G., Daurade, L.E., Fajon, V., Horvat, M., Alcalde, R. and Kestelman, A.J., 2003. Heavy metals in the vicinity of a chlor-alkali factory in the upper Negro River ecosystem, Northern Patagonia, Argentina. Science of the Total Environment. 301 (1-3), 187-203.

Audry, S., Blanc, G. and Schäfer, J., 2005. The impact of sulphide oxidation on dissolved metal (Cd, Zn, Cu, Cr, Co, Ni, U) inputs into the Lot-Garonne fluvial system (France). Applied Geochemistry 20 (5), 919-931.

Audry, S., Blanc, G., Schäfer, J., 2006. Solid state partitioning of trace metals in suspended particulate matter from a river system affected by smelting waste drainage. Science of the Total Environment. 363, 216–236.

Balcom, P., Fitzgerald, W., Hammerschmidt, C., Lamborg, C, and Graham, L., 2004. Mercury sources and speciation in the waters of New York/New Jersey Harbor Estuary. Mater. Geoenviron. 51, 795–798. Environmental Technology 13 (12), 1175-1179.

Bermond, A.P., 1992. Thermodynamics applied to the study of the limits of sequential extraction procedures used for the speciation of trace elements in sediments and soils. Environmental Technology. 13 (12), 1175-1179.

Biester, H., Bindler, R., Martinez-Cortizas, A. and Engstrom, D.R., 2007. Modeling the past atmospheric deposition of mercury using natural archives. Environmental Science and Technology. 41, 4851–4860.

Böning, P., Bard, E. and Rose, J., 2007. Toward direct, micron-scale XRF elemental maps and quantitative profiles of wet marine sediments. Geochemistry, Geophysics, Geosystems. 8 (5), doi:10.1029/2006GC001480.

Botté, S.E., Freije, R.H. and Marcovecchio, J.E., 2010. Distribution of Several Heavy Metals in Tidal Flats

Sediments within Bahía Blanca Estuary (Argentina). Water Air Soil Pollution. 210, 371–388. DOI 10.1007/s11270-009-0260-0.

Boulanger, J-P., Leloup, J., Penalba, O., Rusticucci, M., Lafon, F. and Vargas, W., 2005. Observed precipitation in the Paraná-Plata hydrological basin: long-term trends, extreme conditions and ENSO teleconnections. Climate Dynamics. 24, 393-413.

Brunetto, E. and Iriondo, M.H., 2007. Neotectónica en la Pampa Norte (Argentina). Revista de la Sociedad Geológica de España, 20 (1-2), 17-29.

Bryan, G.W. and Langston, W.J., 1992. Bioavailability, accumulation and effects of heavy metals in sediments with special reference to United Kingdom estuaries: a review. Environmental Pollution. 76 (2), 89– 131.

Bucher, E.H., Gavier Pizarro, G. and Curto, E.D., 2006. Cap. 1. Síntesis geográfica. En: Bañados del Río Dulce y Mar Chiquita (Córdoba, Argentina) (ed. Bucher E.H), pp. 15-27. Academia Nacional de Ciencias (Córdoba, Argentina).

Constantine, E.K., Bluth, G.J.S. and Rose, W.I., 2000. TOMS and AVHRR Observations of Drifting Volcanic Clouds From the August 1991 Eruptions of Cerro Hudson. Mouginis-Mark, P., Crisp, J.A., Fink, J.H. (Eds.), Remote Sensing of Active Volcanism. Geophysical Monograph, Washington, DC, pp. 45–64.

Costa, C., 1999. Tectónica cuaternaria en las Sierras Pampeanas. Geología Argentina. Anales 29. Subsecretaría de Minería de la Nación. Servicio Geológico Minero Argentino. Instituto de Geología y Recursos Minerales. Buenos Aires.

Da Silva, L.S.V., Piovano, E.L., Azevedo, D.d.A., Aquino Neto, F.R.d., 2008. Quantitative evaluation of sedimentary organic matter from Laguna Mar Chiquita, Argentina. Organic Geochemistry. 39 (4), 450-464.

De Marco, S.G., Botté, S.E. and Marcovecchio, J.E., 2006. Mercury distribution in abiotic and biological compartments within several estuarine systems from Argentina: 1980–2005 period. Chemosphere. 65, 213–223.

Depetris, P.J., Kempe, S., Latif, M. and Mook, W.G., 1996. ENSO controlled flooding in the Paraná River (1904-1991). Naturwissenschaften. 83, 127–129.

Diaz, E., 2000. Mercury pollution at gold mining sites in the Amazon environment. Principles of Environmental Toxicology. University of Idaho. pp. 24.

Downs, S. G., Macleod, C. L., and Lester, J. N., 1998. Mercury in precipitation and its relation to bioaccumulation in fish: a literature review. Water Air and Soil Pollution. 108, 149–187.

Etcheber, H., Relexans, J-C., Beliard, M., Weber, O., Buscail, R. and Heussner, S., 1999. Distribution and quality of sedimentary organic matter on the Aquitanian margin (Bay of Biscay). Deep-Sea Research II. 46, 2249-2288.

Elbaz-Poulichet, F., Dezileau, L., Freydier, R., Cossa, D. and Sabatier, P., 2011. A 3500-year record of Hg and Pb contamination in a mediterranean sedimentary archive (The Pierre Blanche Lagoon, France). Environmental Science and Technology. 45 (20), 8642-8647.

Farrah, H. and Pickering W.F., 1993. Factors influencing the potential mobility and bioavailability of metals in dried lake sediments. Chemical Speciation and Bioavailability. 5 (3), 81-96.

Fitzgerald, W.F. and Mason, R.P., 1997. Biogeochemical cycling of mercury in the marine environment. In: Sigel, H., Sigel, A. (Eds.), Metal Ions in Biological Systems, Mercury and its Effects on Environment and Biological Systems, vol. 34. Marcel Dekker Inc., New York, pp. 3–110.

Fitzgerald, W.F. and Lamborg C.H., 2003. Geochemistry of Mercury in the Environment. In: In: Holland, H.D. and Turekian, K.K. (Eds), Treatise on Geochemistry, ed. BS Lollar, pp. 107-148. New York: Elsevier.

Frank, H., 1915. Contribución al conocimiento de las Salinas Grandes y la Mar Chiquita de la Provincia de Córdoba. Revista del Centro de Estudiantes de Ingienería, 3:91-107.

Gagnon, C., Pelletier, É. and Mucchi, A., 1997. Behaviour of anthropogenic mercury in coastal marine sediment. Marine Chemistry. 59, 159-176.

Gaiero D.M., Roman Ross, G., Depetris, P.J. and Kempe, S. 1997. Spatial and temporal variability of total non-residual heavy metals content in stream sediments from the Suquía river system, Córdooba, Argentina. Water, Air and Soil pollution. 93, 303-319.

Gaiero D.M., Brunet, F., Probst, J-L. and Depetris, P.J., 2007. A uniform isotopic and chemical signature of dust

exported from Patagonia: Rock sources and occurrence in southern environments. Chemical Geology. 238 (1-2), 107-120.

Garreaud, R.D., Vuille, M., Compagnucci, R. and Marengo, J., 2009. Present-day Souh American Climate (LOTRED South America). Palaeogeography, Palaeoclimatology, Palaeoecology. 281, 180–195.

Gilli A., Anselmetti F.S. and Ariztegui D., 2005. Seismic stratigraphy, buried beach ridges and contourite drifts: The Late Quaternary history of the closed Lago Cardiel basin, Argentina (49°S). Sedimentology. 51, 1–23.

Hermanns, Y.M. and Biester, H., 2013. Anthropogenic mercury signals in lake sediments from southernmost Patagonia, Chile. Science of the Total Environment. 445-446, 126-135.

Hudson-Edwards, K.A., Macklin, M.G., Miller, J.R. and Lechler, P.J., 2001. Sources, distribution and storage of heavy metals in the Río Pilcomayo, Bolivia. Journal of Geochemical Exploration. 72 (3), 229-250.

Huerta-Diaz, M.A. and Morse, J.W., 1990. A quantitative method for determination of trace metal concentrations in sedimentary pyrite. Marine Chemistry. 29, 119–44.

Huerta-Diaz, M.A. and, Morse, J.W., 1992. Pyritization of trace metals in anoxic marine sediments. Geochimica et Cosmochimica Acta. 56 (7), 2681–702.

Iriondo, M.H.,1989. Major fractures of the Chaco-Pampa plain. In: Mörner, N. (Ed.), Bullettin of the INQUA, Neotectonics Comission, NA, pp. 12–42.

Iriondo, M.H., 1997. Models of deposition of loess and loessoids in the Upper Quaternary of South America. Journal of South American Earth Sciences. 10, 71–79.

Johannessen S.C., Macdonald, R.W. and Eek, K.M., 2005. Historical trends in mercury sedimentation and mixing in the strait of Georgia, Canada. Environmental Science and Technology. 39, 4361-4368.

King, P., Kennedy, H., Newton, P.P., Jickells, T.D., Brand, T., Calvert, S., Cauwet, G., Etcheber, H., Head, B., Khripounoff, A., Manighetti, B. and Miquel, J.C., 1998. Analysis of total and organic carbon and total nitrogen in settling oceanic particles and a marine sediment: an interlaboratory comparison. Marine Chemistry. 60, 203–216.

Kostka, J.E. and Luther III, G.W., 1994. Partitioning and speciation of solid phase iron in saltmarsh sediments. Geochimica et Cosmochimica Acta. 58 (7), 1701–1710.

Kratzmann, D.J., Carey, S. and Naranjo J., 2008. Compositional variations and magma mixing in the 1991 eruptions of Hudson Volcano, Chile. Bulletin of Volcanology. 71 (4), 419-439.

Kratzmann, D.J., Carey, S.N., Fero, J., Scasso, R.A. and Naranjo, J.A., 2010. Simulations of tephra dispersal from the 1991 explosive eruptions of Hudson volcano, Chile. Journal of Volcanology and Geothermal Research. 190, 337–352.

Kröhling, D. and Iriondo, M., 1999. Upper Quaternary Palaeoclimates of the Mar Chiquita area, North Pampa, Argentina. Quaternary International. 57/58, 149-163.

Lacerda, L.D., De Souza, M. and Ribeiro, M.G., 2004. The effects of land use change on mercury distribution in soils of Alta Floresta, Southern Amazon. Environmental Pollution. 129, 247-255.

Lamborg, C.H., Fitzgerald, W.F., Damman, A.W.H., Benoit, J.M., Balcom, P.H. and Engstrom, D.R., 2002. Modern and historic atmospheric mercury fluxes in both hemispheres: Global and regional mercury cycling implications. Global Chemical Cycles. 16 (4), 1104.

Langston, W.J., Burt, G.R. and, Pope, N.D., 1999. Bioavailability of metals in sediments of the Dogger Bank (central North Sea): a mesocosm study. Estuarine, Coastal and Shelf Science. 48 (5), 519– 40.

Larrose, A., Coynel, A., Schäfer, J., Blanc, G., Massé, L. and Maneux, E., 2010. Assessing the current state of the Gironde Estuary by mapping priority contaminant distribution and risk potential in surface sediment. Applied Geochemistry. 25, 1912–1923.

Liang, L., Sun, Y., Yao, Z., Liu, Z. and Wu, F., 2012. Evaluation of high-resolution elemental analyses of Chinese loess deposits measured by X-ray fluorescence core scanner. Catena. 92, 75–82.

Lofi, J. and Weber, O., 2001. SCOPIX - digital processing of X-ray images for the enhancement of sedimentary structures in undisturbed core slabs. Geo Marine Letters. 20, 182-186.

Löwemark, L., Chen, H.F., Yang, T.N., Kylander, M., Yu, E.F., Hsu, Y.W., Lee, T.Q., Song, S.R. and Jarvis, S., 2011. Normalizing XRF-scanner data: A cautionary note on the interpretation of high-resolution records from organic-rich lakes. Journal Of Asian Earth Sciences. 40, 1250–1256.

Ma, Y. and Uren, N.C., 1995. Application of a new fractionation scheme for heavy metals in soils. Communications in Soil Science and Plant Analysis. 26 (19-20), 3291-3303.

Marcovecchio, J.E., Andrade, S., Ferrer, L.D., Asteasuain, R.O., De Marco, S.G., Gavio, M.A., Scarlato, N., Freije, R.H. and Pucci, A.E., 2001. Mercury distribution in estuarine environments from Argentina: The detoxification and recovery of salt marshes after 15 years. Wetlands Ecology and Management. 9 (4), 317-322.

Markgraf, V., 1998. Past climate of South America. In: Hobbs JE, Lindesay JA, Bridgman HA (eds) Climate of the southern continents: Present, past and future. John Wiley & Sons Ltd, Hoboken, NJ.

Martínez, D.E., 1991. Caracterización geoquímica de las aguas de la Laguna Mar Chiquita, Provincia de Córdoba. Universidad Nacional de Córdoba –Facultad de Ciencias Exactas Físicas y Naturales – Doctoral Thesis, 284 pp.

Martínez, D.E., Gómez Peral, M.A. and Maggi, J., 1994. Caracterización geoquímica y sedimentológica de los fangos de la laguna Mar Chiquita, Provincia de Córdoba: aplicación del análisis multivariante. Revista de la Asociación Geológica Argentina. 49 (1-2), 25-38.

Matthews, S.J., Gardeweg, M.C. and Sparks, R.S.J., 1997. The 1984 to 1996 cyclic activity of Lascar Volcano, northern Chile: cycles of dome growth, dome subsidence, degassing and explosive eruptions. Bulletin of Volcanology. 59 (1), 72–82.

Migeon, S., Weber, O., Faugeres, J-C. and Saint-Paul, J., 1999. SCOPIX: A new imaging system for core analysis. Geo-Marine Letters. 18, 251-255.

Mon, R. and Gutiérrez, A., 2009. The Mar Chiquita Lake: An indicator of intraplate deformation in the central plain of Argentina. Geomorphology. 111, 111–122.

Monferrán, M.V., Galanti, L.N., Bonansea, R.I., Amé, M.V. and Wunderlin, D.A., 2011. Integrated survey of water pollution in the Suquía River basin (Córdoba, Argentina). Journal of Environmental Monitoring. 13, 398–409.

Moreno, A., Giralt, S., Valero-Garcés, B., Sáez, A., Bao, R., Prego, R., Pueyo, J.J., González-Sampériz, P. and Taberner, C., 2007. A 14 kyr record of the tropical Andes: The Lago Chungara sequence, 18 S, northern Chilean Altiplano. Quaternary International. 161,4–21.

Nova-López, C. and Huerta-Díaz, M.A., 2001. Degree of trace metal pyritization in sediments from the Pacific coast of Baja California, Mexico. Ciencias Marinas, 27 (2), 289-309.

Nriagu J.O., 1989. A global assessment of natural sources of atmospheric trace metals. Nature. 338, 47–49.

Olivero, J., Johnson, B. and Arguello, E., 2002. Human exposure to mercury in San Jorge river basin, Colombia (South America). The Science of the Total Environment. 289, 41-47.

Osores M.S., Pujol, G., Collini, E. and Folch, A., 2011. Análisis de la dispersión y depósito de ceniza volcánica mediante el modelo fall3d para la erupción del volcán Hudson en 1991. Trabajo para el Servicio de Hidrografía Naval y el Servicio Meteorológico Nacional.

Pasquini, A.I., Lecomte, K.L., Piovano, E.L. and Depetris, P.J., 2006. Recent rainfall and runoff variability in central Argentina. Quaternary Internacional. 158, 127-139.

Pasquini A.I., Formica, S.M. and Sacchi, G.A., 2011. Hydrochemistry and nutrients dynamic in the Suquía River urban catchment's, Córdoba, Argentina. Environmental Earth Science. DOI 10.1007/s12665-011-0978-z.

Pesce, S.F. and Wunderlin D.A., 2000. Use of water quality indices to verify the impact of Córdoba City, Argentina, on Suquía River. Water Research. 34 (11), 2915-2926.

Piovano, E.L., Ariztegui, D. and Damatto, Moreira, S., 2002. Recent environmental changes in Laguna Mar Chiquita (central Argentina): a sedimentary model for a highly variable saline lake. Sedimentology. 49, 1371–1384.

Piovano, E.L., Ariztegui, D., Bernasconi, S.M. and McKenzie, J.A., 2004a. Stable isotopic record of hydrological changes in subtropical Laguna Mar Chiquita (Argentina) over the last 230 years. The Holocene. 14 (4), 525–535.

Piovano, E.L., Larizzatti, F.E., Fávaro, D.I., Oliveira, S.M.B., Damatto, S.R., Mazzilli, B.P. and Ariztegui, D., 2004b. Geochemical response of a closed-lake basin to 20th century recurring droughts/wet intervals in the subtropical Pampean Plains of South America. Journal of Limnology. 63(1), 21-32.

Piovano, E.L., Ariztegui, D., Córdoba, F., Cioccale and M, Sylvestre, F., 2009. Hydrological Variability in South America Below the Tropic of Capricorn (Pampas and Patagonia, Argentina) During the Last 13.0 Ka, in Vimeux, F., Sylvestre, F., Khodri, M. (eds.), Past Climate Variability in South America and Surrounding Regions, From the Last Glacial Maximum to the Holocene, Volume 14: Springer, 323-351.

Quevauviller, P., 1998. Method performance studies for speciation analysis. Cambridge, UK7 Royal Society of Chemistry.

Quintana, E., 2011. Environmental impact of the nuclear tests in Argentina. Comprehensive nuclear-test-ban treaty, science and technology, 8-10 June, 2011. Vienna, Austria.

Raiswel, R., Canfield, D.E., and Berner, R.A., 1994. A comparison of iron extraction methods for the determination of degree of pyritization and the recognition of iron-limited pyrite formation. Chemical Geology. 111(1-4), 101–10.

Reati, G.J., Florín, M., Fernández, G.J. and Montes, C., 1997. The Laguna Mar Chiquita (Córdoba, Argentina): a little known, seculary fluctuating, saline lake. International Journal of Salt Lake Research. 5, 187-219.

Ribeiro Guevara, S., Massaferro, J., Villarosa, G., Arribére, M. and Rizzo, A., 2002. Heavy metal contamination in sediments of lake Nahuel Huapi, Nahuel Huapi National Park, Northern Patagonia, Argentina. Water, Air, and Soil Pollution 137 (1-4), 21-44.

Ribeiro Guevara, S., Rizzo, A., Sánchez, R. and Arribére, M., 2005. Heavy metal inputs in Northern Patagonia lakes from short sediment core analysis. Journal of Radioanalytical and Nuclear Chemistry. 265 (3), 481–493.

Ribeiro Guevara, S., Catán, S.P. and Marvin-Di Pasquale, M., 2009. Benthic methylmercury production in lacustrine ecosystems of Nahuel Huapi National Park, Patagonia, Argentina. Chemosphere 77. (4), 471-477.

Ribeiro Guevara, S., Meili, M., Rizzo, A., Daga, R. and Arribére, M., 2010. Sediment records of highly variable mercury inputs to mountain lakes in Patagonia during the past millennium. Atmospheric Chemistry and Physics. 10, 3443–3453.

Robbins, J.A., Edgington, D.N., 1975. Determination of recent sedimentation rates in Lake Michigan. Geochimica et Cosmichimica Acta. 39, 285-304.

Rodrigues Bastos, W., Oliveira Gomes, J.P., Cavalcante Oliveira, R., Almeida, R., Nascimento, E.L., Bernardi, J.V.E., Drude de Lacerda, L., da Silveira, E.G. and Pfeiffer, W.C., 2006. Mercury in the environment and riverside population in the Madeira River Basin, Amazon, Brazil. Science of the Total Environment. 368, 344– 351.

Ronco, A., Camilión, C. and Manassero, M., 2001. Geochemistry of heavy metals in bottom sediments from streams of the western coast of the Rio de la Plata Estuary, Argentina. Environmental Geochemistry and Health. 23 (2), 89-103.

Rosenberg, E. and Ariese, F., 2001. Quality control in speciation analysis. In: Ebdon L, Pitts L, Cornelis R, Crews H, Donard OFX, Quevauviller Ph, editors. Trace Element Speciation for Environment, Food and Health. Cambridge, UK, Chap 7, The Royal Society of Chemistry; 2001. p. 17– 50.

Rothwell, R.G. and Rack, F.R., 2006. New techniques in sediment core analysis: an introduction. In: Rothwell, R.G. (Ed.), New techniques in sediment core analysis. Special Publications. Geological Society, London, pp. 1–29.

Saari, H-K., Schmidt, S., Castaing, P., Blanc, G., Sautour, B., Masson, O. and Kirk Cochran, J., 2010. The particulate 7Be/210Pbxs and 234Th/210Pbxs activity ratios as tracers for tidal-to-seasonal particle dynamics in the Gironde estuary (France): Implications for the budget of particle-associated contaminants. Science of the Total Environment. 408, 4784–4794.

Sahuquillo, A., Rauret, G., Bianchi, M., Rehnert, A. and Muntau, H., 2003. Mercury determination in solid phases from application of the modified BCR-sequential extraction procedure: a valuable tool for assessing its mobility in sediments. Analytical and Bioanalytical Chemistry. 375 (4), 578–583.

Sanchez-Cabeza, J.A. and Ruiz-Fernández, A.C., 2012. ^{210}Pb sediment radiochronology: An integrated formulation and classification of dating models. Geochimica et Cosmochimica Acta. 82, 183–200.

Schäfer, J., Blanc, G., Audry, S., Cossa, D. and Bossy, C., 2006. Mercury in the Lot-Garonne River system

(France): sources, fluxes and anthropogenic component. Applied Geochemistry. 21, 515–527.

Schmidt, S., Howa, H., Mouret, A., Lombard, F., Anschutz, P. and Labeyrie, L., 2009. Particle fluxes and recent sediment accumulation on the Aquitanian margin of Bay of Biscay. Continental Shelf Research. 29, 1044-1052.

Selin, N., 2009. Global Biogeochemical Cycling of Mercury: A Review. Annual Review of Environment and Resources. 34, 43–63.

Silvestri, G., 2004. El Niño signal variability in the precipitation over southeastern South America during the austral summer. Geophysical Research Letters. 31, L18206.

Streets, D.G., Hao, J., Wu, Y., Jiang, J., Chan, M., Tian, H. and Feng, X., 2005. Anthropogenic mercury emissions in China. Atmospheric Environment. 39, 7789–7806.

Tack, F.M.G., Vossius, H.A.H., and Verloo, M.G., 1996. A Comparison between Sediment Fractions, Obtained from Sequential Extraction and Estimated from Single Extractions. International Journal of Environmental Analytical Chemistry. 63 (1), 61-66.

Tessier, A., Campbell, P.G.C. and Bisson, M., 1979. Sequential extraction procedure for the speciation of particulate trace metals. Analytical Chemistry. 51 (7), 844–51.

Tjallingii, R., Röhl, U., Kölling, M. and Bickert, T., 2007. Influence of the water content on X-ray fluorescence core-scanning measurements in soft marine sediments. Geochemistry, Geophysics, Geosystems. 8 (2). Doi:10.1029/2006GC001393.

Troin, M., Vallet-Coulomb, C., Sylvestre, F. and Piovano, E., 2010. Hydrological modelling of a closed lake (Laguna Mar Chiquita, Argentina) in the context of 20th century climatic changes. Journal of Hydrology. 393, 233–244.

UNSCEAR, 2000. Sources and effects of ionizing radiation. UNSCEAR 2000 report to the General Assembly, with scientific annexes. Sources. New York, United Nations; 2000:1. 654 pp.

Van der Klooster, E., van Egmond, F.M. and Sonneveld, M.P.W., 2011. Maping soil clay contents in Dutch marine districts using gamma-ray spectrometry. European Journal of Soil Science. 62, 743-753.

Weltje, G.J. and Tjallingii, R., 2008. Calibration of XRF core scanners for quantitative geochemical logging of sediment cores: Theory and application. Earth and Planetary Science Letters. 274, 423–438.

Wunderlin D.A., Díaz, M.P., Amé, M.V., Pesce, S.F., Hued, A.C. and Bistoni, M.A.,. 2001. Pattern recognition techniques for the evaluation of spatial and temporal variations in water quality. A case study: Suquía River Basin (Córboba-Argentina). Water Resources. 12, 2881-2894.

Zárate, M., 2003. Loess of Southern America. Quaternary Science Reviews. 22 1987–2006.

Annexe B : 2nd article – Identificación de fases portadoras y flujos de mercurio en el registro sedimentario de la Laguna del Plata, región central de Argentina

Identificación de fases portadoras y flujos de mercurio en el registro sedimentario de la Laguna del Plata, región central de la Argentina

Revista Mexicana de Ciencias Geológicas

Y.V. Stupar [1], M.G. García[2], J. Schäfer[3, 4], S. Schmidt[3, 4], E. Piovano[2], G. Blanc[3, 4], F. Huneau[5, 6], Ph. Le Coustumer[1]

[1]Université de Bordeaux, EA 4592 Géoressources & Environnement, ENSEGID, 1 allée F. Daguin, F-33607 Pessac, France. yohanastupar@yahoo.com.ar.
[2]Centro de Investigaciones en Ciencias de la Tierra (CICTERRA), CONICET y FCEFyN Universidad Nacional de Córdoba, Av. Vélez Sarsfield 1611, X5016CGA, Córdoba, Argentina. ggarcia@efn.uncor.edu
[3]Université de Bordeaux, EPOC, UMR5805, F-33400 Talence, France
[4]CNRS, EPOC, UMR5805, F-33400 Talence, France
[5]Université de Corse Pascal Paoli, Laboratoire d'Hydrogéologie, Campus Grimaldi, BP 52, F-20250 Corte, France
[6]CNRS, UMR 6134 SPE, BP 52, F-20250 Corte, France

RESUMEN

En este trabajo se analiza la variación en las concentraciones de Hg, las fases portadoras del mismo y los flujos de este elemento producidos en la laguna del Plata, en la región central de Argentina, en los últimos ~80 años. Para ello se realizaron análisis químicos, mineralógicos, sedimentológicos y dataciones radiométricas en un núcleo de sedimento de 120 cm de profundidad extraído de la laguna del Plata y de sedimentos de lecho tomados a lo largo de toda la cuenca del río Suquía que desemboca en la mencionada laguna. La determinación de mercurio total particulado (Hg_T) se realizó mediante espectrometría de absorción con vapor frío (vapor de O_2) previa incineración y amalgamación, utilizando un analizador directo de mercurio. Los resultados obtenidos sugieren que las variaciones en los niveles de Hg responden principalmente a cambios hidrológicos registrados en el sistema en los últimos ~80 años. En el período seco que afectó la región antes de 1968, la principal fuente de Hg fueron los sedimentos transportados desde las cabeceras de la cuenca del río Suquía; esto generó concentraciones de Hg más o menos constantes en la base del núcleo de sedimento, que son además similares a las medidas en los sedimentos del resto de la cuenca. En estos sedimentos, el Hg se encuentra principalmente adsorbido a la pirita y en menor medida asociado con la materia orgánica particulada. El aumento en las precipitaciones de la región a partir de 1968 y hasta 2003 coincide con un aumento en las concentraciones de Hg_T, probablemente asociado con un mayor arrastre de sedimentos desde las cabeceras de la cuenca y un mayor aporte de Hg atmosférico desde las precipitaciones. En ese período la mayor parte del Hg determinado pareciera ser de tipo geogénico y habría llegado a la laguna adsorbido sobre pirita y óxidos de Fe y Mn presentes en los sedimentos de lecho. Una vez en la laguna se habría producido una posterior removilización y transporte a partir de diversos procesos biogeoquímicos, que determinaron su preferente asociación con la materia orgánica en los sedimentos acumulados en ese período. El pico de concentración de Hg registrado en sedimentos acumulados entre 1990 y 1995 se atribuye al aporte desde las cenizas volcánicas que alcanzaron la región luego de la erupción del volcán Láscar en 1993. Finalmente, en los sedimentos más modernos (acumulados desde 2003) el incremento continuo de las concentraciones de Hg se atribuye a las mencionadas fuentes geogénicas y al aumento de los flujos globales de Hg atmosférico.

Palabras claves: Hg geogénico – cenizas volcánicas – cambio climático – extracciones selectivas.

Identification of Hg-bearing phases and fluxes in the sedimentary record of laguna del Plata, central Argentina

Abstract:

In this work the variations in the concentrations of Hg, its carrying phases and fluxes in the last ~80 years are analyzed for the sedimentary record of the Laguna del Plata. Chemical, mineralogical and sedimentological analysis were performed as well as the radiometric dating of a 120 cm sediment core extracted from Laguna del Plata and sediments collected from the riverbed along the Suquía River basin that discharges into the mentioned lake. Total mercury (HgT) was determined through cold vapour (O2 flux) Atomic Absorption Spectrometry previous incineration and amalgamation, using a direct mercury analyzer. The results suggest that variations in Hg levels respond mainly to hydrological changes registered in the system in the last ~80 years. During the dry period that affected the region before 1968, the main Hg sources were the sediments transported from the upper Suquía River watershed. Constant Hg concentrations measured in the base of the sedimentary core, are similar to those measured in the sediments of the basin, which support the hypothesis of a contribution from terrigenous Hg. The main Hg-bearing phase determined in these sediments is pyrite and in lesser extent, particulate organic matter. The rise in the regional precipitation from 1972 to 2003 coincide with an augmentation in Hg_T concentrations, probably associated to a higher wash down from the upper part of the basin and a higher atmospheric Hg input from precipitation. In that period, Hg probable reached the lake adsorbed into pyrite and Fe and Mn-(hydr)oxides present in the riverbed sediments. Once in the lake a subsequent remobilization and transport from various biogeochemical processes would have occurred, which explains its association with organic matter in sediments accumulated in that period. The peak of Hg concentrations registered in the sediments accumulated between 1990 and 1995 is attributed to the contribution from volcanic ash that reached the region after the eruption of the Lascar volcano in 1993. Finally, in the most recent sediments (accumulated from 2003) the steady increase in Hg concentrations is attributed to the mentioned geogenic sources, but also to the increase of global atmospheric Hg fluxes.

Key words: geogenic Hg - volcanic ash – climate change – Selective extractions.

INTRODUCCIÓN

Desde su incorporación a la superficie terrestre a partir de erupciones volcánicas, el Hg geogénico es removilizado a través del transporte atmosférico y el intercambio en la interfase aire-agua (Fitzgerald y Lamborg, 2003). Dado que la formación de especies solubles en agua es limitada, el Hg suele quedar atrapado en los sedimentos. El mercurio particulado puede explicar más del 90 % del mercurio total en sistemas de agua dulce, estuarios o zonas costeras (Fitzgerald y Mason, 1997; Balcom *et al.,* 2004; Schäfer *et al.,* 2006) donde aparece asociado a las partículas en suspensión. Es por ello que los sedimentos en esos sistemas acuáticos constituyen trampas efectivas de mercurio, convirtiéndose a lo largo del tiempo en registros óptimos de antiguas acumulaciones (Gagnon *et al.,* 1997; Castelle *et al.,* 2007). Asimismo se ha determinado que en la mayoría de los casos, el Hg queda retenido en los sedimentos asociado con fases más o menos reactivas que permiten su posterior removilización y transporte a partir de varios procesos biogeoquímicos, como puede ser la degradación de la materia orgánica y la oxidación de sulfuros o reducción de sulfatos (Tseng *et al.,* 2001; Laurier *et al.,* 2003; Audry *et al.,* 2005; Gutiérrez-Ruiz *et al.,* 2007). Además, la formación de metilmercurio a partir de procesos microbiológicos que suele ocurrir en los ciclos de sedimentación y resuspensión (Tseng *et al.,* 2001), incrementa la biodisponibilidad del Hg, contribuyendo a su acumulación en la fauna presente en los cuerpos

de agua afectados (por ejemplo, Durrieu *et al.*, 2005).

Si bien los procesos de combustión de carbón son considerados como las mayores fuentes de Hg en el medio ambiente (Environmental Protection Agency, 1997) junto con un gran número de actividades industriales y mineras, existe una importante proporción dentro del balance global de Hg que es aportada a través de erupciones volcánicas (Fitzgerald y Lamborg, 2003). Las fuentes de origen antrópico son las principales responsables de las acumulaciones observadas en sedimentos del Hemisferio Norte que resultan entre tres a cinco veces mayores que en tiempos preindustriales (Selin, 2009).

En Sudamérica se han informado altas concentraciones de Hg en suelos y en sedimentos fluviales y lacustres de regiones cercanas a explotaciones mineras de oro, particularmente en Brasil (Olivero *et al.*, 2002; Rodrigues Bastos *et al.*, 2006), Venezuela, Bolivia y Perú (i.e., Cooke et al., 2009; Cooke et al., 2011; Santos-Francés et al., 2011). En el extremo más austral del continente sudamericano, existen sólo unos pocos estudios que determinan las concentraciones de Hg en sedimentos. Alguno de ellos atribuyen la presencia de Hg en sedimentos fluviales y costeros a un origen antrópico (por ejemplo, Muñiz *et al.*, 2004; De Marco *et al.*, 2006), mientras que en regiones más prístinas de la Patagonia, la presencia de Hg en el registro sedimentario de lagos cordilleranos se atribuye al aporte desde erupciones volcánicas, erosión de suelos y grandes incendios. Además, a partir del año ~1900 AD se observa un incremento gradual de las concentraciones que se ha atribuido al aumento global de los flujos de Hg atmosférico (Ribeiro Guevara *et al.*, 2010; Hermanns y Biester, 2013)

Aun cuando los ecosistemas acuáticos están globalmente expuestos al Hg a través de contribuciones atmosféricas crecientes, existen pocos estudios que se centren en la identificación de fuentes, la determinación de flujos y el análisis del registro histórico de este elemento en cuerpos de agua prístinos del hemisferio sur (Downs *et al.*, 1998; Lamborg *et al.*, 2002; Biester *et al.*, 2007; Ribeiro Guevara *et al.*, 2010; Hermanns y Biester, 2013). Este trabajo es una contribución en este sentido dado que se analiza la distribución espacial y temporal (últimos ~80 años) de las concentraciones de Hg en sedimentos de la cuenca del río Suquía (Región central de Argentina), desde sus cabeceras hasta su desembocadura en la laguna del Plata. A través de análisis mineralógicos y ensayos de extracción secuencial, se definen también las posibles fuentes de aporte de este elemento. Esta cuenca resulta particularmente interesante debido a que está sujeta a un desarrollo industrial y urbano creciente desde mediados del siglo XX y es además altamente sensible a los cambios climáticos registrados en el Sur de Sudamérica.

MATERIALES Y METODOS

Área de estudio

El río Suquía es uno de los mayores cursos de agua superficial en la provincia de Córdoba, Argentina. Sus nacientes se encuentran en las Sierras Pampeanas de Córdoba, donde existen mineralizaciones metalíferas variadas (i.e., Mutti *et al.*, 2005), y desemboca en la Laguna del Plata, pequeño cuerpo de agua asociado a la laguna de Mar Chiquita en su margen suroeste (Figura 1). En su recorrido, el río atraviesa de oeste a este la Ciudad de Córdoba, la segunda ciudad más poblada de Argentina con 1.3 millones de habitantes, y que cuenta con numerosas industrias de tipo automotriz, manufacturera, alimenticia, de pinturas, entre otras (ministerio de economía y finanzas públicas, http://www.mecon.gov.ar). El río cruza también la depresión loéssica de la Llanura Chacopampeana caracterizada por ser una de las zonas agrícolas más importante del país.

El área de Mar Chiquita está compuesta por la Laguna del Plata, la Laguna Mar Chiquita y los bañados del río Dulce y ha sido declarada sitio Ramsar por las Naciones Unidas (Bucher *et al.*, 2006; http://ramsar.wetlands.org) debido a que hospeda muchas especies amenazadas y algunas emblemáticas, así como también una abundante y diversa fauna de aves playeras. Las reconstrucciones paleoclimáticas de la zona se realizaron a partir de estudios llevados a cabo en la Laguna de Mar Chiquita, principal reservorio de agua del sistema (Piovano *et al.*, 2009). En los primeros 75 años del siglo XX, Mar Chiquita estuvo caracterizada por períodos de niveles bajos, intercalados con estadíos altos, el último de los

cuales se produjo entre los años 1999 y 2005 (Leroy *et al.,* 2010). Los niveles bajos y altos están definidos como inferiores o superiores al nivel medio de la laguna (66.5 msnm) los cuales son sincrónicos con la disminución o el aumento de las precipitaciones medias regionales (Piovano et al., 2002). A partir de 2005 los niveles comenzaron a ser decrecientes hasta la actualidad. Como consecuencia de las fluctuaciones en los niveles de la laguna, se produjeron variaciones en los niveles de salinidad desde valores máximos de 360 g l^{-1} registrado en 1911 (Frank, 1915) o 270 g l^{-1} registrado en 1970 (Martínez, 1991) a un valor mínimo de 35 g l^{-1} registrado en 1989 (Martínez *et al.,* 1994). Incluso en los períodos de extrema sequía la laguna nunca estuvo seca gracias a la recarga proveniente de aguas subterráneas (Piovano *et al.,* 2002, 2004 a,b).

El clima actual en el área de estudio es típicamente continental, semihúmedo a semiárido donde el 80 % de las precipitaciones se concentran entre octubre y marzo coincidiendo con el verano austral. Las máximas descargas del río Suquía se registran también durante este período. La temperatura media anual es de 16° C con máximas de 40° C en verano y mínimas de 0° C en invierno (http://climexp.knmi.nl).

En cuanto a la calidad del agua del río Suquía, diversos estudios han demostrado que existe un gradiente creciente de contaminación desde sus nacientes hasta regiones cercanas a la localidad de Corazón de María, ubicada aguas abajo de la ciudad de Córdoba y de la planta de tratamiento de líquidos cloacales (Pesce y Wunderlin, 2000; Wunderlin et al., 2001; Monferrán et al., 2011; Merlo et al., 2011). La contaminación del agua está dada principalmente por la presencia de elevadas concentraciones de materia orgánica disuelta (Merlo et al., 2011) y una marcada disminución en el contenido de oxígeno disuelto. Asimismo, algunos estudios han incluido el análisis de los sedimentos de fondo tomados en distintos puntos a lo largo de la cuenca, y han observado también un incremento en las concentraciones de metales pesados aguas abajo (Gaiero *et al.,* 1997; Merlo *et al.,* 2011). Sin embargo, estas concentraciones no resultan demasiado elevadas cuando se las compara con los valores determinados en sedimentos fluviales de ciudades del hemisferio norte donde el nivel de desarrollo industrial es mucho mayor y más prolongado en el tiempo.

Muestreo y preparación de las muestras

Con el fin de analizar la distribución espacial de las concentraciones de Hg en los sedimentos de cauce de la cuenca del río Suquía, se seleccionaron un total de 16 estaciones de muestreo, cuya ubicación se muestra en la Figura 1. Además, en las lagunas del Plata y de Mar Chiquita se recolectaron sedimentos de fondo y en la primera de ellas se extrajo un núcleo de sedimento de 120 cm de longitud (LP11-1: 30°51'43.3"S, 62°40'47.4"W) desde un sector próximo a la desembocadura del río Suquía. El núcleo de sedimento fue extraído con un muestreador manual Eijkelkamp.

Las muestras de sedimento de cauce se almacenaron en bolsas plásticas hasta el posterior tratamiento en el laboratorio. El núcleo de sedimento se conservó cerrado en cámara fría a 4 °C hasta su traslado al laboratorio EPOC (Environnements et Paléoenvironnements Océaniques et Continentaux) de la Université de Bordeaux 1, Francia.

Una vez en el laboratorio, se abrió el núcleo de sedimento cortándolo longitudinalmente a fin de realizar la descripción sedimentológica correspondiente y tomar las muestras necesarias para los posteriores análisis químicos y mineralógicos. Previo a la toma de muestras, se tomaron radiografías utilizando un equipo de rayos X acoplado a un amplificador de energía de alto brillo y una cámara con dispositivos de carga acoplada que permite obtener una imagen SCOPIX de alta resolución de 256 niveles de grises. La toma de muestras para análisis químicos y mineralógicos se realizó con una resolución de 0.5 cm. Tanto las muestras del núcleo de sedimento como las muestras de sedimentos de río fueron secadas a estufa a 50 °C. Las muestras de río fueron tamizadas a fin de separar las fracciones granulométricas correspondientes a partículas menores a 3 mm (fracción arenosa) y 62 µm (fracción limosa) respectivamente.

Todas las muestras de sedimentos de fueron molidas en mortero de ágata previo a la realización de las determinaciones.

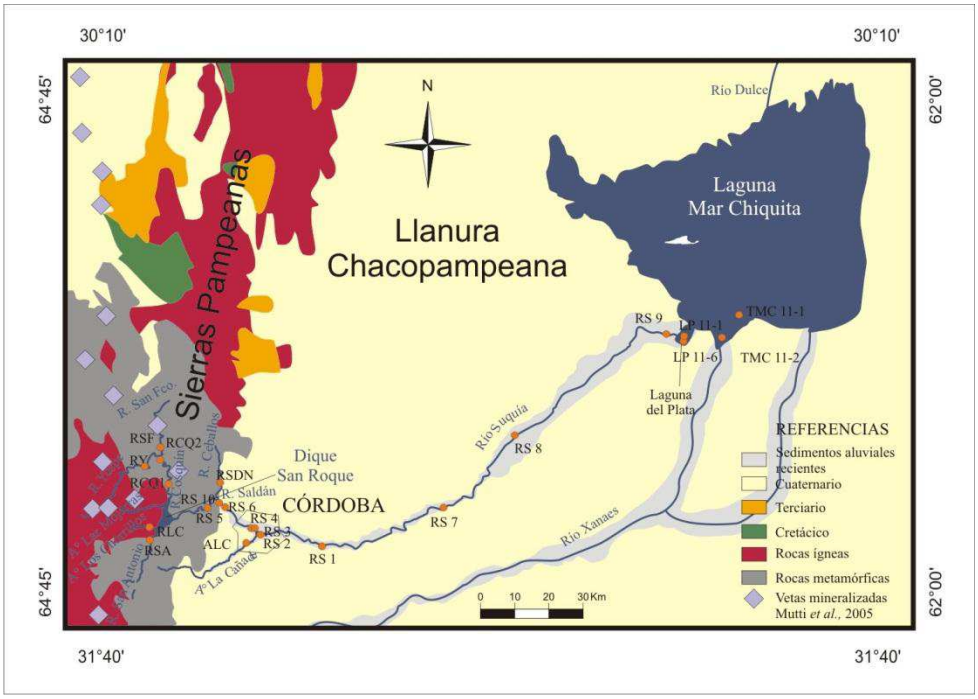

Figura 1. Características litológicas del área de estudio y y localización de los puntos de muestreo.

Determinaciones analíticas y mineralógicas en el núcleo de sedimento y sedimentos de cauce

La concentración total de mercurio (Hg_T) fue determinada en sub-muestras de ~70-100 mg de sedimento seco mediante espectrometría de absorción con vapor frío (vapor de O_2) previa incineración y amalgamación, utilizando un analizador directo de mercurio (Direct Mercury Analyzer – DMA 80, MILESTONE). Con este método se analizaron todas las muestras. Además, en los sedimentos de fondo de cauce las medidas de Hg se realizaron tanto en la fracción arenosa como limosa. La calidad analítica de los resultados se verificó sistemáticamente con sedimentos de referencia certificados internacionalmente (LKSD-4, IAEA 433, 1646a). Las lecturas de los patrones de referencia se realizaron cada cinco muestras y las concentraciones se expresaron en $\mu g\ kg^{-1}$ de peso seco. El límite de detección (3 veces la desviación estándar de 5 valores de muestras en blanco) varió entre 1 y 2 $\mu g\ kg^{-1}$. La precisión (coeficiente de variación de 5 muestras repetidas) fue mejor que 5 %.

Las determinaciones de Carbono total (Ctot), C orgánico (Corg) y azufre total (S%) se realizaron utilizando un analizador de carbono/azufre LECO CS 125. Previamente las muestras fueron primero acidificadas en crisoles con HCl 2M a fin de destruir los carbonatos y luego se secaron a 60 °C durante 24 h para remover el carbono inorgánico, así como el ácido y agua restantes (Etcheber *et al.*, 1999). La calidad se comprobó mediante las determinaciones de materiales de referencia certificados (LECO 501–506) y la precisión fue mejor que 3 %.

La mineralogía de los sedimentos de fondo de la laguna, de los sedimentos de lecho del río y de los sedimentos acumulados en los distintos niveles del núcleo de sedimento se determinó con un difractómetro de rayos X, SIEMENS D500 compuesto por un goniómetro theta/2theta y funciona con un ánodo de cobre (Cu Kα= 1.5406 Å). Las lecturas se registraron en un intervalo de 4 a 90° de 2Θ con intervalos de escaneo de 0.02° y un tiempo de duración de 2 segundos.

Determinaciones isotópicas

A fin de determinar la edad de los niveles reconocidos en el núcleo de sedimento, se midieron las actividades de ^{210}Pb, ^{232}Th, ^{226}Ra y ^{137}Cs usando un detector γ de bajo fondo y alta eficiencia (CANBERRA) (Schmidt *et al.*, 2009). La calibración del detector γ se realizó utilizando materiales certificados de referencia (IAEA-RGU-1; IAEA-RGTh; SOIL-6). Las actividades se expresaron en $mBq\ g^{-1}$ y los errores están basados en conteos estadísticos de 1 SD. El exceso de ^{210}Pb ($^{210}Pb_{xs}$) se calculó sustrayendo la actividad soportada por su

isótopo padre, ^{226}Ra, de la actividad total del ^{210}Pb en el sedimento. Los errores en $^{210}Pb_{xs}$ fueron calculados por propagación de los errores en el par correspondiente (^{210}Pb y ^{226}Ra).

Extracciones selectivas

Las extracciones selectivas se utilizan para determinar la asociación de elementos traza con diferentes fases mineralógicas u orgánicas presentes en suelos y sedimentos (e.g. Tessier *et al.*, 1979, Audry *et al.*, 2005). A fin de determinar las fases portadoras de Hg en el núcleo de sedimento estudiado, se realizaron extracciones selectivas de tres pasos, tal como se describe en Castelle *et al.* (2007). Los esquemas de extracciones paralelas similares al utilizado en este trabajo, evitan limitaciones tales como (i) la transferencia de metales de una fase a la otra (Bermond, 1992), (ii) múltiples riesgos de contaminación de muestras por los sucesivos reactivos usados (Quevauviller, 1998), (iii) posibles cambios en la especiación elemental durante las sucesivas extracciones y (iv) cambios o pérdidas de especies elementales durante el lavado del residuo (Rosenberg y Ariese, 2001). Además este método no muestra riesgos en la pérdida de muestras por lo que un error producido durante una de las extracciones no compromete a la secuencia entera (Tack *et al.*, 1996).

Todas las soluciones utilizadas en los ensayos y determinaciones analíticas se prepararon a partir de reactivos de Grado Analítico y agua Milli-Q®. Todo el material de laboratorio en contacto con las muestras fue lavado previamente con HCl 10 % durante 3 días, enjuagado con agua Milli-Q® y secado bajo campana con flujo laminar.

En el extracto obtenido se realizaron determinaciones de las concentraciones de Hg siguiendo la metodología descrita anteriormente, así como de Fe y Mn que se midieron mediante espectrometría de absorción atómica por llama (Perkin Elmer AAnalyst 300). Los límites de detección (3 veces la desviación típica del blanco) fueron de 0.5 y 0.3 $\mu g\ L^{-1}$ para Fe y Mn y la precisión fue mejor que 2 y 3%, respectivamente. El proceso de extracción selectiva comprendió las siguientes etapas:

Extracción con ascorbato (Hg asociado a la fracción reducible)

Este procedimiento permite extraer los elementos traza asociados con óxidos de Mn y la fracción más reactiva de los óxidos de Fe (i.e. óxidos amorfos; Kostka y Luther III, 1994; Audry *et al.*, 2006). La metodología consiste en suspender 200 mg de sedimento seco en 12.5 ml de solución 0.11M de ascorbato (5:5:2 citrato de sodio/bicarbonato de sodio/mezcla de ácido ascórbico; J.T. Baker). Se agita durante 24 h y luego se separa el residuo sólido mediante centrifugación durante 15 minutos a 9000 rpm. El residuo se enjuaga con agua Milli-Q®, se seca a 50° C y se muele en mortero de ágata hasta alcanzar fracciones de ~4µm. La fracción correspondiente al Hg reducible corresponde a la diferencia entre la concentración de Hg total (Hg_T) y el Hg determinado en el residuo.

Extracción con H_2O_2 (Hg asociado a la fracción oxidable)

El lavado de los sedimentos con H_2O_2 permite extraer los metales asociados con la materia orgánica y sulfuros minerales (Tessier *et al.*, 1979). El método modificado por Ma y Uren (1995) y Audry *et al.* (2006), consiste en suspender 250 mg de sedimento seco en 8 ml de una solución de H_2O_2 al 30 % cuyo pH se fija en 5 mediante el agregado de NaOH. La suspensión resultante se calienta a 85° C durante 5 h. Al cabo de 3 h se agregan 3 ml de H_2O_2 30 % y 5 ml de acetato de amonio 5M mientras continúa calentándose. Después de 5 h, la suspensión se agita nuevamente durante 30 minutos y se centrifuga durante 15 minutos a 9000 rpm. El residuo sólido se lava con agua Milli-Q®, se seca y se muele en mortero de ágata. La fracción de Hg asociada a la materia orgánica y sulfuros se calcula restando a la concentración de Hg_T, la concentración de Hg determinada en el residuo resultante de esta extracción (Sahuquillo *et al.*, 2003; Castelle *et al.*, 2007).

Extracción con HCl (Hg asociado a la fracción soluble en ácido)

La fracción soluble en ácido fue diseñada empíricamente para extraer la mayor parte de los metales traza potencialmente biodisponibles (Bryan y Langston, 1992; Langston *et al.*, 1999). Comprende metales adsorbidos o intercambiados, y aquellos que se encuentran co-precipitados en sales solubles y asociados a sulfuros volátiles ácidos (Huerta-Diaz y Morse 1990, 1992; Nova-López y Huerta-Díaz, 2001). La fracción correspondiente a los sulfuros volátiles ácidos se define operacionalmente como la fracción de sulfuros extraída mediante lavados con HCl 1M a temperatura ambiente. Esta fracción no incluye los óxidos de Fe cristalinos resultantes de la oxidación de monosulfuros (Raiswell *et al.*, 1994).

Para esta extracción se suspenden 200 mg de sedimento seco en 12.5 ml de HCl 1M y se agita durante 24 h. El residuo sólido se separa por centrifugación, se lava con agua Milli-Q®, se seca a 50° C y se muele en mortero de ágata. La concentración de Hg asociada a la fracción soluble se calcula como la diferencia entre la concentración de Hg_T y la concentración de Hg determinada en el residuo resultante de esta extracción (Hg_{HCl}; Castelle *et al.,* 2007).

RESULTADOS

Descripción sedimentológica y geoquímica del núcleo de sedimento de la Laguna del Plata

La Figura 2 a y b muestra la fotografía y la imagen de RX obtenidas para el núcleo de sedimento de la Laguna del Plata (LP11-1) donde se observa una alternancia de laminaciones en tonos grises claros y oscuros que han permitido distinguir 5 unidades sedimentarias. La primera (A) se extiende desde el fondo del núcleo de sedimento (120 cm) hasta los 75 cm y se trata de una secuencia masiva (sin laminaciones) que está separada de la inmediata superior mediante un contacto neto. Entre los 75 y 69 cm se observa una pequeña secuencia (B) que muestra una laminación producida por la alternancia de sedimentos oscuros y claros. Por encima de esta secuencia y hasta los 53 cm se distingue una nueva secuencia (C) caracterizada por la alternancia de capas de sedimento predominantemente claras. Entre los 53 y 16 cm de profundidad, se distingue una nueva secuencia (D) formada por la alternancia de laminaciones oscuras y claras, pero con contactos más netos que en los casos anteriores. Finalmente, en los 16 cm superiores se observa la secuencia superior (E) caracterizada por la acumulación de sedimentos de color verde oliva oscuro.

Las características sediment-ológicas del núcleo de sedimento fueron además contrastadas con algunas de las propiedades físicas y químicas determinadas en él (Figura 2 c-e). De acuerdo con lo observado en estas figuras, los mayores valores de porosidad (75 %) se determinaron cerca de la superficie del núcleo de sedimento mientras que los más bajos (~40 %) fueron registrados en la porción inferior (Figura 2 c). La laminación descrita anteriormente pareciera estar relacionada con estos cambios de porosidad: la sección A muestra los menores valores, las secciones B, C y D valores intermedios, mientras que la secuencia E muestra los valores más altos (Figura 2 c).

La variación del contenido de Corg a lo largo del núcleo de sedimento se muestra en la Figura 2d. Las concentraciones varían entre ~0.5 y ~2.8 %, encontrándose los máximos valores en los primeros 15 cm y entre los 40 y 60 cm de profundidad. En el resto del núcleo de sedimento, los valores permanecen más o menos constantes entre 0.6 y ~0.9 %. Probablemente como consecuencia de las escasas precipitaciones y la elevada salinidad del agua, los niveles de C_{org} medidos en el núcleo de sedimento de la Laguna del Plata son marcadamente inferiores a los medidos en lagos de la Patagonia andina, donde se han reportado valores de entre 6 y 8 % C_{org} en lagos del Norte (i.e. Ribeiro Guevara *et al.,* 2010) y entre 12 y 15 % de C_{org} en lagos más australes (Hermanns y Biester, 2013). Los valores de C_{org} son importantes indicadores de aportes de Hg a partir de la erosión de suelos en las cabeceras de los lagos debido a la fuerte afinidad de este elemento por la materia orgánica (Driscoll *et al.,* 1995; Rydberg *et al.,* 2010; Teisserenc *et al.,* 2010).

Las concentraciones de S a lo largo del núcleo de sedimento oscilan entre ~3 y ~11 %. El perfil de concentraciones (Figura 2 e) muestra tres zonas donde se registran los máximos valores: por debajo de los 100 cm de profundidad, entre los 75 y 35 cm y por encima de los 16 cm de profundidad. Estas concentraciones corresponderían principalmente a sulfuros diseminados en los sedimentos dado que no se ha determinado la presencia de yeso a lo largo del núcleo de sedimento.

Las concentraciones de Fe y Mn fueron medidas en los sobrenadantes de la extracción con ascorbato (Fe y Mn-asc). Desde la parte más profunda del núcleo de sedimento (120 cm) hasta los 74 cm el valor promedio de Fe es de 1670 mg kg^{-1}, en la parte central hasta los 16 cm es de 1270 mg kg^{-1} y en la parte más superficial es de 2240 mg kg^{-1}. En los mismos intervalos, las concentraciones de Mn promedian 1410, 1790 y 1510 mg kg^{-1}respectivamente.

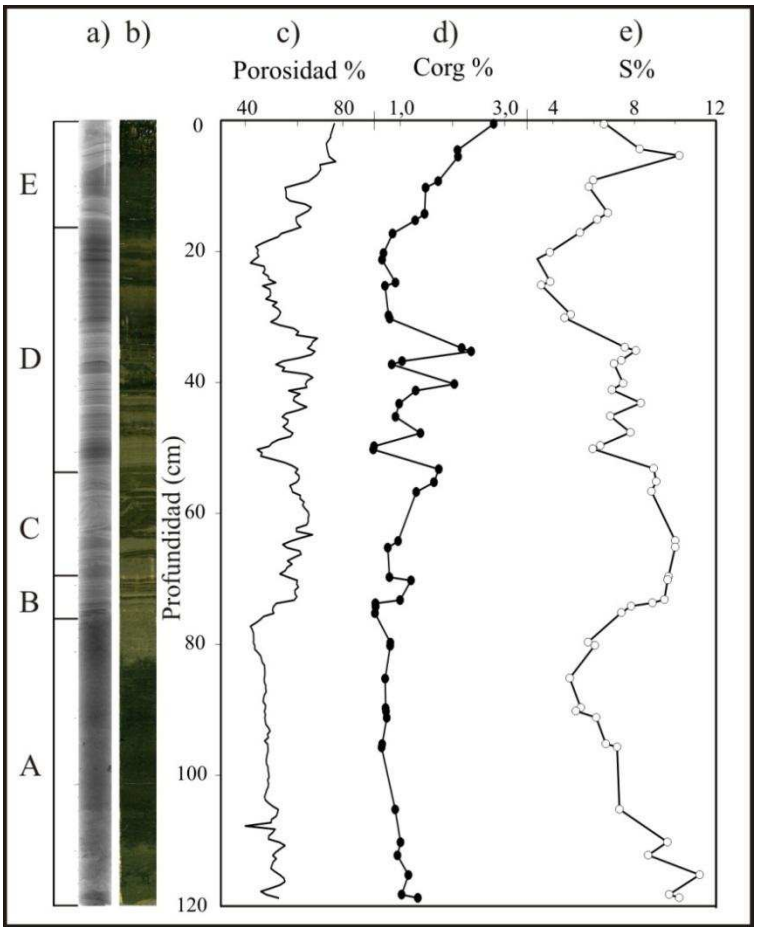

Figura 2. Propiedades sedimentológicas, físicas y químicas del núcleo de sedimento LP; a) radiografía SCOPIX, b) fotografía, c) porosidad expresada en porcentaje, d) concentración del C_{org} (%), e) concentración de S (%).

Composición mineralógica del núcleo de sedimento

Los minerales mayoritarios encontrados a lo largo del núcleo de sedimento LP son cuarzo, albita, muscovita, biotita, calcita y halita; pirita fue el principal mineral accesorio reconocido. Entre los minerales arcillosos se identificaron montmorillonita y caolinita.

En las muestras de sedimentos de lecho analizadas (RS 7 y RS 8) se identificó cuarzo, albita y microclino como minerales mayoritarios, mientras que como accesorios se identificaron Perovskita y Pirita. También se observó escasa illita.

Dataciones radiométricas del núcleo de sedimento

El ^{210}Pb ($T_{1/2}$ = 22.3 años) es un radionucleido natural que es liberado continuamente a la atmósfera por decaimiento radiactivo (Saari *et al.,* 2010) y se adsorbe rápida y fuertemente a la materia orgánica. Este ^{210}Pb es denominado ^{210}Pb en exceso (^{210}Pbxs) para diferenciarlo del isótopo que se origina dentro de las partículas por el decaimiento de su isótopo padre, el ^{226}Ra. A diferencia del ^{210}Pb, el ^{137}Cs ($T_{1/2}$ = 30 años) es un radionucleido artificial; su aparición en el medio ambiente es principalmente el resultado del polvillo radiactivo de los ensayos de armas nucleares realizados en los años sesenta, y al accidente en Chernobyl de 1986 (United Nations Scientific Committee on the Effects of Atomic Radiation, 2000). En la actualidad, los flujos atmosféricos de ^{137}Cs son casi insignificantes (Quintana, 2011). El ^{232}Th existe de forma natural y debido a que posee una larga vida media, se le considera generalmente asociado a la fracción detrítica (Van der Klooster *et al.,* 2011). Por lo tanto, los cambios en sus actividades pueden indicar diferentes proporciones o fuentes litológicas.

El ^{210}Pb ha sido ampliamente utilizado para calcular períodos cortos (años a décadas) de tasas de

sedimentación en ambientes continentales y oceánicos desde hace cuarenta años (Appleby, 2001). La edad se calcula utilizando el exceso de ^{210}Pb (^{210}Pbxs). Una vez incorporado al sedimento, el ^{210}Pb decae con el tiempo en la columna sedimentaria, según la ecuación (1):

$$^{210}Pb_{xs(z)} = {}^{210}Pb_{xs(0)}e^{-\lambda t} \quad (1)$$

donde ^{210}Pb$_{xs(z)}$ y ^{210}Pb$_{xs(0)}$ representan el exceso de ^{210}Pb en la interfase sedimento-agua, o en la base de la capa mezclada, a una profundidad z, λ es la constante de decaimiento de ^{210}Pb (0.0311 año^{-1}) y *t* es la edad en años. Se han desarrollado varios modelos para calcular la edad o la tasa de acumulación: CIC: Concentración Inicial Constante (Robbins y Edgington, 1975); CRS: Flujo Constante (Appleby y Oldfield, 1978); CFCS: Flujo Constante-Sedimentación Constante (Robbins *et al.*, 1977; Sanchez-Cabeza y Ruiz-Fernández, 2012). El modelo CIC en el cual los sedimentos tienen una concentración de ^{210}Pb constante sin tener en cuenta las tasas de sedimentación (Appleby, 2001) se descartó rápidamente debido a que la Laguna del Plata ha sufrido conexiones y desconexiones de la Laguna Mar Chiquita alternantes, influenciando la cantidad y la naturaleza del material sedimentado (Piovano *et al.*, 2002). Por esto se eligió el modelo CFCS para calcular las tasas de sedimentación y la edad para la Laguna del Plata teniendo en cuenta dos suposiciones: la depositación de ^{210}Pb atmosférico es constante al igual que la tasa de masa acumulada (MAR) que se expresa en g cm^{-2} a^{-1} y puede ser calculada mediante la ecuación (2) :

$$^{210}Pb_{xs(z)} = {}^{210}Pb_{xs(0)} \times e^{-m_z \frac{\lambda}{MAR}} \quad (2)$$

donde m (z) es la masa seca acumulada por área (g cm^{-2}) a la profundidad z. Para compensar el efecto de cambios en la composición del sedimento, las actividades de ^{210}Pb$_{xs}$ se normalizaron utilizando las concentraciones de ^{232}Th, medidas simultáneamente para limitar errores. La MAR se calculó de la regresión exponencial de ^{210}Pb$^{n}_{xs}$ graficada con respecto a la masa acumulada (Figura 3 a). El promedio de la tasa de masa acumulada es 1 g cm^{-2} a^{-1}. El tiempo de deposición (en años) se calculó dividiendo la masa seca acumulada por unidad de área por la tasa de la masa acumulada permitiendo determinar las tasas de sedimentación (Figura 3b). El año de depositación esperado para cada capa de sedimento se estimó considerando el año de muestreo (2011) y la interfase agua-sedimento como la capa superficial de referencia para establecer la cronología.

Robins y Edgington (1975) mostraron que es necesario confirmar la precisión del modelo basado en ^{210}Pb usando un marcador cronoestratigráfico independiente tal como el de ^{137}Cs. El pico de ^{137}Cs que se observa en el núcleo de sedimento LP corresponde al año 1966 (Figura 3 c), que se correlaciona con el polvillo atmosférico anual de ^{137}Cs registrado en Buenos Aires desde 1960 (Quintana, 2011).

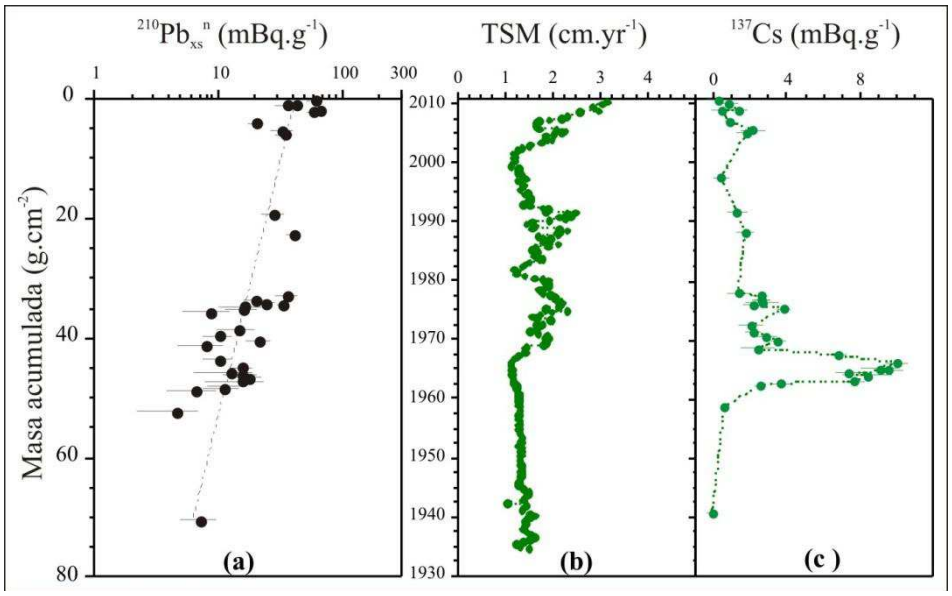

Figura 3. Perfil de datación. a) Tasa de masa acumulada (TMA). b) Tiempo de deposición (en años). c) Medición de ^{137}Cs como marcador cronoestratigráfico independiente.

Concentraciones de Hg total e identificación de fases portadoras en el núcleo de sedimento

Hg_T y tasas de acumulación

Las concentraciones de Hg_T medidas en intervalos de 0.5 cm a lo largo del núcleo de sedimento de la Laguna del Plata, varían entre ~13 y ~131 µg kg^{-1} (Figura 4 a). Las concentraciones más bajas y constantes se midieron desde la base del núcleo de sedimento y hasta los 75 cm de profundidad alcanzando un valor promedio de ~17.4 ± 1.6 µg kg^{-1}. Por encima de los 75 cm, las concentraciones de Hg_T son muy variables. Por ejemplo, entre los 75 y 45 cm de profundidad, la concentración promedio determinada es de 39.8 ± 15.6 µg kg^{-1}. Por encima de los 45 cm y hasta los 16 cm, se encuentran las concentraciones promedio de Hg_T más elevadas de 79.9 ± 27.5 µg kg^{-1} con picos de 89.7, 131.5 y 87.3 µg kg^{-1} observados a los 43.2, 36.7 y 30.2 cm respectivamente. En los primeros 16 cm de profundidad, la concentración promedio de Hg_T es menor, alcanzando un valor de 54.7 ± 16.1 µg kg^{-1}. Estos valores se encuentran dentro del intervalo informado en lagos de la Patagonia y de otras regiones remotas de mundo que no están directamente afectadas por la actividad del hombre (Ribeiro Guevara *et al.,* 2010; Hermanns y Biester, 2013; Conaway *et al.,* 2012; Yang *et al.,* 2010). Por ejemplo en la Patagonia argentina las concentraciones de Hg varían entre 50 y 200 µg kg^{-1} (Ribeiro Guevara *et al.,* 2010) mientras que en la Patagonia chilena lo hacen entre 28 y 73 µg kg^{-1} (Hermanns y Biester, 2013) y en el lago Tanganyika (África) entre 20 y 90 µg kg^{-1} (Conaway *et al.,* 2012). Concentraciones de Hg mayores se midieron en regiones más industrializadas o afectadas por actividades mineras. Por ejemplo, Castelle *et al.* (2007) informan concentraciones entre 490 y 5460 µg kg^{-1} en una zona minera francesa, mientras que Xia *et al.* (2001) informan una concentración promedio de Hg de 90 µg kg^{-1} en una reserva natural de humedales en el sur de China afectada por la contaminación derivada de la quema de combustibles fósiles. De acuerdo con las dataciones radiométricas los sedimentos acumulados en el segmento comprendido entre los 16 y los 75 cm se depositaron entre los años 1968 y 2003, período que además coincide con un máximo hidrológico (Figura 4 b) determinado para el sistema de lagunas del Plata/Mar Chiquita (Piovano *et al.,* 2002, 2004 a,b). Los sedimentos más modernos presentan también concentraciones elevadas, aunque en promedio inferiores a las registradas en el período 1968-2003, con una tendencia creciente hacia la parte más alta del núcleo de sedimento.

La masa acumulada de sedimento por unidad de área se calculó en base a los datos de la densidad efectiva cada 0.5 cm de profundidad. Con este valor se calculó la masa acumulada de Hg por cm^2 a lo largo del registro sedimentario de la laguna (Figura 4 c). Los valores determinados en la parte más baja del núcleo de sedimento (de 120 a 75 cm) son muy constantes y alcanzan un valor promedio de 0.02 ± 0.003 µg cm^{-2} a^{-1}. Por encima de los 75 cm y hasta los 45 cm, la masa acumulada de Hg se incrementa notablemente alcanzando un valor promedio de 0.038 ± 0.016 µg cm^{-2} a^{-1}, lo cual supone un incremento promedio de 1.7 veces, en relación con la tasa determinada en el segmento inmediatamente inferior. Este aumento se intensifica aún más en los sedimentos depositados entre los 45 y 16 cm de profundidad, donde la masa acumulada de Hg alcanza un valor promedio de 0.078 ± 0.022 µg cm^{-2} a^{-1}, con un pico de 0.135 µg cm^{-2} a^{-1} Hg a los 35 cm de profundidad. Los sedimentos más modernos, acumulados por encima de los 16 cm de profundidad, muestran una masa acumulada de Hg que en promedio es ~2 veces inferior (0.041 ± 0.014 µg cm^{-2} a^{-1} Hg) que el período anterior pero al mismo tiempo resulta ~2 veces superior al valor promedio medido en la base del núcleo de sedimento. El aumento gradual de los flujos de Hg hacia la parte superior de los núcleos de sedimento extraídos en lagos de regiones remotas de la Tierra ha sido asignado al aumento del Hg atmóférico global. Para diferenciar estos aportes, se tomó como valor de referencia de condiciones no afectadas por los aportes atmosféricos a las concentraciones promedio de Hg medidas en la base del núcleo de sedimento (sedimentos acumulados antes de 1968). Este supuesto se basa en la constancia de los valores registrados en ese tramo del registro sedimentario y en la similitud de los mismos con las concentraciones de Hg medidas en los sedimentos de la cuenca del río Suquía (Tabla 1), lo cual sugiere que estos sedimentos podrían haber sido la principal fuente de aporte de Hg a la laguna en los años previos a 1968. La Figura 4 d muestra la variación de la relación entre los valores de la masa acumulada de Hg a lo largo del núcleo de sedimento y el correspondiente valor de fondo. En ella se observa el incremento gradual en la tasa de acumulación de Hg a partir del año 1968, alcanzado valores que son ~3.5 veces superiores en los sedimentos acumulados en el año 2011, en relación

con los registrados en sedimentos acumulados antes de 1968. A pesar de este marcado incremento, los máximos valores de acumulación de Hg se produjeron entre 1990 y 1995, cuando se registraron picos entre ~4 y ~7 veces superiores a los valores de fondo.

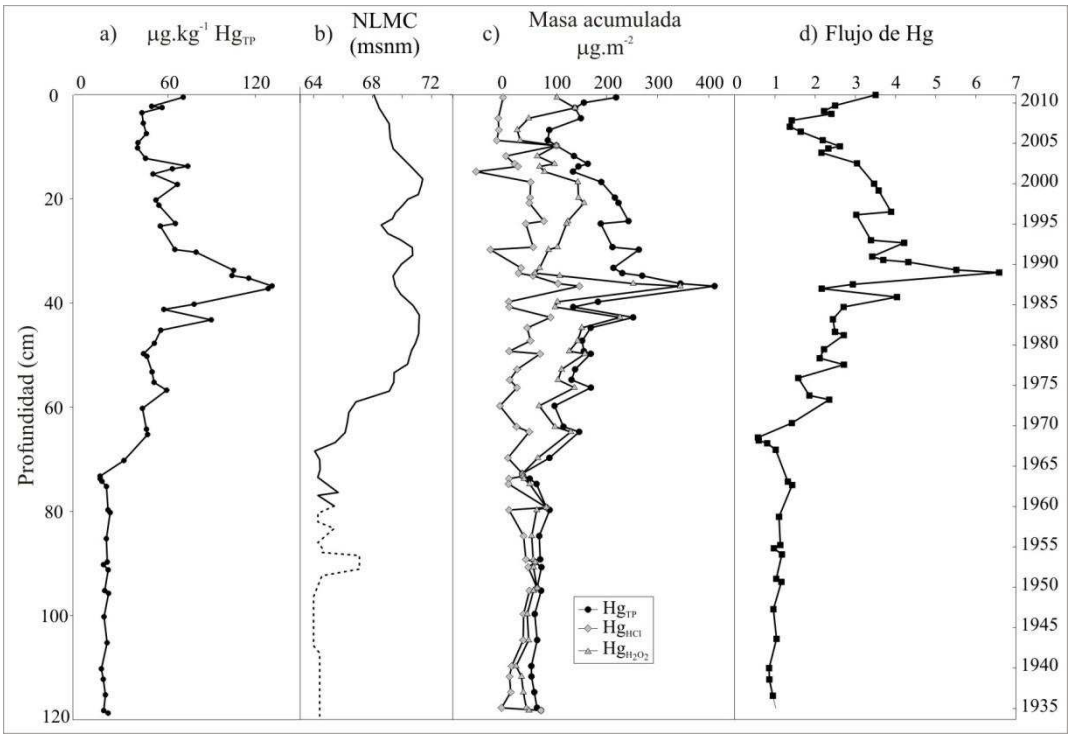

Figura 4. a) Variación de las concentraciones de Hg_T en el núcleo de sedimento LP; b) Variación del nivel de la Laguna Mar Chiquita (NLMC) en el período estudiado. La línea sólida corresponde a valores medidos mientras que la línea punteada corresponde a valores reconstruidos (Piovano *et al.*, 2006); c) masa acumulada de Hg_T, Hg_{H2O2} y Hg_{HCl} en el núcleo de sedimento LP; d) Variación de los flujos de Hg a lo largo del núcleo de sedimento.

Muestra	Fracción limosa µg kg^{-1}	Fracción arenosa µg kg^{-1}
RSF	72.41	25.06
RCQ2	62.52	9.61
RCQ1	34.92	7.39
RS10	63.24	10.31
RY	30.57	2.13
RLC	23.18	15.46
RSA	60.49	5.37
RSDN	180.99	10.09
RS6	40.99	17.97
RS5	46.94	26.69
RS1	20.42	9.14
RS7	23.51	2.59
RS8	34.84	2.75
RS9	29.77	11.82
LP11-1	38.89*	
TMC 11-1	20.70*	

Tabla 1. Concentración de Hg_T en las fracciones arenosa y limosa determinadas en sedimentos de lecho de la cuenca del río Suquía y en la fracción total (*) de sedimentos de fondo de las lagunas del Plata (LP11-1) y Mar Chiquita (TMC11-1).

Fases portadoras de Hg

Los perfiles de Hg asociados a las distintas fracciones obtenidas mediante ensayos de extracciones selectivas se muestran en la Figura 5a. La concentración de Hg asociado a la fracción reductible (Hg_{asc}) es despreciable por lo que no se lo ha incluido en la figura. El resto de las fracciones extraídas explican en gran medida la concentración Hg_T medida a lo largo del núcleo de sedimento. La fracción oxidable (Hg_{H2O2}), que comprende el Hg asociado con la materia orgánica y sulfuros, predomina por sobre la fracción soluble en HCl (Hg_{HCl}) en todo el núcleo de sedimento, sobre todo por debajo de los 40 cm de profundidad donde constituye entre un 70 y un 80 % de la concentración total de Hg (Figura 5 b). La fracción Hg_{HCl}, que corresponde al Hg adsorbido en la superficie de minerales tales como óxidos de Fe o asociado a sulfuros volátiles en ácidos, es siempre minoritaria, aunque en la base del núcleo de sedimento (por debajo de los 74 cm) su participación sobre el Hg_T (Figura 5 c) es mayor comparada con las concentraciones determinadas en los sedimentos más modernos.

Al calcular la masa acumulada por unidad de área de las dos fracciones de Hg, se observa que gran parte del incremento en el flujo de Hg en los sedimentos acumulados entre los 75 y 16 cm de profundidad se explica fundamentalmente por el aporte de Hg asociado con la fracción oxidable (materia orgánica + sulfuros). Esta fracción prácticamente explica el 100 % de la masa acumulada de Hg total hasta aproximadamente el año 1990. En los sedimentos más modernos se observa un exceso de Hg que no puede ser explicado por ninguna de las dos fracciones (Figura 4 c).

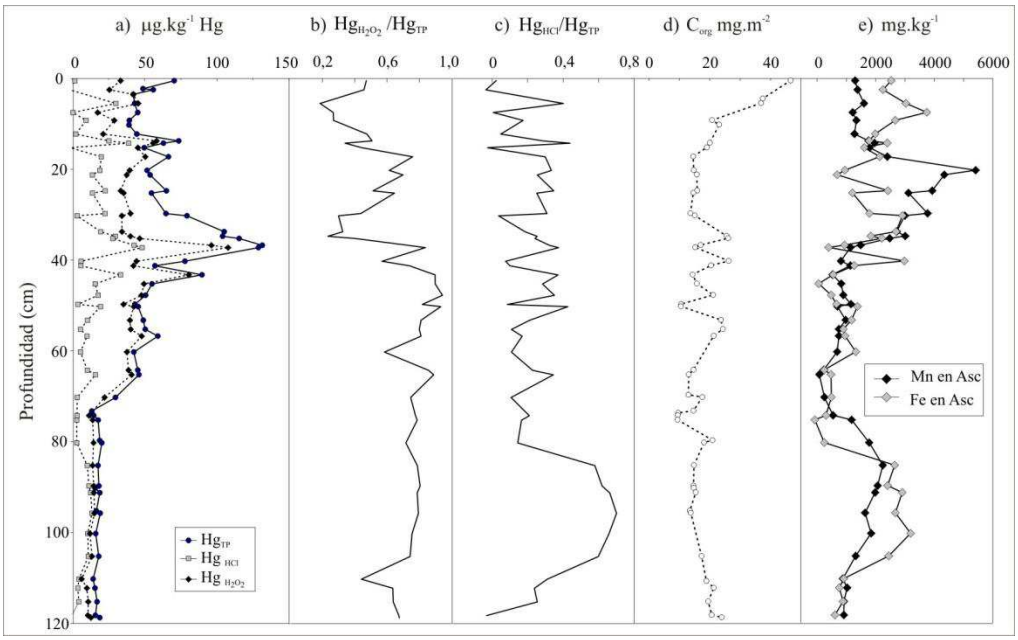

Figura 5. a) variación de las concentraciones de Hg_T, Hg_{H2O2} y Hg_{HCl} a lo largo del núcleo de sedimento LP; b) relación Hg_{H2O2}/ Hg_T a lo largo del núcleo de sedimento; c) relación Hg_{HCl}/ Hg_T a lo largo del núcleo de sedimento, d) masa acumulada de C a lo largo del núcleo de sedimento; e) variación de las concentraciones de Fe y Mn extraídas con ácido ascórbico.

Siguiendo un procedimiento similar, se calculó el flujo de masa acumulada de C_{org} a lo largo del núcleo de sedimento. El perfil obtenido (Figura 5 d) muestra una distribución más o menos constante desde la base del núcleo de sedimento y hasta aproximadamente los 16 cm de profundidad (masa acumulada promedio 5.56 ± 1.52 µg cm^{-2} a^{-1} C). Por encima de este nivel, la masa de C acumulada comienza a incrementarse gradualmente alcanzando un valor promedio de 7.79 ± 3.57 µg cm^{-2} a^{-1} C. Esta distribución sugiere que el aporte de materia orgánica particulada fue más o menos constante entre los años 1935 y 2003 y que el comienzo del período húmedo a partir de 1968 simplemente afectó la variabilidad en el aporte de materia orgánica a la laguna, sin alterar significativamente la masa promedio de materia orgánica acumulada. En consecuencia, el aumento de Hg asociado a la fase oxidable en los sedimentos acumulados entre los 74 y 16 cm de profundidad, podría asignarse no sólo a la materia orgánica, sino

también a la presencia de otras fases oxidables en el sedimento, muy probablemente pirita dado que este mineral ha sido identificado mediante los análisis de difracción de rayos X.

La distribución de las concentraciones de Fe y Mn medidas en los extractos realizados con ácido ascórbico indica una fuerte presencia de los correspondientes óxidos por debajo de los 80 cm de profundidad y por encima de los 40 cm en el núcleo de sedimento estudiado (Figura 5 e). Dado que las concentraciones de Hg determinadas en esos mismos extractos son despreciables, es posible inferir que el Hg presente en los sedimentos acumulados en esos niveles no estaría asociado con patinas de óxidos de Fe y Mn.

DISCUSIÓN

Los perfiles de concentración del Hg_T y de las fracciones de Hg asociado con fases oxidables y con fases biodisponibles indican que a partir del año 1968 se inicia un período de gradual aumento de las concentraciones en relación con lo observado en los sedimentos acumulados previamente y que perdura hasta la actualidad. Este comportamiento coincide con un importante incremento en el nivel de la laguna de Mar Chiquita (Figura 4b) que comenzó a partir del año 1968 y que culminó en el año 2003 cuando se inició un período de bajante. Además del fuerte incremento en las concentraciones de Hg, se observó un aumento en la variabilidad de las mismas, que podría estar relacionado con las fluctuaciones de nivel registradas durante ese período. Debido a que no existen registros de nivel en la laguna del Plata, los valores que aquí se utilizan corresponden a los medidos en la laguna de Mar Chiquita, la cual se mantuvo conectada con la laguna del Plata durante todo el período húmedo.

Los sedimentos acumulados en la laguna antes de 1968 presentan concentraciones bajas de Hg y relativamente constantes. La reconstrucción paleoclimática de la región indica que en este período predominaron condiciones de mayor aridez que dieron lugar a una fuerte contracción de la superficie de la laguna. En consecuencia, durante ese período la principal fuente de aporte de sedimentos a la laguna habría correspondido a los sedimentos transportados por el río Suquía desde las cabeceras de la cuenca y al aporte desde las precipitaciones, fundamentalmente en forma de polvo atmosférico. Considerando que la naturaleza de los sedimentos de lecho se ha mantenido invariable con el tiempo (sobre todo de aquellos que se encuentran en las cabeceras de la cuenca donde no hay una fuerte intervención del hombre) sería válido pensar que las concentraciones de Hg medidas en sedimentos actuales de lecho representan el aporte de este elemento a la laguna a lo largo del tiempo. Las concentraciones más altas de Hg medidas en los sedimentos tomados en las cabeceras de la cuenca (Tabla 1) sugiere que la fuente de este elemento estaría relacionada con la presencia de sedimentos volcaniclásticos predominantes en el sector NO así como también de sulfuros diseminados o en vetas (Mutti *et al.,* 2005). Además, el aporte proveniente de actividades industriales desarrolladas en el tramo medio de la cuenca pareciera ser despreciable dado que los niveles de Hg se mantienen más o menos constantes desde la ciudad de Córdoba hasta la desembocadura del río en la Laguna del Plata. Durante el período seco únicamente los sedimentos más finos pudieron alcanzar la laguna, lo cual refuerza la hipótesis del aporte desde los sedimentos de la cuenca, debido a que el Hg se concentra fundamentalmente en la fracción más fina de los mismos (Tabla 1).

La especiación sólida del Hg en el segmento más profundo del núcleo de sedimento indica que este elemento se encuentra principalmente asociado con la fracción oxidable de los sedimentos. En esta parte del núcleo de sedimento además, la concentración de C_{org} es la menor (Figura 2e) y la de S total es la mayor (Figura 2) lo cual sugiere fuertemente que el Hg acumulado en la laguna del Plata antes de 1968 se encuentra asociado a sulfuros de metal probablemente aportados desde la fracción más fina de los sedimentos provenientes de las cabeceras de la cuenca. El HgS(s) es relativamente insoluble y menos volátil que otras formas de Hg (Barnett y Turner, 2001), lo cual lo convierte en una fase estable en los sedimentos. Sin embargo, la presencia de este mineral no ha sido descrita en la región, por lo que se estima que se encuentra asociado preferentemente con la pirita. Este último, además de ser un mineral muy común en los ambientes sedimentarios y de haber sido identificado tanto en los sedimentos acumulados en la laguna como en los sedimentos de lecho del río Suquía, es capaz de adsorber muchos elementos potencialmente tóxicos como Hg, Pb, Cu, Cd, Cr y As (por ejemplo, Bostick *et al.,* 2003; Doyle *et al.,* 2004; Borah y Senapati, 2006; Ozverdi y Erdem, 2006). El Hg se adsorbe en la superficie de la pirita en un amplio intervalo de pH (Behra *et al.,* 2001) formando principalmente complejos de Hg-Cl y Hg-OH (por ejemplo, Behra *et al.,* 2001; Bower *et al.,* 2008). En la laguna del Plata, la formación de

estos complejos estaría favorecida además por la elevada salinidad y el pH alcalino del agua (~42 g L^{-1} y pH ~9.2).

En los sedimentos acumulados después de 1968 las concentraciones de Hg_T aumentan en relación con los niveles más antiguos. Esta situación coincide con el inicio de un período más húmedo en la región que se tradujo en un aumento en los niveles de las lagunas estudiadas. Al igual que en la parte más baja del núcleo de sedimento, el Hg se encuentra principalmente asociado con la fracción oxidable, pero en este tramo en particular, la concentración de C_{org} es ligeramente mayor, lo cual sugiere que el Hg estaría principalmente asociado con la materia orgánica y en menor medida se encontraría adsorbido tanto en sulfuros (en períodos de mayor humedad y de condiciones reductoras predominantes), como en arcillas y pátinas de (hidr)óxidos de Fe y Mn (en períodos más secos y oxidantes).

En el perfil de Hg_T (Figura 4a) se observa un pico (131 µg kg^{-1}) asociado a sedimentos acumulados aproximadamente entre los años 1990-1995. Este pico coincide además con un con un pico en las concentraciones de Hg_{H2O2} (Figura 5 b) y elevado porcentaje de C_{org} (Figura 5 d) lo cual sugiere que la laguna estuvo afectada por algún factor o evento que dio lugar a una acumulación de Hg superior a la registrada en períodos anteriores y posteriores y que además promovió la actividad biológica en la laguna.

Entre las diferentes fuentes de Hg descritas en sistemas naturales, se menciona el aporte desde emisiones volcánicas (i.e., Fitzgerald y Lamborg, 2003, Selin, 2009). Debido a la proximidad del sistema volcánico andino y a su conocida influencia sobre el área de estudio (i.e., Gaiero *et al.,* 2007; Osores *et al.,* 2011), es posible pensar que los niveles más importantes registrados en el núcleo de sedimento puedan ser consecuencia de aportes desde erupciones volcánicas producidas en los últimos ~80 años. Además, es conocido el efecto de fertilización que tienen los elementos asociados con las cenizas, tales como P, Fe y otros elementos traza, sobre los ecosistemas acuáticos (Hamme et al., 2010; Lin et al., 2011). En ambientes marinos, por ejemplo, se ha demostrado que luego de una erupción volcánica se produce un incremento en la concentración de clorofila, la cual es tomada como un proxy de biomasa planctónica (Hamme *et al.,* 2010; Lin *et al.,* 2011). En consecuencia, un potencial aporte de Hg desde tefras provenientes de una erupción volcánica podría haber generado, no sólo un aporte extraordinario de Hg a la laguna del Plata, sino también podría haber dado lugar a un proceso de fertilización que se ve reflejado en el registro sedimentario como un aumento en el contenido de C_{org}.

El registro de erupciones volcánicas más próximas al área de estudio, indica que la más cercana al momento en que se registró el pico fue la erupción del volcán Láscar (5592 m; 23.22ºS, 67.44ºW), ubicado en el Norte de Chile sobre el límite con Argentina. Desde 1984 hasta 1993, la actividad del volcán Láscar fue intensa y estuvo caracterizada por ciclos de crecimiento y subsidencia de domos dacíticos de lava, desgasificación del magma representada por una actividad fumarólica intensa y eventos eruptivos vulcanianos a plinianos. La erupción del 19 y 20 de Abril de 1993 fue la más intensa del registro histórico del volcán Láscar y durante la misma se formó un extenso penacho de dirección E-SE que alcanzó la costa atlántica sudamericana (Matthews *et al.,* 1997) y muy probablemente la laguna del Plata.

Por encima del mencionado pico de Hg, la masa acumulada de Hg_T por unidad de área comienza a disminuir gradualmente, y conserva esta tendencia hasta los ~7 cm de profundidad, cuando comienza a aumentar nuevamente. Es interesante notar que la masa acumulada de Hg_T no puede ser completamente explicada por las fracciones oxidable y biodisponibles en ese tramo del núcleo de sedimento, lo cual permite suponer un aporte que podría estar asociado al Hg atmosférico.

CONCLUSIONES

Los niveles de Hg medidos en sedimentos actuales y pasados acumulados en la cuenca del río Suquía (en promedio: 47±30 µg kg^{-1}) son bajos en relación con niveles medidos en otras regiones del mundo altamente industrializadas o afectadas por actividades mineras, pero están dentro del intervalo de valores determinados en lagos ubicados en regiones remotas de la Patagonia andina.

Las importantes variaciones en los niveles de Hg observadas en el núcleo de sedimento extraído de la laguna del Plata parecieran responder a los cambios hidrológicos registrados en el sistema en los últimos ~80 años, más que a eventos de contaminación puntuales.

Durante el período seco que afectó la región de la laguna antes de 1968, la principal fuente de aporte de sedimentos a la laguna habría correspondido a los sedimentos transportados por el río Suquía desde las cabeceras de la cuenca y al aporte desde las precipitaciones, fundamentalmente en forma de

polvo atmosférico. La inexistencia de otras fuentes de Hg que afecten la región, así como también de mecanismos que alteren la especiación y distribución del Hg entre las fases sólida y acuosa, explica la constancia en las concentraciones de Hg registradas en la base del núcleo de sedimento y también son similares a las medidas en los sedimentos de la cuenca del río Suquía. En este tramo, el Hg se encuentra principalmente asociado con la fracción oxidable de los sedimentos, atribuible en mayor medida a la pirita (sobre la que el Hg se encontraría adsorbido) y en menor medida a la presencia de materia orgánica particulada.

En los sedimentos acumulados después de 1968 el aumento en las concentraciones de Hg_T coincide con el inicio de un período más húmedo en la región, al menos hasta el año 2003. En ese período el Hg geogénico habría llegado a la laguna adsorbido en pirita y en menor medida asociado a óxidos de Fe y Mn presentes en los sedimentos de lecho. Una vez en la laguna se habría producido una posterior removilización y transporte partir de procesos biogeoquímicos.

El pico de concentración de Hg registrado en sedimentos acumulados entre 1990 y 1995 se atribuye al aporte desde las cenizas volcánicas que alcanzaron la región luego de la erupción del volcán Lascar en 1993. Estas cenizas no sólo aportaron Hg a los sedimentos sino que además desencadenaron un aumento en la actividad biológica de la laguna que se tradujo en la presencia de mayores concentraciones de C_{org} en los sedimentos de ese período y una mayor asociación del Hg con esa fase.

El continuo crecimiento de las concentraciones de Hg en los sedimentos más modernos (acumulados desde 2003), asociado con un ciclo de bajas precipitaciones en la región, se atribuye a la influencia del Hg antropogénico, incorporado desde la atmósfera y cuyo efecto ha sido descrito en otras regiones del extremo sur de América del Sur menos afectadas por la actividad del hombre.

Agradecimientos. Los autores desean agradecer la asistencia del Consejo Nacional de Investigaciones Científicas y Técnicas (CONICET), de la Universidad Nacional de Córdoba y de la Université de Bordeaux 1**.** Este trabajo fue parcialmente financiado con fondos otorgados por SECYT-UNC y PIP-CONICET. Yohana V. Stupar agradece una beca Erasmus Mundus otorgada por la Unión Europea. Asimismo, los autores agradecen las sugerencias de Anne M. Hansen y otros dos revisores anónimos que contribuyeron a mejorar significativamente el presente trabajo.

REFERENCIAS

Appleby, P.G., Oldfield, F., 1978, The calculation of lead-210 dates assuming a constant rate of supply of unsupported ^{210}Pb to the sediment: Catena, 5 (1), 1-8.

Appleby, P.G., 2001, Chronostratigraphic techniques in recent sediments, *in* Last, W.M. and Smol, J.P. (eds.), Tracking Environmental Change Using Lake Sediments, Volume 1: Basin Analysis, Coring and Chronological Techniques: Dordrecht, The Netherlands Kluwer Academic Publishers, 171-203.

Audry, S., Blanc, G., Schäfer, J., 2006, Solid state partitioning of trace metals in suspended particulate matter from a river system affected by smelting waste drainage: Science of the Total Environment, 363, 216-236.

Audry, S., Blanc, G., Schäfer. J., 2005, The impact of sulphide oxidation on dissolved metal (Cd, Zn, Cu, Cr, Co, Ni, U) inputs into the Lot-Garonne fluvial system (France): Applied Geochemistry 20 (5), 919-931.

Balcom, P., Fitzgerald W., Hammerschmidt, C., Lamborg, C., Graham, L., 2004, Mercury sources and speciation in the waters of New York/New Jersey Harbor Estuary: Materials and Geoenvironment, 51, 795-798.

Barnett, M.O., Turner, R.R., 2001, Bioaccessibility of mercury in soils: Soil and Sediment Contamination, 10, 301-316.

Behra, P., Bonnissel-Gissinger, P., Alnot, M., Revel, R., Ehrhardt, J.J., 2001, XPS and XAS study of the sorption of Hg(II) onto pyrite: Langmuir, 17, 3970-3979,

Bermond, A.P., 1992, Thermodynamics applied to the study of the limits of sequential extraction procedures used for the speciation of trace elements in sediments and soils: Environmental Technology, 13 (12), 1175-1179. Biester, H., Bindler, R., Martínez-Cortizas, A., Engstrom, D., 2007, Modeling the past atmospheric deposition of mercury using natural archives: Environmental Science and Technology, 41 (14), 4851-4860.

Borah, D., Senapati, K., 2006. Adsorption of Cd(II) from aqueous solution onto pyrite: Fuel, 85, 1929-1934.

Bostick, B.C., Fendorf, S., 2003, Arsenite sorption on troilite (FeS) and pyrite (FeS_2): Geochimica et Cosmochimica Acta, 67, 909-921.

Bower, J., Savage, K.S., Weinman, B., Barnett, M.O., Hamilton, W.P., Harper, W.F., 2008, Immobilization of mercury by pyrite (FeS2): Environmental Pollution, 156, 504-514.

Bryan, G.W., Llangston, W.J., 1992, Bioavailability, accumulation and effects of heavy metals in sediments with special reference to United Kingdom estuaries: a review: Environmental Pollution, 76(2), 89-131.

Bucher, E.H., Gavier Pizarro, G., Curto, E.D., 2006, Cap. 1. Síntesis geográfica, *en* Bucher E.H. (ed.), Bañados del Río Dulce y Mar Chiquita (Córdoba, Argentina), Academia Nacional de Ciencias, Córdoba, Argentina, 15-27.

Castelle, S., Schäfer, J., Blanc, G., Audry, S., Etcheber, H., Lissalde, J-P., 2007, 50-year record and solid state speciation of mercury in natural and contaminated reservoir sediment: Applied Geochemistry, 22, 1359-1370.

Cauwet, G., Gadel, F., De Souza Sierra, M.M., Donard, O., Ewald, M., 1990, Contribution of the Rhône River to org. C inputs to the Northwestern Mediterranean Sea: Continental Shelf Research, 10, 1025-1037.

Conaway, C.H., Swarzenski, P.W., Cohen, A.S., 2012, Recent paleorecords document rising mercury contamination in Lake Tanganyika: Applied Geochemistry, 27(1), 352-359.

Cooke, C.A., Wolfe, A.P., Hobbs, W.O., 2009, Lake-sediment geochemistry reveals 1400 years of evolving extractive metallurgy at Cerro de Pasco, Peruvian Andes: Geology, 37(11), 1019-1022.

Cooke, C.A., Balcom, P.H., Kerfoot, C., Abbott, M.B., Wolfe, A.P., 2011, Pre-colombian mercury pollution associated with the smelting of argentiferous ores in the bolivian andes: Ambio, 40, 18-25.

De Marco, S.G., Botté S.E., Marcovecchio J.E., 2006, Mercury distribution in abiotic and biological compartments within several systems from Argentina: 1980-2005 period: Chemosphere, 65, 213-223.

Downs, S.G., Macleod, C.L., Lester, J.N., 1998, Mercury in precipitation and its relation to bioaccumulation in fish: a literature review: Water, Air, and Soil Pollution, 108, 149-187.

Doyle, C.S., Kendelewicz, T., Bostick, B.C., Brown, G.E., 2004, Soft X-ray spectroscopic studies of the reaction of fractured pyrite surfaces with Cr(Vl)-containing aqueous solutions: Geochimica et Cosmochimica Acta, 68, 4287-4299.

Driscoll, C.T., Blette, V., Yan, C., Schofield, C.L., Munson, R., Holsapple, J., 1995, The role of dissolved organic carbon in the chemistry and bioavailability of mercury in remote Adirondacklakes: Water, Air and Soil Pollution, 80,499-508.

Durrieu, G., Maury-Brachet, R., Girardin, M., Rochard, E., Boudou, A., 2005, Contamination by heavy metals (Cd, Zn, Cu, and Hg) of eight fish species in the Gironde estuary (France): Estuaries 28, 581-591.

Environmental Protection Agency, 1997, Mercury Study Report to Congress, Volume I: Executive summary, EPA-452/R-97-2003, Office of Air Planning and Standards and Office of Research and Development, U.S. Environmental Protection Agency, Washington, DC, <http://www.epa.gov/ttn/caaa/t3/reports/volume1.pdf>, consulta: 10 de mayo de 2013.

Etcheber, H., Relexans, J-C., Beliard, M., Weber, O., Buscail, R., Heussner, S., 1999, Distribution and quality of sedimentary organic matter on the Aquitanian margin (Bay of Biscay): Deep-Sea Research II, 46, 2249-2288.

Fitzgerald, W.F., Lamborg, C.H., 2003, Geochemistry of Mercury in the Environment. In: Lollar, B.S. (ed.), Treatise on Geochemistry: New York, Elsevier, 107-148.

Fitzgerald, W.F., Mason, R.P., 1997, Biogeochemical cycling of mercury in the marine environment. In: Sigel, H., Sigel, A. (Eds.), Metal Ions in Biological Systems, Mercury and its Effects on Environment and Biological Systems: New York, Marcel Dekker Inc., 34, 3-110.

Frank, H., 1915, Contribución al conocimiento de las Salinas Grandes y la Mar Chiquita de la Provincia de Córdoba: Revista del Centro de Estudiantes de Ingienería, 3, 91-107.

Gagnon, C., Pelletier, É., Mucchi, A., 1997, Behaviour of anthropogenic mercury in coastal marine sediment: Marine Chemistry, 59, 159-176.

Gaiero, D.M., Brunet, F., Probst, J-L., Depetris, P.J., 2007, A uniform isotopic and chemical signature of dust exported from Patagonia: Rock sources and occurrence in southern environments: Chemical Geology, 238 (1-2), 107-120.

Gaiero, D.M., Roman Ross G., Depetris, P.J., Kempe, S., 1997, Spatial and temporal variability of total non-residual heavy metals content in stream sediments from the Suquía river system, Córdoba, Argentina: Water, air and soil pollution. 93, 303-319.

Gutiérrez-Ruiz, M., Romero, F.M, González-Hernández, G., 2007, Suelos y sedimentos afectados por la dispersión de jales inactivos de sulfuros metálicos en la zona minera de Santa Bárbara, Chihuahua, México: Revista Mexicana de Ciencias Geológicas, 24 (2), 170-184.

Hamme, R.C., Webley, P.W., Crawford, W.R., Whitney, F.A., DeGrandpre, M.D., Emerson, S.R., Eriksen, C.C., Giesbrecht, K.E., Gower, J.F.R., Kavanaugh, M.T., Peña, M.A., Sabine, C.L., Batten, S.D., Coogan, L.A., Grundle, D.S., Lockwood, D., 2010, Volcanic ash fuels anomalous plankton bloom in subarctic northeast Pacific: Geophysical Research Letters, 37 (19).

Hermanns, Y.M., Biester, H., 2013, Anthropogenic mercury signals in lake sediments from southernmost Patagonia, Chile: Science of the Total Environment, 445-446, 126-135.

Huerta-Diaz, M.A., Morse, J.W., 1990, A quantitative method for determination of trace metal concentrations in sedimentary pyrite: Marine Chemistry, 29, 119-144.

Huerta-Diaz, M.A., Morse, J.W., 1992, Pyritization of trace metals in anoxic marine sediments: Geochimica et Cosmochimica Acta, 56(7), 2681-702.

Kostka, J.E., Luther III, G.W., 1994, Partitioning and speciation of solid phase iron in saltmarsh sediments: Geochimica et Cosmochimica Acta, 58(7), 1701-1710.

Lamborg, C.H., Fitzgerald, W.F., Damman, A.W.H., Benoit, J.M., Balcom, P.H., Engstrom, D.R., 2002, Modern and historic atmospheric mercury fluxes in both hemispheres: Global and regional mercury cycling implications: Global Biogeochemical Cycles, 16 (4), 51-1–51-11.

Langston, W.J., Burt, G.R., Pope, N.D., 1999, Bioavailability of metals in sediments of the Dogger Bank (central North Sea): A mesocosm study: Estuarine, Coastal and Shelf Science, 48(5), 519- 540.

Laurier, F.J.G., Cossa, D., Gonzalez, J.L., Breviere, E., Sarazin, G., 2003, Mercury transformations and exchanges in a high turbidity estuary: The role of organic matter and amorphous oxyhydroxides: Geochimica et Cosmochimica Acta, 67, 3329-3345.

Leroy, S.A.G., Warny S., Lahijani, H., Piovano, E.L., Fanetti, D., Berger, A.R., 2010, The role of geosciences in the mitigation of natural disasters: Five case studies: Geophysical Hazards, International Year of Planet Earth, 115-147.

Lin, I.-I., Hu, C., Li, Y.-H., Ho, T.-Y., Fischer, T.P., Wong, G.T.F., Wu, J., Huang, C.-W., Chu, D.A., Ko, D.S., Chen, J.-P., 2011, Fertilization potential of volcanic dust in the low-nutrient lowchlorophyll western North Pacific subtropical gyre: Satellite evidence and laboratory study: Global Biogeochemical Cycles, 25.

Ma, Y., Uren, N.C., 1995, Application of a new fractionation scheme for heavy metals in soils: Communications in Soil Science and Plant Analysis, 26(19-20), 3291-3303.

Martínez, D.E, Gómez Peral, M.A., Maggi, J., 1994, Caracterización geoquímica y sedimentológica de los fangos de la laguna Mar Chiquita, Provincia de Córdoba: aplicación del análisis multivariante: Revista de la Asociación Geológica Argentina, 49(1-2), 25-38.

Martínez, D.E., 1991, Caracterización geoquímica de las aguas de la Laguna Mar Chiquita, Provincia de Córdoba: Facultad de Ciencias Exactas Físicas y Naturales, Universidad Nacional de Córdoba, Tesis Doctoral, 284 pp.

Matthews, S.J., Gardeweg, M.C., Sparks, R.S.J., 1997, The 1984 to 1996 cyclic activity of Lascar Volcano, northern Chile: cycles of dome growth, dome subsidence, degassing and explosive eruptions: Bulletin of Volcanology, 59(1), 72-82.

Merlo, C., Abril, A., Amé, M.V., Argüello, G.A., Carreras, H.A., Chiappero, M.S., Hued, A.C., Wannaz, E., Galanti, L.N., Monferrán, M.V., González, C.M., Solís, V.M., 2011, Integral assessment of pollution in the Suquía River (Córdoba, Argentina) as a contribution to lotic ecosystem restoration programs: Science of the Total Environment, 409, 5034-5045.

Monferrán, M.V., Galanti, L.N., Bonansea, R.I., Amé, M.V., Wunderlin, D.A., 2011, Integrated survey of water pollution in the Suquía River basin (Córdoba, Argentina): Journal of Environmental Monitoring, 13, 398-409.

Muñiz, P., Danulat, E., Yannicelli, B., García-Alonso, J., Medina, G., Bícego, M.C., 2004, Assesment of contamination by heavy metals and petroleum hydrocarbons in sediments of Montevideo Harbour (Uruguay): Environmental International, 29, 1019-1028.

Mutti, D., Tourn, S., Caccaglio, O., Herrmann, C., Geuna, S., Di Marco, A, Gonzalez Chiozza, S., 2005, Evolución metalogenética de las Sierras Pampeanas de Córdoba y sur de Santiago del Estero: Ciclos famatiniano, gondwánico y ándico: Revista de la Asociación Geológica Argentina 60(3), 467-485.

Nova-López, C., Huerta-Díaz, M.A., 2001, Degree of trace metal pyritization in sediments from the Pacific coast of Baja California, Mexico: Ciencias Marinas, 27(2), 289-309.

Olivero, J., Johnson, B., Arguello, E., 2002, Human exposure to mercury in San Jorge river basin, Colombia (South America): The Science of the Total Environment, 289, 41-47.

Osores, M.S., Pujol, G., Collini, E., Folch, A., 2011, Análisis de la dispersión y depósito de ceniza volcánica mediante el modelo FALL3D para la erupción del volcán Hudson en 1991: Argentina, Servicio de Hidrografía Naval y Servicio Meteorológico Nacional, informe técnico, 14 pp.

Ozverdi, A., Erdem, M., 2006, Cu^{2+}, Cd^{2+} and Pb^{2+} adsorption from aqueous solutions by pyrite and synthetic iron sulphide: Journal of Hazardous Materials, 137, 626-632.

Pesce, S.F., Wunderlin D.A., 2000, Use of water quality indices to verify the impact of Córdoba City, Argentina, on Suquía River: Water Research, 34(11), 2915-2926.

Piovano, E.L., Ariztegui, D., Damatto Moreira, S., 2002, Recent environmental changes in Laguna Mar Chiquita (central Argentina): A sedimentary model for a highly variable saline lake: Sedimentology, 49, 1371–1384.

Piovano, E.L., Ariztegui D., Bernasconi, S.M., McKenzie, J.A., 2004 a, Stable isotopic record of hydrological changes in subtropical Laguna Mar Chiquita (Argentina) over the last 230 years: The Holocene, 14(4), 525-535.

Piovano, E.L., Larizzatti, F.E., Fávaro, D.I., Oliveira, S.M.B., Damatto, S.R., Mazzilli, B.P., Ariztegui, D., 2004 b, Geochemical response of a closed-lake basin to 20^{th} century recurring droughts/wet intervals in the subtropical Pampean Plains of South America: Journal of Limnology, 63(1), 21-32.

Piovano, E., Villalba, R., Leroy, S., 2006, Holocene environmental catastrophes in South America: from lowlands to the Andes: Quaternary International, 158, 1-3.

Piovano, E.L., Ariztegui, D., Córdoba, F., Cioccale and M, Sylvestre, F., 2009, Hydrological Variability in South America Below the Tropic of Capricorn (Pampas and Patagonia, Argentina) During the Last 13.0 Ka, *in* Vimeux, F., Sylvestre, F., Khodri, M. (eds.), Past Climate Variability in South America and Surrounding Regions, From the Last Glacial Maximum to the Holocene, volume 14: Springer, 323-351.

Quevauviller, P., 1998, Method performance studies for speciation analysis: Royal Society of Chemistry, Cambridge, UK, 71-75.

Quintana, E., 2011, Environmental impact of the nuclear tests in Argentina (poster) *in* Comprehensive nuclear-test-ban treaty, science and technology, Vienna, Austria, 8-10 June.

Raiswell, R., Canfield, D.E., Berner, R.A., 1994, A comparison of iron extraction methods for the determination of degree of pyritization and the

recognition of iron-limited pyrite formation: Chemical Geology, 111(1-4), 101–10.

Ribeiro Guevara, S., Meili, M., Rizzo, A., Daga, R., Arribére, M., 2010, Sediment records of highly variable mercury inputs to mountain lakes in Patagonia during the past millennium: Atmospheric Chemistry and Physics, 10, 3443-53.

Robbins, J.A., Edgington, D.N., 1975, Determination of recent sedimentation rates in Lake Michigan: Geochimica et Cosmichimica Acta, 39, 285-304.

Robbins, J.A.; Krezoski, J.R., Mozley, S.C., 1977, Radioactivity in sediments of the Great Lakes, Post-depositional redistribution by deposit-feeding organisms: Earth and Planetary Science Letters, 36, 325-333.

Rodrigues Bastos, W., Oliveira Gomes, J.P., Calvacante Oliveira, R., Almeida, R., Nascimento, E.L., Bernardi, J.V.E., Drude de Lacerda, L., da Silveira, E.G., Pfeiffer, W.C., 2006, Mercury in the environment and riverside population in the Madeira River Basin, Amazon, Brazil: Science of the Total Environment, 368, 344-351.

Rosenberg, E., Ariese, F., 2001, Quality control in speciation analysis, *in* Ebdon L, Pitts L, Cornelis R, Crews H, Donard OFX, Quevauviller Ph, (eds.), Trace Element Speciation for Environment, Food and Health: The Royal Society of Chemistry, Cambridge, UK, 17-50.

Rydberg, J., Klaminder, J., Rosén, P., Bindler, R., 2010, Climate driven release of carbon and mercury from permafrost mires increases mercury loading to sub-arctic lakes: Science of the Total Environment, 408, 4778-83.

Saari, H-K., Schmidt, S., Castaing, P., Blanc, G., Sautour, B., Masson, O., Kirk Cochran, J., 2010, The particulate $^{7}Be/^{210}Pb_{xs}$ and $^{234}Th/^{210}Pb_{xs}$ activity ratios as tracers for tidal-to-seasonal particle dynamics in the Gironde estuary (France): Implications for the budget of particle-associated contaminants: Science of the Total Environment, 408, 4784-4794.

Sahuquillo, A., Rauret, G., Bianchi, M., Rehnert, A., Muntau, H., 2003, Mercury determination in solid phases from application of the modified BCR-sequential extraction procedure: a valuable tool for assessing its mobility in sediments: Analytical and Bioanalytical Chemistry, 375(4), 578-583.

Sanchez-Cabeza, J.A., Ruiz-Fernández, A.C., 2012, ^{210}Pb sediment radiochronology: An integrated formulation and classification of dating models: Geochimica et Cosmochimica Acta, 82, 183-200.

Santos-Francés, F., García-Sánchez, A., Alonso-Rojo, P., Contreras, F., Adams, M., 2011, Distribution and mobility of mercury in soils of a gold mining region, Cuyuni river basin, Venezuela: Journal of Environmental Management 92, 1268-1276.

Schäfer, J., Blanc, G., Audry, S., Cossa, D., Bossy, C., 2006, Mercury in the Lot-Garonne River system (France): sources, fluxes and anthropogenic component: Applied Geochemistry, 21, 515-527.

Schmidt, S., Howa, H., Mouret, A., Lombard, F., Anschutz, P., Labeyrie, L., 2009, Particle fluxes and recent sediment accumulation on the Aquitanian margin of Bay of Biscay: Continental Shelf Research, 29, 1044-1052.

Selin, N., 2009, Global Biogeochemical Cycling of Mercury: A Review: Annual Review of Environment and Resources, 34, 43-63.

Tack, F.M.G., Vossius, H.A.H., Verloo, M.G., 1996, A comparison between sediment fractions, obtained from sequential extraction and estimated from single extractions: International Journal of Environmental Analytical Chemistry, 63(1), 61-66.

Teisserenc, R., Lucotte, M., Houel, S., 2010, Terrestrial organic matter biomarkers as tracers of Hg sources in lake sediments: Biogeochemistry, 103, 235-244.

Tessier, A., Campbell, P.G.C., Bisson, M., 1979, Sequential extraction procedure for the speciation of particulate trace metals: Analytical Chemistry, 51(7), 844-51.

Tseng, C.M., Amouroux, D., Abril, G., Tessier, E., Etcheber, H., Donard, O.F.X., 2001, Speciation of mercury in a fluid mud profile of a highly turbid macrotidal estuary (Gironde, France): Environmental Science and Technology, 35, 2627-2633.

United Nations Scientific Committee on the Effects of Atomic Radiation, 2000, Sources and effects of ionizing radiation: UNSCEAR 2000 Report to the General Assembly, with Scientific Annexes, United Nations, New York, 1, 654 pp.

Van der Klooster, E., van Egmond, F.M., Sonneveld, M.P.W., 2011, Maping soil clay contents in dutch marine districts using gamma-ray spectrometry: European Journal of Soil Science, 62, 743-753.

Wunderlin, D.A., Díaz, M.P., Amé, M.V., Pesce, S.F., Hued, A.C., Bistoni, M.A., 2001, Pattern recognition techniques for the evaluation of spatial and temporal variations in water quality. A case study: Suquía River Basin (Córboba-Argentina): Water Resources, 12, 2881-2894.

Xia, P., Meng, X., Yin, P., Cao, Z., Wang, X., 2011, Eighty-year sedimentary record of heavy metal inputs in the intertidal sediments from the Nanliu River estuary, Beibu Gulf of South China Sea: Environmental Pollution, 159, 92-99.

Yang, H., Engstrom, D.R., Rose, N.L., 2010, Recent changes in atmospheric mercury deposition recorded in the sediments of remote equatorial lakes in the Rwenzori Mountains, Uganda: Environmental Science and Technology, 44(17), 6570-6575.